Hot Water Supply Using a Transcritical Carbon Dioxide Heat Pump

A thesis presented in fulfilment of the requirement for the degree of
Master of Engineering at Massey University,
Palmerston North, New Zealand.

Roland Kern
Dipl. Ing. FH
2004

Abstract

In New Zealand (NZ) a typical household uses between 160-330 l of hot water per day at 50 to 60°C. Most hot water systems are electrically heated. Heat pumps using carbon dioxide (CO_2) in the transcritical heat pump cycle offer high potential for energy savings. The use of CO_2 also offers further benefits such high volumetric heating capacity, reduced environmental impact, good availability and low costs.

The objective of this project was to design, build and test a hot water supply system (HWSS) using a CO_2 heat pump.

The main components of the HWSS were the heat pump, a stratified hot water storage cylinder (HWC), a water pump and a control system. The heat pump design was based on a prototype Dorin CO_2 compressor which was available. Key features were use of a vented spiral tube-in-tube heat exchanger for the gas cooler, use of a low pressure receiver incorporating an internal heat exchanger after the evaporator and the use of a back-pressure regulator as the expansion valve. The heat pump had a nominal design heating capacity of 8.1 kW with a COP of 3.9 at 0°C/34.8 bar.a evaporation temperature/pressure and 100 bar.a discharge pressure when heating water from 15°C to 60°C.

The prototype heat pump performance was measured for a range of operating conditions including 0°C/33.8 bar.g to 15°C/49.8 bar.g evaporation temperatures/pressures, 18 to 30°C cold water inlet temperature, 40 to 60°C hot water outlet temperature and 90 to 120 bar.g discharge pressures. Liquid refrigerant and/or oil carry over caused by limited LPR separation capacity and/or oil foaming in the LPR was apparent for some trials but could not be completely eliminated. The compressor isentropic and volumetric efficiencies were about 30% lower than stated by the manufacturer. Possible reasons were mechanical and/or compressor oil related problems. The gas cooler was marginal in capacity especially when the heat pump operated at high evaporation pressure conditions.

The measured heat pump heating capacity at the design conditions was 5.3 kW at a COP of 2.6. The heat pump COP was not sensitive to the discharge pressure across a wide range of operating conditions, so constant discharge pressure control was adopted. Overall best heat pump efficiency for 60°C hot water was achieved at 105 bar.g discharge pressure. At these discharge conditions the heating capacity and COP ranged from 4.8 kW and 2.2 at 0°C/33.8 bar.g evaporation temperature/pressure and

30°C cold water inlet temperature to 8.7 kW and 3.9 at 15°C/49.8 bar.g evaporation and 18°C water inlet respectively.

A mathematical model of the HWSS was developed. The model parameters were determined from a small set of separate trials. The overall agreement between measured and the predicted HWSS performance was good. The HWSS performance was predicted for conditions likely to occur in a one or two family home. The biggest efficiency losses were HWC standing losses to the ambient air. The heat pump operated with close to the maximum COP of 2.75 because the water inlet temperature seldom rose above 25°C. There was potential for efficiency improvements if the short on/off intervals caused by the relatively small HWC relative to the heating capacity of the heat pump could be avoided.

Overall, the investigation has shown that the CO_2 heat pump combined with a stratified HWC can provide a very efficient HWSS. The heat pump prototype performance was competitive with conventional heat pumps but there was significant potential for efficiency improvements due to the poor compressor performance. However, the availability and costs of heat pump components and the poor compressor performance constrain the commercial implementation.

Acknowledgement

Thanks in particular to my Supervisor Dr. Don Cleland (Institute of Technology and Engineering (ITE) Massey University, NZ) for guiding the project, supporting on the thesis and for organising a scholarship.

Thanks to other Massey staff, including Dr. Stephen White (ITE) who introduced me to the CO_2 project at Massey University, the staff from the Massey Workshop for their help on building the heat pump test rig, Bruce Collins (ITE) for his support on measurement and electronic devices and Julie Mudford and Jon Hayward (IT) for helping on numerous occasions.

Thanks to Dorin SA for the use of their prototype compressor and to Danfoss SA for access to their prototype CO_2 expansion valve.

Thank you to all those who supported me during the Master degree at Massey University and during the writing of the thesis in Switzerland.

Finally, thanks to the people, who made the study in NZ possible, such as Dr. Max Ehrbar (University of Applied Science NTB Buchs, Switzerland) who organised the internship at Massey ITE and great thanks to my parents for their support.

Table of contents

List of figures

List of tables

1 Introduction

New Zealand (NZ) is about to ratify the Kyoto protocol, a global convention to reduce the global greenhouse gas emissions. Fundamental to the convention is the development of more energy efficient technologies and greater use of renewable energies.

New Zealand's energy production is predominantly fossil fuel based (72% of the total), followed by hydro-powered electricity (23%), geothermal electrical power (5%) and other renewable energies (less than 1%) (Ministry of Economic Development, 2000). The production of sanitary hot water in domestic household accounts for 8.7% of the total energy use and represents 38% of the domestic energy consumption (4000 kWh/year for the average household).

Water heating technology in domestic and commercial applications is dominated by electric (69%) and gas-fired (19%) storage units (Williamson and Clark, 2001). Alternative systems, such as solar thermal, wet-backs and heat pumps represent less than 1% of the market. Even though the gas instantaneous water heaters dominate many world markets, the technology has only 8% of the market in NZ.

World-wide about 90 million heat pumps were installed in the year 1997, predominately for residential space heating, air conditioning and cooling applications (Runacres, 2002). The heat pump market has grown at an average of 15% per year since 1992. The biggest markets are China, Japan and the USA.

Heat pumps have the potential for high-energy efficiency but the high heating temperature required for the domestic hot water production limits their efficiency and use in domestic water heating applications. Therefore the use of heat pumps for water heating has not been as widespread as the use of heat pumps for space heating and air conditioning.

The recent concerns of ozone depletion and global warming caused by the emission of fluorocarbon refrigerants, has increased the research on more sustainable heat pump technology. One alternative is the natural refrigerant carbon dioxide (CO_2), which has high potential for water heating applications when used in a transcritical heat pump cycle (Lorentzen, 1994a).

The overall aim of this research was to develop and test the performance of a water heating heat pump using the transcritical CO_2 cycle based on a prototype CO_2 compressor produced by Dorin SA an Italien compressor manufacturer.

2 Literature Review

The scope of this chapter was to review the requirements of domestic hot water heating in NZ and the state of art technology for hot water supply systems, including conventional heat pump technology. Further the advantages and disadvantages of both conventional and CO_2 heat pumps for water heating and the general applications for CO_2, including the availability of the equipment were reviewed.

2.1 Hot water heating

The technology used for hot water supply systems (HWSS) in NZ has been summarised by Williamson and Clark (2001). This survey of NZ's households covers many aspects of the hot water production such as economic requirements for hot water production and safety standards. Further information about the state of art technologies, used for hot water production in NZ were available on the Energy Efficiency Resource Assessment (EERA) (Rossouw, 2000). Corresponding data for the American situation is available from ASHRAE (1999).

2.1.1 Requirements for hot water production

The HWSS must heat cold fresh water from the main supply to the desired temperature and supply the user with sufficient hot water at any time (Williamson and Clark, 2001). The main requirements for HWSS's are reliability, safety, energy efficiency and low cost. The most common water temperature is in the range of 50-70°C for households and up to 100°C in the commercial sector and/or special circumstances. The amount of hot water typically used in NZ varies between 160 and 330 litres at 60°C per day per household.

New Zealand's building code requires the hot water production temperature to be 60°C or higher to avoid the growth of *Legionella*. However, the delivery temperature to the user is often lower than 55°C to reduce the danger of burns. ASHRAE (1999) provides more detailed information about *Legionella* and other bacterial growth in water supply systems, including their prevention.

2.1.2 Hot water supply systems (HWSS)

The general function of the HWSS is to supply the user with sufficient hot water at any time. The hot water can either be a) produced on-demand or b) supplied out of a water storage tank (hot water cylinder, HWC).

a) On-demand water heating

On-demand water heaters (also called: instantaneous water heaters) operate without a storage tank and the hot water is produced and supplied directly to the user when required. The heating capacity requirement of such an installation is high compared to a hot water supply system operating with a storage tank. Electric installations generally operate at constant power and the water temperature is controlled by the water flow rate, whereas modern gas powered units control the gas combustion to produce the water at the demanded temperature. Electric instantaneous water heaters have efficiencies of about 95%, while gas powered units typically achieve efficiencies of 65 to 80% due to the losses associated with the pilot flame of the gas burner and losses of the flue gas (Williamson and Clark, 2001).

b) Storage systems

Water heaters that operate in combination with a HWC heat the water over the time and store the water at useful temperature in the HWC until needed. The heating capacity is designed to heat the content of the HWC within the desired recovery time of the HWC. Typical recovery time is 4 to 6 hours and the water in the cylinder is often heated during the night using low night power-supply rates. The water heater starts operating when the water temperature at the thermostat, which is installed towards the bottom of the HWC, is lower than the set point.

Gas heated storage systems typically achieve efficiencies of 70-80%. The only losses of electric HWC are the so-called standing losses of the HWC (i.e. convective heat losses to the surrounding air).

HWC models in NZ are graded from 'A' to 'C' depending on their insulation level. Modern A-grade HWC have heat losses in the range of 600-800 kWh/year, while C-grade cylinders (manufactured between 1976-1986) have losses of 1300 to 1800 kWh/year (Williamson and Clark, 2001).

HWC's typically rely on the creation of a thermocline between the hot and the cold water. Hot water is drawn to the top of the HWC and is replaced by cold water entering at the bottom. Density differences prevent mixing of the water until heating starts. Most electric and gas installations heat the water at the bottom of the HWC so that the hot water with a low density rises to the top, while the colder water with a high density sinks to the bottom. Hence during heating the contents of the HWC is mixed. Some HWC use an electric boost-element at the top of the cylinder so the upper part of the cylinder can be recovered faster and a shortage of hot water prevented.

A more enhanced separation of the hot and cold water in the cylinder can be achieved with a fully stratified HWC. The cold water from the bottom of the cylinder circulates through an external water heater, where it is heated to the hot water temperature and returns to the top of the HWC. Similarly when hot water is supplied to the user out of the top of the cylinder, cold water flows through the bottom inlet. Thereby mixing of the hot and cold water is limited and the hot water temperature remains high until the HWC is nearly completely exhausted.

There have been numerous theoretical analysis and experimental investigations into stratified chilled water storage tanks (e.g. Nelson *et al*, 1998). However, investigations into stratified hot water storage tanks have been less frequently reported (e.g. Oppel *et al*, 1986).

2.2 Heat pumps

2.2.1 General heat pump description

Heat pumps transfer heat from a reservoir at low temperature (heat source) to a reservoir at high temperature (heat sink) by using the phase change energy of a working fluid (refrigerant). In the most common vapour compression cycle, the liquid refrigerant evaporates in a heat exchanger (evaporator) at a low pressure and temperature by absorbing heat from the heat source. The vapour is compressed to a higher pressure and temperature and condenses in a second heat exchanger (condenser) by rejecting the heat to the heat sink. A throttling device closes the cycle by expanding the working fluid to the low pressure again. The heat pump process generally operates below the critical point of the working fluid.

The efficiency of a heat pump is usually expressed as the coefficient of performance (COP), which describes the ratio between useful energy output and energy input to the process (ASHRAE, 2001). The ideal theoretical process is the completely reversible Carnot cycle. According to the second law of thermodynamics the heat sink and heat source temperatures determine the Carnot cycle efficiency.

$$COP_{Carnot} = \frac{T_{heat\,sink}}{T_{heat\,sink} - T_{heat\,source}}$$

Practically the efficiency of the Carnot cycle never can be achieved since the heat transfer in the heat exchangers and the compression and expansion are not irreversible. In heating mode the COP of a heat pump is given by:

$$COP_{heat} = \frac{heat\ output}{work\ input} = \frac{heat\ transfered\ in\ the\ condensor}{work\ to\ compressor}$$

Heat pumps are often characterised by their thermal efficiency related to the Carnot cycle (Carnot efficiency):

$$\eta_{Carnot} = \frac{COP_{heat}}{COP_{Carnot}}$$

Heat pumps operating in conventional applications such as air conditioning and space heating in a moderate climate, generally achieve COP's in the range of 3 to 5 and up to 8 in special circumstances. The Carnot efficiency is generally in the range of 0.2-0.5 and seldom higher than 0.6, because approximately 50% of the efficiency losses are caused by the compressor, temperature differences in the heat exchangers and the throttling losses (Neksa, 1994).

2.2.2 Refrigerants

Refrigerants are the working fluid in heat pump cycles. According to the second law of thermodynamics the theoretical energy efficiency of a heat pump system depends only on the thermodynamic process and is independent of the thermodynamic properties of the working fluid. However, in practise the refrigerant properties have substantial effect on the system performance.

The main thermodynamic characteristics of the refrigerants are their critical temperature, thermal conductivity, latent heat of evaporation, specific volume of vapour, and viscosity. Also important are their long-term chemical stability under typical operating conditions, their safety, such as toxicity, flammability and odour, plus their compatibility with the system components, availability, cost and their environmental compatibility (ASHRAE, 2001).

Refrigerants used are dominated by the synthetic fluorocarbon refrigerants so conventional heat pump equipment has been standardised to suit these refrigerants (e.g. maximum pressure rating of 25 bar). For example the frequently used synthetic refrigerants HCFC-22, HFC-134a and HFC-407C have saturation pressures of 5.0 bar, 2.9 bar and 4.9 bar at 0°C and 24.3 bar, 16.8 bar and 26.6 bar at 60°C respectively.

2.2.2.1 Phase out of synthetic refrigerants

The fluorocarbon based synthetic refrigerants, such as CFC's and HCFC's are harmful to the environment, cause long-term global damage to the ozone layer and contribute to global warming due to their high chemical stability and other chemical properties.

The Montreal protocol initially signed in 1987, and its following revisions, successively ban "substances that deplete the ozone layer". The production of CFC's has been prohibited since 1996 and the production of HCFC's will be stopped completely by 2030. The hydro-fluorocarbons (HFC's) do not deplete ozone and their production and use is not restricted by the Montreal protocol. However restrictions to their use may be imposed by individual countries due to the global warming effects (ASHRAE, 2001).

CFC's or HCFC's refrigerants can either be replaced by drop-in refrigerants with similar thermodynamic properties, such as HFC's or replaced by working fluid with no ODP and low GWP, such as natural refrigerants. The high GWP makes the use of the HFC's debatable and critics have proposed the use of natural working fluids with known long-term effects on the environment (e.g. Lorentzen, 1994a; Novelli, 1994; Halozan *et al*, 1994; Pettersen, 1995).

2.2.2.2 Natural refrigerants

The natural substances that are suitable to be used as working fluids are air (R-729), water (R-718), ammonia (R-717), hydrocarbons (e.g. R-290, R-1270 and R-600a), carbon dioxide (R-744), nitrogen (R-728) and noble gases. In the recent past, only ammonia has commonly been used in commercial applications (Lorentzen, 1994b).

The advantages of the natural working fluids are their known short- and long-term effects on the environment. The main disadvantageous compared to the synthetic refrigerants is their chemical properties. In particular, many of the natural working fluids are flammable and/or toxic, which limit their use as commercial refrigerants due to safety reasons. However, Lorentzen (1994b) suggested that the danger of natural working fluid in domestic applications is often overestimated. It is pointed out that natural working fluids are already widely used in (non-refrigerant) domestic and commercial applications.

2.2.3 Conventional heat pumps for water heating

Tap water heating requires relatively large temperature lifts e.g. from an ambient source temperature of 15°C or less to a hot water temperature greater than 60°C.

The hot water temperature of a conventional heat pump for water heating is limited by the condensing temperature of the working fluid at the given operation conditions. The working fluid enters the condenser as superheated gas and cools down until the gas starts to condense at constant temperatures (Figure 2.1). The water is heated counter currently and at a gliding temperature. The driving force for the heat transfer in the heat exchanger decreases as the water heats up and there is a pinch where the working fluid starts to condense. The temperature gradient may become so small, that little further heat can be transferred.

The pinch effect can be minimised with condensing temperatures much greater than the desired hot water temperature. However, this implies a large pressure ratio leading to reduced process efficiency. Therefore the water is often heated by re-circulating it through the heat exchanger several times before reaching the desired end-point temperatures. At the beginning of the heating process, the condensing temperature is low due to the low mean water temperature in the heat exchanger. The water temperature increases with each circulation through the heat exchanger so the condensing temperature increases and the process becomes progressively less efficient. In conclusion, the conventional heat pump process with rejection at constant temperature leads to poor temperature matching between the refrigerant side and the water side.

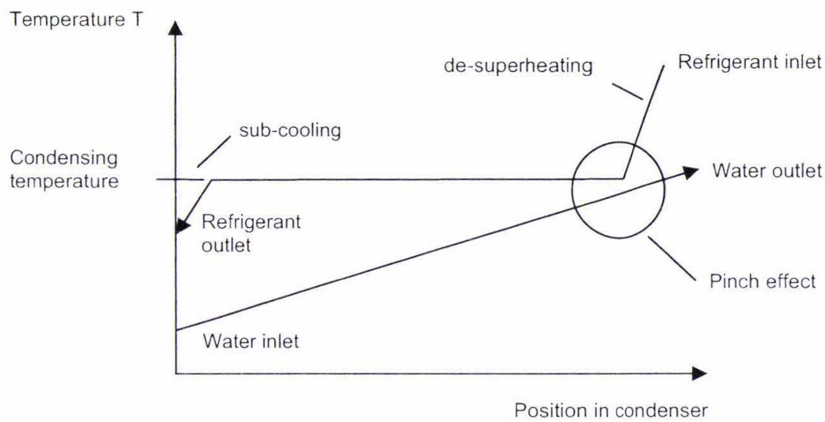

Figure 2.1: Temperature profile during heat rejection in a conventional water heating condenser.

The practical feasible process efficiency of conventional heat pumps is about 50% of the ideal Carnot cycle efficiency, resulting in COP's of 2.5 to 3.0. This is relatively low compared to many other heat pump applications.

Egger (1987) investigated practical improvements to conventional hot water heat pumps. The largest source for improvements was the compressor performance. With recently available components, efficiency improvements were achieved by using a stratified HWC, which reduces the heat pump water inlet temperature and by using an internal heat exchanger (IHX) for suction vapour superheating. The later has increased the COP of the tested heat pump by 10 to 12%. The refrigerant used in the heat pumps was not mentioned. However whether the IHX improves the COP depends on the type of refrigerant because increased superheat is not useful for all refrigerants.

In contrast, investigations carried out by Klein *et al* (1999) have shown, that the effect of a suction side heat exchanger for suction vapour superheating and simultaneous high pressure refrigerant sub-cooling, depends on the process conditions, the refrigerant and pressure drop in the heat exchanger. Higher superheating results in increased compressor discharge temperature but at the costs of reduced refrigerant mass flow rate and leads to poor compressor performance. It was found that the COP changes in direct proportion to the capacity.

From a cost perspective, any gains in the COP and the reduced energy costs may not compensate for the loss of capacity since the lower capacity requires a bigger compressor, which affects the initial system costs.

Carrier Ltd (NZ) produced an air-source heat pump for water heating in domestic applications using HCFC-22. The heat pump has a nominal capacity rating of 1.9 kW at 18°C ambient air temperature and produces water at constant temperature of 60°C. The heat pump gives a seasonal COP of 2.0 to 2.3 in NZ. The heat pump operates in combination with a stratified water storage tank. The heat pump installation is 0.7 m wide by 0.5 m high and 0.28 m deep and can be installed in a ceiling space or outdoors.

Field test data of heat pump water heaters, operation problems and practical experiences such as installations and the costs have been reported by Hiller (2002). The investigation has shown that the first cost of a heat pump water heater, including the installation costs is more than double normal electrical installations.

2.2.4 Trans-critical carbon dioxide heat pump

2.2.4.1 Carbon dioxide as a working fluid

Environmental aspects

Carbon dioxide is a greenhouse gas with a global warming potential (GWP) of one and no ozone depletion potential (ODP). Therefore it has no harmful effects on the ozone layer and there are no unknown long-term effects on the environment. Since carbon dioxide is recovered from the atmosphere or from industrial vent gas, its use as a refrigerant does not have a negative impact on the greenhouse effect (Lorentzen, 1994a, 1994b; Pettersen, 1995).

Thermodynamic properties

The characteristics of carbon dioxide have been described in many publications, such as by Pettersen (1995). Important characteristics are the low temperature of the critical point (31.1°C and 73.8 bar), the high saturation pressure at normal operating conditions resulting in high volumetric refrigerating capacity, and the rapid changes in the specific enthalpy above the critical point.

Thermodynamic and transport property data and methods for their evaluation, including the deviation from the ideal gas behaviour in the supercritical region, have been presented by Vesovic *et al* (1990) and Fenghour and Wakeham (1998). In general terms, carbon dioxide transport properties lead to low pressure-drop and high rates of heat transfer.

Chemical properties

The chemical properties of carbon dioxide are well known. Carbon dioxide is a colourless and odourless gas. Below 2000°C it remains stable and inert. It is non-flammable and non-toxic (unlike all other natural alternatives that are toxic and/or combustible), although it can lead to asphyxiation. Carbon dioxide is harmful and causes headache, dizziness, fainting and finally death, when in concentrations higher than 15% (v/v) in air. Since the gas is 1.5 times heavier than air it can accumulate to a deadly concentration in closed rooms or cellars.

When releasing high-pressure liquid carbon dioxide at normal ambient temperatures to atmospheric pressures, two thirds of the liquid evaporates and the rest becomes solid "dry ice" at -80°C. The dry ice slowly sublimates under atmospheric conditions.

Carbon dioxide is compatible with normal lubricants and construction materials. However, zinc should not be used since it will react to zinc-hydroxide ($Zn(OH_2)$). Leisenheimer and Fritz (2000) studied the compatibility of carbon dioxide with elastomers, focusing on the leakage of the refrigerant. It was shown that fluorinated elastomers performed well in carbon dioxide systems.

2.2.4.2 Carbon dioxide heat pump process

In heat pump applications, CO_2 must generally be operated in a transcritical cycle, because of the low critical temperature. The system pressures in a transcritical refrigerant cycle are generally higher than in a conventional system. The behaviour of heat pumps based on the trans-critical carbon dioxide cycle has been described by many authors (e.g. Lorentzen, 1994a, 1994b; Neksa, 1994; Pettersen, 1995; Halozan and Rieberer, 1999, 2000).

The main characteristic of the transcritical vapour cycle is the heat rejection above the critical point and the heat absorption below the critical pressure of the working fluid (Figure 2.2, left) whereas in a conventional (Evan-Perkins, E-P) refrigerant process the conditions remain below the critical point (sub-critical) (Figure 2.2, right).

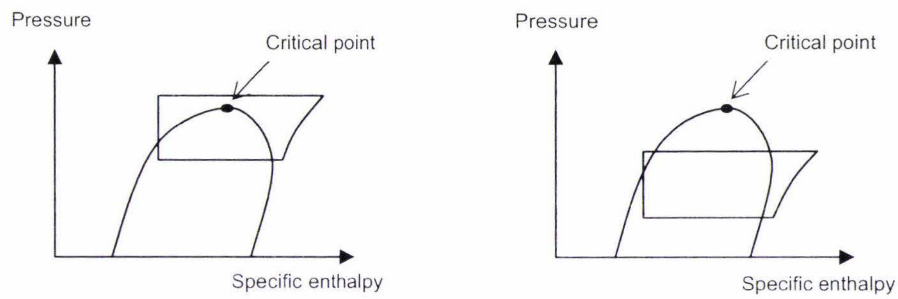

Figure 2.2: Pressure-Enthalpy diagram for transcritical (left) and conventional (right) heat pump cycle.

Above the critical point the working fluid is no longer a liquid or a gas but a supercritical fluid. A supercritical fluid is a gas-like medium with strong deviation from the ideal gas laws. Saturated conditions do not exist and the fluid does not change phase. Hence it cannot condense, and unlike the saturated condition in the two-phase area, the pressure and temperature are independent of each other. The heat rejection in the supercritical region takes place at gliding temperatures in the gas cooler (GC: equivalent to the condenser in a sub critical heat pump). The supercritical process can theoretically supply unlimited amount of heat by increasing the high pressure. However, practically the heating capacity is limited by the compressor efficiency, because increased discharge pressure implies higher compressor pressure ratio.

Discharge pressure control

The discharge pressure in the supercritical area is not determined by the condensing temperature and some kind of pressure control is required. For the selection of the discharge pressure, the heat pump heating capacity, efficiency and gas cooler length and costs have to be considered. At given heat pump conditions, the discharge pressure can be optimised. Due to the shape of the isotherms above the critical point, there exists an optimum pressure where the gain in the rejected heat does not compensate the additional compressor work and the associated heat pump efficiency losses so the COP is maximised (Neksa *et al*, 1997, 1998).

The term optimum discharge pressure for maximum COP is ambiguous in the literature and the difference between the theoretical maximum COP and the maximum feasible COP in a practical system should be made. Theoretically the heat transfer process in the gas cooler is reversible and the optimum discharge pressure is a pure function of the process enthalpies. Practically, the heat rejection process in the heat exchanger has a significant influence on the system efficiency and the feasible COP is mainly limited by the temperature approach at the end of the gas cooler.

The optimum discharge pressure has been studied by many authors such as Pettersen and Skaugen (1994), Liao and Jakobsen (1998) and Vaisman (2000, 2002). The pressure is mainly affected by the heat sink inlet temperature, the heat source temperature and the compressor efficiency; in particular the heat sink inlet temperature has a strong influence on the COP. The usage of an internal heat exchanger reduces the efficiency losses when operating at a non-optimum discharge pressure.

Experimental studies, including those by Pettersen and Skaugen (1994), Grohmann and Wobst (1998) and Rieberer *et al* (2000) have shown less influence of the discharge pressure on the system efficiency than expected from theoretical cycle calculations.

Pettersen and Skaugen (1994) measured process efficiency losses of 5% with deviations of about 4 to 5 bar from the optimum discharge pressure when operating at heat sink inlet and outlet temperatures of 35°C and 50°C and an evaporation temperature of 5°C. Similar observations have been made by Rieberer *et al* (2000). The performance of a heat pump was measured at a heat source inlet temperature between -10°C and 20°C and a temperature of 10°C and 60°C at the heat sink inlet and outlet respectively. The measured COP changes were ±2.5% for deviations of ±10 bar from the optimum discharge pressure.

More significant changes in the optimum discharge pressure were observed when varying the heat sink inlet temperature between 10°C and 50°C. For a constant heat sink outlet temperature of 60°C and a constant heat source temperature of 10°C, the COP decreased from 3.9 at 10°C heat sink inlet temperature to 3.2 at 30°C (18% drop in COP) and 2.4 at 50°C (38.5% drop in COP). Hence a discharge pressure control is required to achieve satisfactory efficiency if the heat sink inlet temperature varies (Rieberer *et al*, 2000).

In conclusion, the studies have shown that a discharge pressure control is only required when the heat sink temperatures varies in a wide range exceeding approximately 30°C. However, the measured efficiency losses depend on cycle configuration, the discharge pressure and the component performance.

2.2.4.3 Refrigerant cycle

The existence of the optimum heat rejection pressure for maximum COP has to be considered for the cycle design and its control strategy. Possible cycle configurations, aiming to produce simple and cost-effective discharge pressure control at a maximum or near maximum efficiency have been proposed by many authors (e.g. Lorentzen and Pettersen, 1993); Pettersen and Skaugen, 1994; Pettersen, 1999a). The main differences relate to the use of liquid receivers. The most frequently investigated configurations are:

a) Cycle with a low pressure receiver
b) Cycle with an intermediate pressure receiver
c) Cycle without a receiver

a) Cycle with a low pressure receiver (LPR)

Lorentzen (1993) patented a cycle with a low-pressure receiver that is suitable for the transcritical carbon dioxide process. It is known as the Lorentzen cycle and has proven satisfactory performance in air conditioning and water heating applications. The cycle has been described and tested by Pettersen and Skaugen (1994), Neksa *et al* (1997) and Rieberer *et al* (2000) among others.

The cycle consists of a compressor, gas cooler (GC), internal heat exchanger (IHX), expansion valve, evaporator and LPR. The expansion valve controls the discharge pressure. The evaporation process in the flooded evaporator unit is not controlled. The LPR receiver has multiple functions, such as the separation of the vapour/liquid mixture at the end of the evaporator, it provides buffer refrigerant to maintain the optimum refrigerant charge at changing operation conditions, it provides surge volume and it prevents liquid carry over to the suction of the compressor. The advantage of this configuration is the self-balancing low-pressure side, operating at maximum evaporation pressure at all operation conditions and the simple cycle control with only one valve. A disadvantage is that the oil has to be recovered from the LPR.

b) Cycle with a intermediate pressure receiver (IMP)

The refrigerant cycle with an IMP has been described by Pettersen (1999a), and experimentally investigated by Rieberer *et al* (2000) and Grohmann and Wobst (1998) and others. In this cycle the high-pressure refrigerant is expanded to intermediate pressures in the receiver. In a second expansion, the refrigerant is expanded to the evaporation pressure using a conventional thermostatic expansion valve. The discharge pressure is controlled by the first expansion valve, which controls the refrigerant flow to produce a constant suction vapour superheat. The IMP stores refrigerant at changing conditions. Oil is carried back to the compressor by the suction vapour. Difficulties sizing the receiver and the expansion valve have been reported but it was suggested that the performance is as good as the cycle with a LPR (Rieberer *et al*, 2000).

c) Cycle without a receiver

Grohmann and Wobst (1998) and Rieberer *et al* (2000) tested systems without a receiver.

The cycle operates with a thermostatic valve, which controls the evaporation so that the discharge pressure becomes a function of the refrigerant charge and the operating conditions. The main advantage is the simplicity but it is at the cost of reduced control flexibility. Also, the system is sensitive to refrigerant charge.

Rieberer *et al* (2000) investigated the effect of the refrigerant charge on the system efficiency. The heat rejection pressure remained near the optimum discharge pressure when undercharged while 15% overcharge result in excessive (40 bar) deviations from the optimum discharge pressure at -10°C heat source temperatures. However the significance of the refrigerant charge on the system efficiency depends on the system design, such as the volume of the high and low-pressure side components.

Refrigerant cycle control

In a transcritical heat pump two parameters may have to be controlled: (a) the discharge pressure and (b) the system capacity. The heat rejection pressure affects both the system efficiency and the capacity.

a) Control of the discharge pressure

The discharge pressure can be actively controlled by an expansion valve or passively controlled by the conditions in the low-pressure side. Options for active control are to control the optimum pressure or to hold the pressure at a constant pressure near the optimum.

Pressure control at optimum pressure has been described by many authors (e.g. Pettersen and Skaugen, 1994; Rieberer *et al*, 2000). Most controlled the pressure using the refrigerant temperature at the gas cooler outlet as the control parameter. It was suggested that a linear pressure control, proportional to the increasing refrigerant gas cooler outlet temperature is appropriate for a wide range of operating conditions. Rieberer *et al* (2000) controlled the discharge pressure by sensing the compressor discharge temperature, rather than the refrigerant temperature at the gas cooler outlet.

Grohmann and Wobst (1998) proposed that the gain in the efficiency does not justify the equipment costs for exact heat rejection pressure control. The efficiency of an air-conditioning system varied less than 4% when changing the discharge pressure between 95 and 110 bar. Similar observation have been made by Pettersen and Skaugen (1994) and Rieberer *et al* (2000).

b) Capacity control

Lorentzen (1993) suggested the possibility of capacity control through discharge pressure adjustments. Later experimental results showed that the capacity control is limited by the compressor inefficiency and by the reduced refrigerant mass flow (Pettersen and Skaugen, 1994). It was suggested that conventional capacity control based on speed control of the compressor would be both more efficient and simpler.

2.2.4.4 Heat pump performance

General methods for efficiency evaluations of the transcritical cycle based on the modified cryogenic approach have been described by Vaisman (2000, 2002). Equations for the evaluation of the process efficiency determined by the heat pump conditions and the CO_2 properties were given. The method distinguishes between the possible process efficiency and the process losses and allows significant factors affecting process losses to be identified.

Neksa (1994) identified the fundamental advantages of a transcritical heat pump for water heating applications. The study compared the efficiency and the costs of a transcritical carbon dioxide heat pump process for water heating with corresponding conventional CFC-12 and HCFC-143a processes. In both processes, conventional and transcritical, the efficiency losses are mainly caused by the compressor (about 50% of the total process losses). In terms of the heat rejection, the transcritical process performs significantly better than the conventional CFC-12 process. Higher throttling losses are caused by the expansion valve in the transcritical process but the losses are less significance on the overall process efficiency than for the conventional process. The investment cost was theoretically estimated to be about the same for both systems, with higher compressor costs but lower heat exchanger costs for the transcritical system.

In theoretical cycle evaluations CO_2 can not compete with conventional refrigerants such as CFC-12, HCFC-22 or HFC-134a. Pettersen (1995) calculated the theoretical coefficient of performance (COP) of carbon dioxide operating in a simple E-P cycle to be less than 75% of that for CFC-12.

Practically, the efficiency losses of the refrigerant process are smaller than in a conventional system and the transcritical CO_2 process achieves superior efficiency in applications with limited heat sink, low heat sink inlet temperature, high temperature glide of the heated medium and an unlimited heat source. The real advantages of such an application is the close match between the refrigerant temperature and the heat sink temperature in the gas cooler, and the possibility of gas being cooled close to heat sink temperatures leading to highly efficient heat transfer and reduced heat losses.

Disadvantageous is the rapid loss of efficiency at increasing heat sink inlet temperatures. Because of the high throttling losses, the process is not suitable for applications where small temperature glide, low heat sink outlet temperature and/or high heat sink inlet temperature occur. This may be improved by two stage compression cycles or by using an expansion device for work recovery (Lorentzen, 1994a, 1994b; Pettersen, 1995; Heyl *et al*, 1998; Halozan *et al*, 1994).

Besides the thermodynamic advantages in certain applications, carbon dioxide has a number of practical benefits, such as:

- Reduced component size

The high system pressures of a carbon dioxide system leads to high volumetric refrigerating capacity and constructional advantages, such as reduced compressor displacement (5-10 times smaller than for conventional refrigerants with the same refrigeration capacity), compact heat exchangers and small pipe diameters. The reduced weight and the compact design are favourable for transport refrigeration applications (Lorentzen, 1994a, 1994b, Halozan *et al*, 1994).

- Improved compressor efficiency

The high saturation pressures of CO_2 lead to small compressor pressure ratio and efficient compression. This is in particular favourable since the compressor causes the biggest energetic losses in every heat pump process (Pettersen and Skaugen, 1994).

- Practical use of refrigerant

Carbon dioxide is gained from the ambient air at low costs, the gas is already widely in use, necessary infrastructure exists and the handling is simple and well known. The refrigerant does not have to be recovered from refrigerant systems or recycled (Pettersen, 1995).

- Compatibility

CO_2 has no harmful effect on the ozone layer and its global warming potential is low compared to the conventional refrigerants so it will not be banned for any environmental reasons.

The main disadvantage is the availability and the cost of the heat pump components. However, Halozan and Reiberer (2000) suggested that ultimately the system costs of a transcritical system are mainly dependent on whether the components, in particular the compressor, will be mass-produced. At this stage the availability of the components is certainly a critical factor for the commercial applications.

2.2.4.5 Heat pump performance modelling

Simulation of the transcritical heat pump process, the appropriate control strategy and the performance of the individual components, in particular of the gas cooler, require a steady-state mathematical model. Such a model has been described by Skaugen and Svensson (1998). The investigation focused on the heat rejection process in the gas cooler at varying high pressure between 70 and 110 bar and varying water mass flow rates from 0.13 to 0.23 l/s. The results of the model were in good agreement with the measured data.

The modelling of an air-conditioning unit based on a carbon dioxide heat pump was described by Robinson and Groll (2000). The model evaluates the overall cycle performance as well as the performance of the individual components. The predictions were in good agreement to the data for an air conditioning model for conventional refrigerants, however, the verification of the model with experimental CO_2 data was not described.

A carbon dioxide heat pump for simultaneous heating and cooling has been modelled based on experimental data for a full-scale laboratory prototype by White *et al* (1999). The investigation showed that hot water between 65 and 120°C could be produced with at a moderate reduction of the COP by 33%. Further potential for improvements in the efficiency by increasing the gas cooler size were suggested.

2.2.5 Applications of carbon dioxide heat pumps

Carbon dioxide heat pumps can perform thermodynamically and/or environmentally equal or better than conventional heat systems in many applications, such as low temperature district space heating, air conditioning, drying and dehumidifying processes and water heating (Lorentzen, 1994a).

2.2.5.1 Air conditioning

Theoretical and experimental investigation of carbon dioxide in air-conditioning systems have shown that CO_2 can compete with a conventional HCFC-22 systems (Aarlien *et al*, 1996). Similar studies has been reported by Yin *et al* (1998), Beaver *et al* (1999) and Richter *et al* (2000). Compared to conventional systems, the carbon dioxide heat pumps operate at competitive efficiencies with slightly higher efficiency in heating mode and slightly lower efficiencies in air cooling mode.

Experimental investigations for car air-conditioning have shown that carbon dioxide performs similarly to a conventional air conditioning system with COP's in the range of 1.5 to 2.5. (Pettersen and Skaugen, 1994; Preissner *et al*, 2000; Hafner, 2000). Environmentally, carbon dioxide has a high potential to improve transport heat pump applications, since this sector has been by far the biggest source of emissions of gases with high ODP (Pettersen and Skaugen, 1994; Toshio and Kenichi, 1998).

2.2.5.2 Space heating

The development of carbon dioxide heat pumps for space heating in existing buildings using different heat sources has been reported by Brandes and Kruse (2000). With an air-to-water heat pump, annual COP's higher than 3.2 have been achieved. A ground water source water-to-water heat pump operated with annual COP of approximately 2.3.

Richter *et al* (2000) compared the performance of a conventional and a carbon dioxide heat pump for space heating. The carbon dioxide system operated at a slightly lower COP than the HFC-410a system but had a higher capacity at low ambient temperatures.

Space heating in modern low-energy houses and commercial buildings was investigated by Rieberer and Halozan (1998, 1999). CO_2 heat pumps had potential for heat recovery and achieved COP's in the range of 5 to 10, depending on the operation conditions and the heat source.

2.2.5.3 Drying / dehumidifying

The design and experimental data of an laundry drier, using a transcritical carbon dioxide heat pump has been presented by Schmidt *et al* (1998) and Schmidt and Fredsted (1999). The heat pump dehumidifies the moist airflow from the drying process and recovers the heat. The performance was similar to a conventional system, and considerable environmental benefits were also achieved.

2.2.5.4 Water heating

Several transcritical carbon dioxide water heaters using laboratory compressor prototypes have been developed and described in the literature (e.g. Hwang *et al*, 1997a; Neksa *et al*, 1997, Kasper and Halozan, 1997). However, the test rigs have often been used for investigations into the general characteristics of the transcritical cycle, the process control or component performance, rather than evaluating the applications itself.

A prototype air-source 4.5 kW hot water supply unit with a storage tank for domestic buildings has been described by Hashimoto and Saikawa (1997) and Saikawa and Hashimoto (1998, 2000). The heat pump uses the Lorentzen refrigerant cycle and a semi-hermetic scroll compressor. The water temperature was kept constant at 65°C. The high pressure was controlled at optimum pressure by an electronic expansion valve. Field tests showed an overall yearly COP of over 3 in Tokyo's climate with estimated heat source and fresh water temperatures between 5°C and 23°C and 3°C and 23°C respectively.

Zakeri *et al* (2000) presented preliminary performance results for a commercial water heater with a design capacity of 22 kW (earlier design descriptions were reported by Neksa *et al* (1998). The pilot plant was installed in a food-processing factory. At design conditions, water was heated from 9°C to 75°C giving a COP of 4.3 with an evaporation temperature of 20°C. The seasonal COP was approximately 4. The system uses the Lorentzen cycle, with a semi-hermetic 2-cylinder compressor (single stage) and a manually adjustable backpressure regulator for discharge pressure control. As a heat source, the condenser heat of an ammonia cascade refrigerant plant was used.

The characteristics of a heat pump water heater in combination with a stratified tank has been described by Lemke *et al* (1999). The aim of the investigation was to improve the performance of a hot water supply unit operating with a transcritical carbon dioxide heat pump by reducing the water temperature at the heat pump inlet. The first experiments were based on the re-heating characteristics of the water in the storage tank and showed promising results. Although the improvements were not quantified, further research work was proposed.

A prototype for industrial water heating, combined with simultaneous cooling, has been built and tested by Yarrall (1998) and Yarrall *et al* (1998). The prototype had a heating capacity of 130 kW when heating water from 10 to 90°C and simultaneous cooling capacity of 90 kW at -5°C evaporation temperature. The combined heating and cooling COP was 5.4 at 0°C and 4.8 at -6°C evaporation temperature.

2.3 CO_2 heat pump equipment

Conventional refrigerant equipment cannot be used in transcritical carbon dioxide systems where pressure is often at 100-150 bar. The high pressures require new technology, in particular for the compressor. Several compressors have recently become available on the market. Other components, such as expansion valves, have recently become available as prototypes and maybe available for research purposes.

2.3.1 Personal safety

Safety aspects in terms of an explosive discharge of a carbon dioxide system have been studied by Pettersen (1999b). This investigation showed that the explosive discharge energy of a conventional HCFC-22 heat pump and a carbon dioxide heat pump system of equal heating capacity are comparable. The carbon dioxide has the higher explosive discharge energy at temperatures below 60°C but the explosive discharge energy equalises at temperatures around 60°C. Above that temperature, the carbon dioxide system has less explosion energy than the conventional system.

Overall, carbon dioxide is proposed as being as safe for the user as the widely used conventional refrigerants, including the halocarbons. The high pressure has to be considered for the component design due to the safety factor, but it does not lead to general construction difficulties (Lorentzen, 1994a, 1994b; Pettersen, 1995).

2.3.2 Carbon dioxide compressors

The high operating pressure of carbon dioxide systems requires new compressor design and technology. Design criteria for compressors in transcritical carbon dioxide cycle have been investigated by Suess and Kruse (1997a, 1997b) and Suess (1998).

Dorin SA (Italy) developed a one and two stage semi-hermetic piston compressor series with 0.5 to 12.7m^3/h swept volume and a cooling capacity of 0.6 to 15 kW at -35°C evaporation temperature. The compressor performance data were presented by Neksa *et al* (1999), Dorin and Neksa (2000) and later by Hubacher and Groll (2003).

A small hermetic oil free compressor with 1.25 m^3/h swept volume, driven by a 0.5 kW motor was described by Baumann (2001). The compressor development was supported by the Swiss Federal Office of Energy (SFOE).

Preliminary results of the performance of an 2-stage reciprocating compressor prototype, built by the company Bock, have been published by Foersterling *et al* (2000). The compressor prototype was based on design of a conventional compressor for HFC-134a.

Yanagisawa *et al* (1999, 2000) and Suzai *et al* (1999) reported the development of small rotary (rolling piston) compressors with a 0.35 cm^3 displacement volume operating at 30-60 Hz frequency.

The design of a scroll compressor with a displacement volume of 7.23 cm^3 has been investigated by Hasegawa *et al* (2000) The compressor was built by the company Denso in Japan.

While the commercial availability of such compressor types has been reported, none are yet freely available in NZ.

2.3.3 Expanders

Expanders achieve little work recovery at the operating pressures in a conventional refrigerant cycle. However, the use of expanders in combination with the transcritical carbon dioxide process has been suggested by Lorentzen (1994a) and Pettersen (1995). The properties of carbon dioxide may make the use of expanders for work recovery feasible and may improve the process efficiency. This could improve the poor energy efficiency of the carbon dioxide process in the ordinary E-P cycle so that the process can compete with conventional heat pumps and become suitable for a wider range of applications.

Suess (2001) describes different options for possible full or part-load work recovery and their potential for increased system performance. It was concluded that suitable applications were not obvious and further research work was necessary.

Prototypes of work recovery devices have been presented by Heyl and Quack (1999, 2001, 2002). The expanders extract up to 80% of the expansion work. Ongoing research investigated the integration of work recovery devices into the compressor for the direct use of the recovered work. The possibility of discharge pressure control by the work recovery devices is also under development.

No expanders suitable for CO_2 in a heat pump cycle were available at reasonable cost in NZ.

2.3.4 Expansion valves

Refrigerant valves for carbon dioxide are not available on the market at this stage so the use of ordinary valve types often used in the petrochemical industry is the most common approach used. In a transcritical cycle the expansion valve may be used as a control valve for the discharge pressure. Pettersen and Skaugen (1994) proposed an expansion valve similar to the conventional thermostatic valve with a temperature sensor measuring the compressor discharge temperature and actuating the valve to maintain the discharge pressure at the optimum level.

A prototype of an electronic refrigerant expansion and control valve for carbon dioxide, developed by Danfoss SA (Denmark) has been mentioned by Suess (2001). Specific information about the valve and the control strategy were not given.

Non-refrigerant back-pressure regulators have been used for active discharge pressure control (Petterson and Skaugen, 1994). Such valves regulate the up-stream pressure at a set level, which can be adjusted manually or with an automatic actuator.

2.3.5 Heat exchangers

The high volumetric refrigeration capacity of carbon dioxide and its favourable transport properties leads to compact heat exchangers with highly efficient heat transfer.

2.3.6 Gas cooler (GC)

The supercritical heat rejection takes place at gliding temperatures and the gas cooler design is based on predicted steady-state temperature gradients, refrigerant properties and pressure drops.

A numerical model for heat transfer performance prediction in a counter-flow refrigerant-to-water gas cooler has been described by Hwang and Radermacher (1997b). The model was based on steady state refrigerant properties and accounts for the varying temperature difference for the heat transfer process at gliding temperatures. The model was in good agreement with experimental results. The capacity was predicted within 2.6% and the difference between the predicted temperature distribution and the experimental data was negligible. A similar model based on partial differential equations has been described by Schoenfeld and Krauss (1997).

Olson (1999) investigated experimentally the prediction accuracy of different carbon dioxide heat transfer correlations. Best predictions were achieved with the Krashnoschekov-Protopopov and the Ghajar-Asadi correlation, which predicted the supercritical heat transfer within ±8%. Pettersen *et al* (2000a) proposes a new correlation for in-tube cooling of turbulent carbon dioxide based on the Gnilenski correlation. The prediction accuracy was within ±20%.

Kim *et al* (2001) suggest that the heat transfer of supercritical carbon dioxide near the critical point is often underestimated and proposes a new correlation based on the Jackson-Fewster's correlation, which predicted the experimental data within ±20%.

The effect of the pressure drop on the supercritical heat transfer has been investigated by Rieberer and Halozan (1997). The pressure drop has little significance on the heat transfer and may be treated as negligible for the heat transfer predictions. The measured pressure drop of the supercritical carbon dioxide inside a 7.7 mm tube at 90 bar and a gas velocity of 8-12 m/s, was in the range of 0.03 - 0.12 bar per meter, causing a negligible temperature change of 0.6 K.

The effect of the compressor oil on the heat transfer and the pressure drop during supercritical heat rejection have been measured by Zingerli and Groll (2000). The oil reduced the carbon dioxide heat transfer coefficient by 15% and 25% at oil concentrations of 2% and 5% receptively. The measured pressure drop did increase proportionally with increasing oil concentration. With 2% oil in carbon dioxide, the pressured drop increased by 12% while 5% oil resulted in 20% increased pressure drop. A similar study for CFC-12 by Silvares and Huerta (1999) for the sub-critical heat transfer process showed that 5% oil concentration in CFC-12 caused less then 10% refrigerant heat transfer losses. In conclusion, the effect of the compressor oil on the heat transfer in a carbon dioxide system was greater than in a conventional system.

2.3.7 Evaporator

The evaporation process on the low-pressure side is similar to a conventional system and new heat exchanger rating methods are not required. The refrigerant properties and the process characteristics of the carbon dioxide process, such as the small effect of pressure drops on the process performance make the use of compact micro-channel heat exchangers feasible. The use of micro-channel heat exchangers has been most frequently documented for car air conditioning units (Man-Hoe and Clark, 2001). Micro-channel heat exchangers for residential space heating and air conditioning applications were used by Richter *et al* (2000).

Performance predictions have been carried out by Ortiz and Groll (2000) and Beaver *et al* (1999) for micro-channel evaporator for a car air conditioning units. The accuracy of the predictions was reasonable compared to experimental data, and further investigations into the pressure drop in order to improve the model were discussed.

The heat transfer of boiling carbon dioxide deviates strongly from correlations for synthetic refrigerants. Hwang *et al* (1997a) compared the performance of different heat transfer correlations for boiling carbon dioxide at saturated conditions with experimental data. A modified correlation with improved accuracy for heat transfer calculations, fully based on experimental data, has been suggested.

Experimental studies of boiling carbon dioxide in a 6, 7 and 10 mm tube have been carried out by Yun *et al* (2001), Bredesen *et al* (1997) and Knudsen and Jensen (1997). The heat transfer in small tubes of 0.79 to 1.8 mm diameter has been studied by Koyama *et al* (2001), Hihara and Tanaka (2000) and Pettersen *et al* (2000b). Due to the low surface tension of liquid CO_2, the heat transfer was underestimated. New correlations for the heat transfer, as well as the pressure drop, based on experimental data were proposed.

2.3.8 Compressor oil

Carbon dioxide compressors are operating at high pressures. At the same time the low swept volume reduces the geometric space for bearing rings and sealing leading to high load on the bearings. Therefore the oil must provide a thin film between piston and compressor body to ensure sufficient lubrication between the moving parts. The oil film between the moving parts also has a sealing function (Hesse, 1997).

Fahl (1998), Hauk *et al* (2001) and Heide and Fahl (2001) studied the possible lubricants for use with CO_2, such as the frequently used polyolester's (POE's) oils. The main characteristics such as miscibility, solubility and low temperature fluidity were discussed. The performance of POE oils were favourable for carbon dioxide compressors, due their high thermal stability and a high miscibility (dissolution of liquid refrigerant into the lubricant) and solubility (dissolution of gaseous refrigerant in the lubricant) in CO_2 at operating pressures, resulting in reduced viscosity. Because of the high solubility of the carbon dioxide in the oil, the mixture tends to foam with changing operation pressures. Using chemical additives can reduce foaming problems.

Hesse (1997) and Hesse and Spauschus (1996) studied the effect of the oil on the refrigerant transport properties. Methods for their evaluation and information about the viscosity and density of the oil-CO_2 mixtures were given.

2.3.9 Oil recovery

Due to compressor leakage, oil will enter into the refrigerant cycle. This oil has to be recovered to avoid shortage in the compressor and heat transfer inefficiency caused by oil accumulating in the heat exchangers. In systems where a low- pressure receiver is used, the oil will tend to accumulate in the receiver. The appropriate recovery method depends on the phase behaviour of the oil-carbon dioxide mixture. Rieberer *et al* (2000) recovered the oil out of the bottom of the receiver directly into the compressor suction line. Conventional oil recovery methods with a discharge line oil separator have rarely been described in the literature.

2.4 Summary of the literature

Heat pumps are an efficient method for water heating. However, the performance of the conventional heat pumps for water heating is limited by their efficiencies (typically COP's of 2 to 3) and due to the harmful effect of the synthetic refrigerant on the environment. Carbon dioxide has proven potential as an alternative refrigerant.

Carbon dioxide is a non-toxic and non-flammable natural gas with zero ODP. It has a low critical temperature at 31.5°C and 73.5 bar pressure. Above the critical point the working fluid is supercritical gas-like fluid with strong deviation from the ideal gas behaviour. Due to the relatively high pressure at the critical temperature of carbon dioxide, the system pressure in a carbon dioxide heat pump is higher than in a conventional system.

Carbon dioxide heat pumps for water heating generally operate in a transcritical cycle with discharge pressure between 80 and 130 bar and low side pressure below the critical point. The main advantage of carbon dioxide heat pumps is the efficiency of the heat rejection process at gliding temperatures, leading to a close match between the refrigerant and the heat sink. The main disadvantage is efficiency losses at high heat sink temperatures. Besides energy use and environmental advantages, the high volumetric refrigerant capacity of CO_2 can lead to a compact system design which is particularly advantageous for transport application where system weight and size is limited.

In the transcritical heat pump process, the compressor discharge pressure is not determined by the condensing temperatures and has to be controlled. Due to the thermodynamic properties of carbon dioxide, there is a pressure where maximum system efficiency is achieved. Experimental results have shown little effect of the discharge pressure on the COP over a wide range of operation conditions, except when the heat sink inlet temperature exceeds 30°C.

Several simple system designs have been described for carbon dioxide but the discharge pressure control is not always straightforward and has to be designed considering the application. Promising options for the discharge pressure control are control at the optimum pressure for maximum COP or control to a constant pressure near the optimum.

The high pressure for carbon dioxide requires new technology, particular for the compressor design. Components such as compressors, refrigerant valves and heat exchangers are under development and their availability on the market has been announced.

Numerous studies based on the use of carbon dioxide as refrigerant are going on and heat pump applications, such as car air conditioning systems, space heating and heat recovery, drying processes and water heating have been evaluated.

Several laboratory prototypes of water heaters operating with COP between 3 and 5 have been built for investigating the general characteristics of the transcritical heat pumps. The first commercial heat pump for domestic water heating with a seasonal COP of 3 has recently been announced.

In conclusion, carbon dioxide has proven its potential in both theoretical and experimental investigations for a wide range of applications. Commercial applications are constrained because of limited availability of components. Further investigations into the cycle design, the heat pump control and the component design are necessary to bring the technology to market.

3 Objectives

The overall aim of the project was to develop a prototype of a small-scale hot water supply system suitable for domestic or commercial applications, based on the transcritical carbon dioxide heat pump cycle. A prototype CO_2 compressor from Dorin SA was available to the research group at Massey. Therefore specific objectives of the projects were to:

- Design a carbon dioxide heat pump for water heating based on the available compressor.
- Construct and commission the system to achieve stable and reliable heat pump operation.
- Measure the performance of the individual components over the full range of expected operation conditions.
- Investigate methods to improve the heat pump efficiency using alternative refrigerant cycle configurations, expansion valves and control strategies.
- Integrate the heat pump with a typical hot water storage cylinder.
- Measure the performance of the modified and integrated system.
- Develop a model of the overall hot water supply system and validate the model against the measured data for typical operation conditions.
- Suggest system improvements and tasks for further investigations.

4 Prototype Description

4.1 Background

A full-scale prototype of the hot water supply system (HWSS) was designed and built, to gain experience in the system design, components design / selection and to enable experimental performance trials. The experimental data were also used to validate the model of the overall performance of the HWSS.

The requirement of the HWSS was to produce hot water at 60°C with high efficiency and at low costs, while operating in typical climatic conditions likely to occur in NZ. The hot water had to be potable and available to the user at any time of the day.

A 60°C hot water outlet temperature was chosen to be consistent with the NZ building code and meet the current practise in terms of prevention of Bacteria grow, such as *Legionella*. However, the supply hot water temperature to the user would typically be lower than 55°C for safety reasons (e.g. via a tempering valve).

The average water consumption in domestic households is between 120 and 300 L of hot water per day, leading to a typical domestic electric hot water system capacity rating of 3.0 kW so that recovery time is less than 6 hours (Williamson and Clark, 2001). Therefore it was preferable that the heat pump heating capacity was at least 3 kW to match or better this recovery rate.

CO_2 heat pump technology is still at the research stage so the commercial availability of the refrigeration components was limited. However a Dorin compressor prototype for use with CO_2 (Pre-series model: CD4.017S) with a nominal swept volume of 1.7 m^3/h and a power rating of 2.0 kW was available. The size of the compressor combined with the characteristics of the transcritical CO_2 cycle led to a nominal heat pump capacity of 8 to 10 kW, which corresponds to the combined capacity of a HWSS for several family houses or a small commercial building.

The heat pump had to be integrated into a typically HWSS used in NZ and it had to operate automatically using air as the heat source to enable flexible installation such as in ceiling spaces or outdoors.

4.2 System design procedure

The objectives of the system design procedure were to:

- Design the hot water supply system (HWSS)
- Design the heat pump cycle and process
- Select / design the HWSS and the heat pump components

The HWSS was designed first. The heat pump process was then designed based on the expected HWSS operating conditions, the likely climatic operating conditions and the manufacturer's compressor efficiency data. Knowing the design heat pump performance, the HWSS and heat pump components were then designed and/or selected. Detail of the heat pump process and component design calculations are described in appendix A.2.

4.2.1 Hot water supply system (HWSS) design

The function of the HWSS was to deliver the hot water from the heat pump to the user and to supply the heat pump with cold water. The HWSS had to be capable of supplying the user with sufficient hot water at the specified temperature despite highly variable demand.

HWSS's considered were:

- Instantaneous

The water is heated instantly from cold and directly supplied to the user. This implies heating capacity must be equal or greater than the maximal demand.

- Storage

The hot water is stored in a HWC, which provides a buffer between the supply of and the demand for hot water. The heating capacity is usually designed to heat the HWC within a typical recovery time of 4 to 6 hours so the capacity requirements is typically 2 to 6 times the average heat load depending on the size of the HWC relative to the demand.

A storage system with a HWC was considered to be the most suitable system for a domestic hot water heat pump due to the variable hot water flowrates. The advantages of such a system are longer heat pump operating periods (the HWC is fully recovered in a single period so short on/off periods do not occur) and reduced heat pump capacity requirements leading to reduced heat pump capital cost. Disadvantages are the extra cost of the HWC, the heat losses of the HWC, and the risk of hot water shortage at times of peak demand.

There were two options for the hot water production using a heat pump:

- Water re-circulation (multi-pass)

The water, which is stored at relatively uniform temperature (mixed storage), circulates between the heat pump and the HWC until the whole HWC is heated to the specified temperature in a multi-pass arrangement.

- One pass heating

The cold water is heated from cold to the specified temperature in one pass and is delivered to the top of the HWC. Because of its lower density, the hot water remains at the top while the colder water stays at the HWC bottom resulting in a thermocline in the HWC (stratified storage).

The one pass heating configuration was chosen because the transcritical CO_2 heat pump process is particularly suitable for large temperature splits with low heat sink inlet (heat pump water inlet) temperature. Other advantages of the stratified HWC were the efficient storage of the hot water (because of the thermocline, the supplied water remains at the specified hot water temperature until the HWC volume is nearly exhausted) thereby given faster apparent recovery, and slightly reduced heat losses through the HWC wall.

4.2.2 Heat pump design

The function of the heat pump was to heat the cold water at 10 to 30°C to a minimum of 60°C. The ambient air was used as the heat source. Desirable characteristics of the heat pump were stable and reliable operation, simple control and cost-effective design.

4.2.2.1 Thermodynamic and transport properties

The thermodynamic properties of carbon dioxide and water were evaluated using ASHRAE refrigerant data, which were electronically available from the software Coolpack V1.46 (Department of Mechanical Engineering, Technical University of

Denmark). The transport properties of supercritical CO_2 given by ASHRAE (2001) such as the viscosity and the thermal conductivity deviated significantly from the literature data proposed by Vesovic *et al* (1990) and Fenghour and Wakeham (1998). Hence the literature data was used to develop an equation that gives the viscosity and the thermal conductivity in the supercritical region at constant pressure and as a function of the temperature (full details are described in Appendix A.1).

4.2.2.2 Heat pump design and operating conditions

Table 4.1 summarises climatic conditions in various NZ locations.

Table 4.1: Typical NZ climatic data (ASHRAE, 2001)

	Heating dry bulb temperature [°C] (occurrence does not exceed 88 h/y)	Mean dry bulb temperature of the coldest month [°C] (occurrence does exceed 88 h in coldest month)	Mean value of extreme annual daily temperature [°C] Maximum / minimum
Auckland	1.8	11.9	29.6 / 1.7
Christchurch	-2.2	8.7	33.2 / -4
Taiaroa Head	1.8	9.9	25.3 / 1.6
Wellington	3.1	6.8	28.7 / 1.9
Average in NZ	1.1	9.3	29.2 / 0.3
Design conditions	**0**	**10 ***	**30**

* Nominal design condition

The three conditions used for the heat pump design are also given in Table 4.1. The nominal heat pump design condition of 10°C air represents an average winter day in NZ while the other operating conditions of 30°C and 0°C represent the extreme summer and winter conditions respectively.

The available tap water temperature was assumed to be approximately 15°C throughout the whole year. However, the water inlet temperature to the heat pump might be higher when partially heated water from the HWC enters the heat pump. This is most likely to occur for short periods at the end of the recovery period only so for the heat pump design conditions, a 15°C gas cooler water inlet temperature was chosen.

4.2.2.3 Heat pump cycle design

The following options for the liquid receiver and evaporator control in the transcritical heat pump cycle were considered:

- Intermediate pressure receiver (IPR)

Refrigerant cycle with an intermediate pressure receiver, an expansion valve for active discharge-pressure control and a thermal expansion valve for the evaporator control, Figure 4.1, left).

- Low pressure receiver (LPR)

A refrigerant cycle with a low-pressure receiver (LPR), a valve for active discharge-pressure control and refrigerant expansion and no evaporator control (Figure 4.1, right).

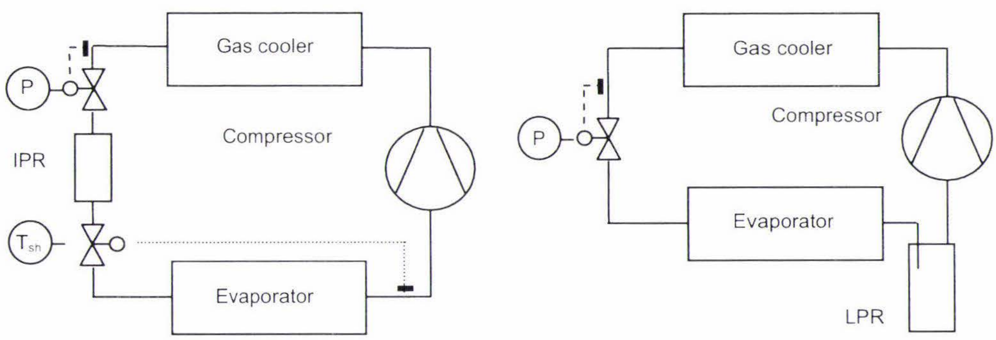

Figure 4.1: Schematic diagrams of the refrigerant cycles with intermediate-pressure receiver (IPR) (left) and low-pressure receiver (LPR) (right).

The LPR option was chosen because of the advantage of only one expansion valve, simple sizing of the components and the lower pressure rating of the LPR. Disadvantages were the need for an oil recovery system and a larger receiver size.

There were two options for the location of the LPR:

- before the evaporator (Figure 4.2)

The high-pressure refrigerant is expanded directly into the LPR located above the evaporator and circulates through the flooded evaporator driven by the force of a thermosiphon. The evaporation pressure can be limited (optional) by starving the evaporator (controlling the refrigerant mass flowrate through the evaporator inlet valve.

- after the evaporator (Figure 4.1, right)

The expanded refrigerant flows directly through the flooded evaporator then enters the LPR where the liquid / vapour mixture is separated.

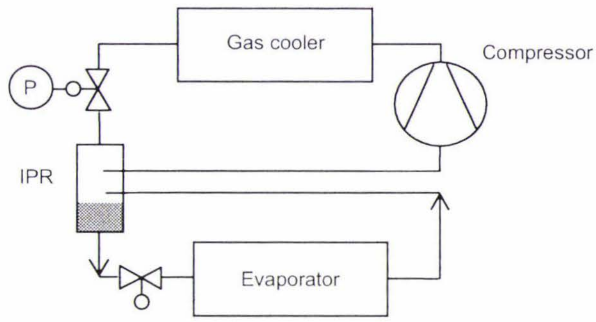

Figure 4.2: Refrigerant cycle with low pressure receiver (LPR) and thermosiphon

The refrigerant cycle with the LPR located after the evaporator was adopted because of the simple cycle design and the simpler oil recovery system. Disadvantages are the potential loss in the evaporation temperature and pressure control at high ambient air temperature.

An internal heat exchanger (IHX) was used to sub-cool the high-pressure refrigerant before expansion. This improves the efficiency and capacity requirements of the evaporator and keeps the system efficiency high across a wider range of discharge pressures than when an IHX is not used. Two options for the location of the internal heat exchanger were considered.

- IHX in the suction line to the compressor

The recovered heat is used to superheat the suction vapour only.

- IHX inside the LPR

The recovered heat is used both to evaporate liquid refrigerant at the bottom of the LPR and to provide slight vapour superheat.

The IHX located inside the LPR was chosen. The main advantage was the balancing effect of the evaporator and LPR (the liquid carried over from the evaporator must be equal to the refrigerant evaporated in the LPR), which leads to more constant superheat with varying IHX capacity.

4.2.2.4 Heat pump process design

The heat pump process design was based on the nominal heat pump operating conditions of 10°C ambient air temperature and water heating from 15°C to 60°C. At the nominal heat pump condition the following temperature approaches in the heat exchangers were assumed:

- 10 K temperature difference in the air-source evaporator.
- 5 K temperature approach between the GC water inlet and the GC refrigerant outlet
- 5 K temperature approach between the refrigerant at the IHX high-pressure outlet and the refrigerant evaporating temperature in the evaporator
- 5 K vapour superheat at the compressor suction

A steady-state model of the transcritical CO_2 heat pump cycle was developed so that the required heat exchanger size at the nominal design condition could be determined. Details of the model are given in Appendix A.2. The compressor performance data published by Neksa *et al* (1999) were assumed to apply for the available Dorin compressor prototype (as described in 4.5.7). The heat pump process predictions included iterative calculation of the cycle process parameters, such as the compressor discharge temperature, the GC and IHX refrigerant outlet temperature and the evaporation temperature. The calculations methods used are described in the Appendix A.2 and were implemented in an Excel spreadsheet.

The key decision was the choice of the discharge pressure because it has a significant effect on the performance of the GC due to the effect of rapidly changing refrigerant specific heat capacity near the critical point.

It was desired to operate the heat pump at constant discharge pressure for the whole range of likely operation conditions. The design criteria for the discharge pressure was to guarantee water heating up to 60°C at every operating condition. To avoid constraints in the GC heat transfer due to an internal pinch effect within the GC (near the critical point), the minimum temperature difference between the water and refrigerant within the GC was chosen to be at least 5 K.

Figure 4.3 shows the predicted temperature profiles in the GC at 100 bar.g discharge pressure and when heating water from 15°C to 60°C for both the nominal design and the extreme heat pump operating conditions. The temperature approach at the GC outlet was 5 K and the compressor suction superheat was 5 K. At the nominal and the extreme winter condition the heat transfer was most constrained at the GC refrigerant outlet. However for the summer extreme condition there is an internal pinch point about 20% of the way through the GC from the refrigerant inlet end.

The design discharge pressure was chosen to be 100 bar.g (101 bar.a) because the pinch effect would not be significant except at very high air temperatures. Overall, this was a conservative approach and the discharge pressure was higher than the required pressure to avoid pinch-effect related constraints in the heat transfer for most of the operating conditions, other than at very high air temperatures.

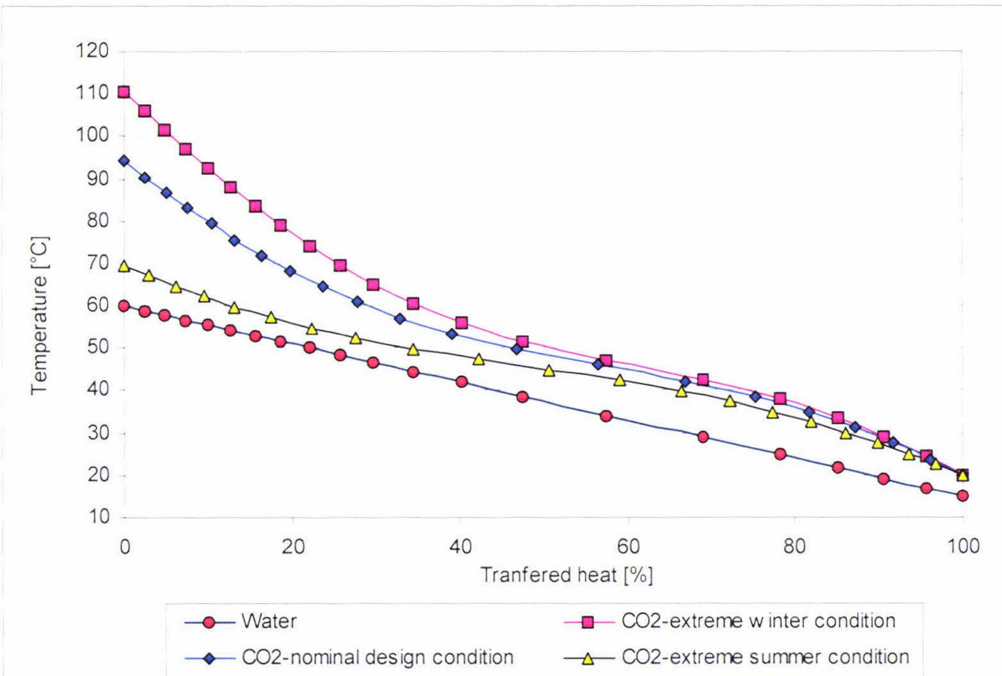

Figure 4.3: Temperature profile in the GC at 100 bar.g discharge pressure, 15°C to 60°C water temperature, 5 K temperature approach at the GC outlet and 5 K compressor suction superheat.

Table 4.2 summaries the nominal design heat pump conditions and gives the corresponding requirements for the heat exchanger UA-values predicted by the heat pump model. Given that these nominal UA-values do not change, the heat pump performance was predicted for different operating conditions. Figure 4.4 to Figure 4.6 show the predicted heat pump heat capacity, the overall heat pump efficiency (COP) and the Carnot efficiency at a hot water temperature of 60°C as a function of the gas cooler cold-water inlet temperature and air temperature.

Table 4.2: Nominal heat pump design criteria's and corresponding heat exchanger requirements

Ambient air temperature	10°C
Hot water temperature	60°C
Cold water temperature	15°C
Compressor discharge pressure	100 bar.g
Suction vapour superheat	5 K
Evaporator temperature difference	10 K
Evaporation temperature / pressure	0° C / 33.9 bar.g
Evaporator UA-value	637 W/K
Temperature approach between the refrigerant and the water at the GC refrigerant-side outlet	5 K
Nominal design GC UA value	664 W/K
Temperature approach between the refrigerant at the high-side IHX outlet and the refrigerant evaporating temperature	5 K
Nominal design IHX UA-value	127 W/K

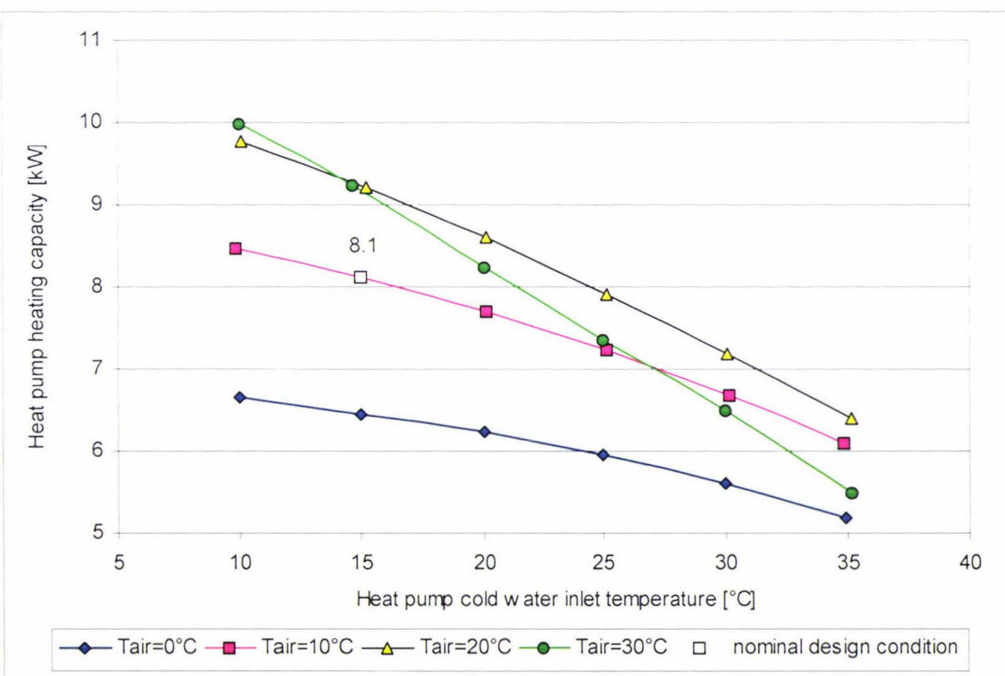

Figure 4.4: Predicted heat pump capacity at 100 bar.g discharge pressure and at 0, 10, 20 and 30°C air temperature as a function of the cold water inlet temperature.

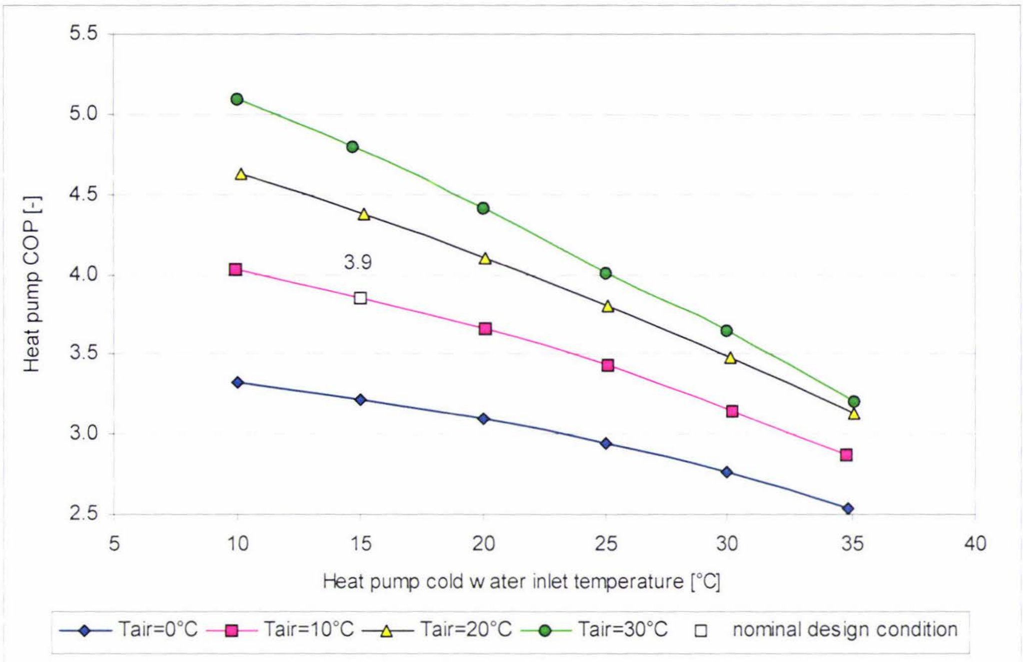

Figure 4.5: Predicted heat pump COP at 100 bar.g discharge pressure and at 0, 10, 20 and 30°C air temperature as a function of the cold water inlet temperature.

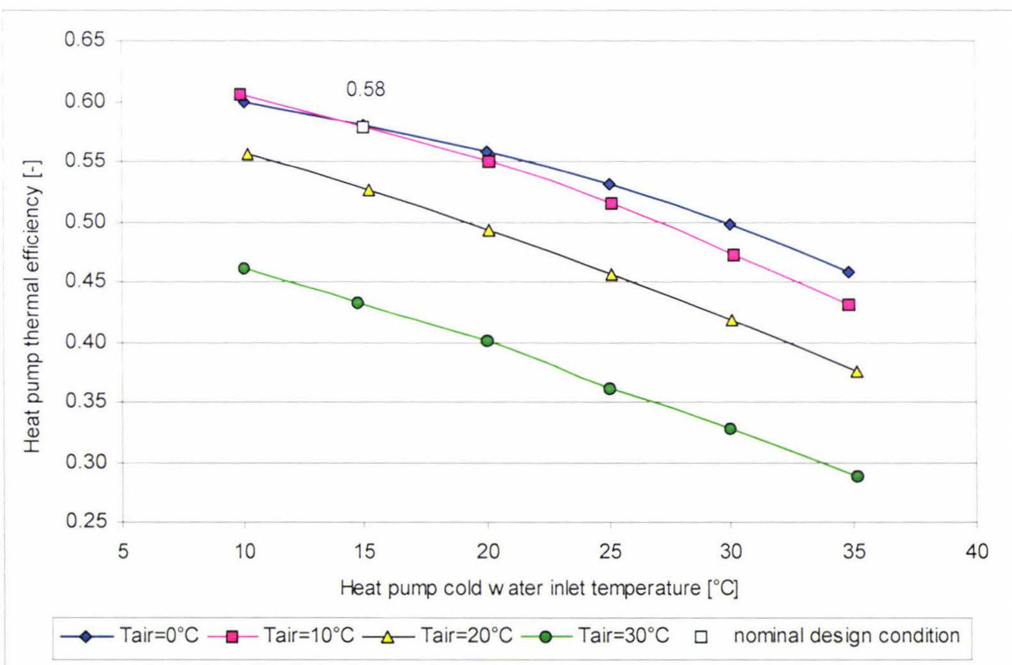

Figure 4.6: Predicted heat pump thermal efficiency based on the Carnot efficiency at 100 bar.g discharge pressure and at 0, 10, 20 and 30°C air temperature as a function of the cold water inlet temperature.

Due to the size of the compressor the heat pump was expected to have a heating capacity of 8.1 kW at the nominal design operating condition. The predicted COP was 3.9 and the Carnot efficiency was 0.6. At varying GC cold water inlet temperatures and a ambient air temperature of 10°C, the predicted heat pump energy efficiency decreased by approximately 24% when changing the water inlet temperature from 10°C to 35°C. The efficiency losses increased to 37% at 30°C ambient air temperature because of constrained heat transfer at the GC pinch point (Figure 4.3).

Table 4.3 summaries the predicted heat pump performance at the nominal, extreme summer and extreme winter conditions.

Table 4.3: Predicted heat pump performance at the nominal design and other operating conditions

	Extreme winter condition	Nominal design condition	Extreme summer condition
Ambient air temperature [°C]	0	10	30
Cold water temperature [°C]	15 / 30	15 / 30	15 / 30
Hot water temperature [°C]	60	60	60
Compressor discharge pressure [bar.g]	100	100	100
Evaporation pressure [bar.g]	27.2 / 28.3	33.8 / 36.0	50.0 / 59.4
Evaporation temperature [°C]	-7.6 / -6.2	0 / 2.3	15.2 / 22.3
Gas cooler heat transfer rate [kW]	6.5 / 5.6	8.1 / 6.7	9.2 / 6.5
IHX heat transfer rate [kW]	1.0 / 2.1	1.2 / 2.6	2.0 / 2.5
Evaporator heat transfer rate [kW]	4.8 / 4.0	6.4 / 4.9	7.5 / 4.9
Compressor power consumption [kW]	2.0 / 2.0	2.1 / 2.1	1.9 / 1.8
Compressor heat losses [kW]	0.40 / 0.39	0.36 / 0.35	0.23 / 0.20
Heating COP [-]	3.2 / 2.8	3.9 / 3.1	4.8 / 3.6
Heating capacity [% of nominal design capacity]	79 / 69	100 / 82	114 / 80

4.2.2.5 Heat pump process control

The heat pump process could be controlled to achieve maximal efficiency or maximal heating capacity. Desired features of the control strategy and equipment were simplicity and cost effectiveness.

Heat pump efficiency

The heat pump process for given operating conditions (air and water temperatures) and heat pump component performance can be optimised by changing the refrigerant discharge pressure. Two options were considered:

- Maximum heat pump efficiency

The discharge pressure could be continuously controlled to the optimum pressure for maximal heat pump energy efficiency, which varies as the operating conditions change.

- Control to near maximum heat pump efficiency

The discharge pressure could be controlled to a constant pressure, which is set reasonably close to the optimum pressure to give maximum heat pump energy efficiency across the full range of heat pump operating conditions.

The constant discharge pressure control was adopted because the efficiency of the process in the real system tends to be insensitive to deviations from the optimum high pressure for water inlet temperatures below approximately 30°C (Rieberer *et al*, 2000). The constant pressure control is both simple and cost-effective.

Capacity control

For the compressor used the options for the capacity control were:

- Capacity control by the discharge pressure

The capacity of a transcritical heat pump could be controlled by the discharge pressure, however, the control is restricted because of the capacity maximum occurs near the pressure for maximum COP and deviating too far from the pressure will reduce the energy efficiency.

- No capacity control

If capacity of the heat pump is not controlled, then the water flowrate through the heat pump gas cooler must be controlled to keep the outlet hot water temperature constant.

The capacity of the heat pump was not controlled. Again this was the simpler control strategy and only required low cost components, such as a water-flow control valve. Compressor speed control would be an effective method to achieve capacity control without compromising system effectiveness but was not available to the research team.

4.3 General prototype description

The prototype of the hot water supply system (HWSS) consisted of the HWC, the heat pump, and the measurement equipment. The hot water supply and the heat pump components were attached to a steel frame with the dimensions 1.8 x 1.0 m. The height of prototype was 1.7 m.

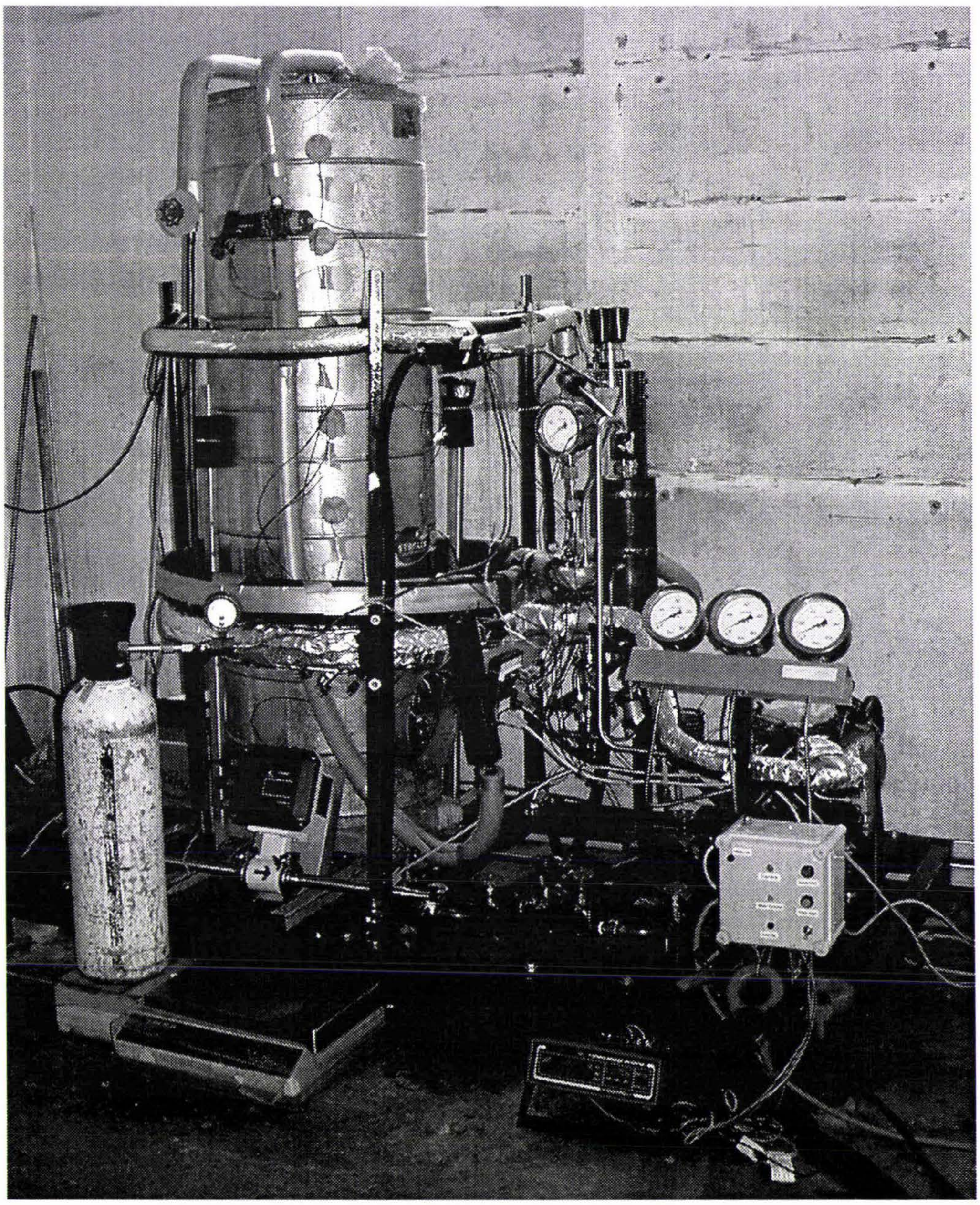

Figure 4.7: Photo of the HWSS prototype

The heat pump consisted of the gas cooler (equivalent to the condenser in a conventional heat pump), the water control valve, the evaporator, the low-pressure receiver with internal heat exchanger and the refrigerant expansion valve.

The heat pump and HWC were arranged in a loop system (Figure 4.8). The cold water flowed out of the bottom of the HWC through the heat pump where it was heated to the desired hot water temperature. The hot water was either supplied directly to the user or flowed into the top of the HWC depending on the hot water use. The main water supply was connected to the bottom of the HWC. A pressure-reducing valve reduced the water pressure from the main supply. If water use was higher than the flow from the heat pump, the make-up cold water enters the HWC at the bottom, pushing the thermocline higher in the HWC.

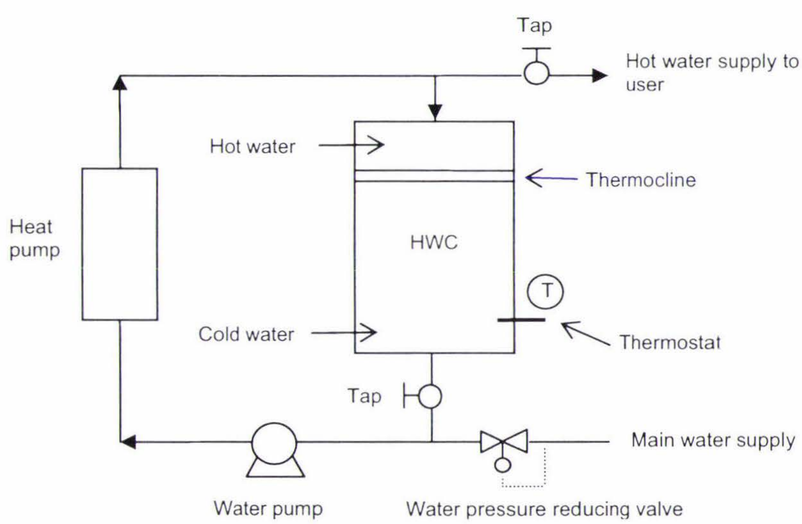

Figure 4.8: Schematic diagram of the hot water supply system

The heat pump ran when the water temperature at the thermostat, (which was installed towards the bottom of the HWC) indicated that the hot water temperature was lower than the set point, and stopped when the HWC was fully recovered (i.e. water at the thermostat was greater than the set point).

Figure 4.9 shows a schematic of the heat pump operating at the design conditions assuming no heat losses. The carbon dioxide leaves the compressor supercritical at 100 bar.g pressure and approximately 94°C. The refrigerant cools down to 20°C in the gas cooler while the water heats up from 15°C to 60°C. The high-pressure refrigerant sub-cools in the IHX to 5°C and then expands to saturated conditions at 33.9 bar.g and

0°C as it passes through the BPR valve. Most of the liquid refrigerant evaporates in the evaporator; however, some liquid carries over into the LPR where vapour and liquid separate. The remaining liquid refrigerant evaporates and superheats to 5 K by the internal heat exchanger in the LPR and returns to the compressor suction at 5°C.

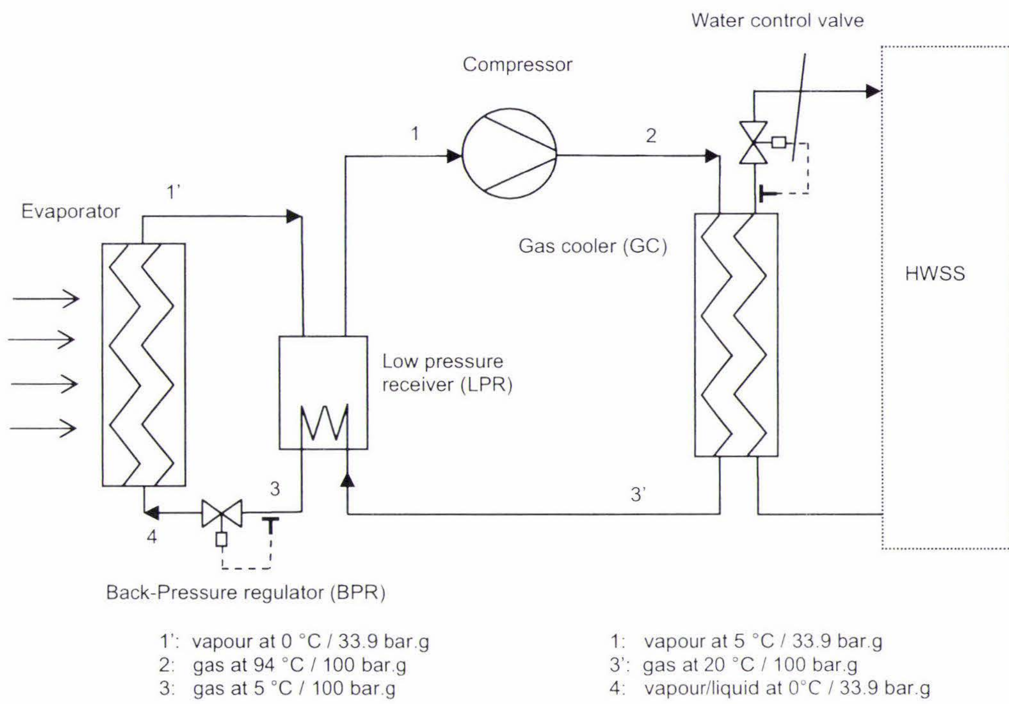

Figure 4.9: Schematic diagram of the heat pump and refrigerant temperatures at the nominal design operating condition.

4.4 HWSS component designs and descriptions

4.4.1 Stratified hot water storage cylinder (HWC)

The function of the HWC was to:

- store the hot water until the water was consumed by the user
- provide a buffer between the production and the supply

Table 4.4 summarises the data for the HWC used. The HWC thermostat was located at a height of 0.34 m of the HWC bottom.

Table 4.4: Hot water storage cylinder specifications

Model	Stainly water heater
Year manufactured	1970
Grade	Type D (Pre 1976)
Dimensions	ϕ 0.45 x 1.5 m
Dimensions of inner shell	ϕ 0.35 x 1.43 m
Volumetric capacity	137 l
Maximal head pressure	7.6 m

4.4.2 Main water supply pressure reducer

A pressure reducer (Model: Nefa NFV3715) was used to maintain the pressure in the HWC at 3.7 m of head.

4.4.3 Water flow control valve

The function of the water flow control valve was to control the hot water to the specified outlet temperature by adjusting the water mass flowrate through the gas cooler.

A thermostatic type valve was used (Table 4.5). The device consisted of a valve body and a temperature sensor, which was connected via capillary tube to the valve body. The sensor was installed inside the water tube, directly at the gas cooler outlet to achieve a short time constant (C5, Figure 4.14). The valve body was by-passed by approximately 0.2 l/min so that there was a small water flow to maintain a representative signal when the valve was fully closed.

Table 4.5: Water flow-control valve specifications

Model	Danfoss / AVTA-15
Range of mass flowrate	Unknown
Control temperature range	25-65°C
Control accuracy	Unknown
Maximal operating pressure	10 bar
Maximal pressure drop	7 bar

4.4.3.1 Water pump

The water pump supplies the heat pump with cold water from the bottom of the HWC. The centrifugal pump summarised in Table 4.6 was used. It had a nominal power use of 110 W (stage 3) and was installed between the HWC cold water inlet and the heat pump gas cooler. The pump was cooled and lubricated by the water-flow, so the pump bearing had to be vented at start-up and there had to be a minimal flow passing through the pump, which was provided by the water flow control valve by-pass. The pump was operated only when the GC was provided with water from the mains supply (C4, Figure 4.14).and/or when the HWC shut off valve was opened (WSS4, Figure 4.14).

Table 4.6: Water pump specifications

Model	Nowax MR 63
Supply voltage [V ~ Hz]	230 ~ 50
No. of operation stages [-]	3
Power rating [W]	60 / 83 / 110
Maximum head pressure [bar]	0.48 / 0.6 / 0.64
Maximum volumetric flow rate [m^3/h]	2.3 / 3.2 / 4.3
Volumetric flow rate at 3 meter head pressure [m^3/h]	0.5 / 1.4 / 2.5
Minimal required flow rate [m^3/h]	>0

4.4.4 Tubing

Standard plumbing ½" (12.2 mm) copper pipes and ½" (12.2 mm) rubber hoses were used for the water supply system.

4.5 Heat pump component designs and descriptions

4.5.1 Pressure rating and safety factors

The maximum heat pump operating pressures were set by the compressor specifications at a maximum of 150 bar.a on the discharge side and 100 bar.a on the suction side. The refrigerant system was protected by relief valves (Table 4.20), which were set to these maximum operation pressures. The refrigerant system design pressures were 160 bar.a on the discharge side and 110 bar.a on the suction side, which corresponds to pressures about 10% higher than the relief pressure (Sinnott, 1999).

The design safety factor for all custom-made components was 2 to 3. However, the strength of the components also depended on the quality of the weld joints so the custom made components were pressurised to 1.5 times the design pressure to test their construction before commissioning (Sinnott, 1999).

4.5.2 Gas cooler (GC)

The function of the gas cooler was to transfer the heat from the supercritical refrigerant to the water, so the water had to flow counter-flow to the refrigerant to achieve close temperature matching. Oil flow through the GC had to be guaranteed to avoid excessive oil fouling. As a rule of thumb 5 to 7 m/s gas velocity is required for sufficient oil carry through a vertical tube. In this case the oil return was assumed to be less critical than in a conventional system due to the high solubility of the oil in the supercritical CO_2. The pressure drop of the refrigerant in the gas cooler had to be reasonably small to avoid GC efficiency losses; however, modelling showed that the overall efficiency of the transcritical CO_2 heat pump was not sensitive to the pressure drop. It was also desirable to avoid the potential contamination of the hot water with refrigerant or oil in case of a leak in the heat pump GC.

Table 4.7 summarises the gas cooler design specifications:

Table 4.7: GC specifications

Design heat load	8.1 kW
Refrigerant pressure	100 bar.g
Mass flowrate of CO_2	116 kg/h
Temperature carbon dioxide inlet	94°C
Temperature carbon dioxide outlet	20°C
Nominal UA value	664 W/K
Minimal design gas velocity	5 m/s
Maximal design pressure drop	1 bar
Mass flow rate of water	155 kg/h
Temperature water inlet	15°C
Temperature water outlet	60°C
Temperature approach at the GC end	5 K

The gas coolers selected were the Spiralex vented tube heat exchangers manufactured by Vaportec Ltd (Napier, NZ). These heat exchangers incorporate 3 tubes arranged in a conventional double pipe heat exchanger but with the inner tubes twisted together. If there was a leakage in the refrigerant tube the gas and oil could escape through the gap between the two inner tubes to the ambient atmosphere without endangering the water quality (Figure 4.10).

The advantages of the twisted tubes was the increased turbulence of the flow inside the tubes, the extended heat transfer surface and closer contact and hence reduced losses between the vented tubes compared with standard double pipe design (the straight tubes were assembled and twisted until the two inner pipes made contact at multiple points). The disadvantages were that the twisting process had dimensional constraints, particularly minimum tube diameter, wall thickness and length.

Due to cost considerations, the gas coolers were constructed in one piece with an overall length of 5 meters and formed into a coil with a diameter of 0.7 meter. Full heat transfer performance data for these heat exchangers were not available so a full design could not be performed, but it was expected that the nominal design capacity could not be achieved with 5 meters so two heat exchangers were built. To get more experience with the gas cooler design, the units had different designs:

- Gas cooler 1 (GC 1)

The refrigerant flowed in the spiral-shape annulus between the outer and inner tubes and the water flowed in the inner tube (Figure 4.10, left). Twisted copper tubes were used for the inner tube and the inside tube of annulus. The outside tube of the heat exchanger was not twisted.

- Gas cooler 2.1 (GC 2.1)

The refrigerant flowed in a straight inner (aluminium) tube and water in the annulus (Figure 4.10, right). The inside tube of the annulus was a twisted copper tube; the outside tube was not twisted.

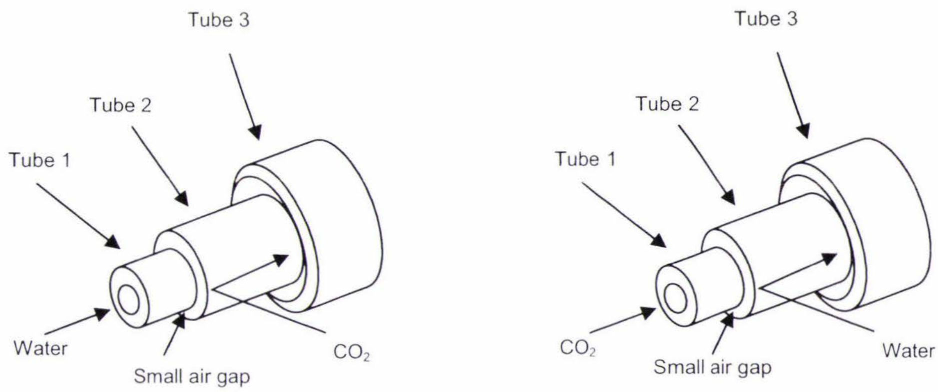

GC 1
Tube 1: Ø 1/2" x 0.9 mm, copper, twisted
Tube 2: Ø 3/4" 0.9 mm, copper, twisted
Tube 3: Ø 1" x 2 mm, steel, straight

GC 2:1
Tube 1: Ø ¾" x 2.1 mm, aluminium, straight
Tube 2: Ø 5/8" 1.25 mm, copper, twisted
Tube 3: Ø 1 1/8 " x 1 mm, copper, straight

Figure 4.10: Design of the gas cooler units 1 and 2.1

- Gas cooler 2.2 (GC 2.2)

GC 2.1 was modified by reducing the cross-sectional for flow of the inner tube, by inserting a 9.0 mm diameter flexible steel cable into the tube. The modified unit was designated as gas cooler 2.2.

To obtain the highest possible heat transfer capacity, the units were connected in series in two ways for some trials:

- Gas cooler 3.1 (GC 3.1)

Gas cooler 1 upstream of the gas cooler 2.2 on the refrigerant side.

- Gas cooler 3.2 (GC 3.2)

Gas cooler 2.2 upstream of gas cooler 1 on the refrigerant side.

GC 1 had the advantage of the reduced refrigerant side cross-sectional area. A disadvantage was the higher heat losses through the outside of the gas cooler because the main disadvantage of the gas cooler 2.1 was the low refrigerant velocity and the reduced turbulence in the straight inner tube. GC 2.2 improved this problem at the cost of the additional insert. The likely advantage of GC 3.2 over GC 3.1 was the reduced heat losses due to the refrigerant being in the outer tube when it was cooler.

Pressure rated tubes were used for the gas cooler construction. However, pressure rating data for the tubes after the twisting process were not available. It was assumed that the geometry of the twisted double pipe construction increased the actual strength due to the contact points created between the tubes.

Pressure rating data for external pressure such as the inner pipe of the annulus of GC 1 (Figure 4.10, left; Tube 2) were not available. The required wall thickness of the twisted tube was predicted for a single straight tubes using equations purposed by (Sinnott, 1999). The calculations were performed for a pressure safety factor of 3 and a thermal safety pressure factor of 1.5 (Swagelok tubing data) resulting in a minimum wall thickness of the copper tube of 1.4 mm. Due to the limited range of available tubes and manufacturing constraints (in the twisting process) a tube with 0.9 mm wall thickness was used, which corresponds to a pressure safety factor of 0.8 for a straight tube. However, the pressure rating calculation was grossly simplified, so it was assumed that the twisted double pipe construction increased the resistance of the tube to external pressure and any failure of the second tube would contained by the outer tube so this lower than desired safety factor was tolerated.

The gas cooler performance was predicted using steady-state temperatures and refrigerant properties (as described in the Appendix A.2.2) by applying a heat balance between the water and the refrigerant flow (Hwang and Radermacher, 1997b). The carbon dioxide heat transfer coefficient was predicted by using a modified version of the Jackson-Fewster correlation (Kim *et al*, 2001), which takes the wall and bulk temperature into account to consider the rapid properties changes near the critical point. For the water-side heat transfer the McAdams correlation (ASHRAE, 2001) was used. For the twisted tube a heat transfer coefficient enhancement factor of 1.4 was applied (Chen *et al*, 1996a and 1996b). According to the manufacturer of the twisted tube a reduction (for other water heating applications) of approximately 30% had to be expected due to the vented tube configuration so the overall heat transfer coefficient was corrected by a heat transfer correction factor of 0.7. To simplify the overall heat transfer predictions the fin effects of the twisted tubes were neglected.

For the pressure drop prediction, the Darcy-Weissbach correlation with the friction factor for smooth tubes (ASHRAE, 2001) was used as a correlation for the twisted tube geometry was not available.

Table 4.8 and Table 4.9 summarise the gas cooler dimensions and the expected performance at the design conditions.

Table 4.8: Dimensions and predicted performance of the gas coolers 1, 2.1 and 2.2 at the nominal design conditions.

GC units	**Gas cooler 1**	**Gas cooler 2.1**	**Gas cooler 2.2**
Overall predicted length required for total design heat load (8.1 kW) [m]	11.8	20.6	16.3
Actual overall gas cooler length [m]	5.0	5.0	5.0
Heat transfer rate [kW]	4.6	4.1	4.9
Heat transfer surface area CO_2 side [m^2]	0.478	0.233	0.233
Heat transfer surface area water side [m^2]	0.171	0.558	0.558
Heat transfer surface area ratio (water to refrigerant side) [-]	0.36	2.39	2.39
Average water side heat transfer coefficient [W/m^2K]	1699	840	846
Average refrigerant side heat transfer coefficient [W/m^2K]	6023	1736	3243
Heat transfer coefficient ratio (refrigerant to water side) [-]	3.54	2.06	3.83
UA [W/K]	181	148	197
LMTD [K]	25.7	28.0	24.8
U mean [W/m^2K]	379	374	500
Temperature approach at the GC end (CO_2 to water) [K]	30.7	33.0	29.6
GC effectiveness [-]	0.61	0.58	0.62
Nominal refrigerant mass flux [kg/m^2s]	233	187	295
Nominal water mass flux [kg/m^2s]	266	116	136
Average velocity CO_2 [m/s]	0.7	0.6	0.9
Pressure drop CO_2 [bar]	0.26	0.03	0.22
Velocity water [m/s]	0.3	0.6	1.0

LMTD: Logarithmic temperature difference between the refrigerant and the water side

Table 4.9: Dimensions and predicted performance of the gas coolers 3.1 and 3.2 at design conditions

GC units	**Gas cooler 3.1**	**Gas cooler 3.2**
Configuration	GC1 upstream of GC2.2	GC 2.2 upstream of GC1
Overall length [m]	10.0 (5.0 / 5.0)	10.0 (5.0 / 5.0)
Heat transfer rate [kW]	7.4 (4.3 / 3.1)	8.1 (3.2 / 4.9)
Heat transfer surface CO_2 side [m^2]	0.592	
Heat transfer surface water side [m^2]	0.591	
Heat transfer surface area ratio (water to refrigerant side) [-]	1.00	
UA [W/K]	466 (258 / 209)	655 (196 / 459)
LMTD [K]	15.8 (16.5 / 14.9)	12.4 (16.7 / 10.5)
U mean[W/m^2K]	638 (718 / 527)	900 (496 / 960)
Average water side heat transfer coefficient [W/m^2K]	2272	2945
Average refrigerant side heat transfer coefficient [W/m^2K]	6102	8469
Heat transfer coefficient ratio (refrigerant to water side) [-]	2.68	2.87
Temperature approach (CO_2 to water) [K]	13.3 (13.5 / 13.3)	5.3 (10.9 / 5.2)
GC effectiveness [-]	0.83 (0.78 / 0.59)	0.93 (0.79 / 0.86)
Average velocity CO_2 [m/s]	0.6 (0.7 / 0.4)	0.7 (1.0 / 0.3)
Pressure drop CO_2 [bar]	0.4 (0.3 / 0.1)	0.4 (0.3 / 0.1)
Velocity water [m/s]	0.3 (0.4 / 0.2)	0.3 (0.2 / 0.5)

Based on predictions of the heat transfer coefficients from first principles, only GC 3.2 was predicted to provide the desired heat transfer performance at the nominal design condition. Constraints on the gas cooler construction meant that alternative designs were not considered.

For effective heat transfer the ratio of the water and refrigerant heat transfer surface areas should be inversely proportional to the ratio of the water and refrigerant heat transfer coefficients. In this way the overall heat transfer would be neither water-side nor refrigerant-side constrained. This situation was achieved for GC 2.1 and GC 2.2. However GC 1 was constrained by the water side heat transfer surface which was about 10 times too small. Similarly for GC 3.1 and GC 3.2 the heat transfer was expected to be slightly constrained on the water side due to the use of GC 1.

4.5.3 Evaporator

Conventional air-cooling evaporators (fin and tube heat exchangers) could not be used because of the high pressure rating. Custom-made air-cooled evaporator unit were investigated but were eliminated because of the high manufacturing costs in NZ. A micro-channel evaporator unit was also investigated but standardised units were not commercially available on the market. Therefore the evaporator built was a water-source unit to mimic an air-source unit operating at varying ambient temperatures.

The objective was to operate the compressor suction pressure at the full range of conditions it would experience with an air-source evaporator. However, the range of the refrigerant evaporating conditions the water-source evaporator could mimic was therefore limited by the freezing point of the water. The evaporator was designed to operate flooded so there were no special requirements for the minimal vapour velocity for oil recovery.

Table 4.10: Evaporator specifications

Nominal design heat load	6.4 kW
Nominal design evaporation pressure	33.9 bar.g
Nominal design evaporation temperature	0°C
Range of evaporation temperatures	>0°C
Nominal design evaporator water inlet temperature	20°C
Nominal design evaporator water outlet temperature	≥ 5°C
Nominal design CO_2 mass flowrate	116 kg/h
Nominal design water mass flow rate	6.1 l/min
Nominal design LMTD	10.8 K
Outer tube (diameter x wall thickness)	1' (24.4 mm) x 2 mm
Inner tube (diameter x wall thickness)	¾' (19.1 mm) x 0.9 mm
Overall length	3 m
Approximate mean heat transfer surface area of the twisted tube	0.23 $m^{2\,*}$
Evaporator UA requirements at nominal operating conditions	637 W/K

Table 4.10 summarises the water source evaporator design specification. The evaporator was designed by Vaportec (NZ) based on this specification, hence no predictions of heat transfer performance based on first principles were made. The evaporator was constructed as a twisted tube pipe unit (similar to the gas cooler

design) with an overall length of 3 meters. The tube was formed into a coil with a diameter of 0.7 meters. The water flowed in the inner twisted tube (made of a 4 m straight ¾' copper tube that was twisted to 3 m in length) and the refrigerant in the spiral-shape annulus of the heat exchanger in a co-current configuration. The outer pipe of the annulus was straight and made of steel.

To give different refrigerant temperatures/pressures the evaporator water inlet temperature and/or the water flowrate were reduced/increased.

4.5.4 Internal heat exchanger (IHX)

The purpose of the internal heat exchanger was to:

- recover heat from the high-pressure refrigerant before the expansion
- evaporate liquid refrigerant out of the bottom of the LPR
- superheat the suction vapour

The internal heat exchanger was made of a coiled copper tube, which was located inside at the bottom of the LPR (Figure 4.11). The size of the IHX was constrained to 3.5 m cooper tube by the tube diameter and the available space in the LPR. The range of suitable cooper tubes with sufficient pressure rating (150 bar.a) in NZ was limited so the IHX was made of a 3/16" (4.8 mm) copper tube. Therefore prediction of heat transfer performance was not performed.

The pressure drop of the refrigerant in the coil of the IHX was predicted (as described in Appendix A.2.4) for a straight tube using the Darcy-Weissbach correlation with the friction factor for smooth tubes (ASHARE, 2001). The predicted pressure drop varied between 1.4 and 12.1 bar (2.7 bar at design conditions) depending on the mass flowrate and the operating condition. The largest pressure drop of 12.1 bar in the IHX at extreme summer conditions was unavoidable to construction constraints on the diameter of the tube used. Overall it would not have a significant impact on the overall heat pump efficiency.

Table 4.11 summarises the IHX design:

Table 4.11: IHX specifications

Nominal design heat load	1.2 kW
Temperature sub cooling	15 K
High pressure refrigerant in / outlet temperature	20 / 5°C
Low pressure refrigerant temperature (evaporation temperature)	0°C
UA requirements at nominal heat pump operating condition	127 W/K
Pipe dimensions (diameter x wall thickness)	3/16" (4.76 mm) x 0.9 mm
Coil dimensions (mean diameter x height)	60 x 100 mm
Overall length of coil	3.5 m
Mean heat transfer surface area	0.04 m^2
Predicted pressure drop (low/high flow)	1.4 / 12.1 bar

4.5.5 Low pressure receiver (LPR)

The low pressure receiver had several functions:

- It provided volume for the separation of the refrigerant vapour/liquid mixture entering from the evaporator.
- It provided surge volume for liquid refrigerant at the heat pump start-up and at changing operating conditions.
- It provides a reservoir for additional refrigerant, which prevent the system from starving in case of leakage (ballast volume).
- It provided volume for refrigerant expansion at changing operating conditions and volume to prevent liquid carry over caused by oil foaming.
- It incorporates the IHX.

For the LPR design the full range of the expected operating conditions were considered which gave volumetric flow rates between 1.1 and 1.5 m^3/h.

For the separation process the single droplet model was adopted (Wiencke, 2001). It proposes that the liquid refrigerant has the shape of a droplet with uniform diameter. The droplet in the vapour flow will stay in suspension when the vapour velocity is equal to the terminal velocity, which is given by the Navier-Stokes equation and it will separate out when the vapour velocity is smaller. Other unknown parameters of the gravity separation were taken into account using an artificial droplet diameter (e.g. interaction of the droplets and/or turbulent flow).

Applying a droplet size of 0.1 mm gave a terminal velocity of 0.09 to 0.19 m/s depending on the flowrate and conditions, and led to a minimum LPR diameter requirement for the separation section of 75.5 mm (as described in Appendix A.2.5). The LPR was designed with an inner diameter of 85 mm, resulting in vapour velocity safety factor at operating conditions of 1.3 to 3.4.

The separation length (Figure 4.11) was 170 mm, which corresponds to 1.5 times the LPR diameter between the refrigerant inlet and outlet pipe, and 0.5 times the diameter between the inlet and the liquid surface (Sinnott, 1999).

The LPR was designed to contain 100 g of liquid refrigerant (ballast volume) at the nominal design condition; however, additional volume for 100 g compressor oil was added. Surge volume of 200 g liquid CO_2 was added for start-up conditions (30% of the evaporator volume (Wiencke, 2001) and for mass fluctuations in the refrigerant system. For the swell and foam volume, 10% of the total LPR liquid volume was recommended (Wiencke, 2001). Furthermore, additional space for the volume of the IHX coil was added. Therefore the total volume of the LPR was 1.7 l which corresponded to an active height of 300 mm.

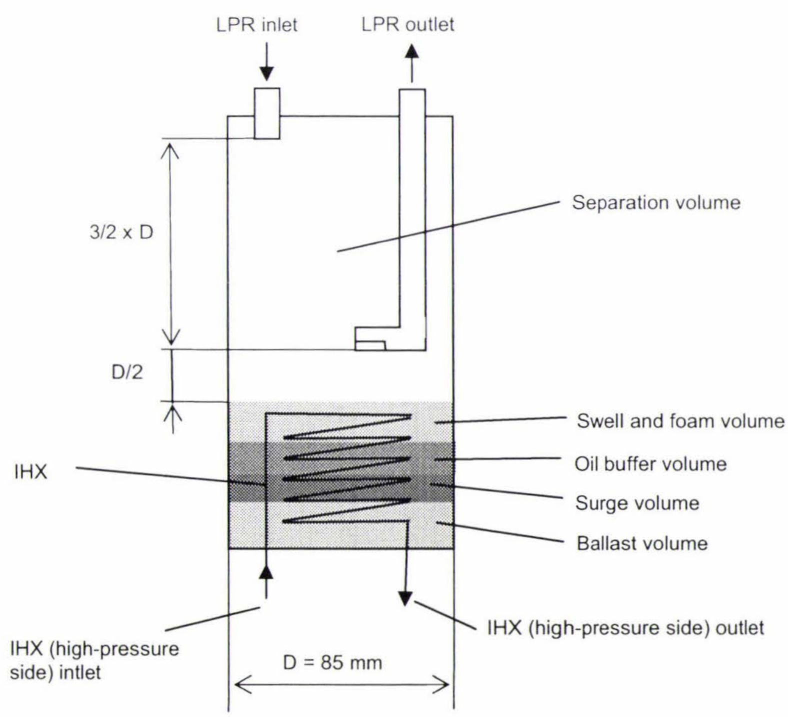

Figure 4.11: LPR design

For the LPR design, the constructional recommendations proposed by Wiencke (2001) were adopted. The LPR was made off a pressure rated hydraulic tube. The refrigerant entered the LPR through the top of the vessel, while the IHX was connected at the bottom (not shown in Figure 4.12). Table 4.12 summarises the LPR specifications:

Table 4.12: LPR specification

Overall length	320 mm
Active length	300 mm
Outer diameter	115 mm
Inner diameter	85 mm
Inner volume	1708 cm^3
Vapour velocity	0.06 to 0.07 m/s
Vapour velocity safety factor	1.3 to 3.4
Total separation length	170 mm
Mass liquid CO_2 at the nominal design conditions	100 g
Pressure rating (tube)	206 bar.a (3000 psi.a)

4.5.6 Expansion valve / back-pressure regulator (BPR)

The expansion valve had two functions:

- Throttling the refrigerant from the high pressure to the low pressure side in a single stage expansion.
- Controlling the discharge pressure in the gas cooler.

The design discharge pressure was 100 bar.g, however it was desired to operate the heat pump between 80 bar.g and approximately 130 bar.g.

Conventional refrigerant expansion valves were not suitable because of the high pressures so a back-pressure regulator valve manufactured by Tescom (US) was used (Table 4.13). The valve controlled the up-stream pressure, which was manually adjustable.

Table 4.13: Expansion valve specifications

Model	Tescom back pressure regulator 26-1700
Control pressure range	1 - 172.4 bar.g (15-2500 psig)
Flow capacity factor (cv)	0.10
Control accuracy	+/-1%
Actuator	Spring-loaded screw

4.5.7 Compressor

The function of the compressor was to compress the gaseous refrigerant at the suction side to higher pressure and temperature at the discharge side.

A semi-hermetic single stage compressor (CD 4.017 S/L) of the Dorin pre-series was used (Table 4.14). The compressor was designed for a supercritical or near transcritical vapour compression cycle. The compressor was driven by a 4-pole electric motor with 2 kW nominal power rating.

Table 4.14: Compressor specifications

Model	CD 4.017 S/L
Refrigerant	CO_2
Nominal swept volume at 50 Hz/230 V	1.7 m^3/h
Number of pistons	2
Compression-stage	Single stage
Bore size	34 mm
Stroke length	11 mm
Discharge pressure	100-150 bar.a
Maximum suction pressure	100 bar.a
Oil pressure	0-100 bar.a
Overall dimensions (length x wide x height)	503 x 290 x 342 mm
Compressor body surface area	~1.5 m^2

The compressor volumetric and isotropic efficiency were available for the next larger model with a swept volume of 2.7 m^3/h (compressor model: CD 4.027 S) (Neksa *et al*, 1999). Figure 4.12 shows these efficiencies plus the indicated isentropic efficiency at a discharge pressure of 95 bar.a and 80 bar.a respectively. The suction superheat was constant at 10 K and the compressor body cooled with a fan.

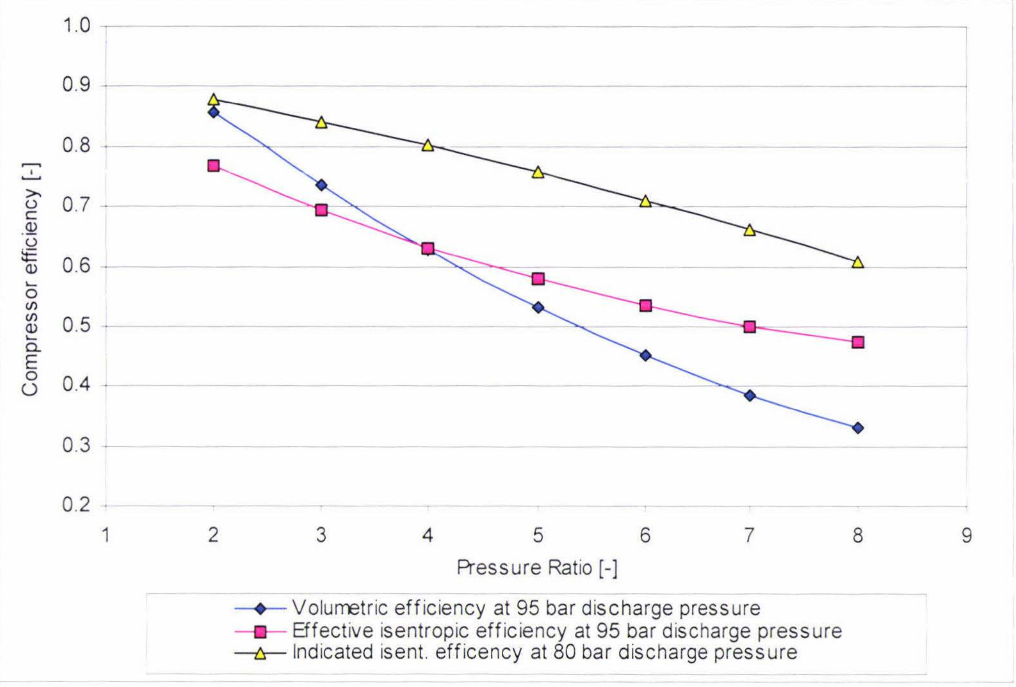

Figure 4.12: Volumetric, isentropic and indicated isentropic efficiency for a single-stage pre-series Dorin CO_2 compressor as a function of the pressure ratio at 95 bar.a discharge pressure and constant superheat of 10 K (Neksa *et al*, 1999).

Based on this data, the compressor performance at the nominal design and extreme heat pump operating conditions was predicted assuming heat losses other than from of the compressor body were insignificant (Table 4.15). The method used for the performance calculations are described in Appendix A.2.1.

At 100 bar.g discharge pressure the compressor power has a maximum at about 36 bar.g suction pressure (as described in Appendix A.2.1.1). Hence the compressor power at the extreme operating conditions was lower than at the nominal design conditions (Table 4.15).

The motor of the compressor was oil-cooled. This was advantageous because low vapour superheat improves the compressor efficiency (Neksa *et al*, 1999). The compressor oil was cooled in the external air-cooled coil with a surface area of approximately 0.75 m^2. The minimum oil return temperature was 30°C; a maximum return temperature was not given by the manufacturer.

Table 4.15: Expected compressor performance data at the various design operating conditions

Operating condition	Extreme winter condition	Design condition	Extreme summer condition
Pressure ratio [-]	3.6	2.9	2.0
Compressor suction pressure [bar.g]	27.2	33.8	50.0
Compressor discharge pressure [bar.g]		100.0	
Compressor motor power consumption [kW]	2.0	2.1	1.9
Compressor heat losses [W]	400	360	230
Volumetric efficiency [-]	0.67	0.75	0.88
Isentropic efficiency [-]	0.66	0.70	0.78
Indicated isentropic efficiency [-]	0.82	0.85	0.88
Suction temperature [°C]	-2.6	5.0	23.3
Discharge temperature [°C]	106	94	72
Volumetric flow rate at suction density [m^3/h]	1.1	1.3	1.5
CO_2 flow rate [kg/h]	82	116	240
Oil leakage rate [w/w-%]		unknown	

Compressor oil discharge rate data were not available. The oil level in the crankcase was controlled visually at the oil sight glass. Due to the high solubility of carbon dioxide in the oil, the compressor was supplied with a crankcase heater, which boiled the carbon dioxide off in the oil sump.

To reduce the compressor load at the start-up, the compressor suction and discharge were connected with a by-pass, which was controlled by a manual needle valve.

4.5.8 Compressor oil and oil recovery

The functions of the oil in the compressor were:

- lubrication and cooling of moving compressor parts
- sealing of the pistons and cooling of the compressor motor

The function of the oil recovery system was to return the oil, which was carried over in the refrigerant system and accumulated in the LPR back into the compressor.

The compressor was supplied with Polyolester oil (POE) with a viscosity class of 100 cST. General properties data are shown in Table 4.16, however, specific data of the oil at heat pump operation conditions were not available.

Table 4.16: Compressor oil data

Type	Emkakare RL 100S
Viscosity at 40 / 100°C	98.8 / 12.5 kg/ms
Density at 20°C	974 kg/m^3

For the oil recovery the miscibility and solubility behaviour of the oil in carbon dioxide was important. Some data were available for POE oils of the viscosity class 68, 108 and 220 cST (Fahl, 1998; Hauk *et al*, 2001). Figure 4.13 shows the miscibility behaviour of a POE 108cST.

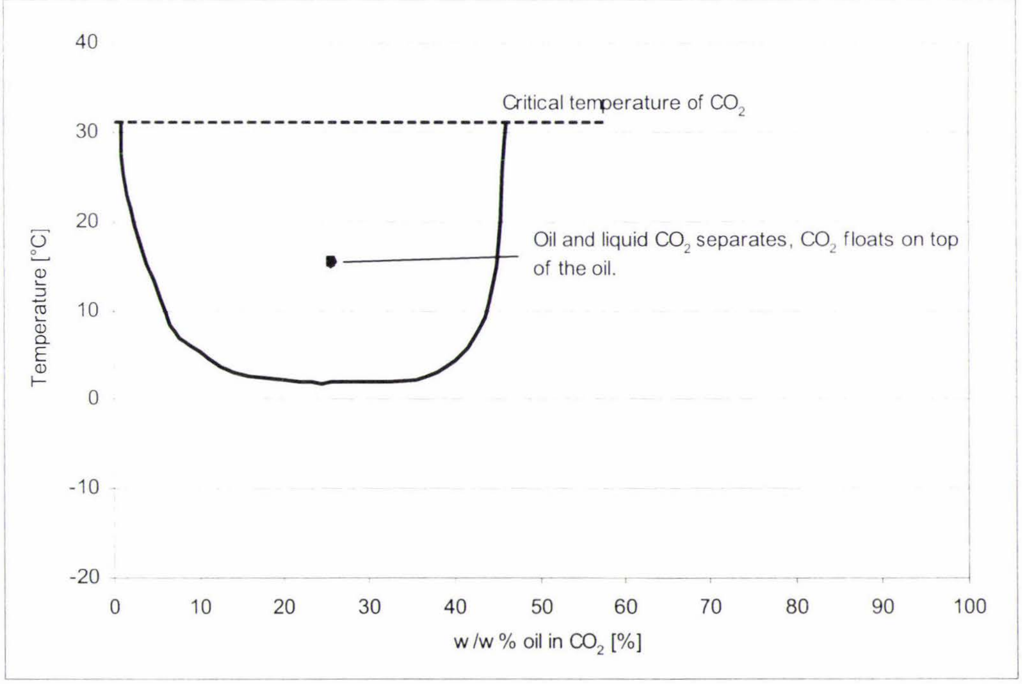

Figure 4.13: Compressor oil and refrigerant miscibility behaviour between -15°C and 31°C.

From the data it was expected that the oil used would remain miscible (oil does not separate) at:

- every concentration when the temperatures is below approximately 3°C
- concentrations higher than 50% w/w oil in CO_2

In conclusion, it was assumed that the oil would not separate at all operating condition and oil-CO_2 concentrations. To guarantee sufficient oil return to the compressor, the oil-CO_2 mixture or oil only was recovered from the bottom of the LPR through a manual needle valve (as specified in Table 4.18) to the compressor suction. To boil any liquid refrigerant off, the mixture was drained (by gravity) through a 2 m long recovery line, made of a ¼" (6.35 mm) copper tube.

4.5.9 Pipe work

Tubes and fittings

The tubes and fittings connect the components of the heat pump. Key design features were low pressure drop but a sufficient velocity (5 to 15 m/s for the tubes where the oil had to be carried over) to overcome the oil dragging force and ensure oil did not accumulate. The gas velocity was not considered critical due to the high solubility of the oil in the supercritical CO_2. Stainless steel tubes and fittings were selected to avoid corrosion.

Table 4.17 summarises the tube dimensions, and the expected gas velocity and pressure drop at the design discharge pressure for the range of operating conditions and the corresponding mass flowrates. The pressure drop of the gaseous refrigerant in the line between the evaporator and the LPR (assuming no liquid) was predicted using the Darcy-Weissbach equation (ASHRAE, 2001) and friction factors for smooth tubes.

Table 4.17: Tube specifications design conditions

Location of tube	Inner tube diameter [mm]	Tube length [m]	Gas velocity [m/s]	Pressure drop [bar]
Compressor to GC	10.6	1.5	1.4 - 3.2	0.01 - 0.02
Gas cooler to IHX	4.6	1.0	1.6 - 5.4	0.05 - 0.34
IHX to BPR	4.6	1.0	1.4 - 4.9	0.03 - 0.24
Evaporator to LPR	10.6	1.0	3.4 - 4.1	0.01 - 0.02
LPR to Compressor	10.6	2.0	3.4 - 4.6	0.01 - 0.04

Swagelok tubes and fittings were used. The fittings were sealed with thread sealer (Loctite 542), however the thread sealer was later replaced wherever possible by Teflon sealing tape due to leakage problems (as described in section 7.1).

Valves

The valves as specified in Table 4.18 were used to connect measurement devices and to allow the connection of the refrigerant charging equipment such as a CO_2 pressure bottle and a vacuum pump (The full piping and instrumentation diagram is shown in Figure 4.14). Further needle valves were used to control the oil recovery, the refrigerant charging and the compressor by-pass line. A 3-way valve was installed to allow the internal heat exchanger to be bypassed if required and a non-return valve (check valve) was used for the CO_2 pressure bottle.

Table 4.18: Refrigerant valve specifications

Ball-valves	
Model	Swagelok-SS-42S4
Operating pressure (max.)	172 bar.a
Operating temperature	10 to 65°C
Orifice size	3.2 mm
Needle valves	
Model	Swagelok-SS-1RS4
Operating pressure (max.)	266 bar.a
Operating temperature	-53 to 148°C
Orifice size	4.4 mm
3-way valve	
Model	Swagelok-SS-43XF4
Operating pressure (max.)	172 bar.a
Operating temperature	10 to 65°C
Orifice size	4.8 mm
Check valve	
Model	Swagelok-SS-4C410
Operating pressure (max)	3000 psi.a / 207 bar.a
Maximum back pressure	1000 psi.a / 69 bar.a
Temperature range	-23 to 191°C

4.5.10 Refrigerant charge

The refrigerant charge was predicted to provide a guideline for the refrigerant charging procedure.

The charge of all individual components at design conditions was summed for the various gas cooler arrangements. The evaporator was assumed to contain 1/3 liquid and 2/3 gaseous refrigerant by volume. The inner volume of the compressor was unknown and was neglected in the calculations. Table 4.19 summarises the expected refrigerant in the high- and low-pressure side of the refrigerant cycle at design conditions.

Table 4.19: Volume and refrigerant charge of the low- and high-pressure side of the system at design conditions.

GC configuration	GC1	GC2.1	GC2.2	GC3.1	GC3.2
Volume high pressure side [cm^3]	938	1102	784	1477	1477
CO_2 mass high pressure side [kg]	0.34	0.37	0.29	0.67	0.81
Volume low pressure side [cm^3]	2307				
CO_2 mass low pressure side [kg]	0.485				
Total volume [cm^3]	3245	3409	3091	3784	3784
Total mass of refrigeration [kg]	0.82	0.86	0.77	1.15	1.29

The refrigerant was charged with liquid carbon dioxide out of a standard CO_2 pressure bottle. The pressure bottle was directly connected to the system without using a pressure reducer. A manual needle valve (as specified in Table 4.18) was used to control the mass flowrate; additionally a non-return valve (as specified in Table 4.18) protected the gas bottle from compressor oil and high pressures.

4.5.11 Safety devices

The following safety devices were used to both protect the refrigeration equipment and for personal safety.

Refrigerant relief valves

Spring-loaded pressure relief valves protected the refrigeration system from pressure above the maximum operating pressure. The valves were installed in the high and low-pressure sides of the refrigerant cycle (Table 4.20). The relief valve in high-pressure side releases refrigerant at pressures above 150 bar.a to the low-pressure side. The valve in the low-pressure side was set to 100 bar.a pressure and releases the refrigerant to the atmosphere. The relief valves were calibrated and certified by the supplier.

Table 4.20: Relief valve specifications

Model	Swagelok SS-4R3
Release pressure discharge side	150 bar.a
Release pressure suction side	100 bar.a
Actuator type	Spring loaded

Compressor discharge non-return valve

A non return valve protected the compressor from liquid refrigerant in the discharge line. Table 4.21 describes the check valve used, which acted as a non-return valve.

Table 4.21: Compressor discharge non-return valve specifications

Model	Lift-check valve Swagelok-SS-53S4
Maximal operation pressure	413 bar.a
Operating temperature	-53 to 482°C
Orifice size	4 mm

Compressor temperature switch

A temperature-switch protected the compressor motor from overheating by cutting the main compressor power supply. The compressor had to be manually reset after such a trip.

Fusible plugs

Fusible plugs (Swagelok SS-400-1-4) were used to prevent unintentional release of refrigerant by accidental opening of the ball valves when the valves where not connected to pressure measurement equipment or the refrigerant charging line.

4.5.12 Control of the HWSS

The system was controlled to obtain reproducible operating conditions. The water mass flowrate which was drawn off the HWC was controlled by a tap (C1, Figure 4.14). The heat pump operating conditions were set by four control parameters, as follows:

- Refrigerant evaporation temperature and pressure

The evaporating conditions were controlled based on the measured CO_2 evaporating temperature rather than by the suction pressure (P2, Figure 4.14) because of uncertainties with the pressure readings (as described in section 4.5.13.2). The evaporating temperature was adjusted by controlling the evaporator water inlet temperature and/or the water mass flowrate using a valve system at the evaporator inlet (C2, Figure 4.14).

- Discharge pressure

The discharge pressure was set using the manual BPR valve (HP5, Figure 4.14).

- Gas cooler water inlet temperature

The water temperature at the gas cooler inlet was controlled (when water was not circulated from the HWC) by a valve system at the gas cooler inlet (C4, Figure 4.14), where cold and warm water from an external supply where mixed to achieve the desired gas cooler water inlet temperature.

- Hot water outlet temperature at the gas cooler outlet

The hot water temperature was set using the water-flow control valve (C5, Figure 4.14).

Table 4.22 summarises the ranges and the expected control precision of the HWSS control parameters.

Table 4.22: Heat pump control parameters

Parameter	Control range of parameter	Precision of the HWSS control parameters
HWC water outlet flowrate	0 - 10 l/min	-
Evaporation pressure	33.9 - 49.8 bar.g	±1.4 - ±1.8 bar
Evaporation temperature	0 - 15°C	±1.5 K
Discharge pressure	90 - 130 bar.g	±1.5 bar
Hot water temperature	40 - 60 °C	±2.0 K
GC water inlet temperature	15 - 35 °C	±2.0 K

4.5.13 Measurement system and data acquisition

Figure 4.14 shows all the measurement instrumentation.

4.5.13.1 Temperature

Refrigerant and water temperatures through the system were measured with thermocouples (T1-T24, Figure 4.14). The thermocouples were connected to aluminium wells, which were mounted onto the outside of the refrigerant and water tubes and the outside of the HWC respectively. To achieve good heat contact, heat conducting paste was applied between the ports and the tubes, and most of the measurement points were covered with insulation.

Two dataloggers with each 8 channels, a PC computer (Win95) and datalogger-software (PicoLog R5.06.3, Pico Technology Ltd) were used to monitor the temperatures.

Calibration of the thermocouples was performed using ice-water and boiling water as reference points to evaluate the temperature offset and scaling factors. However, the temperature readings of the thermocouples at the two reference points were always within ± 0.3 K so no adjustments were necessary.

Table 4.23 summarises the specifications of the thermocouples and the datalogger.

Table 4.23: Thermocouple and datalogging specifications

Thermocouples	
Type	T
Temperature range	-210 to 1370 °C
Measurement accuracy (-20 to 1150°C)	±0.025 K
Datalogger	
Model	Picolog TC-08
Channels	8
Bus	8 bit
Measurement accuracy (not calibrated)	±0.5 K
Software	Picolog for win95

4.5.13.2 Pressure

Pressure gauges with visual analog displays were used to measure the pressures in the refrigerant system (Table 4.24). The pressure gauges at the compressor suction and discharge were installed permanently (P1 to P4, Figure 4.14). An additional pressure gauge was used to measure the pressures in other locations around the refrigerant system. For safety reasons the latter gauge was not moved while the heat pump was operating.

The pressure gauges were calibrated by the manufacturer as described in Table 4.24. The three pressure gauges used for the refrigerant pressure measurements (P1, P2 and P4, Figure 4.14) agreed within the precision of the pressure gauges when measuring the pressure of the equilibrated system.

Table 4.24: Pressure gauges specifications

Permanent gauge at the compressor discharge and movable gauge	
Model	Buchanan 1122
Pressure range	0-160 bar.g
Accuracy	1.5 % full scale (min. 2.4 bar)
Permanent gauge at the compressor suction and crankcase (oil pressure)	
Model	Buchanan 1122
Pressure range	0-100 bar.g
Maximum accuracy	1.5 % full scale (min. 1.5 bar)

The pressure readings on the display of the pressure gauge at the compressor suction were difficult to read due to pressure fluctuations and vibrations (which occurred despite a coil shaped tube of about 0.8 meter tube length between the refrigerant system and the pressure gauge). The average deviation of the measured suction pressure and the pressure back-calculated from the CO_2 evaporation temperature readings was 0.3±0.8 bar, which was within the data uncertainty of the measurement devices.

4.5.13.3 Flowrates

The refrigerant mass flow rate was not measured directly because of the measurement difficulties in the supercritical region and the unavailability of a suitable flowmeter.

The water flowrates through the gas cooler and the HWC respectively were measured either manually, using a stopwatch, a scale and a bucket or by a magnetic type flowmeter (Table 4.25). The flowmeter was insensitive to rapid changes in the flow so the device was only used to measure the water flowrate through the gas cooler when the HWC was in use.

The water flowrate through the evaporator was measured manually with a stop watch and a bucket. The accuracy was expected to be within 5% of the actual flow.

The flowmeter was calibrated by the manufacturer but the flowmeter readings were checked using the bucket and stopwatch method. The difference in the measured flowrate was less than 0.1 l/min at a flowrate of 1.8 l/min.

Table 4.25: Water flowmeter specifications

Model	ADMAG-AM100A (Yokogawa)
Nominal size	25 mm
Measuring span (min/max)	0 - 0.54 m^3/h / 0 - 17.6 m^3/h
Operating temperature	-30 to 60°C
Set flow-span	0 - 6.0 l/min
Accuracy within flow span	0.25% of span (0.015 l/min)

4.5.13.4 Compressor power consumption

The compressor power consumption was measured with an energy analyser (Table 4.26), which measured the current, voltage and phase angle and displayed the power consumption. The current and the power phase angle were measured inductively using ampere clamps and the voltage was measured directly at the poles of the motor.

The energy analyser was calibrated by the manufacturer who quoted a precision of the electric power measurements better than 5% of the actual load.

Table 4.26: Energy analyser specifications

Model	Microvip 3 (Elcontrol)
Power supply	120 V, 60Hz
Measurements range with used clamp meters	0 - 750 Vrms / 0.05-1000A, 48 - 1000 Hz
Measurement frequency	1.2 seconds
Precision of voltage and current measurement	0.3% full scale + 0.3% load.
Precision of clamp	±0.8% load ± 0.05A; phase angle error: 60'
Measurement accuracy of the power consumption	<5% load

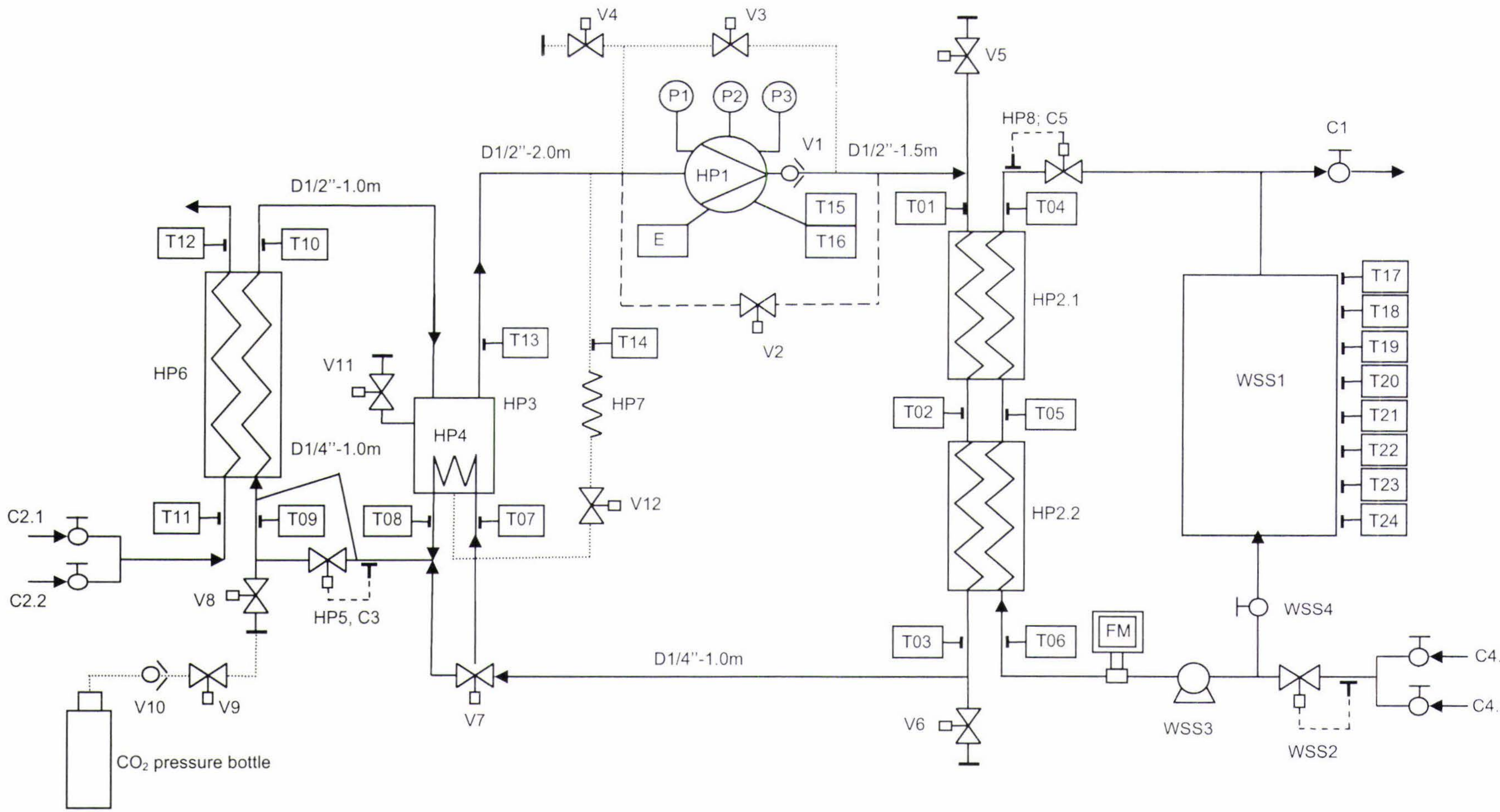

Figure 4.14: Piping and instrumentation diagram for the heat pump and the HWSS (Table 4.26 gives the code description).

Table 4.27: Piping and instrumentation of the heat pump and the HWC

Water supply system (WSS) components			
WSS1	Hot water cylinder (HWC)	WSS3	Water pump
WSS2	Main water supply pressure reducer	WSS4	HWC shut off valve
Heat pump (HP) components			
HP1	Compressor	HP5	Expansion valve (BPR)
HP2.1	1st gas cooler (GC)	HP6	Evaporator (E)
HP2.2	2nd Gas cooler (GC)	HP7	Oil return coil
HP3	Low pressure receiver (LPR)	HP8	Water flow control valve
HP4	Internal heat exchanger (IHX)		
Refrigerant valves			
V1	Non-return lift check valve	V7	3-way valve
V2	Compressor by-pass needle valve	V8	Refrigerant charging ball valve
V3	Pressure relief valve high-pressure side	V9	CO_2 charging needle valve
V4	Pressure relief valve low -pressure side	V10	Pressure bottle non-return check valve
V5	Ball valve (port for pressure gauge)	V11	Ball valve (port for pressure gauge)
V6	Ball valve (port for pressure gauge)	V12	Oil return needle valve
Heat pump control			
C1	HWC water flowrate control valve	C4.1	GC water inlet temperature cold water control valve
C2.1	Evaporator cold water control valve	C4.2	GC water inlet temperature hot water control valve
C2.2	Evaporator temperature hot water control valve	C5	GC hot water outlet temperature control valve
C3	Discharge pressure control		
Measurement system			
T1-16	Thermocouples HP	P1	Pressure gauge CO_2 high-pressure side
T17-24	Thermocouples HWC	P2	Pressure gauge CO_2 low-pressure side
FM	Water flow meter	P3	Pressure gauge oil pressure
E	Energy analyser	P4	Additional pressure gauge

5 Experimental Procedure

5.1 Commissioning

The heat pump was fully commissioned before carrying out the performance tests as described below. The commissioning procedure was repeated after every change in the heat pump equipment configuration.

5.1.1 Leak testing

The refrigerant system was flushed with carbon dioxide to remove air and dirt from the pipe system. Afterwards the refrigerant system was charged to 5 bar.g pressure and the pipe connections (fittings) were checked for gas tightness with soapy water. After the sealing procedure, the system was evacuated with a vacuum pump to remove remaining air for approximately 1 hour.

Once the heat pump was fully charged (see below), the gas tightness checking procedure was repeated. The refrigerant system was then pressure tested up to 130 bar.g (high-side) and 50 bar.g (low-side).

5.1.2 Refrigerant charging

The heat pump was charged with liquid carbon dioxide from a 6.8 kg pressure bottle, which was connected to the low pressure-side of the refrigerant system (Figure 4.14). The charge was continually measured by weighting the carbon dioxide pressure bottle with an electronic scale.

The refrigerant charging procedure consisted of the following steps:

1. Fully close the refrigerant expansion valve (BPR, HP5 in Figure 4.14).
2. Open the refrigerant charging port (V8, Figure 4.14) and quickly pre-charge the system to approximately 40 bar pressure by opening the refrigerant charging valve (V9, Figure 4.14).
3. Open the BPR, the compressor by-pass (V3, Figure 4.14) and the gas cooler water flow-control valve (HP8) and provide sufficient evaporator cooling water flowrate to avoid freezing.
4. Start the compressor and close the compressor by-pass.

5. Slowly close the expansion valve to give a pressure 5 bar below the desired discharge pressure while adding CO_2 until a fully flooded evaporator was obtained (the evaporator was assumed to be flooded when the temperature at the evaporator outlet approached the temperature at the evaporator inlet).
6. Adjust the hot water temperature to the desired temperature using the water flow control valve.
7. Adjust the CO_2 discharge pressure to the desired pressure and add CO_2 charge until the evaporator operated fully flooded.
8. Charge 50 to 100 g additional CO_2 to achieve the design ballast volume in the LPR.

Problems with charging occurred due to leakage of refrigerant valves, such as the 3-way valve (V7, Figure 4.14) and the ball valves at the refrigerant charge port caused by cooling and thereby shrinkage of the valve seals. Therefore, ultimately the ball valve (V8, Figure 4.14) was removed and the carbon dioxide pressure bottle was permanently connected to the charging port. Excessive cooling of the 3-way valve was prevented by quickly pre-charging the system and by fully closing the expansion valve so that no liquid carbon dioxide flowed directly to the 3-way valve.

When changes to the equipment were undertaken, the refrigerant was released through the ball valves on the LPR (V11, Figure 4.14) very slowly to avoid excessive cooling of the valve seals. The released carbon dioxide was not recovered or recycled. The laboratory was ventilated during the releasing procedure for safety reasons.

5.1.3 Heat pump start-up / shut down procedure

The measurement system, water supply system (flow from water mains and the water pump to the HWC if required), GC water and the evaporator cooling water were started first. The compressor crankcase heater was also switched on for at least 30 minutes to boil off dissolved carbon dioxide in the oil sump before starting the compressor.

The compressor was started with the compressor by-pass needle valve fully opened (V2, Figure 4.14). The valve was closed when the compressor reached normal operating speed, thereafter the compressor discharge pressure quickly rose to the desired pressure while the evaporation and suction pressures rapidly declined before slowly recovering to a steady pressure.

To shut down the heat pump, the compressor was switched off. The pressure in the system rapidly balanced through the expansion valve. The water pump to the HWC and the mains water supply were switched off immediately after the compressor.

5.1.4 Precision of the heat pump control

Table 5.1 summarises the estimated reproducibility of the heat pump operating conditions for replicate trials. These estimates include the precision of the heat pump control parameters (Table 4.22), the precision of the measurement devices (Table 4.23 to Table 4.26) and random uncertainty.

Table 5.1: Heat pump control precision

Control parameter	Precision of heat pump control	Precision of measurement device	Overall precision of the heat pump control
Gas cooler water inlet temperature	±2.0 K	±0.5K	±2.1 K
Gas cooler water inlet temperature	±2.0 K	±0.5K	±2.1 K
Discharge pressure	±1.5 bar	±1.2 bar	±1.9 bar
Evaporation temperature	±1.5 K	±0.5 K	±1.6 K
Suction Pressure*	±1.4 bar / ±1.8 bar	±0.75 bar	±1.6 bar / ±2.0 bar

* matching the temperature control error at 0°C / 15°C evaporation temperature

5.1.5 Preliminary trials

Preliminary trials were carried out to evaluate whether the heat pump operation was stable and the heat pump process behaved in the expected manner.

The trials were performed with discharge pressures between 80 and 130 bar.g and evaporation temperatures between 0 and 15°C, corresponding to a suction pressure between 33.8 and 49.8 bar.g. The hot water temperature was not controlled to 60°C in the preliminary tests.

The first tests showed that:

a) There was significant cooling of the refrigerant in the compressor resulting in compressor discharge temperatures being lower than expected even if there was isentropic compression. The extent of the cooling effect tended to be lower at decreasing pressure ratio and remained at higher suction superheat.

b) There was a significant imbalance (more than ±15%) in the overall refrigerant mass flowrate balance based on evaporator and GC energy balances.

c) There was a significant oil level fluctuation in the compressor oil sump (the oil level at the sight glass dropped approximately ½ the height at the initial start up) and significant variation of the oil level during operation at constant compressor operation conditions.

d) There was little cooling (smaller than 3 K) of the compressor oil in the compressor oil-cooling coil.

Possible explanations for these observations were:

a) Compressor mechanical problems

Problems with the valve plates of the compressor pre-series models were reported by (Neksa *et al*, 1999). However, significant refrigerant leakage in the compressor cylinder would probably result in increased compressor discharge temperature, which was not observed.

b) Liquid refrigerant in the suction line

The cooling effect could have been caused by refrigerant droplets in the suction vapour entering the compressor. This could be the case if the refrigerant system was overcharged, if the separation capacity of the LPR was limited, if oil foaming occurred and/or if turbulent flow patterns in the LPR receiver caused liquid carry over. Any such droplets were less likely to persist at superheated conditions, but the cooling effect was observed at 20 K superheat at the compressor suction so this cause was unlikely. However, liquid refrigerant carry-over could help explain the observed mass flowrate (energy) imbalance.

c) Compressor oil foaming

The compressor oil tended to foam when the dissolved carbon dioxide in the oil evaporates. In particular, this occurred at rapid changing pressures and could be observed in the oil sump sight glass of the compressor. Foaming of the accumulated oil in the LPR could increase the possibility of liquid droplets. However, the possibility of foaming in the LPR could not be observed nor measured.

d) Oil leakage and/or oil carry over from the LPR

The cooling effect could be due to excessive oil leakage from the compressor into the discharge line and/or oil carry-over from the LPR into the suction line, with the oil cooling the vapour and subsequently being re-cooled itself as it circulated with the CO_2 through the heat exchangers and accumulated in the LPR. Hubacher and Groll (2003) reported more than 14% by mass oil flowrate in the discharge from a similar compressor. It was difficult to measure if such oil leakage occurred but it would help explain some of the observed energy imbalance based on refrigerant only circulation calculations.

In conclusion, the cooling effect of the refrigerant in the compressor could not fully be explained but it was assumed that it was caused by either liquid refrigerant and/or oil droplets carry over from the LPR into the suction of the compressor and/or excessive oil carry over from the compressor.

The LPR design was improved by increasing the overall lenght of the LPR from 220 mm to 320 mm (adding ballast volume for liquid refrigerant and an additional 100 g of compressor oil, and volume for oil foaming) and modifying the refrigerant inlet pipe (the initially straight pipe was replaced with a pipe which was designed as proposed by Wiencke (2001)). Additionally the pressure measurement system was improved to achieve better control by adding refrigerant ports to the gas cooler inlet and the LPR where there was less vibration (V5 and V11, Figure 4.14).

The performance of the heat pump improved with the changed LPR. The mass flowrate imbalance significantly decreased and the compressor discharge temperature increased. However, measured volumetric and isentropic compressor efficiency and discharge temperature remained lower than expected suggesting liquid (CO_2 and/or oil) carry over might still be significant. The manufacturer could not fully explain the observed compressor performance.

To provide a baseline for the compressor performance and its potential change during further trials, the compressor performance at different loads (pressure ratios) was measured once at the beginning of the overall experimental procedure. Table 5.2 summarises the trial conditions of these reference processes.

Table 5.2: Reference process trial conditions

Condition No.	ref1	ref2	ref3
Heat pump setup	GC1, IHX on, oil return off		
Evaporating temperature	0 °C		
Suction pressure	33.9 bar.g		
Discharge pressure	90 bar.g	100 bar.g	110 bar.g
GC water inlet temperature	20 °C		
GC water outlet temperature	45 °C		

The second reference process compressor operating conditions (that is suction and discharge pressures in ref2 trial) was used to check compressor performance changes before each of the heat pump trials.

5.2 Performance trials

Experimental trials were carried out to characterise the performance and behaviour of the heat pump, the HWC system as a whole, the individual heat pump components, and to evaluate the system parameters required for the HWSS model.

The full experimental data is given in the Appendix A.3. Table 13.1 summarises the experimental trials, while Table 13.2 and Table 13.3 give the heat pump and HWC trial raw data respectively.

5.2.1 Trial conditions and experimental setup

Table 5.3 summarises the heat pump operating conditions used in the trials. They covered the full range of likely operating conditions, except ambient air temperatures below 10°C and GC water inlet temperatures below 20°C. The refrigerant evaporation conditions correspond to ambient air temperatures between 10°C and 30°C at an evaporator temperature difference of 10 to 15 K (as described in Table 4.3).

Table 5.3: Heat pump operating conditions used in the trials

Operating condition No.	GC water inlet temperature [°C]	Hot water temperature [°C]	Evaporation temperature [°C]	Suction pressure [bar.g]	Discharge pressure [bar.g]
C1	20	60	0	33.8	90
C2	25	60	0	33.8	90
C3	30	60	0	33.8	90
C4	20	60	7.5	41.3	90
C5	20	60	15	49.8	90
C6	20	60	0	33.8	95
C7	25	60	0	33.8	95
C8	30	60	0	33.8	95
C9	20	60	7.5	41.3	95
C10	20	60	15	49.8	95
C11*	20	60	0	33.8	100
C12	25	60	0	33.8	100
C13	30	60	0	33.8	100
C14	35	60	0	33.8	100
C15	20	40	0	33.8	100
C16	20	50	0	33.8	100
C17	20	60	7.5	41.3	100
C18	20	60	15	49.8	100
C19	20	60	0	33.8	105
C20	25	60	0	33.8	105
C21	30	60	0	33.8	105
C22	20	60	7.5	41.3	105
C23	20	60	15	49.8	105
C24	20	60	0	33.8	110
C25	25	60	0	33.8	110
C26	30	60	0	33.8	110
C27	20	60	7.5	41.3	110
C28	20	60	15	49.8	110
C29	20	60	15	49.8	120

* C11: Nominal heat pump operating condition. This condition was similar to the heat pump nominal design condition but with higher heat pump water inlet temperature due to the overall higher mains water temperature in the lab than the expected average mains temperature in NZ.

The heat pump and the HWC performance trials were performed with different system configurations and measurement set-ups as described in Table 5.4.

The measurement system set-up was changed during the performance trials. The pressure gauge P4 (Figure 4.14) was used to measure the pressure either after the gas cooler or after the IHX in addition to the pressure gauge (P1) at the compressor discharge. The water flowmeter was only used when the HWC performance was investigated (the hot water from the GC was supplied to the top of the HWC while cold water from the bottom of the HWC flowed to the heat pump); in all other trials the hot water mass flowrate was measured by the bucket and stopwatch method.

The heat pump always ran with the IHX operating to guarantee slight superheating of the compressor suction vapour. The oil return was closed for all experiments except when the oil recovery was being specifically investigated. The HWC was shut off during the heat pump trials (except when the oil recovery was investigated) and the heat pump was supplied with water from the mains so that the supply temperature was more constant.

Table 5.4: The experimental set-ups used for the experimental trials

<table>
<tr><td>Experimental set-up no.</td><td>S1</td><td>S2</td><td>S3</td><td>S4</td><td>S5</td><td>S6</td><td>S7</td><td>S8</td></tr>
<tr><td>Heat pump</td><td colspan="7">on</td><td>off</td></tr>
<tr><td>Gas cooler unit</td><td>GC1</td><td>GC2.1</td><td>GC2.2</td><td>GC3.1</td><td>GC3.2</td><td>GC3.1</td><td>GC3.1</td><td>GC3.1</td></tr>
<tr><td>IHX</td><td colspan="7">on</td><td>-</td></tr>
<tr><td>Oil return</td><td colspan="6">off</td><td>on</td><td>-</td></tr>
<tr><td>HWC</td><td colspan="7">off</td><td>-</td></tr>
<tr><td>Location of pressure gauge P4</td><td>GC outlet</td><td>GC outlet</td><td>GC outlet</td><td>GC outlet</td><td>GC outlet</td><td>IHX outlet</td><td>IHX outlet</td><td>-</td></tr>
<tr><td>Measurement method of hot water flowrate</td><td colspan="6">Bucket and stopwatch</td><td>Flow meter</td><td>-</td></tr>
</table>

5.2.2 Heat pump trials

The objective of these trials was to evaluate the overall heat pump performance and the performance of the individual heat pump components. During the heat pump performance trials, the heat pump was progressively improved by changing the heat pump configuration and/or the heat pump process based on the outcomes of the individual performance trials. The aim was to maximize heat pump efficiency. Four set of trials were undertaken:

1. Gas cooler trials

These trials measured the performance of the various gas coolers configurations (GC 1, GC 2.1, GC 2.2, GC 3.1 and GC 3.2) so that maximum gas cooler capacity could be achieved. Table 5.5 summarises the trial objectives and conditions.

Table 5.5: Gas cooler performance trial objectives, heat pump operating conditions and experimental set-ups

Trial name	Objectives	Operating condition no.	Experimental set-up no.
GC1	Investigate: GC heat transfer performance Refrigerant-side pressure drop	C1, C11, C12, C13, C17, C18, C24, C29	S1
GC2.1			S2
GC2.2			S3
GC3.1		C1, C11, C12, C13, C17, C18, C24	S4
GC3.2			S5

2. Compressor trials

Uncertainties about the compressor performance during the gas cooler trials lead to individual compressor performance trials. The main objective of these trials was to evaluate the compressor performance reproducibility and the effect of compressor operating temperature, oil temperature and the oil level on the overall compressor performance. Table 5.6 summarises the trial conditions.

Table 5.6: Compressor performance trial objectives, heat pump operating conditions and experimental set-up

<table>
<tr><th>Trial name</th><th>Objectives</th><th>Operating condition No.</th><th>Experimental set-up no.</th></tr>
<tr><td>comp 1</td><td rowspan="3">Investigate:
reproducibility of compressor performance
effect of the compressor body and oil temperature on the overall performance
effect of the oil level on the compressor performance
oil leakage rate</td><td rowspan="4">C11</td><td rowspan="4">S6</td></tr>
<tr><td>comp 2</td></tr>
<tr><td>comp 3</td></tr>
<tr><td>comp 4</td><td>Investigate the effect of the compressor body cooling on the compressor performance</td></tr>
</table>

3. Heat pump performance trials

These trials measured the overall performance of the heat pump (COP) as well as the performance of the individual heat pump components and aimed to improve the process control strategy (discharge pressure control) so that maximum energy efficiency was achieved. Table 5.7 summarises the conditions used for the overall heat pump performance trials.

Table 5.7: Heat pump performance trial objectives, heat pump operating conditions and experimental set-up

<table>
<tr><th>Trial name</th><th>Objectives</th><th>Operating condition No.</th><th>Experimental set-up no.</th></tr>
<tr><td>HP90</td><td rowspan="5">Investigate:
Heat pump COP
Improve discharge pressure control to maximum heat pump COP</td><td>C1 to C5</td><td rowspan="5">S6</td></tr>
<tr><td>HP95</td><td>C5 to C10</td></tr>
<tr><td>HP100</td><td>C11 to C13;C17,C18</td></tr>
<tr><td>HP105</td><td>C19 to C23</td></tr>
<tr><td>HP110</td><td>C23 to C28</td></tr>
</table>

4. CO_2 charge trials

These trials evaluated the required refrigerant charge (for S6, the final system configuration) to obtain an optimally charged system at all operation conditions. Table 5.8 summarises the trial conditions.

Table 5.8: Refrigerant charge trial objectives, heat pump operating conditions and experimental set-up

Trial name	Objectives	CO_2 charge	Operating condition No.	Experimental set-up no.
CO2-charge1	Evaluate required CO_2 charge Investigate LPR volumetric capacity	1.685 kg	C19 to C23	S6
CO2-charge2		1.760 kg		
CO2-charge3		1.815 kg		
CO2-charge4		1.915 kg		

5.2.3 Hot water cylinder (HWC) trials

The objectives of the HWC trials was the measurement of the performance of the hot water cylinder, such as the heat standing losses, the heat distribution (thermocline) in the HWC, and the water temperature at the HWC bottom outlet (heat pump inlet). The experimental data was used to evaluate the HWSS model parameters, particularly the overall heat transfer coefficient U_{HWC} and the effective thermal conductivity λ_{HWC}.

Three sets of trials were carried out:

1. Heating trial

The temperature distribution in the HWC was measured while heating the water by the heat pump starting with the tank at mains water temperature. The trial was performed with the final heat pump configuration. Table 5.9 summarises the trial experimental set-up:

Table 5.9: HWC heating trial objectives, heat pump operating conditions and experimental set-up

Trial name	Objectives	Initial heat pump operating condition No.	Experimental set-up no.
heating	Investigate HWC temperature distribution during heating	C19	S7

2. Cooling trial

The temperature distribution of the water in the HWC was measured while drawing hot water from the top and supplying cold water make-up from the bottom. The water was withdrawn for different periods and at varying flowrate, starting with a fully recovered (heated) HWC. The heat pump was switched off in this trial. Table 5.10 summarises the experimental set-up.

Table 5.10: HWC cooling trial objectives, heat pump operating conditions and experimental set-up

Trial name	Objectives	Period No. [-]	Time [min]	Mass flowrate [l/min]	Experimental set-up no.
Cooling	Measure temperature distribution of the water in the HWC during withdrawal periods	1	0:00 - 0:02	2.9 (m1)	S8
		2	0:20 - 0:22	2.9 (m2)	
		3	0:37 - 0:39	3.0 (m3)	
		4	1: 10 - 1:12	4.6 (m4)	
		5	1:45 - 1:47	4.6 (m5)	
		6	2:48 - 2:52	7.5 (m6)	
		7	3:50 - 3:54	7.5 (m7)	

3. Standing losses

The objective of these trials was to measure the HWC standing heat losses when there was no water flow through the HWC. Table 5.11 summarises the conditions used.

Table 5.11: HWC standing losses trial objectives, heat pump operating conditions and experimental set-up

Trial name	Objectives	Initial HWC conditions	Experimental set-up
Heat-loss1	Evaluate HWC standing losses	Fully mixed HWC at 55°C	S8
Heat-loss2		Stratified HWC with 55°C on the top and 18°C at the bottom	

5.2.4 Trial order

At the beginning of each trial the heat pump was run at the nominal heat pump operating conditions (C11) to check whether the heat pump operation was stable and whether the expected components performance (in particular, the compressor discharge temperature of the ref2 trial) was achieved.

Due to limitations in the heat pump controls and heat pump operational problems the order of the trials could not be fully randomised. Table 13.1 and Table 13.2 give the trials listed in chronological order.

5.3 Data analysis

The following summarises the data analysis undertaken for the trials.

5.3.1 Thermodynamic properties of water and CO_2

The water and CO_2 properties were electronically available from the software Coolpack V1.46 (Department of Mechanical Engineering, Technical University of Denmark). Literature values were used (as described in section 4.2.2.1) for the viscosity and the thermal conductivity of supercritical CO_2 (Vesovic *et al*, 1990; Fenghour and Wakeham, 1998).

5.3.2 Gas cooler (GC)

Heat transfer rate

The heat transfer rate for the gas cooler units was calculated from the water-side energy balance:

$$\phi_{GC} = \phi_{W,GC} = m_{W,GC}\, c_W \left(T_{W,GC\_out} - T_{W,GC\_in}\right) \qquad \text{Equ. 5.1}$$

The refrigerant-side energy balance is:

$$\phi_{CO2,GC} = m_{CO2,GC} \left(h_{CO2,GC\_in} - h_{CO2,GC\_out}\right) \qquad \text{Equ. 5.2}$$

Where:

ϕ_{GC}	Heat transfer rate for the gas cooler [W]
$\phi_{W,GC}$	Rate of heat gain by the water in the gas cooler [W]
$\phi_{CO2,GC}$	Rate of heat rejection by the CO_2 in the gas cooler [W]
$m_{W,GC}$	Water mass flowrate in the gas cooler [kg/s]
$m_{CO2,GC}$	Refrigerant mass flowrate in the gas cooler [kg/s]
c_W	Specific heat capacity of water [J/kgK]
T_{W,GC_in}	Water temperature at the gas cooler inlet [°C]
T_{W,GC_out}	Water temperature at the gas cooler outlet [°C]

$h_{CO2,\ GC\_in}$ Enthalpy of the refrigerant at the gas cooler inlet [J/kg]

$h_{CO2,\ GC\_out}$ Enthalpy of the refrigerant at the gas cooler outlet [J/kg]

Refrigerant mass flowrate

The refrigerant mass flowrate for the gas cooler (single units and two units in series) was back-calculated from the overall heat balance:

$$m_{CO2,GC} = \frac{\phi_{GC}}{h_{CO2,GC\_in} - h_{CO2,GC\_out}} \qquad \text{Equ. 5.3}$$

CO_2 enthalpies were calculated from measurements of pressure and temperatures at the relevant positions in the refrigerant cycle.

Gas cooler 3.1 and 3.2

The energy balance of the gas cooler configuration with two units in series was calculated for each of the two gas coolers separately.

$$\phi_{GC} = \phi_{GC-1st} + \phi_{GC-2nd} \qquad \text{Equ. 5.4}$$

$$m_{CO2,GC} = \frac{m_{CO2,GC-1st} + m_{CO2,GC-2nd}}{2} \qquad \text{Equ. 5.5}$$

with:

$$\phi_{GC-1st} = m_{W,GC}\ c_W\ \left(T_{W,GC\_in} - T_{W,GC\_centre}\right) \qquad \text{Equ. 5.6}$$

$$m_{CO2,GC-1st} = \frac{\phi_{GC-1st}}{h_{CO2,GC\_in} - h_{CO2,GC\_centre}} \qquad \text{Equ. 5.7}$$

and:

$$\phi_{GC-2nd} = m_{W,GC}\ c_W\ \left(T_{W,GC\_centre} - T_{W,GC\_out}\right) \qquad \text{Equ. 5.8}$$

$$m_{CO2,GC-2nd} = \frac{\phi_{GC-2nd}}{h_{CO2,\ GC\_centre} - h_{CO2,\ GC\_out}} \qquad \text{Equ. 5.9}$$

Where:

$\phi_{GC\text{-}1st}$	Heat transfer rate for the first gas cooler unit [W]
$\phi_{GC\text{-}2nd}$	Heat transfer rate for the second gas cooler unit [W]
$m_{CO2,\ GC\text{-}1st}$	Refrigerant mass flowrate back-calculated from the heat balance of the first GC [kg/s]
$m_{CO2,\ GC\text{-}2nd}$	Refrigerant mass flowrate back-calculated from the heat balance of the second GC [kg/s]
$T_{W,\ GC\_centre}$	Water temperature between the first and the second gas cooler unit [°C]
$h_{CO2,\ GC\_centre}$	Enthalpy of the refrigerant between the first and the second gas cooler unit [J/kg]

Heat transfer coefficients

The overall heat transfer coefficient U was calculated using the segmented gas cooler temperature model (as described in section A.2.2) and the overall heat balance for the gas cooler:

$$\phi_{GC} = \sum_{1}^{n} \phi_{GC,n} = \sum_{1}^{n} \left(UA_{GC,n}\ LMTD_{GC,n} \right) \qquad \text{Equ. 5.10}$$

Solving for the overall U value (based on the mean heat transfer surface):

$$U_{GC} = \frac{\sum_{1}^{n} UA_{GC,n}}{A_{mean,\,GC}} = \frac{1}{A_{mean,\,GC}} \sum_{1}^{n} \frac{\phi_{GC,n}}{LMTD_{GC,n}} \qquad \text{Equ. 5.11}$$

Where:

U_{GC}	Overall U value of the gas cooler, based on the mean heat transfer surface area [W/m²K]
$\phi_{GC,\ n}$	Heat transfer rate of the n^{th} gas cooler segment [W]
$LMTD_{GC,n}$	Log mean temperature difference of the n^{th} gas cooler segment [K]
$A_{mean,\ GC}$	Mean heat transfer surface of the gas cooler [m²]
$A_{mean,\ GC,\ n}$	Mean heat transfer surface of the n^{th} segment of the gas cooler [m²]

The water side heat transfer coefficient ($h_{W,GC}$) was calculated using the McAdams correlation (ASHRAE, 2001) with water properties based on the mean bulk temperature. Hence the refrigerant side heat transfer coefficient was back-calculated from the equation for the overall heat transfer resistance:

$$\frac{1}{U_{GC}\ f_{vent}\ A_{mean,GC}} = \frac{1}{h_{CO2,GC}\ A_{CO2,GC}} + \frac{\dfrac{r_{i,GC}\ ln\left(r_{o,GC}/r_{i,GC}\right)}{\lambda_{tube}}}{A_{mean,GC}} + \frac{1}{h_{W,GC}\ A_{W,GC}} \quad \text{Equ. 5.12}$$

Solving for the CO_2-side heat transfer coefficient gives:

$$h_{CO2,GC} = \frac{1}{\left(\dfrac{1}{U_{GC}\ f_{vent}\ A_{mean,GC}} - \dfrac{r_{i,GC}\ ln\left(r_{o,GC}/r_{i,GC}\right)}{A_{mean,GC}\ \lambda_{tube}} - \dfrac{1}{h_{W,GC}\ A_{W,GC}}\right) A_{CO2,GC}} \quad \text{Equ. 5.13}$$

Where:

$h_{CO2,GC}$	Refrigerant-side heat transfer coefficient [W/m^{2}K]
$h_{W,GC}$	Water-side heat transfer coefficient [W/m^{2}K]
$A_{CO2,GC}$	Heat transfer surface area of the refrigerant-side [m^2]
$A_{W,GC}$	Heat transfer surface at the water-side [m^2]
$r_{i,GC}$	Radius of the inner tube [m]
$r_{o,GC}$	Radius of the inner tube of the annulus [m]
λ_{tube}	Thermal conductivity of the tube [W/mK]
f_{vent}	Overall heat transfer reduction factor due to the vented GC design [-]

Gas cooler effectiveness

The gas cooler effectiveness was calculated by:

$$\varepsilon_{GC} = \frac{T_{CO2,GC\_in} - T_{CO2,GC\_out}}{T_{CO2,GC\_in} - T_{W,GC\_in}} \quad \text{Equ. 5.14}$$

Where:

ε_{GC}	Gas cooler effectiveness [-]
T_{CO2,GC_in}	Refrigerant temperature at the gas cooler inlet [°C]
T_{CO2,GC_out}	Refrigerant temperature at the gas cooler outlet [°C]

If the gas coolers were in series then equivalent calculations were also performed for each unit.

5.3.3 Internal heat exchanger (IHX)

Heat transfer rate

The heat transfer rate was calculated from the high pressure refrigerant side properties entering and leaving the IHX and the mean refrigerant mass flowrate:

$$\phi_{IHX} = m_{CO2}\left(h_{CO2,IHX\_in} - h_{CO2,IHX\_out}\right) \qquad \text{Equ. 5.15}$$

Where:

ϕ_{IHX}	Heat transfer rate for the IHX [W]
m_{CO2}	Mean CO_2 mass flowrate [kg/s]
h_{CO2,IHX_in}	Enthalpy of carbon dioxide at the IHX inlet [J/kg]
h_{CO2,IHX_out}	Enthalpy of carbon dioxide at the IHX outlet [J/kg]

Low-pressure refrigerant calculations could not be done because the refrigerant inlet condition (quality) to the IHX (inside the LPR) was not known.

Heat transfer coefficient

The heat transfer rate based on the outer heat transfer surface area (low-pressure side) of the IHX was given by:

$$\phi_{IHX} = U_{IHX}\; A_{O,IHX}\; LMTD_{IHX} \qquad \text{Equ. 5.16}$$

Hence the overall heat transfer coefficient for the IHW was estimated using:

$$U_{IHX} = \frac{\phi_{IHX}}{A_{O,IHX}\; LMTD_{IHX}} \qquad \text{Equ. 5.17}$$

The temperature profile of the IHX was unknown because the liquid level in the LPR was not measured so a simplified approach for the LMTD was applied. It was assumed that the IHX operates as counter-current heat exchanger:

$$LMTD_{IHX} = \frac{\left(T_{CO2,IHX\_in} - T_{CO2,LPR\_out}\right) - \left(T_{CO2,IHX\_out} - T_{CO2,LPR\_in}\right)}{ln\left(\dfrac{T_{CO2,IHX\_in} - T_{CO2,LPR\_out}}{T_{CO2,IHX\_out} - T_{CO2,LPR\_in}}\right)} \qquad \text{Equ. 5.18}$$

Note that for a flooded evaporator it follows that:

$$T_{CO2,LPR\_in} = T_{CO2,E} \qquad \text{Equ. 5.19}$$

Where:

U_{IHX}	Overall IHX heat transfer coefficient [W/m^{2}K]
$A_{O,IHX}$	Heat transfer surface outer of the IHX [m^2]
$LMTD_{IHX}$	Approached LMTD of the IHX [K]
T_{CO2,IHX_in}	High-side refrigerant temperature at the IHX inlet [°C]
T_{CO2,IHX_out}	High-side refrigerant temperature at the IHX outlet [°C]
T_{CO2,LPR_in}	Refrigerant temperature at the LPR inlet [°C]
T_{CO2,LPR_out}	Refrigerant temperature at the LPR outlet [°C]
$T_{CO2,E}$	Refrigerant evaporation temperature [°C]

IHX effectiveness

The heat transfer in the IHX was also described by the heat exchanger effectiveness (ASHRAE, 2001):

$$\varepsilon_{IHX} = \frac{T_{CO2\,IHX\_in} - T_{CO2,IHX\_out}}{T_{CO2\,IHX\_in} - T_{CO2,LPR\_in}} \qquad \text{Equ. 5.20}$$

Where:

ε_{IHX} IHX effectiveness [-]

5.3.4 Evaporator

Heat transfer rate

The heat transferred in the evaporator was calculated from the water-side measurements:

$$\phi_E = \phi_{W,E} = m_{W,E}\; c_W \left(T_{W,E\_out} - T_{W,E\_in}\right) \qquad \text{Equ. 5.21}$$

Where:

ϕ_E	Heat transfer rate in the evaporator [W]
$\phi_{W,E}$	Heat transfer rate rejected by the evaporator water [W]
$m_{W,E}$	Water mass flow rate in the evaporator [kg/s]

c_W	Specific heat of water [J/kgK]
T_{W,E_in}	Water temperature at the evaporator inlet [°C]
T_{W,E_out}	Water temperature at the evaporator outlet [°C]

Evaporator refrigerant mass flowrate

To calculate the refrigerant evaporator mass flowrate, the heat balance for the whole low pressure side was used because the exact refrigerant properties (in particular the vapour fraction) at the outlet of the flooded evaporator were unknown. Between the expansion valve and the compressor suction, the low pressure CO_2 absorbs heat from both the water in the evaporator and the high pressure CO_2 in the IHX.

$$\phi_{CO2,lps} = m_{CO2,E}\left(h_{CO2,LPR\_out} - h_{CO2,E\_in}\right) = \phi_E + \phi_{IHX} \qquad \text{Equ. 5.22}$$

Solving for the refrigerant mass flow rate in the evaporator:

$$m_{CO2,E} = \frac{\phi_E + \phi_{IHX}}{h_{CO2,LPR\_out} - h_{CO2,E\_in}} \qquad \text{Equ. 5.23}$$

Where:

$\phi_{CO2,lps}$	Heat rate required for the evaporation and superheating of the refrigerant flow at the low-pressure side [W]
$m_{CO2,E}$	Refrigerant mass flowrate back-calculated of the low-side heat balance [kg/s]
h_{CO2,E_in}	Enthalpy of the refrigerant at evaporator inlet [J/kg]
h_{CO2,LPR_out}	Enthalpy of the refrigerant at LPR outlet [J/kg]

Heat transfer coefficient

The overall heat transfer coefficient for the flooded evaporator was calculated based on the mean evaporator heat transfer surface by using:

$$U_E = \frac{\phi_E}{LMTD_E \, A_{mean,E}} \qquad \text{Equ. 5.24}$$

$$LMTD_E = \frac{\left(T_{w,E\_in} - T_{w,E\_out}\right)}{ln\left(\dfrac{T_{w,E\_in} - T_{CO2,E}}{T_{w,E\_out} - T_{CO2,E}}\right)} \qquad \text{Equ. 5.25}$$

Where:

U_E	Overall heat transfer coefficient of the evaporator [W/m^{2}K]
$LMTD_E$	Log mean temperature difference in the evaporator [K]
$A_{mean,E}$	Mean heat transfer surface of the evaporator [m^2]

Evaporator CO_2 heat transfer coefficient

The CO_2 heat transfer coefficient for the evaporator was back-calculated from the overall heat transfer coefficient which was based on the mean evaporator surface area. The difference in the water and refrigerant side heat transfer areas was small so it was not considered. Also to simplify the calculations, the fin effect of the twisted tube construction was neglected. Hence the overall heat transfer coefficient was approximated by:

$$\frac{1}{U_E} = \frac{1}{h_{CO2,E}} + \frac{t_{tube,E}}{\lambda_{copper}} + \frac{1}{h_{W,E}} \qquad \text{Equ. 5.26}$$

The water-side heat transfer coefficient ($h_{W,E}$) was calculated using the McAdams correlation (ASHRAE, 2001) with water properties based on the mean bulk temperature.

Solving for the CO_2 heat transfer coefficient gives:

$$h_{CO2,E} = \frac{1}{\frac{1}{U_E} - \frac{1}{h_{W,E}} - \frac{t_{tube}}{\lambda_{tube}}} \qquad \text{Equ. 5.27}$$

Where:

$h_{CO2,E}$	Refrigerant side heat transfer coefficient [W/m^{2}K]
$h_{W,E}$	Water side heat transfer coefficient [W/m^{2}K]
t_{tube}	Wall thickness of the tube [m]
λ_{tube}	Thermal conductivity of the tube [W/mK]

5.3.4.1 Refrigerant mass flowrate

The refrigerant mass flowrate m_{CO2} was estimated as the mean value of that back-calculated from the gas cooler and the evaporator heat flows:

$$m_{CO2} = \frac{m_{CO2,GC} + m_{CO2,E}}{2} \qquad \text{Equ. 5.28}$$

The evaporator energy balance requires m_{CO2} to be known so an iterative solution of Equ. 5.28 and Equ. 5.23 was required.

If the energy balance was perfect then the mass flowrate of the evaporator and the GC would be equal. However, in the real system there occurs an energy imbalance causing a difference in the refrigerant mass flowrate:

$$\Delta m_{CO2,imbalance} = \frac{m_{CO2,GC} - m_{CO2,E}}{m_{CO2}} \times 100 \qquad \text{Equ. 5.29}$$

Where:

$\Delta m_{CO2,\ imbalance}$ Refrigerant mass flowrate imbalance [%]

The refrigerant mass flowrate imbalance was taken as guideline for the quality of the experimental data. Experimental heat pump data with a mass flowrate uncertainty higher than 15% were dismissed from the data analysis.

5.3.5 Compressor

Pressure ratio:

$$PR = \frac{p_{discharge} + 1.013\,bar}{p_{suction} + 1.013\,bar} \qquad \text{Equ. 5.30}$$

Where:

PR Compressor pressure ratio [-]

$p_{discharge}$ Compressor discharge pressure [bar.g]

$p_{suction}$ Compressor suction pressure [bar.g]

Volumetric Efficiency

The volumetric efficiency was calculated using:

$$\eta_{vol} = \frac{m_{CO2}}{V_{theo}\ \rho_{CO2,comp\_in}} \quad \text{Equ. 5.31}$$

Where:

η_{vol}	Overall compressor volumetric efficiency [-]
m_{CO2}	Refrigerant mass flow rate [kg/s]
V_{theo}	Nominal swept volume of the compressor [m^3/s]
$\rho_{CO2,\ comp\_in}$	Refrigerant (vapour) density at the compressor inlet [kg/m^3]

Isentropic efficiency

The overall isentropic efficiency was calculated using:

$$\eta_{is,eff} = \frac{m_{CO2}\left(h_{CO2,comp\_out,is} - h_{CO2,\ comp\_in}\right)}{P_{el}} \quad \text{Equ. 5.32}$$

The refrigerant enthalpy $h_{CO2,comp\_out,is}$ was back-calculated from discharge pressure and the refrigerant entropy at the discharge, which was (if the compression was isentropic) equal to the entropy at the compressor suction

$$h_{CO2,comp\_out,is} = f\left(s_{CO2,comp\_in}, p_{discharge}\right) \quad \text{Equ. 5.33}$$

Where:

$\eta_{is,\ eff}$	Effective isentropic compressor efficiency [-]
m_{CO2}	Overall refrigerant mass flowrate [kg/s]
P_{el}	Power consumption of the compressor motor [W]
$h_{CO2,comp\_out\text{-}is}$	Enthalpy of the refrigerant at the compressor outlet if the compression was isentropic [J/kg]
$h_{CO2,comp\_in}$	Enthalpy of the refrigerant at the compressor inlet [J/kg]
$s_{CO2,comp\_in}$	Entropy of the refrigerant at the compressor inlet [J/kg]

The indicated efficiency describes the apparent efficiency of the actual compression process including heat losses and is given by the ratio between the actual change in the enthalpy during the compression and the enthalpy change of the refrigerant if there was isentropic compression.

$$\eta_{is,ind} = \frac{h_{CO2,comp\_out-is} - h_{CO2,comp\_in}}{h_{CO2,comp\_out} - h_{CO2,comp\_in}} \qquad \text{Equ. 5.34}$$

Where:

$\eta_{is,\ ind}$	Indicated isentropic compressor efficiency [-]
$h_{CO2,comp\_out}$	Enthalpy of the refrigerant at the compressor outlet [J/kg]

Compressor heat losses

The heat losses were estimated by an energy balance about the compressor:

$$\phi_{losses,comp} = P_{el} - m_{CO2}\left(h_{CO2,comp\_out} - h_{CO2,comp\_in}\right) \qquad \text{Equ. 5.35}$$

Where:

$\phi_{losses,\ comp}$	Heat losses of the compressor calculated by the compressor energy balance [W]

The heat losses were also estimated by the heat transferred by natural convection through the outside of the compressor.

$$\phi_{losses-conv,comp} = A_{O,comp}\ h_{air}\left(T_{O,comp} - T_{air}\right) \qquad \text{Equ. 5.36}$$

Where:

$\phi_{losses-\ conv,\ comp}$	Heat losses of the compressor calculated by the heat convection to the ambient air [W]
$A_{O,\ comp}$	Surface area of the compressor [m^2]
h_{air}	Overall heat transfer coefficient at the compressor body surface [W/m^2K]
$T_{O,\ comp}$	Average compressor body surface temperature [°C]
T_{air}	Ambient air temperature near the compressor surface [°C]

For the heat transfer to the ambient air an overall heat transfer coefficient of 10 W/m^2K was applied. The heat transfer surface of the compressor body was estimated to be 1.5 m^2.

5.3.6 Heat pump efficiency

Heat pump coefficient of performance (COP)

The heat pump coefficient of performance (COP) was calculated using:

$$COP_{hp} = \frac{\phi_{GC}}{P_{el}} \qquad \text{Equ. 5.37}$$

Where:

COP_{hp} Coefficient of performance of the heat pump [-]

Carnot Efficiency

The maximal possible efficiency of the heat pump process is given by the Carnot efficiency, which is a function of the heat sink and the heat source temperatures. The Carnot efficiency implies an unlimited heat source, which was not the case for the heat pump prototype since the evaporation temperature was controlled by the flowrate and temperature of the water flowing through the evaporator as it mimicked an air-sourced unit. Therefore the Carnot efficiency was calculated for an equivalent air-source evaporator unit, assuming a constant LMTD of 10 K at all operating conditions.

$$COP_{Carnot} = \frac{T_{W,GC\_out} + 273}{T_{W,GC\_out} - \left(T_{CO2,E} + 10\right)} \qquad \text{Equ. 5.38}$$

Were:

COP_{Carnot} Carnot coefficient of performance of the heat pump [-]

Thermal efficiency

The overall thermal efficiency was defined as the ratio between the actual heat pump COP and the Carnot COP:

$$\eta_{hp} = \frac{COP_{hp}}{COP_{Carnot}} \qquad \text{Equ. 5.39}$$

Where:

η_{hp} Thermal efficiency of the heat pump [-]

5.3.7 Energy balance

The energy balance for the overall heat pump system was given by the sum of the energy inputs and outputs.

$$\phi_{GC} + \phi_{IHX(high-side)} + \phi_{losses,comp} = \phi_E + P_{el} + \phi_{IHX(low-side)} \quad \text{Equ. 5.40}$$

In the real system unspecified losses/gains occurred. Hence give that by definition $\phi_{IHX\,(high\text{-}side)}$ and $\phi_{IHX\,(low\text{-}side)}$ are equal the energy imbalance was given by:

$$\Delta\phi_{unspecified} = \phi_{GC} - \phi_E - P_{el} + \phi_{losses,comp} \quad \text{Equ. 5.41}$$

Where:

$\phi_{unspecified}$ Unspecified energy imbalance [W]

5.3.8 Low pressure receiver (LPR)

The separation capacity could not be measured directly but if there was insufficient separation that may cause liquid carry over into the suction of the compressor then the indicated compressor isentropic efficiency would be significantly different from that expected and the energy balance that assumes superheated vapour at the compressor suction will be affected.

The liquid level in the LPR was estimated by the relative refrigerant charge in the system, starting at the charge (absolute mass of CO_2) where the evaporator just started to operate flooded and knowing the extra amount of CO_2 added thereafter. It was assumed that the refrigerant cycle was balanced, so that there was similar refrigerant charge in the other components at similar heat pump conditions, and that the accumulation of oil in the LPR was negligible.

$$H_{CO2-level,LPR} = \frac{M_{CO2} - M_{CO2,E-flooded}}{\rho_{CO2-l,LPR}\, A_{CS,LPR}} \quad \text{Equ. 5.42}$$

Where:

$H_{CO2\text{-}level,\ LPR}$	Height of liquid CO_2 level in the LPR [m]
M_{CO2}	Refrigerant charge [kg]
$M_{CO2,\ E\text{-}flooded}$	Refrigerant charge when the evaporator starts to be flooded [kg]
$\rho_{CO2\text{-}l,\ LPR}$	Density of the liquid refrigerant in the LPR [m^3/kg]
$A_{CS,LPR}$	Cross sectional area of the LPR [m^2]

The liquid level in the LPR was likely to affect the IHX effectiveness, however it was not possible to back-calculate the height of the liquid refrigerant in the LPR from the heat exchanger effectiveness.

The gas velocity in the LPR was estimated using:

$$v_{CO2,LPR} = \frac{m_{CO2}}{A_{CS,LPR}\ \rho_{CO2-g,LPR\_out}} \qquad \text{Equ. 5.43}$$

Where:

v_{CO2}	Vertical velocity of the refrigerant vapour in the LPR [m/s]
$\rho_{CO2\text{-}g,\ LPR\_outlet}$	Density of the refrigerant vapour at the LPR outlet [kg/m^3]

5.4 Hot water cylinder (HWC) data analysis

The water temperature in the HWC was measured with 8 thermocouples (T17-T24, Figure 4.14), which were equally distributed over the HWC height. Each thermocouple measured the temperature of a horizontal segment of the HWC.

HWC heat losses

The heat losses through the shell of the HWC were estimated from the rate of cooling of each part of the HWC using:

$$\phi_{losses,HWC} = M_{HWC}\ c_W\ \frac{\Delta T_{W-mean,HWC}}{\Delta t} \qquad \text{Equ. 5.44}$$

with:

$$T_{W-mean,HWC} = \frac{\sum_{j=1}^{8} M_{HWC,j}\ T_j}{M_{HWC}} = \frac{1}{8}\sum_{j=1}^{8} T_j \qquad \text{Equ. 5.45}$$

Where:

$\phi_{losses,\ HWC}$	Heat losses of the HWC to the ambient air [W]
$M_{HWC,\ j}$	Mass of the j[th] HWC segment [kg]
M_{HWC}	Total mass of the HWC [kg]
$T_{w\text{-}mean}$	Mean temperature of the water in the HWC at the time t [°C]
T_j	Water temperature measured for the j[th] segment [°C]
Δt	Time interval in-between the temperature measurements [s]

Overall heat transfer coefficient of the HWC

The overall heat transfer coefficient was derived from the HWC heat balance based on the inner shell of the HWC:

$$U_{HWC} = \frac{\phi_{losses,HWC}}{A_{i,HWC}\ (T_{W-mean,HWC} - T_{air})} \qquad \text{Equ. 5.46}$$

with:

$$A_{i,HWC} = d_{HWC}\ \pi \left(\frac{d_{HWC}}{2} + H_{HWC} \right) = 1.76\ m^2 \qquad \text{Equ. 5.47}$$

Where:

U_{HWC}	Overall heat transfer coefficient [W/m^{2}K]
$A_{i,\ HWC}$	Surface of the inner HWC shell [m^2]
d_{HWC}	Diameter of the inner HWC shell [m]
H_{HWC}	Height of the inner HWC shell [m]

This implies that the HWC was at uniform temperature represented by the average temperature and neglects the larger surface area of the top and bottom segments in the HWC.

6 Hot water supply system (HWSS) model description

The control and measurement set-up of the HWSS prototype was not fully automated so that the overall system performance and the performance of the HWSS components could not be measured with completely realistic hot water consumption profiles. Therefore the HWSS was modelled to evaluate the overall system performance at likely operating conditions that occur over a 24 hour period. Of interest was the function, reliability and efficiency of the HWSS and the efficiency of the heat pump, which were indicated by the temperature distribution in the HWC, the HWC delivery temperature and the heat pump energy use.

6.1 Hot water usage

Two hot water consumption profiles were defined based on average hot water consumption data (Williamson and Clark, 2001) and typical domestic routines (Table 6.1). Profile A represents moderate hot water usage of 160 l of hot water at 60°C per day while Profile B represents excessive hot water usage of 330 l of hot water. The HWSS had a nominal heating capacity of 8.5 kW which was likely to be sufficient for a 2 or 3 family building. Hence the performance of the HWSS was investigated when delivering household A, household B or both A and B water flowrates.

6.2 Initial condition

Any model requires an initial condition. That chosen was a fully mixed HWC filled with cold water at 15°C at midnight. The ambient air temperature was assumed constant at 10°C and the mains cold water was taken to be 15°C.

Table 6.1: HWSS water consumption profiles for a household with moderate (profile A) and excessive (profile B) hot water usage.

Time and length of the event [h:min]	Type [-]	Flow rate [l/min]	Temperature of supplied water [°C]	Total Volume [l]	Volume at 60°C [l]	Volume at 15°C [l]
Household A: Moderate hot water consumption of 160 l at 60°C per day						
6:00 - 6.05	Shower	7	45	35	23.3	11.7
6:10 - 6:15	Kitchen	3	40	15	8.3	6.7
6:25 - 6:27	Hand basin	4	25	8	1.8	6.2
7:15 - 7:23	Shower	7	45	56	37.3	18.7
7:55 - 8:00	Kitchen	3	40	15	8.3	6.7
8:10 - 8:13	Hand basin	2	25	6	1.3	4.7
16:25 - 16:30	Hand basin	3	25	15	3.3	11.7
17:30 -17:40	Kitchen	3	45	30	20.0	10.0
18:00 -18:10	Kitchen	5	55	50	44.4	5.6
19:00 - 19:05	Hand basin	3	35	15	6.7	8.3
21:00 - 21:05	Hand basin	3	30	15	5.0	10.0
Total water consumption:				**260.0**	**159.9**	**100.1**
Household B: Excessive hot water consumption of 330 l at 60°C per day						
7:50 - 8:00	Shower	7	45	70	46.7	23.3
8:10 - 8:15	Kitchen	3	55	15	13.3	1.7
8:30 - 8:45	Shower	7	45	105	70.0	35.0
9:00 -9:02	Kitchen	3	45	6	4.0	2.0
9:05 - 9:35	Washing	2	55	60	53.3	6.7
11:50 - 11:54	Hand basin	2	25	8	1.8	6.2
12:00 - 12:02	Kitchen	5	55	10	8.9	1.1
15:00 - 15:08	Shower	7	45	56	37.3	18.7
16:50 - 16:55	Hand basin	2	25	10	2.2	7.8
18:00 - 18:10	Bath	5	45	50	33.3	16.7
18:05 - 18:09	Kitchen	5	45	20	13.3	6.7
19:00 - 19:05	Kitchen	10	55	50	44.4	5.6
22:00 - 22:04	Hand basin	2	25	8	1.8	6.2
Total water consumption:				**468.0**	**330.4**	**137.6**

6.3 Mathematical model of the HWSS

The model consisted of the following main parts:

- Water supply system (WSS)
- Heat pump
- Hot water storage cylinder (HWC)

Figure 6.1 shows the HWSS as it was modelled, including the model variables.

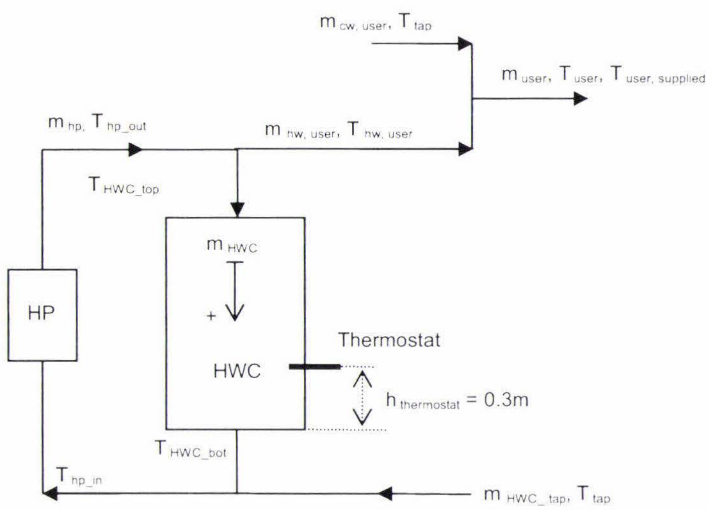

Figure 6.1: Schematic diagram of the water supply system (WSS) showing the model nomenclature.

The nomenclature used was:

T_{user}	Temperature of the water demanded by the user [°C] [1]
$T_{user,\ supplied}$	Temperature of the water supplied to the user [°C] [2]
$T_{hw,\ user}$	Temperature of the hot water supplied to the user [°C] [2]
$T_{HWC,\ top}$	Temperature of the water at the HWC top outlet [°C] [4]
$T_{HWC,\ bot}$	Temperature of the water at the HWC bottom outlet [°C] [4]
$T_{hp,\ in}$	Temperature of the water at the heat pump inlet [°C] [2]
$T_{hp,\ out}$	Temperature of the water at the heat pump outlet [°C] [3]
T_{tap}	Cold water supply temperature [°C] [1]
m_{user}	Mass flowrate of water supplied to the user [l/s] [1]
$m_{cw,\ user}$	Mass flowrate of cold water supplied to the user [l/s] [2]
$m_{hw,\ user}$	Mass flowrate of hot water supplied to the user [l/s] [2]

m_{hp}	Mass flowrate of water produced by the heat pump [l/s] [3]
m_{HWC}	Mass flowrate of water down though the HWC [l/s] [2]
$m_{HWC,\ tap}$	Mass flowrate of cold water at the HWC supply [l/s] [2]
$h_{thermostat}$	Position of the thermostat from the bottom of the HWC [m]

1: System input variables
2: Variables calculated in the WSS model
3: Variables calculated in the heat pump model
4: Variables calculated in the HWC model

6.3.1 Assumptions

Following assumptions were made for the performance modelling:

General:

- Constant thermophysical properties of the water

WSS:

- Constant cold water supply (tap) temperature
- Constant water flowrates to the user
- Infinitely small volume of the pipes
- No heat losses from the pipes to the ambient air

Heat pump:

- Instantaneous production of hot water at the set temperature
- Constant hot water temperature of 60°C (i.e. flowrate control is perfect)
- Constant discharge pressure control at 105 bar.g
- No heat losses to the ambient air, except for the compressor heat losses

HWC:

- Constant ambient air temperature
- Initial perfect mixing of the water in the HWC
- Perfect mixing of the water in the radial direction of the HWC
- Limited mixing of the water in the radial direction of the HWC
- Pure plug-flow of the water through the HWC

6.3.2 Water supply system (WSS)

The water supply system model described the water temperatures and mass flowrates in the pipe system and the water mass flowrate in the HWC, such as the:

- Total amount of hot and cold water consumed by the user
- Temperature and flowrates of the hot and cold water and the water temperature supplied to the user
- Temperature of the cold water at the heat pump inlet
- Water flowrate through the HWC
- Flowrate of cold water make-up in the HWC

The water temperature supplied to the user was given by:

$$T_{user,supplied} = \frac{m_{cw,user}\ T_{tap} + m_{hw,user}\ T_{hw,user}}{m_{user}} \qquad \text{Equ. 6.1}$$

Depending on the demanded water temperature, cold water, hot water or a mixture of both was supplied the user:

If $T_{user} > T_{hw,user}$ *then*

$$m_{cw,user} = 0 \qquad \text{Equ. 6.2}$$

$$m_{hw,user} = m_{user} \qquad \text{Equ. 6.3}$$

Else if $T_{user} \leq T_{hw,user}$ *then*

$$m_{cw,user} = m_{user}\left(\frac{T_{hw,user} - T_{user}}{T_{hw,user} - T_{tap}}\right) \qquad \text{Equ. 6.4}$$

$$m_{hw,user} = m_{user} - m_{cw,user} \qquad \text{Equ. 6.5}$$

Conditional on the demanded flowrate, the hot water will be delivered directly from the heat pump, from the top of the HWC or from both. There were two cases depending on the flow direction in the HWC:

- Case A: Water flows from the HWC top to the bottom
- Case B: Water flows from the HWC bottom to the top

For case A it follows that:

$$m_{HWC} \geq 0$$

$$T_{hw,user} = T_{hp,out} = T_{HWC,top} \qquad \text{Equ. 6.6}$$

$$T_{hp,in} = \frac{m_{HWC}\ T_{HWC,bot} + m_{HWC,tap}\ T_{tap}}{m_{hp}} \qquad \text{Equ. 6.7}$$

For case B if follows that:

$$m_{HWC} < 0$$

$$T_{hw,user} = \frac{m_{HWC}\ T_{HWC,top} + m_{hp}\ T_{hp,out}}{m_{hw,user}} \qquad \text{Equ. 6.8}$$

$$T_{hp,in} = T_{tap} \qquad \text{Equ. 6.9}$$

The mass flowrate in the HWC and at the cold water supply main were calculated by:

$$m_{HWC} = m_{hp} - m_{hw,user} \qquad \text{Equ. 6.10}$$

$$m_{HWC,tap} = m_{hw,user} \qquad \text{Equ. 6.11}$$

6.3.3 Heat pump

The heat pump performance, such as the heat pump heating capacity and the heat pump COP were described as a function of the gas cooler water inlet temperature and the evaporation temperature by fitting polynomials to the experimental data for the prototype.

The performance of the heat pump was modelled for a constant discharge pressure of 105 bar.g where overall maximum heat pump efficiency was achieved. However, heat pump performance data at 105 bar.g and varying heat pump cold water inlet temperature were only available at 0°C/33.8 bar.g evaporation temperature/pressure (as shown in Figure 7.26 and Figure 7.27). Hence a simplistic model of the heat pump was used to predict the performance at constant evaporation temperature only. The evaporation temperature of 0°C corresponded to an air-source heat pump operating with an air temperature of about 10°C. Table 6.2 summaries the valid range of the heat pump performance equations.

Table 6.2: Valid range of the heat pump performance equations

Heat pump water inlet temperature $T_{hp,\,in}$	17-30°C
Hot water temperature $T_{hp,\,out}$	60°C
Evaporation temperature $T_{CO2,E}$	0°C
Discharge pressure $p_{discharge}$	105 bar.g
Suction vapour superheat T_{sh}	5 K

The heat pump heating capacity was given by:

$$\phi_{hp} = \left(1.09\, T_{hp,in}{}^{2} - 1.28 \times 10^{2}\, T_{hp,in} + 7.53 \times 10^{3}\right) switch \qquad \text{Equ. 6.12}$$

The heat pump COP was given by:

$$COP_{hp} = 4.09 \times 10^{-4}\, T_{hp,in}{}^{2} - 5.66 \times 10^{-2}\, T_{hp,in} + 3.54 \qquad \text{Equ. 6.13}$$

Where:

ϕ_{hp} Heat pump heat capacity [W]

COP_{hp} Heat pump heating COP [-]

switch Heat pump switch indicating whether the heat pump is on (1) or off (0) [-]

The heat pump hot water flowrate was calculated from the heat pump heat capacity and the hot water temperature:

$$m_{hp} = \frac{\phi_{hp}}{c_W \left(T_{hp,out} - T_{hp,in}\right)} \qquad \text{Equ. 6.14}$$

It was assumed that the heat pump control was perfect and set to give hot water at 60°C so:

$$T_{hp,out} = 60^{\circ}C \qquad \text{Equ. 6.15}$$

The overall control of the heat pump by the thermostat was modelled as follows:

$$If \quad T_{thermostat} < T_{hp,on} \quad then$$

$$switch = 1 \qquad \text{Equ. 6.16}$$

$$Else\,if \quad T_{thermostat} > T_{hp,on} + \Delta T_{DB} \quad then$$

$$switch = 0 \qquad \text{Equ. 6.17}$$

Where:

$T_{thermostat}$	Temperature at the HWC thermostat [°C]
$T_{hp,\,on}$	Heat pump temperature set-point [°C]
ΔT_{DB}	Temperature dead band for thermostat [K]

The HWSS control parameters, such as the heat pump temperature set-point and the temperature dead band were initially set to be 20°C and 10 K respectively, however the settings were optimised in the HWSS performance modelling so as to maximize the amount of hot water in the HWC at useful temperature, give low heat pump inlet water temperature and to keep heat pump operating intervals as long as possible.

The electric power requirements were given by the heat pump COP and the heat pump capacity.

$$P_{el,hp} = \frac{\phi_{hp}}{COP_{hp}} \qquad \text{Equ. 6.18}$$

Where:

$P_{el,\,hp}$ Power consumption of the heat pump [W]

6.3.4 Hot water cylinder (HWC)

6.3.4.1 Differential equation

The temperature distribution in the HWC was described by a one-dimensional partial differential equation. Figure 6.2 shows the schematic of the HWC and the nomenclature used for the HWC-model.

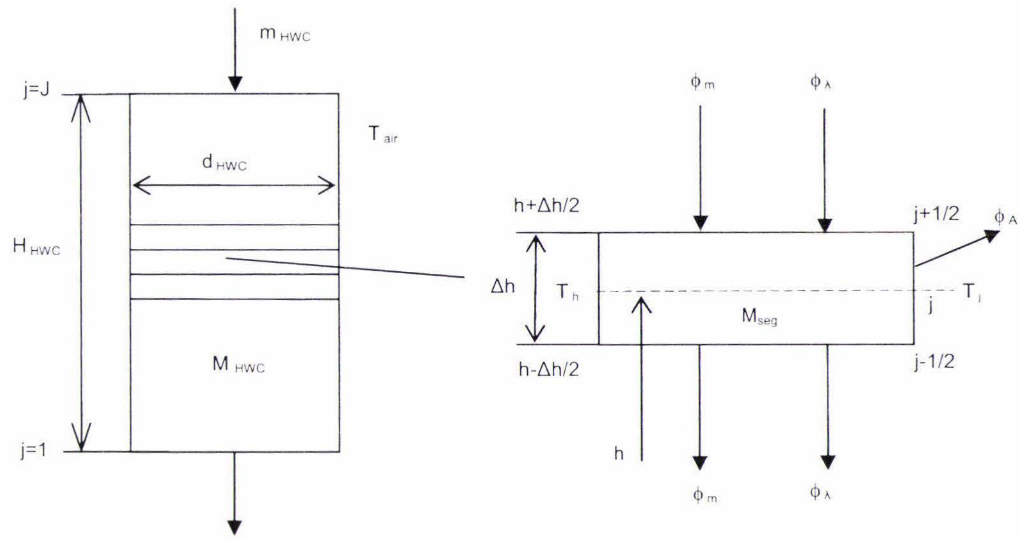

Figure 6.2: Schematic of the HWC and a general segment somewhere in the HWC

Where:

T_h	Water temperature at the height h of the HWC [°C]
T_j	Water temperature of the j^{th} segment in the HWC [°C]
T_{air}	Ambient air temperature [°C]
m_{HWC}	Water mass flowrate through the HWC [l/s]
d_{HWC}	Inner diameter of the HWC [m]
H_{HWC}	Height of the HWC [m]
M_{HWC}	Mass of the water in the HWC [kg]
M_{seg}	Mass of the water in the segment [kg]
Δh	Thickness of the segment [m]
ϕ_A	Heat losses to the ambient air [W]
ϕ_m	Heat transferred by the water mass flowrate [W]
ϕ_λ	Heat transferred by heat conduction [W]
H	Distance from bottom at the HWC [m]
J	Number of segments [-]

Ideally, heat would be transferred between the segments and to the ambient air by the plug-flow of water, heat conduction and convective heat losses only. However some mixing occurs due to the natural convection and turbulent flow patterns (imperfect stratification) in the HWC. The natural convection and the turbulence caused by the mass flow were modelled by pseudo-conduction by correcting the thermal conductivity of water with a conduction enhancement factor. The magnitude of the natural convection was assumed to be the same, independent of the direction of the plug-flow water flow rate in the HWC. Hence the differential equation for the thermocline in the HWC considered:

- the temperature changes of the water with height h caused by the mass flow rate of water through the HWC (flow term)
- the mixing process of the hot and cold water in the HWC by natural convection in the HWC plus the heat conduction through the water (conduction term)
- the heat losses through the outside of the HWC (heat-loss term)

It follows that:

$$\underbrace{\phi_{seg,h}}_{I} = \underbrace{\left(\phi_{m,h+\Delta h/2} - \phi_{m,h-\Delta h/2}\right)}_{II} + \underbrace{\left(\phi_{\lambda,h+\Delta h/2} - \phi_{\lambda,h-\Delta h/2}\right)}_{III} \qquad \text{Equ. 6.19}$$

I) Heat accumulation

The heat accumulated in the segment at the height h is proportional to the temperature change with time:

$$\phi_{seg,h} = \frac{\rho_w\, c_w\, \Delta h\, d_{HWC}^{\;2}\, \pi}{4}\frac{dT_h}{dt} \qquad \text{Equ. 6.20}$$

Where:

$\phi_{seg,h}$	Heat accumulated in the segment at the height h of the HWC [W]
c_W	Specific heat capacity of water [J/kgK]
ρ_W	Density of water [kg/m^3]
t	Time [s]

II) Flow-term

The heat transfer rate due to water flow is given by the transferred mass of the water, the temperature of the water in the segment above or below the segment h and the specific heat capacity of water. Due to the changing direction of the mass flow rate in the HWC, the heat transfer rate has to be estimated differently for case A and B.

Case A ($m_{HWC} \geq 0$):

$$\phi_{m,h+\Delta h/2} = m_{HWC}\, c_W\, T_{h+1} \qquad \text{Equ. 6.21}$$

$$\phi_{m,h-\Delta h/2} = m_{HWC}\ c_W\ T_h \qquad \text{Equ. 6.22}$$

Case B ($m_{HWC} < 0$):

$$\phi_{m,h+\Delta h/2} = m_{HWC}\ c_W\ T_h \qquad \text{Equ. 6.23}$$

$$\phi_{m,h-\Delta h/2} = m_{HWC}\ c_W\ T_{h-1} \qquad \text{Equ. 6.24}$$

Where:

$\phi_{m,\ h\pm\Delta h/2}$ Heat transferred through the surface h+Δh/2 or h-Δh/2 of the segment at the height h in the HWC [W]

III) Convection-term

The heat transfer rate due to heat conduction is given by the effective heat conduction coefficient divided by the thickness of the segment times the cross section area between the segments and the temperature difference of the segments:

$$\phi_{\lambda,h+\Delta h/2} = \frac{\lambda_{eff,h+\Delta h/2}\ d_{HWC}^{\ 2}\ \pi}{4}\ \frac{T_{h+1} - T_h}{\Delta h} \qquad \text{Equ. 6.25}$$

$$\phi_{\lambda,h-\Delta h/2} = \frac{\lambda_{eff,h-\Delta h/2}\ d_{HWC}^{\ 2}\ \pi}{4}\ \frac{T_h - T_{h-1}}{\Delta h} \qquad \text{Equ. 6.26}$$

Where:

$\phi_{\lambda,h\pm\Delta h/2}$ Heat transferred through the surface h+Δh/2 or h-Δh/2 of the segment at the height h of the HWC [W]

$\lambda_{eff,h\pm\Delta h/2}$ Pseudo conduction thermal conductivity at the surface h+Δh/2 or h-Δh/2, which considered heat conduction, natural convection and/or mixing of the water between the segments [W/mK]

Different enhancement factors for the pseudo conduction thermal conductivity were applied depending on the temperature and the flow to account for the likely natural convection and mixing due to turbulent flow. If the water in the HWC was perfectly stratified, heat would be transferred in the direction of the temperature gradient by conduction only when $T_{h+1}>T_h$ (positive temperature gradient). In this case there could be little natural convection because the less dense warmer water is above the cooler water with higher density. However some convection enhancement in the direction of the temperature gradient (driving force) might occur because of radial temperature gradients or imperfect plug-flow entry or exit at the HWC top and bottom. If $T_{h+1}<T_h$

(negative temperature gradient) then natural convection will be significant due to corresponding density differences and the enhancement factor would be expected to be higher. Hence, two enhancement factors for convection with a positive temperature gradient (f_{λ,nat_conv_pos}) and convection with a negative temperature gradient (f_{λ,nat_conv_neg}) were applied.

If $T_{h+1} \geq T_h$ & $m_{HWC} = 0$ *then*

$$\lambda_{eff,h+\Delta h/2} = \lambda_W \, f_{\lambda,nat\_conv\_pos} \qquad \text{Equ. 6.27}$$

Else if $T_{h+1} < T_h$ & $m_{HWC} = 0$ *then*

$$\lambda_{eff,h+\Delta h/2} = \lambda_W \, f_{\lambda,nat\_conv\_neg} \qquad \text{Equ. 6.28}$$

Else if $T_{h+1} \geq T_h$ & $m_{HWC} \neq 0$ *then*

$$\lambda_{eff,h+\Delta h/2} = \lambda_W \, f_{\lambda,nat\_conv\_pos} \, f_{\lambda,flow} \qquad \text{Equ. 6.29}$$

Else

$$\lambda_{eff,h+\Delta h/2} = \lambda_W \, f_{\lambda,nat\_conv\_neg} \, f_{\lambda,flow} \qquad \text{Equ. 6.30}$$

Where:

λ_W	Thermal conductivity of water [W/mK]
$f_{\lambda,\ nat\_conv\_pos}$	Conductivity enhancement factor for the natural convection with a positive temperature gradient between the segments [-]
$f_{\lambda,\ nat\_conv\_neg}$	Conductivity enhancement factor for natural convection with a negative temperature gradient between the segments [-]
$f_{\lambda,\ flow}$	Conductivity enhancement factor for mixing due to the flow [-]

Similar equations were applied to estimate $\lambda_{eff,h-\Delta h/2}$

V) Heat loss-term

Heat losses to the ambient air through the HWC shell were given by:

$$\phi_{A,h} = U_{HWC} \, d_{HWC} \, \pi \, \Delta h \left(T_h - T_{air}\right) \qquad \text{Equ. 6.31}$$

Where:

U_{HWC} Overall heat transfer coefficient of the HWC based on the inner surface [W/m^{2}K]

Applying Equ. 6.20 to Equ. 6.31 in the heat balance of the general segment (Equ. 6.19):

Case A:

$$\frac{dT_{0<h<H}}{dt} = \varpi \frac{(T_{h+1} - T_h)}{\Delta h} + a \frac{\lambda_{eff,h+\Delta h/2}(T_{h+1} - T_h) - \lambda_{eff,h-\Delta h/2}(T_h - T_{h-1})}{\Delta h^2} - b(T_h - T_{air})$$

Equ. 6.32

Case B:

$$\frac{dT_{0<h<H}}{dt} = \varpi \frac{(T_h - T_{h-1})}{\Delta h} + a \frac{\lambda_{eff,h+\Delta h/2}(T_{h+1} - T_h) - \lambda_{eff,h-\Delta h/2}(T_h - T_{h-1})}{\Delta h^2} - b(T_h - T_{air})$$

Equ. 6.33

with:

$$\varpi = \frac{4\, m_{HWC}}{d_{HWC}^{\;2}\, \rho_W\, \pi}$$ Equ. 6.34

$$a = \frac{1}{\rho_W\, c_W}$$ Equ. 6.35

$$b = \frac{4\, U_{HWC}}{d_{HWC}\, \rho_W\, c_W}$$ Equ. 6.36

As $\Delta h \to 0$, the partial differential equations for both cases become:

$$\frac{\partial T_h}{\partial t} = \varpi \frac{\partial T_h}{\partial h} + a\, \lambda_{eff,h} \frac{\partial^2 T_h}{\partial h^2} - b\,(T_h - T_{air})$$ Equ. 6.37

Table 6.3 summarises the boundary conditions for the differential equation:

Table 6.3: Boundary conditions for the HWC model

	Top of HWC (h=H)	Bottom of HWC (h=0)
Case A	$\frac{dT}{dh}=-\frac{U_{HWC}}{\lambda_{eff,H}}(T-T_{air})$ $T=T_{hp,out}$	$\frac{dT}{dh}=\frac{U_{HWC}}{\lambda_{eff,0}}(T-T_{air})$
Case B	$\frac{dT}{dh}=-\frac{U_{HWC}}{\lambda_{eff,H}}(T-T_{air})$	$\frac{dT}{dh}=\frac{U_{HWC}}{\lambda_{eff,0}}(T-T_{air})$ $T=T_{tap}$

6.3.4.2 Finite difference approximation of the differential equation

The differential equation and the boundary conditions were approximated with finite difference equations for different water flow directions in the HWC (Case A and B). The HWC was divided into a finite difference grid with J segments of the height Δh. The finite difference equations were solved with MathLab V6.5.

- Case A:

Top segment ($j=J$):

$$\frac{T_J^{i+1}-T_J^i}{\Delta t}=\varpi\frac{T_{hp,out}-T_J}{\Delta h}-a\frac{\lambda_{eff,J-1/2}\left(T_J-T_{J-1}\right)}{\Delta h^2}-b\left(1+\frac{d_{HWC}}{4\,\Delta h}\right)\left(T_J-T_{air}\right) \qquad \text{Equ. 6.38}$$

Bottom segment ($j=1$):

$$\frac{T_1^{i+1}-T_1^i}{\Delta t}=\varpi\frac{T_2-T_1}{\Delta h}-a\frac{\lambda_{eff,1+1/2}\left(T_2-T_1\right)}{\Delta h^2}-b\left(1+\frac{d_{HWC}}{4\,\Delta h}\right)\left(T_1-T_{air}\right) \qquad \text{Equ. 6.39}$$

Generalised segment ($1<j<J$):

$$\frac{T_j^{i+1}-T_j^i}{\Delta t}=\varpi\frac{T_{j+1}-T_j}{\Delta h}+a\frac{\lambda_{eff,j+1/2}\left(T_{j+1}-T_j\right)-\lambda_{eff,j-1/2}\left(T_j-T_{j-1}\right)}{\Delta h^2}-b\left(T_j-T_{air}\right) \qquad \text{Equ. 6.40}$$

- Case B:

Top segment ($j=J$):

$$\frac{T_J^{i+1}-T_J^i}{\Delta t}=\varpi\frac{T_J-T_{J-1}}{\Delta h}-a\frac{\lambda_{eff,J-1/2}\left(T_J-T_{J-1}\right)}{\Delta h^2}-b\left(1+\frac{d_{HWC}}{4\,\Delta h}\right)\left(T_J-T_{air}\right) \qquad \text{Equ. 6.41}$$

Bottom segment (*j=1*):

$$\frac{T_1^{i+1} - T_1^i}{\Delta t} = \varpi \frac{T_1 - T_{tap}}{\Delta h} + a \frac{\lambda_{eff,1+1/2}\,(T_2 - T_1)}{\Delta h^2} - b\left(1 + \frac{d_{HWC}}{4\,\Delta h}\right)(T_1 - T_{air}) \qquad \text{Equ. 6.42}$$

Generalised segment (*1<j<J*):

$$\frac{T_j^{i+1} - T_j^i}{\Delta t} = \varpi \frac{T_j - T_{j-1}}{\Delta h} + a \frac{\lambda_{eff,j+1/2}\,(T_{j+1} - T_j) - \lambda_{eff,j-1/2}\,(T_j - T_{j-1})}{\Delta h^2} - b\,(T_j - T_{air}) \qquad \text{Equ. 6.43}$$

with:

$$\Delta h = \frac{H_{HWC}}{J} \qquad \text{Equ. 6.44}$$

Stability and accuracy

Instability and inaccuracy can occur because of the finite difference approximation of the differential equation and the highly variable mass flowrates (e.g. numerical dispersion). The following criteria had to be fulfilled to meet the numerical stability criteria and ensure accuracy of the finite differential equations:

a) The temperature change of any segment caused by the heat conduction had to be bigger than the temperature change caused by the heat loss term to make the conduction and the heat loss terms numerically stable. It follows that:

Top segment (*j=J*):

$$\Delta t_{cond+heat\_losses,J} \le \frac{\rho_W\; c_W}{\dfrac{\lambda_{eff,J-1/2}}{\Delta h^2} + U_{HWC}\left(\dfrac{4}{d_{HWC}} + \dfrac{H}{H_{HWC}}\right)} \qquad \text{Equ. 6.45}$$

Bottom segment (*j=1*):

$$\Delta t_{cond+heat\_losses,1} \le \frac{\rho_W\; c_W}{\dfrac{\lambda_{eff,1+1/2}}{\Delta h^2} + U_{HWC}\left(\dfrac{4}{d_{HWC}} + \dfrac{H}{H_{HWC}}\right)} \qquad \text{Equ. 6.46}$$

General segment (*1<j<J*):

$$\Delta t_{cond+heat\_losses,j} \le \frac{\rho_W\; c_W}{\dfrac{\lambda_{eff,j+1/2} + \lambda_{eff,j-1/2}}{\Delta h^2} + \dfrac{4\,U_{HWC}}{d_{HWC}}} \qquad \text{Equ. 6.47}$$

Where:

$\Delta t_{cond+heat\_losses}$ Maximal time step for a numerically stable conduction and heat loss term [s]

b) The mass of the water transferred between the segments during the time period Δt had to be equal to or smaller than the mass of the segments to fulfil the numerical stability criteria for the plug-flow term.

$$m_{HWC}\ \Delta t_{plug-flow} \leq M_{seg} \quad \Rightarrow \quad \Delta t_{plug-flow} \leq \frac{d_{HWC}^{\ 2}\ \pi\ \Delta h\ \rho_W}{4\left|m_{HWC}\right|} \qquad \text{Equ. 6.48}$$

To prevent inaccuracy due to numerical dispersion when $m_{HWC} \neq 0$, Δt must be equal to this criteria.

Where:

$\Delta t_{plug-flow}$ Time step for a numerically stable plug-flow-term [s]

To fulfil the criteria for numerically stable and accurate (numerical dispersion-free) modelling of the plug-flow, the time step had to be adjusted for every mass flowrate. However if the mass flowrate declines toward zero, the Δt increases to an extent that the criteria for accurate "plug-flow" modelling could not be practically fulfilled.

6.3.5 Numerical buffer model

To obtain both stable and accurate modelling, a buffer model was applied (Oppel *et al*, 1986). This model uses constant Δt, fulfilling the stability criteria for the heat conduction and heat loss terms. The flow-term was considered by accumulating the flow mass in a buffer segment while integrating the other terms. The integration was interrupted when the flow reached the face of the buffer segment (i.e. buffer volume equates to the segment volume) during the time step Δt and then the buffer volume was added into or removed from the HWC at once by shifting the temperature profile of the cylinder by one segment up or down. The integration then continued for the remaining time of the time step.

The accumulation of the buffer segment was calculated by:

$$M_{buffer} = \sum_{0}^{\Delta t} m_{HWC}\ t \qquad \text{Equ. 6.49}$$

Where:

M_{buffer} Mass accumulated in the buffer segment [kg]

Δt Time step [s]

At the end of the modelled period the remaining accumulated mass in the buffer was added uniformly into the HWC, giving a temperature change of:

If $M_{buffer} > 0$

$$\frac{T_J^{i+1} - T_J^i}{\Delta t} = \frac{4\left|M_{buffer}\right|}{d_{HWC}^{\ 2}\ \pi\ \rho_W}\ \frac{T_{hp,out} - T_J}{\Delta h} \qquad j = J \qquad \text{Equ. 6.50}$$

$$\frac{T_1^{i+1} - T_1^i}{\Delta t} = \frac{4\left|M_{buffer}\right|}{d_{HWC}^{\ 2}\ \pi\ \rho_W}\ \frac{T_2 - T_1}{\Delta h} \qquad j = 1 \qquad \text{Equ. 6.51}$$

$$\frac{T_j^{i+1} - T_j^i}{\Delta t} = \frac{4\left|M_{buffer}\right|}{d_{HWC}^{\ 2}\ \pi\ \rho_W}\ \frac{T_{j+1} - T_j}{\Delta h} \qquad 1 < j < J \qquad \text{Equ. 6.52}$$

Else if $M_{buffer} < 0$

$$\frac{T_J^{i+1} - T_J^i}{\Delta t} = \frac{4\left|M_{buffer}\right|}{d_{HWC}^{\ 2}\ \pi\ \rho_W}\ \frac{T_J - T_{J-1}}{\Delta h} \qquad j = J \qquad \text{Equ. 6.53}$$

$$\frac{T_1^{i+1} - T_1^i}{\Delta t} = \frac{4\left|M_{buffer}\right|}{d_{HWC}^{\ 2}\ \pi\ \rho_W}\ \frac{T_1 - T_{tap}}{\Delta h} \qquad j = 1 \qquad \text{Equ. 6.54}$$

$$\frac{T_j^{i+1} - T_j^i}{\Delta t} = \frac{4\left|M_{buffer}\right|}{d_{HWC}^{\ 2}\ \pi\ \rho_W}\ \frac{T_j - T_{j-1}}{\Delta h} \qquad 1 < j < J \qquad \text{Equ. 6.55}$$

For the buffer model, the maximum Δt was given by the criteria for stability and accuracy of the heat conduction and heat loss term (Equ. 6.45 to Equ. 6.47). However, as a rule of thumb, accurate modelling was achieved with a time step at least 10 times smaller than that implied by the stability criteria.

6.3.6 HWSS performance

The overall coefficient of performance for the HWSS was calculated over the full simulation period by using:

$$COP_{HWSS} = \frac{E_{hw}}{W_{el,hp}}$$ Equ. 6.56

with:

$$E_{hw} = \Delta t \sum_{0}^{t} \left(c_w \, m_{hp} \left(T_{hp,out} - T_{hp,in} \right) - \sum_{1}^{H} \left(\phi_{A,h} \right) \right)$$ Equ. 6.57

$$W_{el,hp} = \sum_{0}^{t} \left(P_{el,hp} \, \Delta t \right)$$ Equ. 6.58

Where:

COP_{HWSS}	HWSS coefficient of performance [-]
E_{hw}	Total useful energy created by the HWSS [J]
$W_{el,hp}$	Electric work of the heat pump [J]

To quantify the hot water supply reliability, the period for which the HWSS was able to meet the users demand was calculated.

$$t_{reliable\_supply} = \sum_{0}^{t_{supply}} \Delta t_{T\_user,supply \geq T\_hw,user}$$ Equ. 6.59

$$t_{supply} = \sum_{0}^{t} \Delta t_{m\_user > 0}$$ Equ. 6.60

Where:

$t_{reliable\_supply}$	Total time at which the HWSS was able to meet the users demand [s]
$\Delta t_{T\_user,\, supply \geq T\_hw,\, user}$	Periods for which the user was supplied with the demanded hot water temperature [s]
t_{supply}	Total time hot water is required [s]
$\Delta t_{m\_user>0}$	Periods for which the user was supplied with the hot water [s]

6.4 HWSS model checking

6.4.1 Time and space discretisation

Due to the approximation of the differential equation, the accuracy of the HWC model depends on the time step and the segment size used. These had to be chosen accounting for the numerical stability, the model accuracy and the computer calculation time required to perform the modelling procedure.

To allow a direct match between the measurement positions and model segments the number of the segments needed to be a multiple of 8.

The effect of the time step and the number of segments on the model accuracy was assessed by making predictions for a one hour period, with an overall HWC U-value of 1.5 W/m^{2}K, conduction enhancement factors of 40 for both f_{λ,nat_conv_pos} and f_{λ,nat_conv_neg} and a flow enhancement factor of 2.5. The heat pump hot water outlet temperature was set to 60°C, the ambient air temperature to 10°C and the mains water temperature to 15°C. The initial condition was a fully mixed HWC at 60°C when the heat pump was off (modelling HWC standing losses), and 15°C when the heat pump was running (modelling HWC heating).

Figure 6.3 shows the predicted HWC temperature for the HWC segment where maximum change in the temperature occurred at the end of the modelled period for varying time steps. The number of HWC segments was 96.

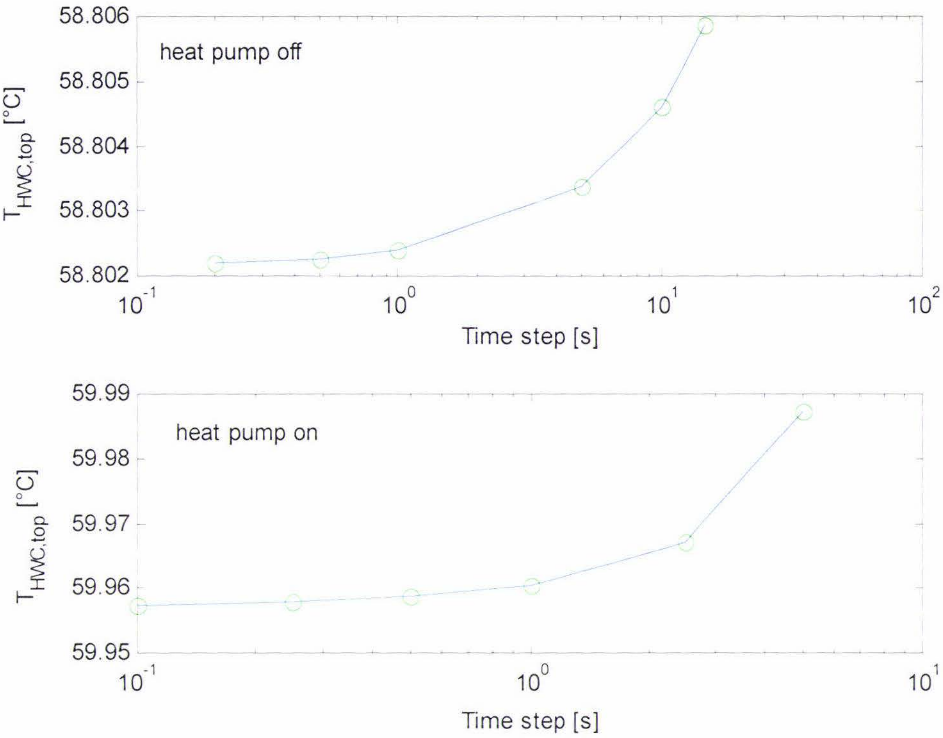

Figure 6.3: Predicted HWC temperature in the top segment of HWC after a one hour period with the heat pump either on (bottom graph) or off (top graph) for varying time step.

For both heat pump on and off conditions, maximum change in temperature occurred in the top segment. The predicted change in the HWC water temperature was bigger when the heat pump was on because of the varying mass of the buffer segment, which was added into the HWC at the end of the modelling period. The maximum allowed time step to fulfil the stability criteria was 18.8 seconds for the heat pump off condition and 7.5 seconds when the heat pump was on. The maximum time step reduced when the heat pump was running due to the 2.5 times higher conductivity caused by the flow factor.

The predicted temperature reduced as the time step decreased. However there were little changes when the time step was set to be 1.0 second or less. However the computing time rapidly increased as the time step was reduced and became excessive when the time step was smaller than 1.0 second.

Figure 6.4 shows the predicted HWC temperature at the end of the modelled period for the HWC segment where maximum change in the temperature occurred (Figure 6.4, top graph) and the maximum time step for numerically stability (Figure 6.4, bottom graph) for varying number of segments. The heat pump was switched off and the time step was set to 1.0 second.

Maximum change in temperature occurred for the top segment and the predicted HWC water temperature reduced as the number of segments was increased. However, the overall change in temperature at 96 segments and above was small. The maximum time step for numerically stability decreased rapidly as the number of segments increased. The computing time became excessive at a number of segments above 96 and a time step below 1.0 seconds respectively.

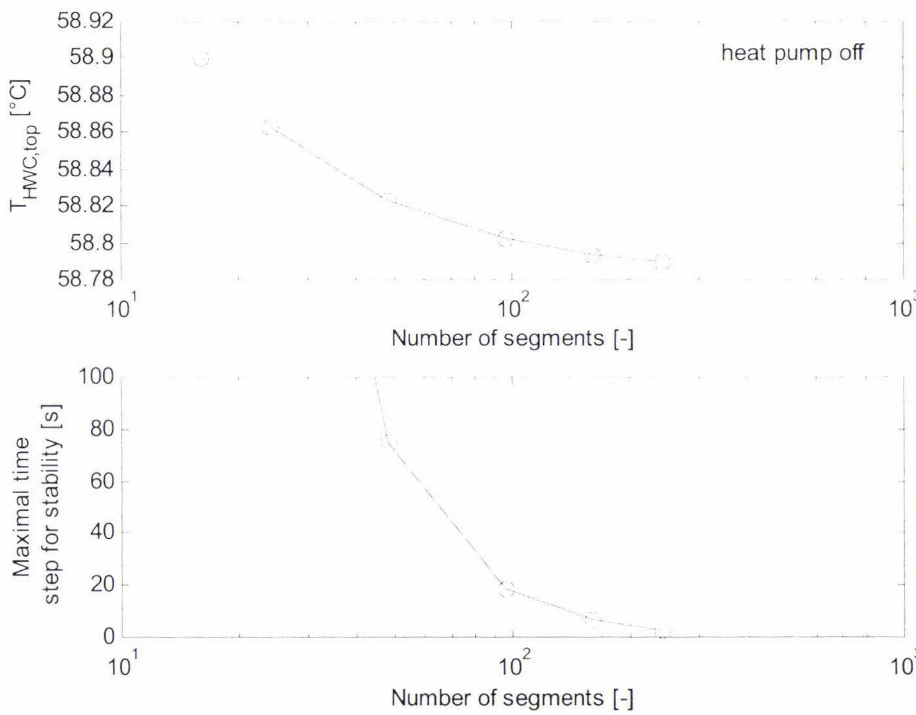

Figure 6.4: Predicted HWC temperature in the top segment of the HWC after a one hour period and the maximum time step for stability with the heat pump off for varying number of segments.

Figure 6.5 shows the temperature of the HWC top segment at varying number of segments when the heat pump was on. Due to the buffer segments the temperature change caused by the plug-flow was not steady but went through step change in temperature when the buffer segment was filled up. The length of the interval between adding the buffer segment into the HWC depended on the water flowrate and the buffer segment size, which was given by the number of segments.

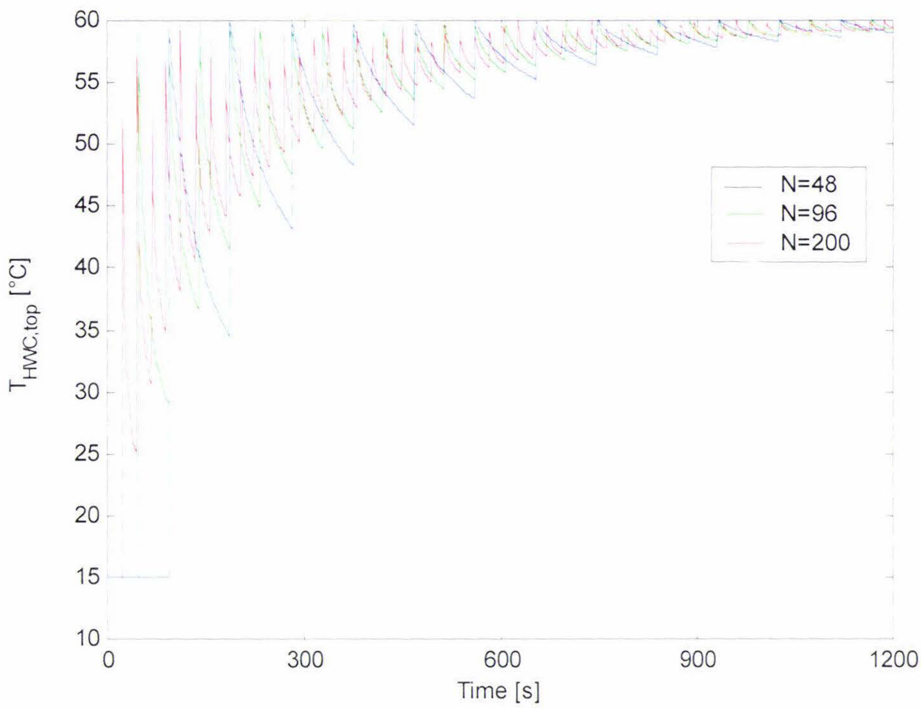

Figure 6.5: Predicted HWC temperature in the top segment of HWC with the heat pump running and varying number of segments.

The water in the top segment approaches the heat pump outlet temperature of 60°C. With a high number of segments (e.g. 200) the buffer is added into the HWC more often giving less deviation of the predicted water temperature from the actual water temperature (heat pump water outlet temperature), and hence less overall prediction error. However, the maximum time step for stability and subsequently *Δt* reduced with increasing number of segments.

Overall, 96 segments and a time step of 1.0 seconds gave adequate modelling precision and computing time. Hence all further HWSS performance modelling was carried out with these model parameters.

adding the buffer segment into the HWC depended on the water flowrate and the buffer segment size, which was given by the number of segments.

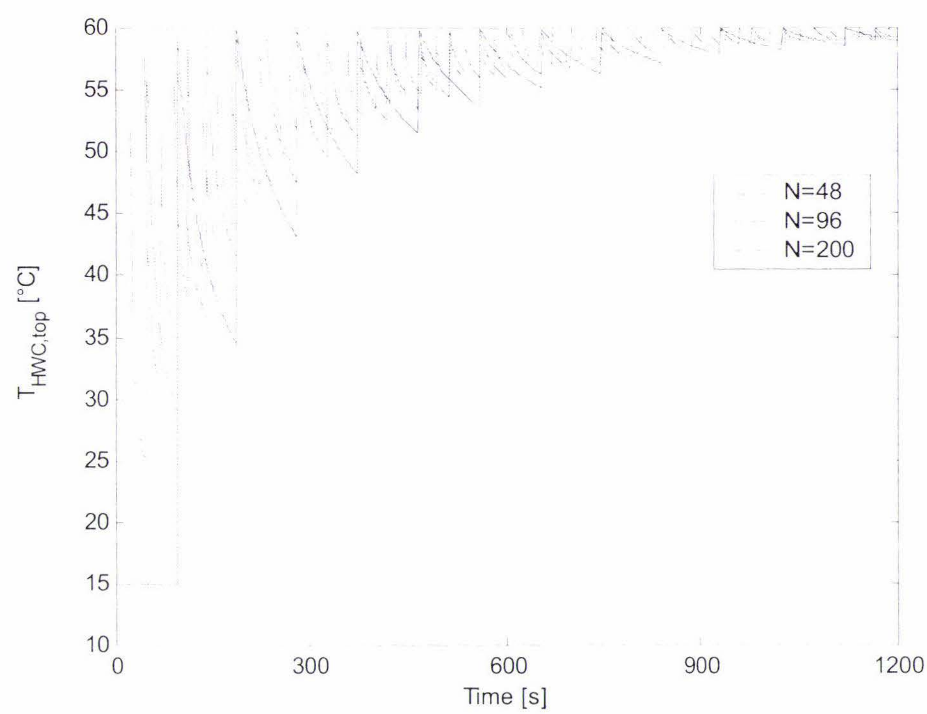

Figure 6.5: Predicted HWC temperature in the top segment of HWC with the heat pump running and varying number of segments.

The water in the top segment approaches the heat pump outlet temperature of 60°C. With a high number of segments (e.g. 200) the buffer is added into the HWC more often giving less deviation of the predicted water temperature from the actual water temperature (heat pump water outlet temperature), and hence less overall prediction error. However, the maximum time step for stability and subsequently Δt reduced with increasing number of segments.

Overall, 96 segments and a time step of 1.0 seconds gave adequate modelling precision and computing time. Hence all further HWSS performance modelling was carried out with these model parameters.

6.4.2 Model checking

To check the implementation and the accuracy of the model, predictions were carried out with high pseudo conduction enhancement factors (f_{λ,nat_conv_pos} and f_{λ,nat_conv_neg}) to mimic a perfectly mixed HWC. Under these conditions the approximated analytical solution is:

$$T(t) = T_{air} + \left(T_{t=0} - T_{air}\right) e^{-\frac{M_W\, c_W}{U_{HWC}\, A_{HWC}} t} \qquad \text{Equ. 6.61}$$

Where:

$T_{t=0}$ Initial water temperature in the HWC [°C]

Figure 6.6 shows the difference between the predicted average water temperature and the temperature calculated by Equ. 6.61. The HWC was modelled with an overall heat transfer coefficient of 1.5 W/m^{2}K and a time step of 1 second. Due to the high effective thermal conductivity the number of segments had to be reduced to 48 to get practical computing time.

The difference between the predicted HWC average temperature and the analytical solution increased over time, however overall the difference was less than 8 x 10^{-4} K after 24 hours. The good agreement between the analytical solution and the predicted temperature suggests that the model was properly formulated and implemented and that the time step and number of segments used were appropriate.

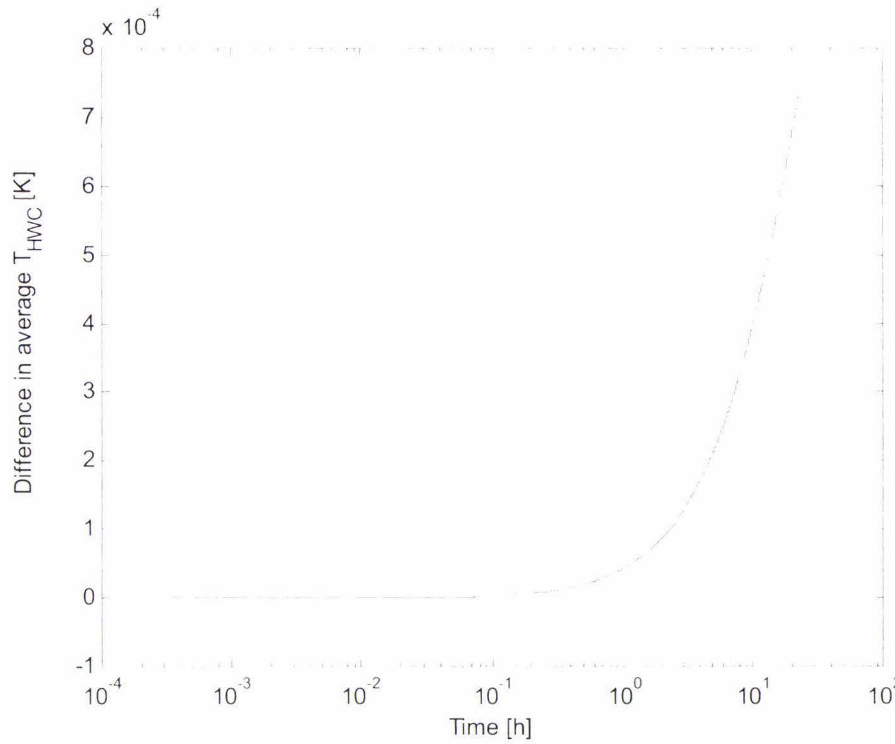

Figure 6.6: Difference between the predicted average HWC water temperature and the analytical solution for a HWC with high water thermal conductivity (well mixed).

To investigate whether the plug-flow term was implemented correctly, the overall HWC U-value and the conductivity were set to a low value of 10^{-10} W/m^{2}K. Under these conditions the changes in mean water temperature in the HWC was given by:

Case A:

$$\Delta T_{HWC} = \frac{m_{HWC}\ \Delta t\ \left(T_{hp,out} - T_{HWC,bot}\right)}{M_{HWC}} \qquad \text{Equ. 6.62}$$

Case B:

$$\Delta T_{HWC} = \frac{m_{HWC}\ \Delta t\ \left(T_{HWC,top} - T_{tap}\right)}{M_{HWC}} \qquad \text{Equ. 6.63}$$

Where:

ΔT_{HWC} Change of the mean HWC temperature [K]

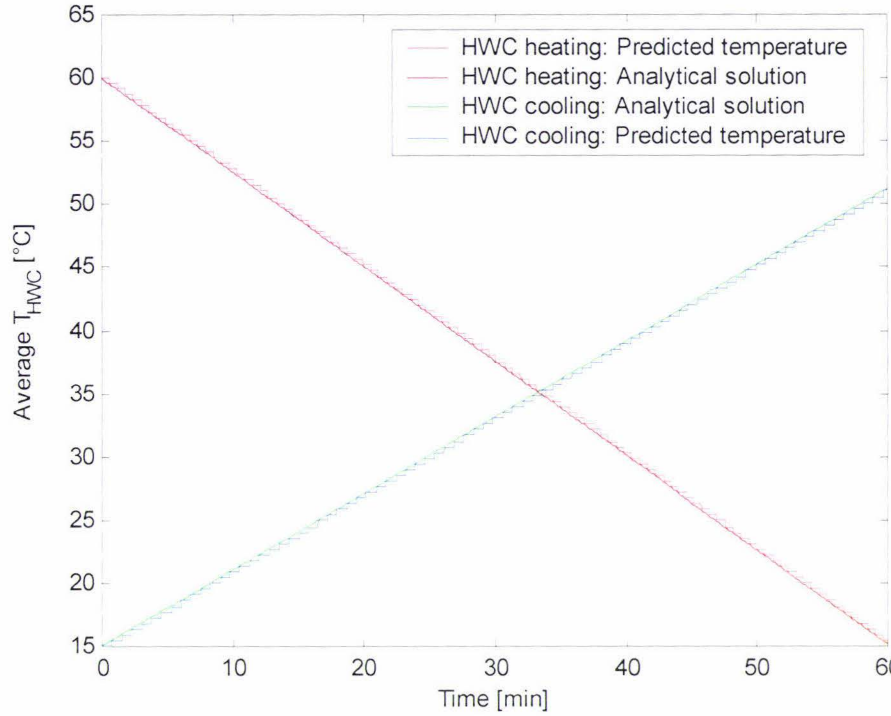

Figure 6.7: Predicted average HWC temperature and analytical solution for a HWC with low U-value and low water thermal conductivity.

Figure 6.7 shows the predicted average HWC temperature and the analytical solution for a HWC heating period of 1 hour and either with the heat pump running (HWC heating) or a period of hot water withdrawal (HWC cooling).

The average water temperature increased/reduced in a stepwise fashion due to the buffer model. Overall, the predicted average water temperature was in good agreement to the analytical solution so it was likely that the plug-flow mechanism was properly formulated and implemented.

The implementation of the HWSS in the model was represented by the average supplied hot water temperature (Equ. 6.1) which was given for the user profiles by the mixed temperature of the hot and cold water, except when there was a hot water shortage. The predicted temperature was equal to the analytically calculated temperature for all user profiles (as described in Table 6.1) so it was expected that the HWSS was implementation was correct.

7 Results and Discussion

7.1 CO_2 charge and leakage

The heat pump with gas cooler unit GC 3.1 was fully charged (flooded evaporator) with 1.61 kg at 105 bar.g discharge pressure, 0°C evaporation temperature and 20°C to 60°C water temperature in the gas cooler. To keep the evaporator flooded at all operating conditions a charge of 1.92 kg CO_2 was required. With this charge the refrigerant system equilibrated at an ambient temperature of approximately 18°C to a saturated pressure of approximately 55 bar.g. The required refrigerant charge was significantly higher than the predicted value of 1.15 kg at 100 bar.g discharge pressure. Possible reasons for the high charge were:

- refrigerant overcharge
- higher refrigerant mass in the discharge side of the refrigerant cycle due to the higher pressure
- underestimated volume of the refrigerant system
- higher fraction of liquid in the evaporator than assumed
- high solubility of the CO_2 in the compressor oil

Occasionally the system displayed characteristics consistent with being overcharged (excessively low compressor discharge temperature) after running the heat pump at various conditions and returning to a condition where earlier the system operation had been stable. Possible reasons were:

- unstable refrigerant mass distribution in the refrigerant cycle
- oil refrigerant solubility changes (as described in section 7.2)

The refrigerant leaked from the system at a rate of approximately 30 g/day. The leakage mainly occurred at the fittings where thread sealant (as described in section 4.5.9) was used, which was probably affected by the compressor oil. The charge had to be adjusted (according to the charging procedure) before performing each trial, so the exact charge in the system was unknown for most of the trials.

7.2 Heat pump operational problems

A number of heat pump operational problems occurred through the trials. These included refrigerant charging problems, compressor performance problems and highly variable oil level in the compressor crankcase. There were several possible reasons, such as:

- Liquid droplets

Droplets of refrigerant and/or compressor oil may have entered the compressor suction despite vapour superheat at the LPR outlet. The droplets were carried over from the LPR.

- Compressor mechanical problems

Poorer compressor performance than expected remained unexplained, so mechanical compressor problems could not be excluded (e.g. valve plate damaged) although there were no other indications of such a problem (e.g. excessive noise or high discharge temperature).

- Oil foaming

Significant oil foaming was observed at the compressor oil sight glass when the CO_2 evaporated out of the oil at changing heat pump operation conditions. Similar behaviour of the oil was expected to occur at the LPR and the oil foaming could had caused and/or increased the liquid carry over.

- Refrigerant-oil behaviour

At saturated conditions, the oil and refrigerant combined to form a viscous mixture. The behaviour of the oil-refrigerant mixture caused difficulties with the charging procedure. In particular, there was varying amount of refrigerant dissolved in the compressor oil depending on the heat pump operating condition and time. Because of the slow evaporation of the CO_2 from the viscous mixture and the refrigerant charging at the beginning of each trial, the CO_2 may have separated from the oil after the system was charged leading to system overcharge.

7.3 Heat pump control

Overall, the heat pump operation was stable over a wide range of operating conditions. Oscillations in the temperatures and/or pressure as well as excessive discharge pressures did not occur at any operating conditions nor when changing the heat pump conditions.

Instabilities, such as rapidly increasing liquid level in the LPR, occasionally occurred when lowering the discharge pressure or when reducing the gas cooler water inlet temperature from 30°C to 25°C or lower. Further, instability occurred because of the large pressure drops in the high-side of the IHX at high refrigerant mass flowrate and at low water flow through the hot water control valve by-pass.

The heat pump was reasonably simple to control when cold water (at the GC inlet and for the evaporator cooling) from the mains was used. However GC water inlet temperature and evaporation temperature and pressure were difficult to control within the desired control precision (as described in Table 5.1) when water from the warm water supply had to be used (i.e. at GC water inlet temperature above the mains water temperature). The reason was the temperature variation of the supplied warm water.

At constant operating conditions, the BPR controlled the discharge pressure with a precision of ±2 bar, which was not as good as specified by the manufacturer (±1 bar at 100 bar.g discharge pressure). Further, the pressure drifted at changing refrigerant flowrate and had to be reset for each heat pump operating condition. A similar characteristic was observed for the GC water-flow control valve. The hot water temperature drifted with changing refrigerant flowrate while at constant heat pump conditions the hot water temperature was controlled with a precision of approximately ±0.5 K.

7.4 Experimental uncertainty

7.4.1 Energy balance

Figure 7.1 shows the energy imbalance of all experimental trials in chronological order as well as the mean imbalance of the individual trials including the standard deviation. A positive difference in the energy balance indicates that the measured energy output into water heating was higher than the measured energy input of the evaporator and compressor.

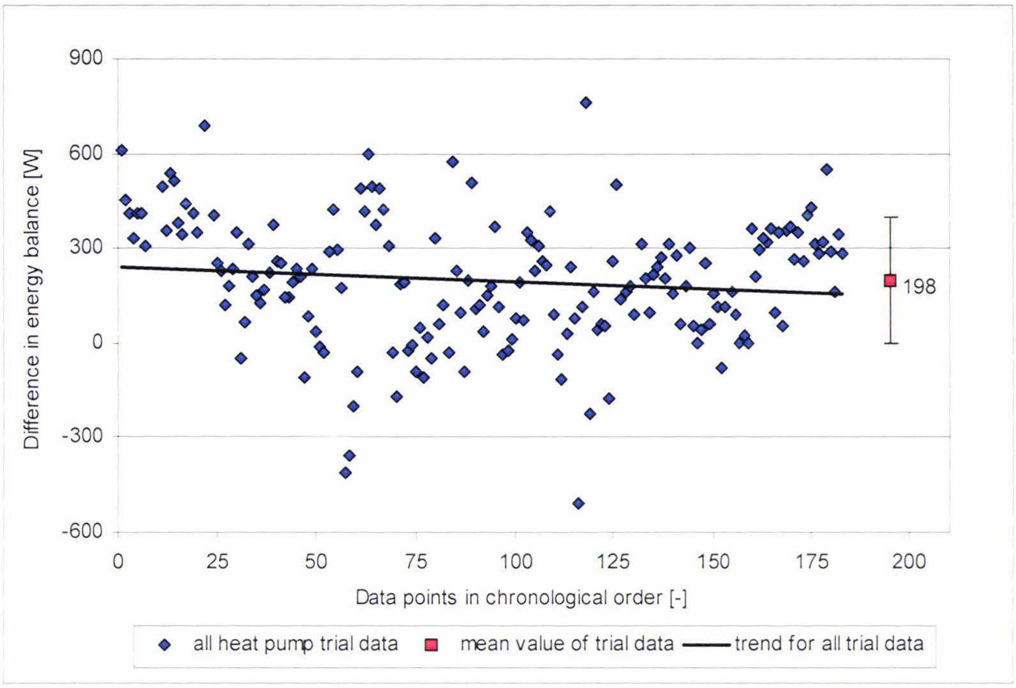

Figure 7.1: Energy imbalance for all experimental trials

The energy imbalance ranged from -512 to 760 W giving an average error of 198±200 W. The range of the imbalance was set by the elimination of data with refrigerant mass flowrate imbalances higher than 15% (as defined in Equ. 5.29). Overall there is no clear time trend in the energy imbalance over the period of the experimental work.

Figure 7.2 shows the average energy imbalance as a percentage of the GC heat transfer rate for the different heat pump configurations (as described in Table 5.4). Again a positive deviation in the energy balance indicates that the measured energy output into water heating was higher than the energy inputs.

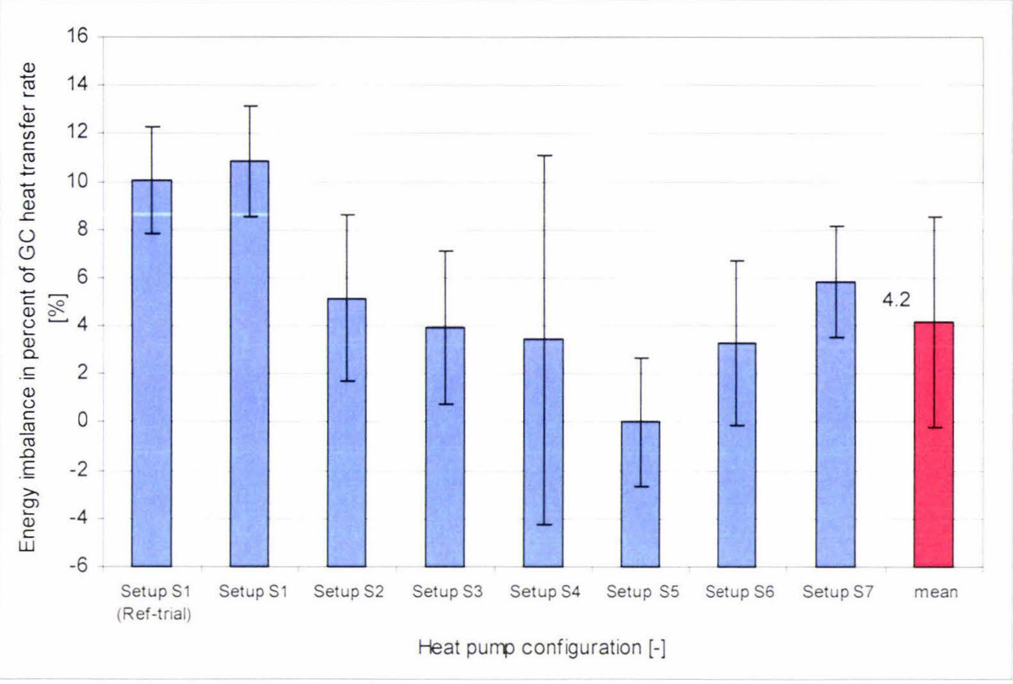

Figure 7.2: Energy imbalance for the different heat pump configurations (bars indicate means, stub's indicate standard deviation)

On average, heat output was 4.2% more than heat input which was a reasonable result considering the relative crudeness of some aspects of the experimental measurement setup. However there was no clear trend in the energy imbalance such as higher imbalance at higher energy input and output.

The effect of the locations of pressure gauge P4 in the heat pump (setup S6 and setup S7) on the overall energy balance was within the overall data uncertainty. The refrigerant enthalpy was relatively insensitive to temperature and pressure for the range of refrigerant GC outlet conditions investigated so this result was expected.

It had been expected that the measured heat input would exceed heat output because heat losses were expected to be higher than the heat gains. Possible reasons for the positive energy imbalance were:

- Liquid CO_2 from the LPR that would lead to higher calculated heat output than heat input because the liquid that was carried over would reject heat in the GC but would not require heat for evaporation in the evaporator or IHX. This is supported by the higher imbalance (and the mass flowrate imbalance as described in section 7.4.2) for configuration S7 where (unlike setup S6) refrigerant/oil-mixture was recovered from the LPR and returned to the compressor, thereby affecting the energy balance in the same way as liquid carry over.

- Systematic measurement errors, particularly for the GC and evaporator water side measurements and the compressor power measurement. Error in other heat pump measurements would contribute to the uncertainty of the compressor heat losses but their effect on the overall energy imbalance was smaller.
- Higher heat gains on the low-pressure (low-temperature) side of the heat pump than heat losses on the discharge-pressure side.
- Refrigerant property uncertainty, particularly in the supercritical region.
- Excessive oil carry over from the compressor that would lead to higher calculated energy output than heat input because the oil would reject heat at the high-pressure side but would not require heat for evaporation in the evaporator.

Indicators for liquid refrigerant and/or oil carry over were the suction vapour superheat (because the possibility of CO_2 droplets that remain in the refrigerant vapour decreased as the superheat increased) and the gas velocity in the LPR respectively. Figure 7.3 shows the energy imbalance as a function of the vapour superheat.

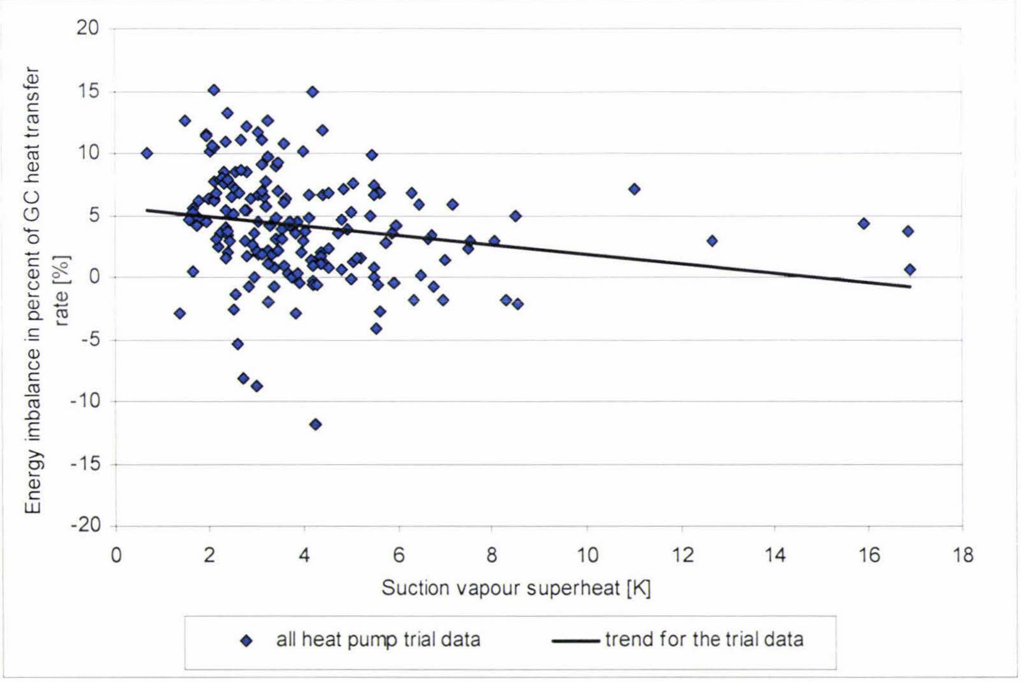

Figure 7.3: Energy imbalance as a function of the compressor suction vapour superheat.

Overall, the general trend was that the energy imbalance improved slightly as the superheat increased. This could indicate that liquid droplets were carried over at low superheat, however the correlation was weak. Further the superheat increased as the vapour velocity in the LPR increased (as described in section 7.5.5 and Figure 7.20) and at high gas velocity it was more likely that droplets were carried over into the compressor suction. Hence the existence of droplets and their effect on the energy imbalance could not be explained by the superheat only.

However several observations, such as the gas cooling in the compressor particularly at high gas velocity in the LPR (section 7.5.5), and the effect of the recovered liquid oil/CO_2 mixture on the compressor efficiency (section 7.5.7) support the theory that liquid was carried over to the compressor from the LPR and that these droplets contributed to the energy imbalance.

7.4.2 Refrigerant mass flowrate balance

Overall refrigerant mass flowrate balance

Figure 7.4 shows the average difference and the standard deviation of the GC and evaporator refrigerant mass flowrate as a percent of the mean mass flow for different heat pump setups. A positive difference corresponds to a higher refrigerant mass flowrate back-calculated for the GC than for the evaporator.

The refrigerant mass flowrate for the high- and low pressure sides were on average within 4.4% (±2.2%) which was a reasonable precision considering the measurement setup for the laboratory prototype. The average refrigerant imbalance ranged from ±5.5% for heat pump setup S1 to ±0% for setup S5. The trend of the mass flowrate imbalance was consistent to the energy imbalance and on average a higher refrigerant mass flowrate was back-calculated from the GC heat balance (except for configuration S5). Explanations for the higher mass flowrate in the GC are the same as for the energy imbalance (as described in section 7.4.1).

The mass flowrate imbalance increased by 2.8% (configuration S6 compared to S7) when the oil was recovered from the LPR and the oil/CO_2-mixture was returned to the compressor. However the change in the imbalance was within the data uncertainty.

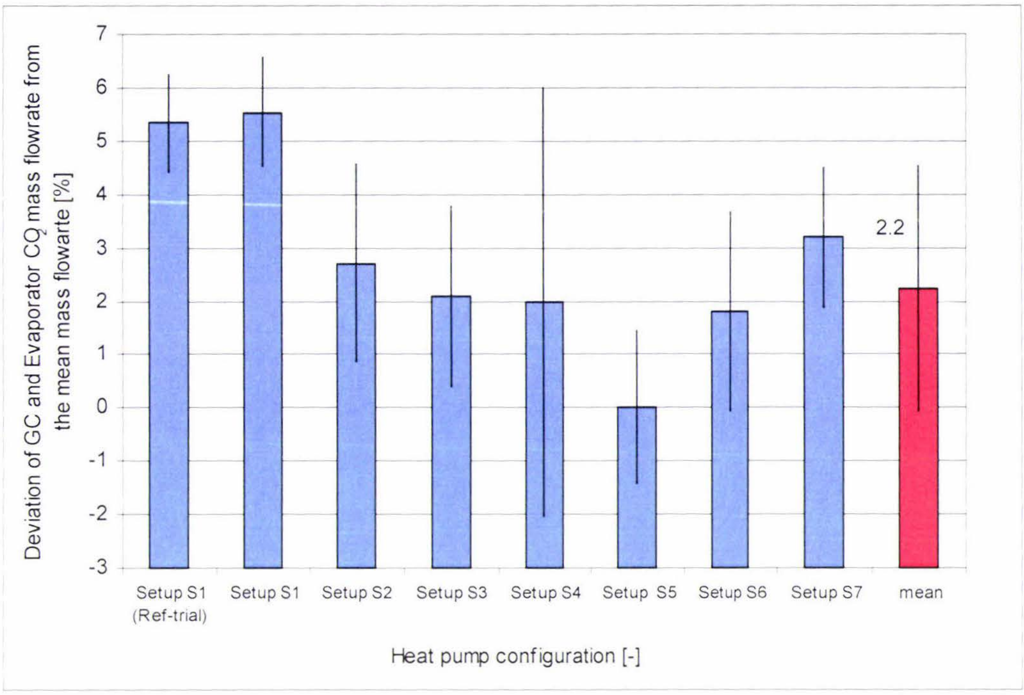

Figure 7.4: Mass flowrate imbalance for the different measurement setups and heat pump configurations

Gas cooler mass flowrate balance

Significant differences occurred in the mass flowrate for the GC units connected in series (GC3.1 and 3.2). Figure 7.5 shows the difference between the mass flowrate calculated for the first GC unit and the second GC as a function of the heat output of the overall GC unit. A negative difference in the mass flowrate corresponds to a higher mass flowrate measured at the second GC unit.

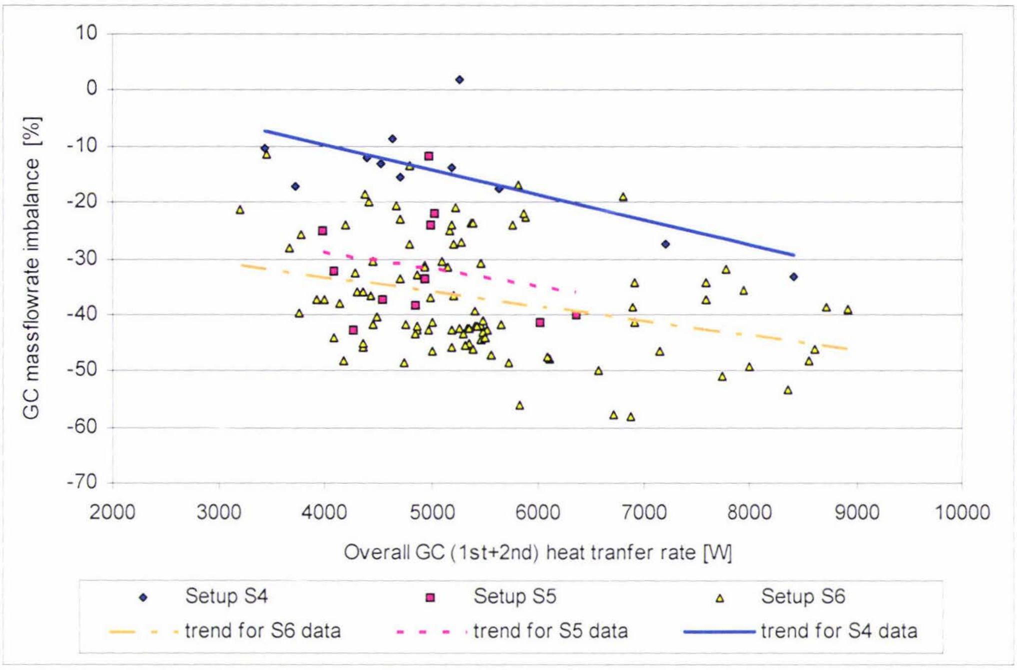

Figure 7.5: Refrigerant mass flowrate imbalance for the GC units that were connected in series as a function of the heat output of the overall GC unit

The mass flowrate back-calculated from the heat balance for the first GC unit of configuration S4 and S6 (GC 1) was on average 15% and 37% lower than the flowrate back-calculated for the second unit (GC2.2). The average imbalance in the refrigerant mass flowrate for configuration 5 (GC 3.2 with GC 2.2 in front of GC 1) was about 32%.

Possible reasons for the overall lower mass flowrate in the first gas cooler than measured at the second unit were:

- Systematic measurement error of the GC temperatures (T1 to T6)
- Pressure drop in the gas cooler (the massflow rate calculations were based on the GC inlet pressure)
- Temperature and pressure sensitive refrigerant enthalpy near the critical point of the working fluid. The GC mass flowrate imbalance was particularly sensitive to the refrigerant temperature and pressure at the conditions that occurred between the two GC units.
- Thermodynamic property uncertainty

Of these reasons, the last two were considered the most significant as the condition between the two GC units was often close to the critical point.

7.5 Heat pump performance

7.5.1 Compressor

The compressor ran at low noise level at all operating conditions. Very occasionally short periods of rattling occurred due to liquid refrigerant entering the compressor during the charging procedure, the compressor start-up and/or when rapidly changing the operation conditions.

The compressor load at the start-up was low because the discharge and the suction pressure quickly equilibrated as soon as the compressor was stopped, so the compressor by-pass valve did not needed to be opened at start-up.

Figure 7.6 and Figure 7.7 show the measured volumetric and isentropic compressor efficiency for all heat pump trial data as a function of the pressure ratio and suction conditions. The predicted compressor performance based on the manufacturer's data for the same compressor model range is also shown (Neksa *et al*, 1999; Dorin and Neksa, 2000). The vapour superheat was 0.7 to 16.9 K.

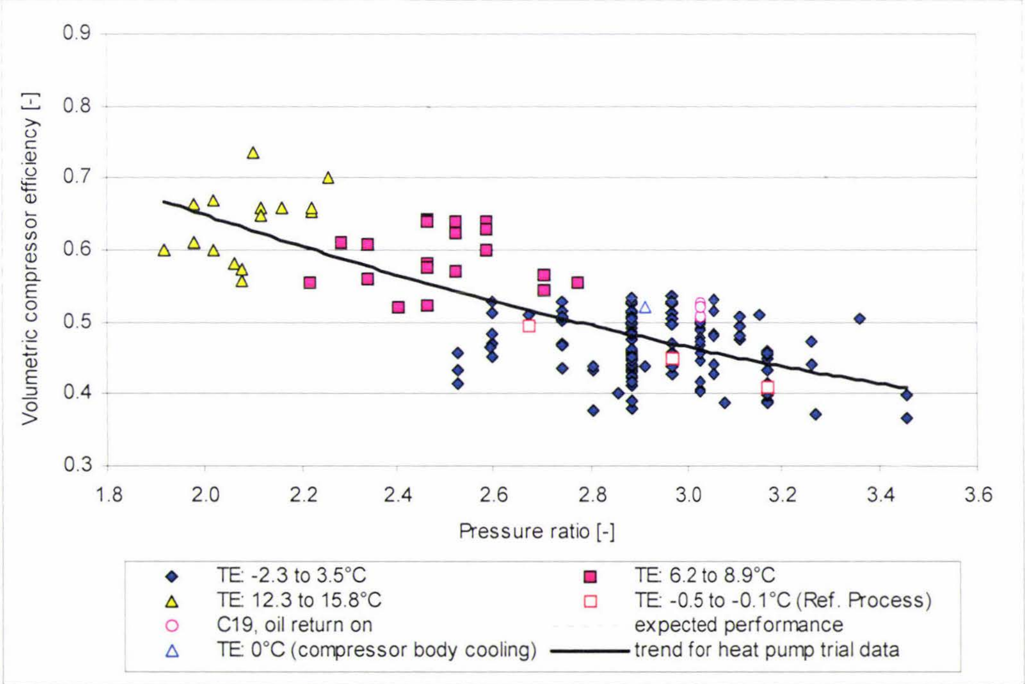

Figure 7.6: Compressor volumetric efficiency as a function of the pressure ratio at 0, 7.5 and 15°C evaporation temperature (TE) and with vapour superheat between 1 and 17 K.

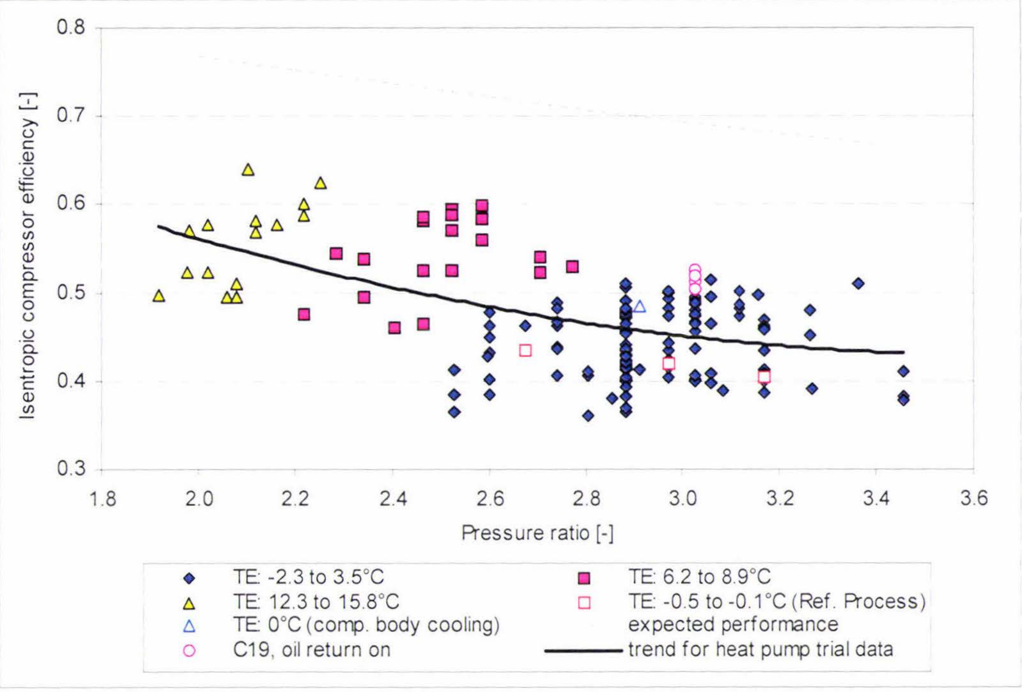

Figure 7.7: Compressor isentropic efficiency as a function of the pressure ratio at 0, 7.5 and 15°C evaporation temperature (TE) and with vapour superheat between 1 and 17 K.

The volumetric efficiency decreased almost linearly with the pressure ratio. The average volumetric efficiency ranged between 0.40 at a pressure ratio of 3.5 to 0.67 at a pressure ratio of 1.9. At the nominal heat pump operating condition (C11, with a pressure ratio of 2.9±0.1) the volumetric efficiency was 0.49±0.04 giving a nominal refrigerant mass flowrate of 76±5 kg/h.

The isentropic efficiency at the nominal heat pump operating condition was 0.47±0.04 and the average isentropic compressor efficiency ranged between 0.43 and 0.58. The effect of the vapour superheat on the compressor performance was within the data uncertainty. A drop in the efficiency at low pressure ratio caused by reduced motor efficiency at low compressor load as suggested by Hubacher and Groll (2003) could not be observed.

Volumetric and isentropic efficiency were both significantly lower than the literature values for the compressor model of the same range (Neksa *et al*, 1999; Dorin and Neksa, 2000). For example at the nominal heat pump operating condition (pressure ratio of 2.9) volumetric and isentropic efficiencies were about 34% lower than expected. However, the literature values were measured for a bigger compressor model with compressor body cooling and at constant discharge pressure of 95 bar.a so a direct comparison of the literature values was not possible.

Figure 7.8 shows the indicated compressor efficiency for all heat pump trials as a function of the pressure ratio. The average indicated compressor isentropic efficiency ranged from 0.75 at a pressure ratio of to 3.5 to 1.0 at 1.9 pressure ratio. The measured values were on average slightly higher at low pressure ratio and lower at high pressure ratio than the manufacturer compressor data which were given for 80 bar.a discharge pressure. As expected the indicated compressor efficiency increased with decreasing pressure ratio (Hubacher and Groll, 2003).

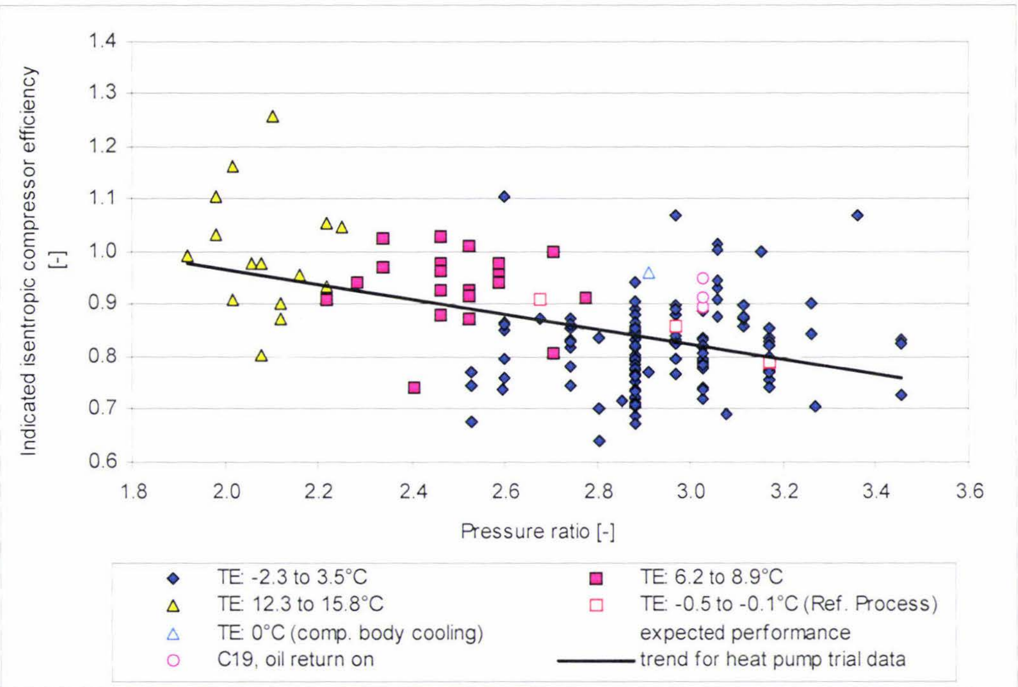

Figure 7.8: Indicated compressor isentropic efficiency as a function of the pressure ratio at 0, 7.5 and 15°C evaporation temperature (TE) and for vapour superheat between 1 and 17 K.

Indicated isentropic efficiency values higher than one imply that the compressor discharge temperature was lower than that for isentropic compression and that there was significant gas cooling during the compression process. Possible explanations for the cooling were:

- Liquid droplet carried over from the LPR leading to refrigerant evaporating in the compressor piston chamber.

- Heat transmission from the gas to the compressor body during the compression (Neksa *et al*, 1999; Dorin and Neksa, 2000).

Droplets in the compressor suction would lead to uncertainties in the back-calculated isentropic and volumetric compressor efficiency because the calculation was based on the mean refrigerant mass flowrate and the refrigerant density for superheated vapour at the compressor suction conditions which were (in case of droplets in the suction) lower than the effective values. However, the compressor efficiencies were only 2.1% higher when the GC based refrigerant mass flowrate (Equ. 5.3) was used for efficiency calculation, rather than the mean mass flowrate (Equ. 5.28).

It was expected that presence of refrigerant and/or oil droplets would increase the apparent volumetric efficiency of the compressor because the actual refrigerant density at the compressor suction would be higher than the density used for the efficiency calculations. Hence the poor volumetric efficiency could not be explained by the droplets alone, however possible reasons for the low compressor volumetric efficiency were:

- Piston leakage problems. A piston leakage problem would be expected to lead to high compressor discharge temperature and/or high convective compressor heat losses. However high discharge temperatures were not measured.
- Excessive vapour superheat inside the compressor suction, leading to low vapour density and thereby reduced refrigerant mass flowrate (Neksa *et al*, 1999).

The effect of the heat transmission from the gas to the compressor body and the convective heat losses respectively on the compressor efficiency was investigated by enhancing cooling of the compressor body with compressed air (comp 4 trial). Under these conditions it was expected that the vapour superheat inside the compressor would reduce due to the enhanced heat losses to ambient air and subsequently the volumetric and isentropic efficiency would improve.

The volumetric and the isentropic efficiency improved by approximately 17% and 11% respectively when the compressor body was cooled (Figure 7.6 and Figure 7.7). However, overall the difference was less than the data uncertainty so it was expected the compressor performance did not suffer from excessive heat transmission from the compressor body to the suction vapour (e.g. caused by a piston leakage problem). This was supported by the overall low compressor discharge temperature and low indicated isentropic efficiency for these trials.

Figure 7.9 shows the measured compressor power consumption of all heat pump trials and the expected performance as a function of the pressure ratio for different evaporation conditions. The average compressor power consumption is indicated by trend lines.

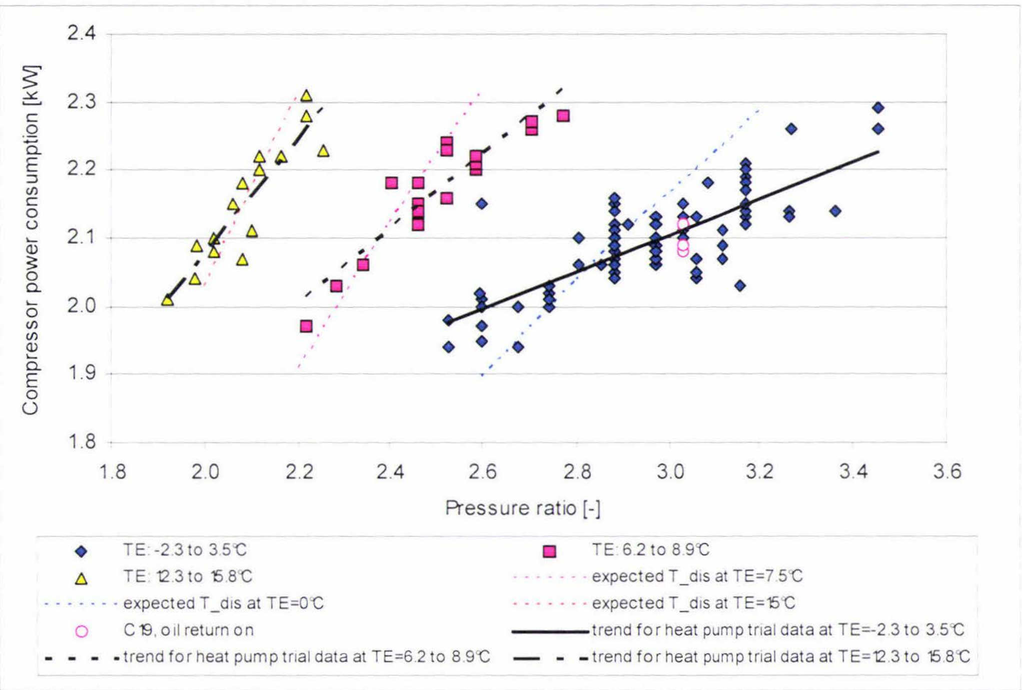

Figure 7.9: Compressor motor power as a function of the pressure ratio at about 0, 7.5 and 15°C evaporation temperature (TE) and with vapour superheat between 1 and 17 K

The power consumption was in the expected range despite reduced refrigerant mass flowrate, except at high pressure ratio where the measured compressor power was lower. This supports the possibility that there was a mechanical compressor problem that reduced the compressor performance at high pressure ratio (e.g. broken valve plate).

Other evidence for a mechanical compressor problem such as noises, excessive rattling, low compressor motor speed, highly variable compressor power consumption and/or compressor overheating were not observed. Figure 7.6 to Figure 7.8 show the compressor performance measured for the compressor reference trial conditions, which was performed once at the beginning of the overall experimental procedure. The volumetric and indicated isentropic efficiency of the reference trial were within the data uncertainty of the compressor performance in the other trials so there was no evidence for compressor performance losses over the experimental period.

Compressor heat losses

The compressor heat losses that were calculated for all the heat pump trials varied widely from 760 W to 1250 W. The correlation between the calculated heat losses and the compressor load and/or the discharge temperature was weak. At the nominal heat pump operating condition the compressor lost on average 718±244 W heat to the ambient air and the heat losses increased by approximately 32% when the compressor body was actively cooled (comp 4 trial).

The heat losses calculated from the energy balance (Equ. 5.36) were on average 1.3 times higher than the losses calculated from the convective heat losses (Equ. 5.37). However, there were considerable uncertainties in the average compressor surface temperature, the surface area of the compressor body and the estimation of the heat transfer coefficient.

Compressor oil

The oil temperature slowly rose to the compressor discharge temperature during each of the trials. Manufacturer recommendations and/or literature values on the maximum oil temperature were not available. The temperature split across the oil cooling coil was about 3 K so it was questionable whether the oil was circulating through the oil cooling coil. However, the oil pressure in the compressor was about 1.9 bar higher than the measured suction pressure of the compressor and excessive body temperature or/and compressor overheating (power cut-off) did not occur, so there was no evidence of a compressor oil pump problem. A possible explanation was a high oil leakage into the compressor discharge so that there was little oil passing through the oil cooling coil.

At the compressor start-up, significant changes in the liquid level in the oil sight glass were observed. The level instantly decreased to approximately 1/3 of the sight glass. The sudden drop in the liquid level was most probably caused by the dissolved CO_2 which evaporated out of the oil as the suction pressure decreased. After shutting down the compressor, the liquid level in the sight glass re-filled by approximately 1/3 within 12 hours. It was expected that considerable amounts of CO_2 (up to 65% at 20°C as described in Figure 4.13) was dissolved in the compressor oil, despite the oil sump heating.

The compressor oil carry-over rate measured in the compressor trials (comp 1, comp 2 and comp 4) was moderate. During stable compressor operation at operating condition C11 the oil level at the sight glass dropped by approximately 0.25 mm/min (0.48 kg/h). This carry-over rate corresponds (at an average CO_2 mass flowrate during the investigated oil leakage trials of 79.2 kg/h) to 0.6% w/w oil in CO_2. Hence it was expected that the oil carry over had marginal affect on the energy imbalance. Much higher oil carry-over rates were reported by Hubacher and Groll (2003) who measured oil leakage up to 14% w/w with the same compressor type.

7.5.2 Gas cooler (GC)

Table 7.1 summarises the average performance of the GC units GC1, GC 2.1, GC 2.2, GC 3.1 and GC 3.2 (all heat pump trials performed with the individual GC unit) at the nominal heat pump operating condition (C11).

Table 7.1: GC performance at the nominal heat pump operating condition (C11)

GC Unit:	GC1	GC2.1	GC2.2	GC3.1	GC3.2
Heat transfer rate [W]	3651	3910	4311	5320	4892
GC UA-value [W/K]	198	220	271	472	394
GC U-value [W/m^{2}K]	748	674	830	798	666
GC effectiveness [-]	0.71	0.75	0.82	0.94	0.90
Design GC UA-value [W/K]	181	148	179	466	655
GC U-value [W/m^{2}K]	379	374	500	638	900

Of the single GC units, the GC design 2.2 performed best at the nominal heat pump operating condition and achieved highest overall heat transfer coefficient. The GC 2.1 heat transfer rate improved by about 10% (GC2.2) when the refrigerant velocity was increased (by approximately 35%) by adding an insert in the refrigerant side. The heat transfer capacity of the single units was too low to efficiently transfer the full heat load of 5.3 kW at the investigated nominal heat pump operating condition (C11).

GC3.1 performed about 9% better than GC 3.2. The higher heat losses that were expected to occur for the GC unit 3.1 were obviously compensated by overall better heat transfer. GC 3.1 achieved a good temperature approach of about 5 K at the refrigerant outlet end of the heat-exchanger, giving a GC effectiveness of 94%. However it was expected that the GC effectiveness would decrease if the design compressor mass flowrates had been achieved because the increase in the overall heat transfer coefficient due to increased refrigerant and water flowrates would not improve at the same rate as the additional heat load. However, the GC refrigerant inlet temperature would also be higher if design compressor performance was achieved and the increased discharge temperature may partly compensate the poor heat transfer coefficient.

Figure 7.10 and Figure 7.11 show the overall GC heat transfer coefficient (U) for the GC 1, GC 2.1, GC 2.2, GC3.1 and GC 3.2 for all heat pump trials performed with the individual GC units as a function of the heat transfer rate. The mean U-value at the design condition (C11) is given as well.

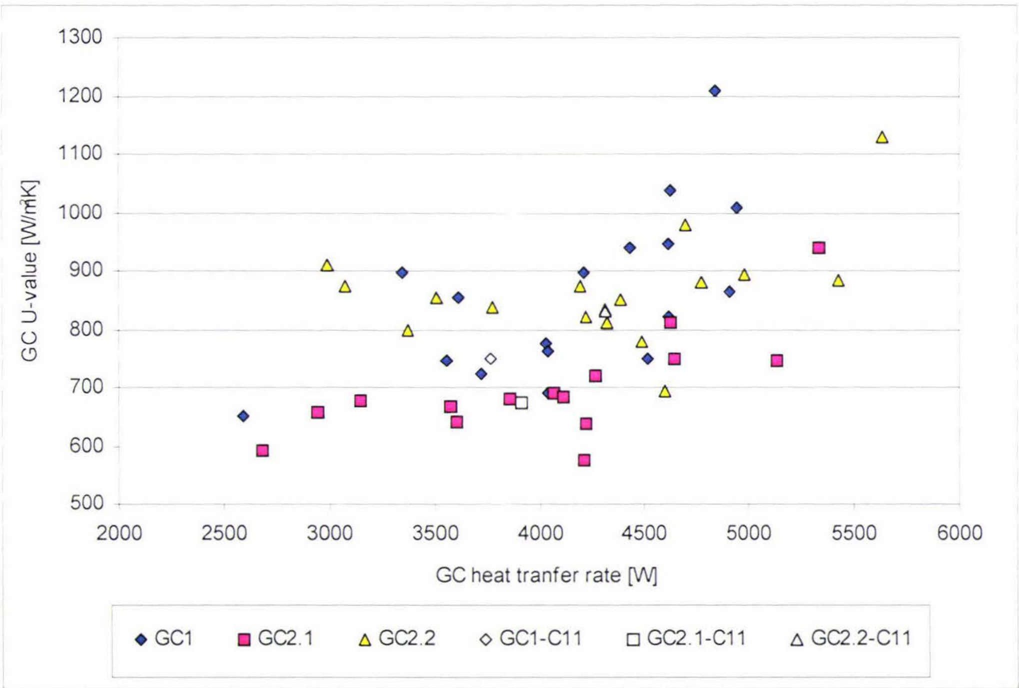

Figure 7.10: U-values of GC 1, GC 2.1 and GC 2.2 as a function of the heat transfer rate.

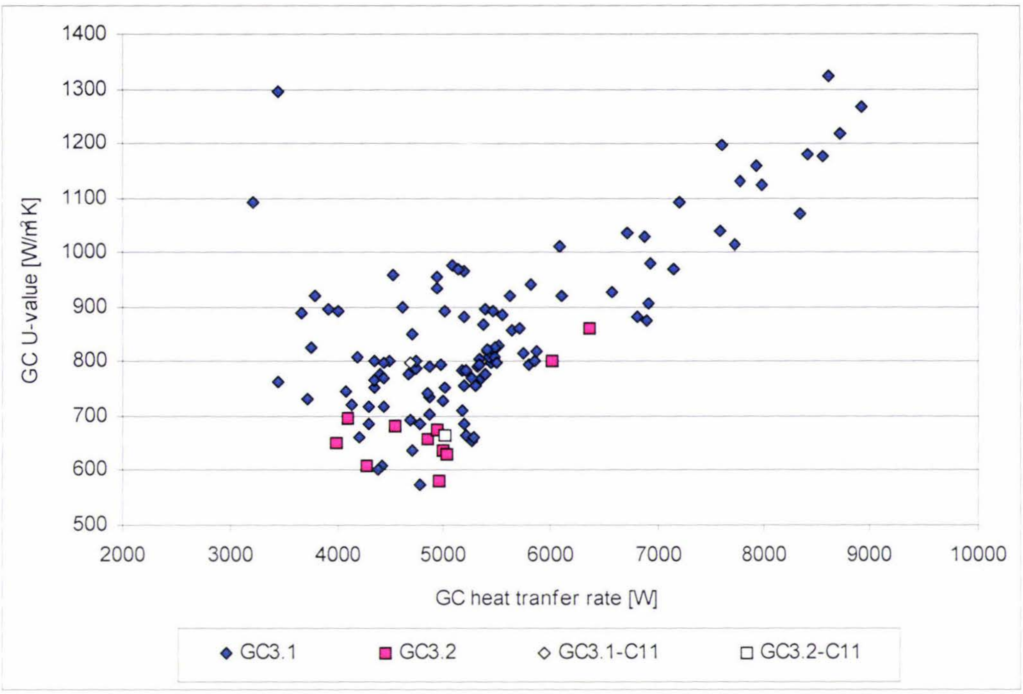

Figure 7.11: U-value of the GC 3.1 and GC 3.2 as a function of the heat transfer rate.

The overall U value for the single GC units (GC 1, GC 2.1 and GC 2.2) ranged from 577 W/m^{2}K to 1207 W/m^{2}K. The U-value of the GC units in series was between 574 W/m^{2}K and 1323 W/m^{2}K for the GC 3.1 and 579 W/m^{2}K to 860 W/m^{2}K for the GC 3.2. The heat transfer coefficient data were broadly consistent with literature values. For example, Yarrall (1998) measured overall heat transfer coefficients between 550 and 1550 W/m^{2}K for a shell and tube gas cooler.

Figure 7.12 shows the U-values of the each GC unit (trial data GC1, GC2.1 and GC2.2 for the conditions C11 to C16) as a function of the water mass flux for constant refrigerant mass flowrate and at 100 bar.g discharge pressure. The trend line is also shown.

The overall heat transfer coefficient changed little above about 430 kg/m^{2}s water mass flux (corresponding to 115 l/h) for GC 1 and above 240 kg/m^{2}s (corresponding to 165 l/h) for GC 2.1 and GC 2.2. This indicates that at higher water flowrate the heat transfer of the GC units was mainly limited by the refrigerant-side heat transfer. However all the GC trials were carried out with significantly lower mass flowrates than the design flowrate so it could not be assessed whether the GC units would suffer from shortage of refrigerant side heat transfer surface if the design nominal heat pump heating capacity was achieved.

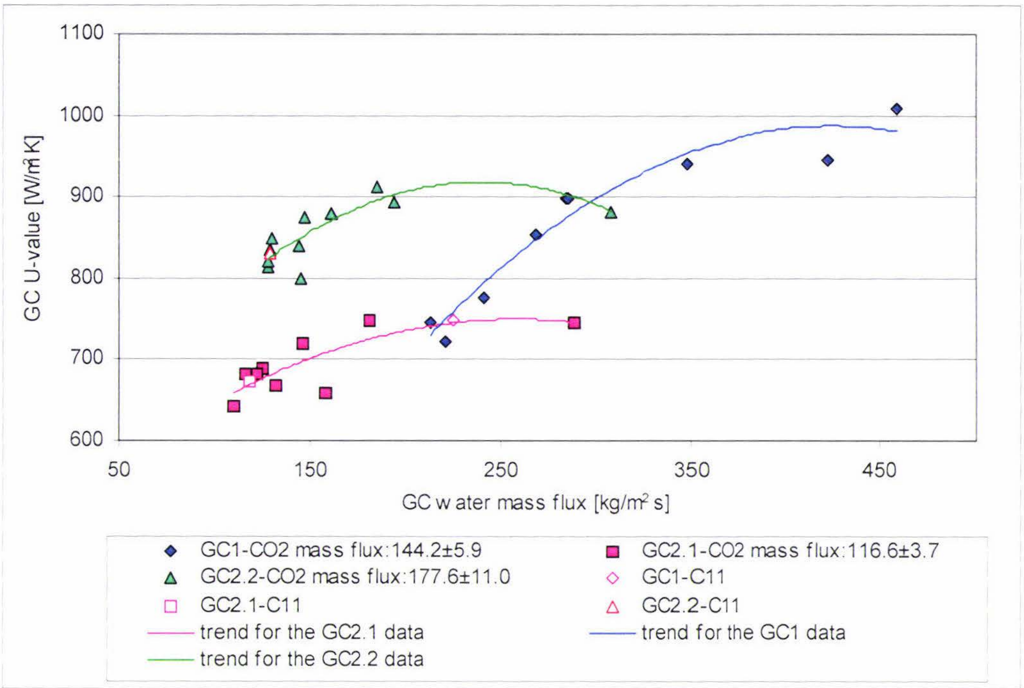

Figure 7.12: U-value of the GC 1, GC 2.1 and GC 2.2 at constant refrigerant mass flowrate as a function of the water mass flux.

The heat transfer coefficients in the single GC units ranged from 1760 W/m^2K to 6250 W/m^2K for the water-side and 835 W/m^2K to 2535 W/m^2K for the refrigerant side. (Figure 7.13). Yarrall (1998) measured values between 700 and 3100 W/m^2K for CO_2 flowing in the annulus of a shell and tube GC. However, the heat transfer coefficients were low compared to those reported by Kim *et al* (2001). They reported 1200 W/m^2K to 8000 W/m^2K measured at 85 bar.g refrigerant pressure, 215-430 kg/m^2s mass flux and 50°C to 40°C refrigerant tube wall temperature.

Figure 7.13 shows the effect of the refrigerant mass flux on the CO_2-side heat transfer coefficient (trial data GC1, GC 2.1 and GC 2.2 at the conditions C11, C17 and C18). At the nominal design condition the GC performance suffered from the low refrigerant heat transfer coefficient due to the refrigerant mass flowrate being significant lower than expected.

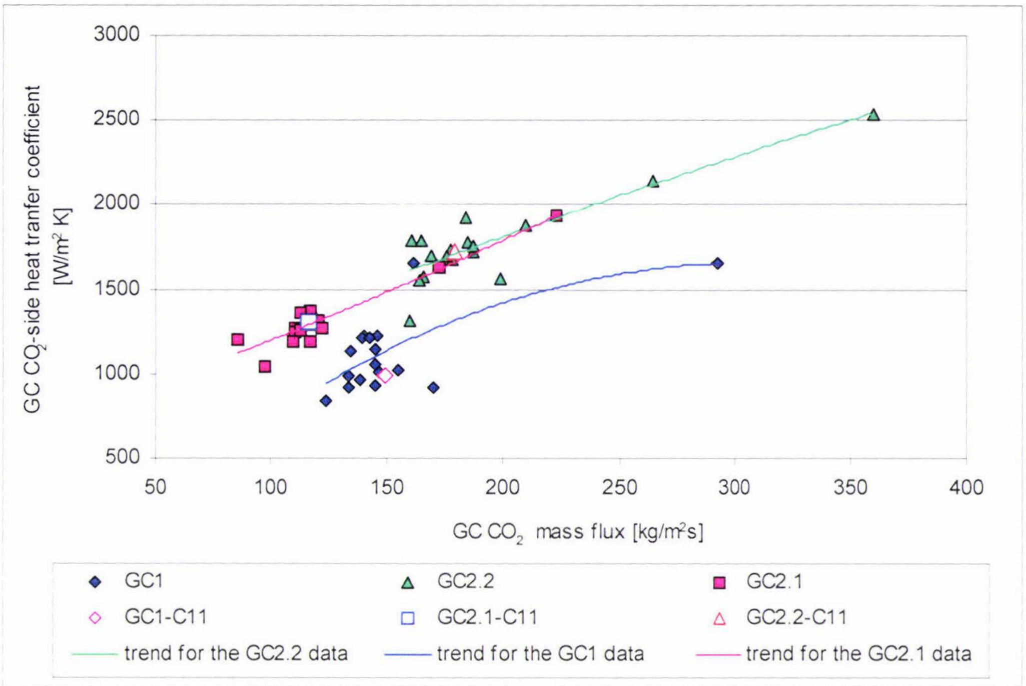

Figure 7.13: Refrigerant side heat transfer coefficient as a function of the refrigerant mass flux and at the nominal heat pump operating condition (C11)

GC 3.1 performed better than GC 3.2 across the whole range of investigated GC conditions (Table 7.1). Hence the main heat pump trials were carried out with the GC 3.1 configuration.

Figure 7.14 shows the effectiveness of GC 3.1 (data for all heat pump trials performed with configurations S4 and S6) at a hot water temperature of 60±1°C as a function of the gas cooler refrigerant inlet temperature and for different GC water inlet temperatures.

The effectiveness of the GC declined with decreasing GC refrigerant inlet temperatures from close to 1 at refrigerant inlet temperatures above 100°C to 63% at 73°C CO_2 inlet temperature. The low refrigerant inlet temperature occurred at high evaporation temperature/pressure and/or low discharge pressure and would lead to a significant temperature pinch effect in the GC. At those conditions, the overall heat pump efficiency could have been significantly improved by operating at higher discharge pressure or by adding additional GC length.

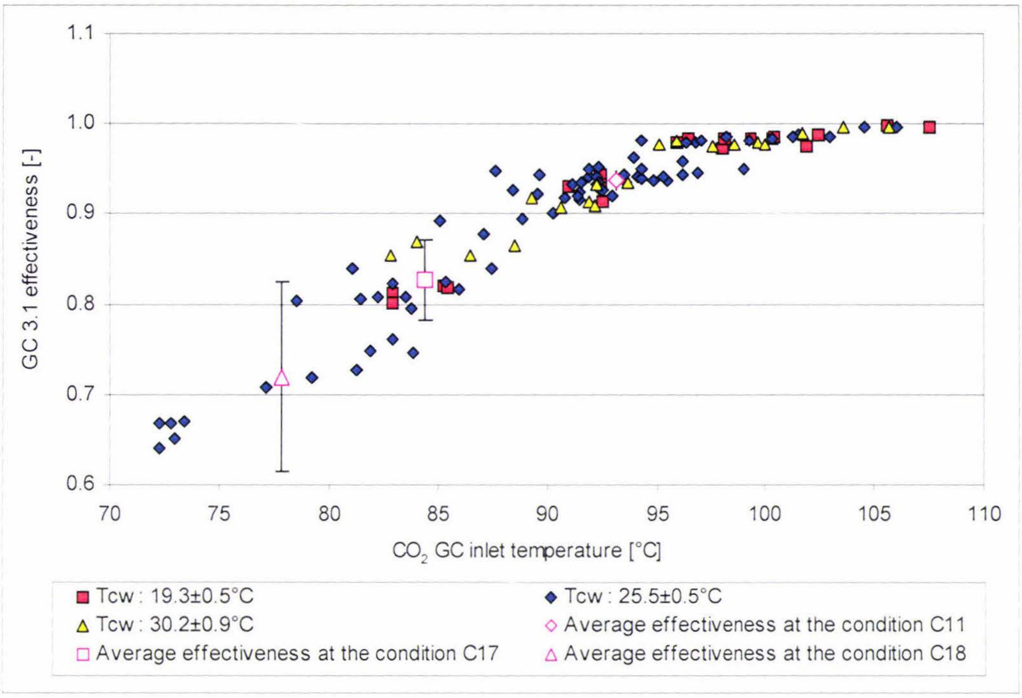

Figure 7.14: GC3.1 effectiveness as a function of the GC refrigerant inlet temperature for 60°C hot water temperature.

The refrigerant pressure drop across GC 1 and GC 2.2 was about 3 bar at a refrigerant mass flowrate of 150 kg/h while the pressure drop across the GC 2.1 was within the data uncertainty of the pressure gauges (less than 1.5 bar). For the GC in series a pressure drop of 4 bar at a mass flowrate of approximately 150 kg/h was measured. This pressure drop was relatively large compared to condensers in conventional heat pumps. However, significant losses due to pressure drop were only expected if the GC refrigerant outlet temperature/pressure was near the critical point of CO_2 (31°C/72 bar.g) because in this range temperature refrigerant enthalpy is sensitive to pressure changes.

The measured GC performance was not directly comparable with the predicted GC design performance because the GC design conditions were significant different from effective GC operation conditions due to low compressor performance. Hence the performance of the GC units was predicted using the design model for the effective operating conditions of the heat pump replicate data (C11, 13 and 18) using measured the GC temperatures, pressures and flowrates as GC input model parameters. Figure 7.15 compares the predicted and the measured GC heat transfer rates of the single and double GC units.

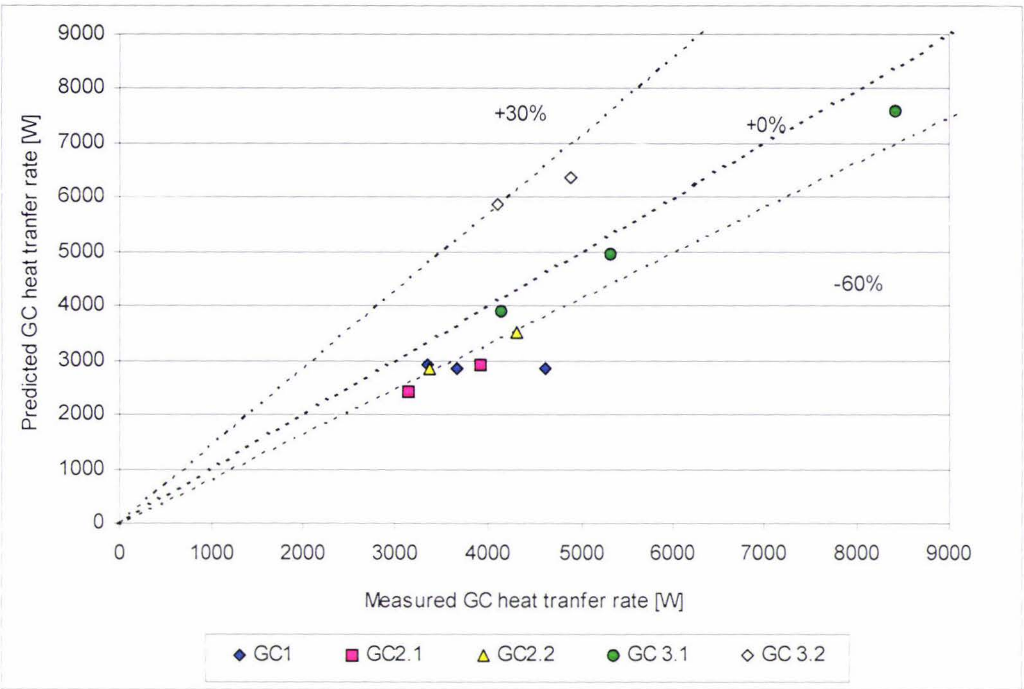

Figure 7.15: Precession of the modelled data

The predicted heat transfer rate of the single GC units was 20 to 60% lower than the measured performance. Good agreement was achieved for the GC unit 3.1 where the heat transfer rate was predicted within 10%. The predicted heat transfer rate of the GC 3.2 was about 20-30% higher than the measured performance. Table 7.1 shows similar trends.

Overall the predicted heat transfer of the GC units was on average 18% too low, expect for the GC 3.2 calculations. However, there were considerable uncertainties such as the heat transfer calculation for supercritical CO_2, the heat transfer enhancement factor for the twisted tubes and the resistance of the double pipe GC construction. For example, it was difficult to assess whether there was less than 30% increase in the tube resistance due to heat conduction of the vented tubes or more than 40% heat transfer enhancement in the corrugated tubes (Chen *et al*, 1996a, 1996b).

The GC 3.2 design predictions were a lot poorer than for other GC units. A possible explanation was over predicted heat transfer towards the refrigerant side outlet of the GC due to an overestimated heat transfer enhancement factor for the CO_2-side corrugated tube. Because the CO_2-side heat transfer coefficient has a peak towards the end of the GC, an overestimated heat transfer enhancement factor significantly affects the overall heat transfer calculation, in particular when low refrigerant side GC outlet temperatures were achieved, such as for the GC in series.

Overall, despite the crudeness of some of the design prediction methods, they were shown to be reasonable accurate.

7.5.3 Internal heat exchanger (IHX)

Figure 7.16 shows the IHX heat transfer rate for all heat pump trials as a function of the IHX effectiveness for different evaporation conditions.

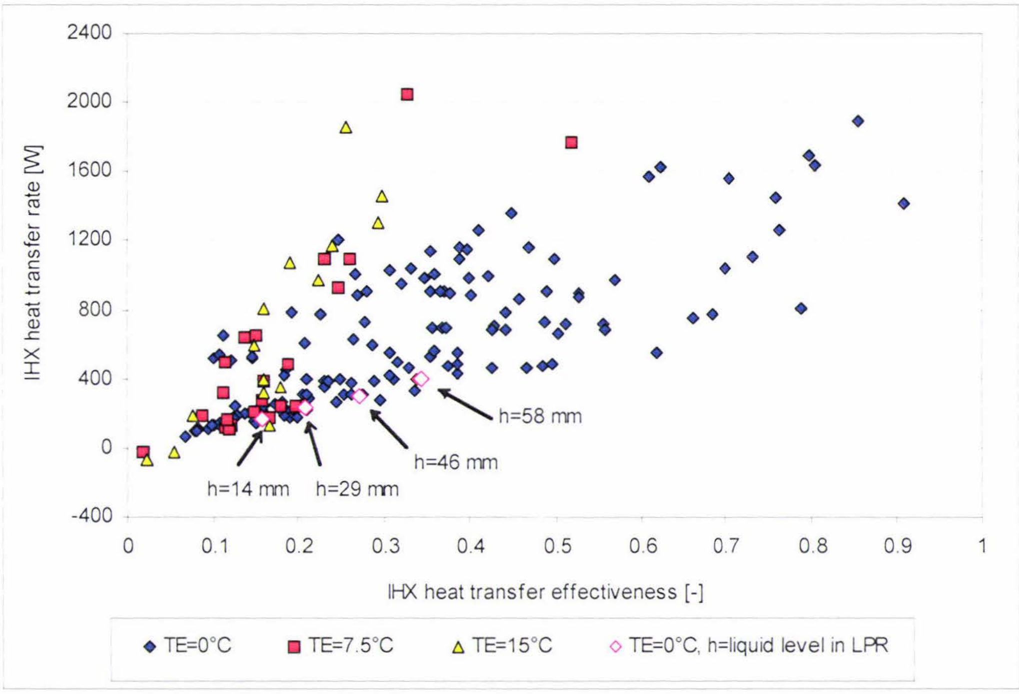

Figure 7.16: IHX transfer heat rate as a function of the IHX efficiency

The IHX transferred 14 to 2050 W to the low pressure refrigerant, depending on the liquid level in the LPR and the refrigerant temperature at the gas cooler outlet. At the nominal heat pump operating condition (C11) the IHX heat transfer rate ranged from 205 to 850 W. The high pressure refrigerant was thereby sub-cooled by 2 to 33 K and the suction superheated by 1.5 to 8 K (over and above some evaporation of refrigerant).

The range of the IHX effectiveness was from 10% for an empty LPR to a maximum of 91%. At 14 and 58 mm height of liquid CO_2 in the LPR (neglecting the accumulation of oil), 105 bar.g discharge pressure and 20°C GC cold water inlet temperature (trial data: CO2-charge 1-4, heat pump condition C19) the IHX effectiveness was 16% and 34% respectively.

The measured IHX UA value ranged from 6 W/K to 149 W/K. At the nominal design condition it was on average 28±28 W/K while at 14 and 58 mm height of liquid CO_2 in the LPR and the heat pump conditions C19 (CO2-charge trial 1-4) the IHX UA was 10 W/K and 26 W/K respectively.

The nominal design IHX heat transfer rate of 1.2 kW and the UA value of 127 W/K were not achieved. An IHX effectiveness higher than 50% was only achieved at high liquid level in the LPR, which occurred at low suction pressure/temperature. Reasons for the poorer than desired heat transfer was the small heat transfer surface, in particular on the low-pressure side and the refrigerant mass flowrate being lower than expected.

Figure 7.17 shows the overall IHX U-value based on the low-pressure side surface area as a function of the IHX effectiveness for different evaporation conditions. The U value varied between 100 W/m^{2}K (empty LPR) and 2800 W/m^{2}K. At 58 mm liquid CO_2 in the LPR (CO2-charge4 trial, condition C19) the U-value was 482 W/m^{2}K; at this condition approximately 59% of the low side IHX surface was in the liquid refrigerant. The effect of the oil accumulation was not measured.

The IHX U-Value increased approximately linearly with the IHX effectiveness except above about 0.6 where the increase in the U-value was enhanced. A possible reason for this effect was that the low pressure- side of the IHX was fully covered by liquid CO_2 (liquid level >100 mm) so that the U-value mainly depended on the CO_2 flow in the high-side.

Yarrall (1998) measured IHX U-values in the range of 600 W/m^{2}K and 1400 W/m^{2}K, however their IHX configuration was located after the LPR and hence was operating with only refrigerant vapour phase on the low side.

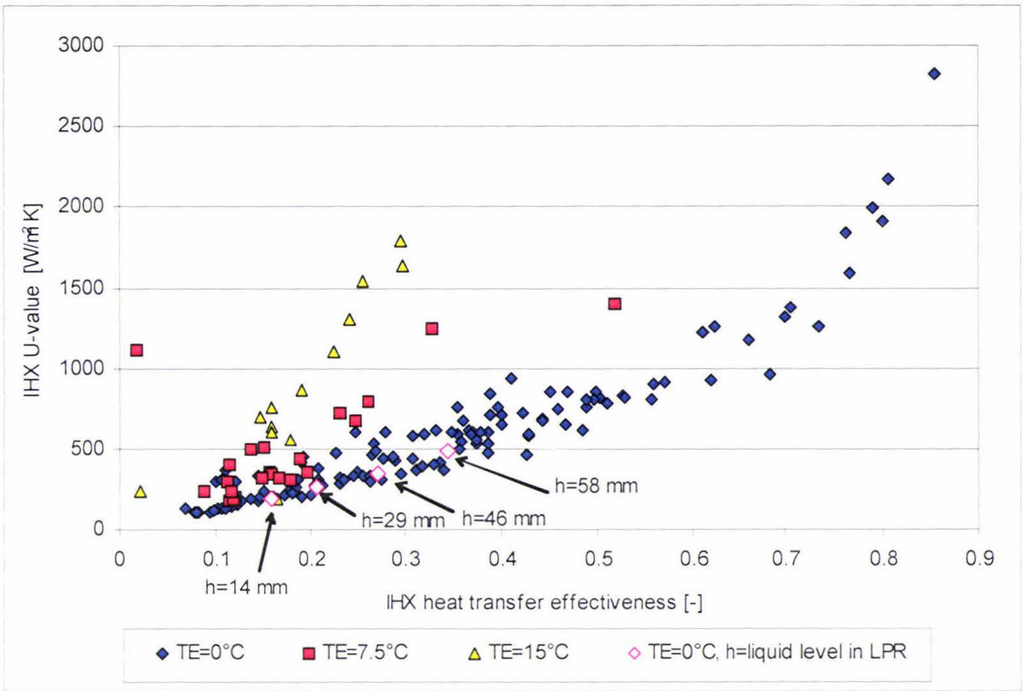

Figure 7.17: Overall heat transfer coefficient of the IHX as a function of the IHX effectiveness

The measured pressure drop in the high-side of the IHX ranged from 2 bar at a volumetric flowrate at the IHX inlet of 0.7 m^3/h (C24 to C26) to 12 bar at 1.2 m^3/h (C5). An effect of the oil fouling on the pressure drop was not expected to occur nor measured in the experiment because of the high solubility of the oil in the CO_2 in the supercritical region (Hauk *et al*, 2001). The reason for the high pressure drop was the undersized inner diameter of the IHX coil (as described in section 4.5.4).

The measured pressure drops were in the range of the predicted values for a straight tube however the actual refrigerant flow was significantly lower than the design flowrate used for the pressure drop calculations. A possible reason for the apparent higher pressure drop was the coil-shaped tube.

7.5.4 Evaporator

The evaporator was initially designed as co-current heat exchanger, however more precise evaporation temperature control was achieved with the water flowing counter-current to the refrigerant.

The measured evaporator heat transfer rate in all heat pump trials varied from 1450 W to 7333 W depending on the heat pump operating conditions and the heat transfer rate of the internal heat exchanger. At the nominal heat pump operating condition (C11), the average evaporator heat transfer rate was 3625±670 W.

The measured evaporator UA value was 200 W/K to 930 W/K giving an overall heat transfer coefficient between 730 W/m^{2}K and 3390 W/m^{2}K. At the nominal heat pump design condition (C11) an average UA value of 475±70 W/K was measured, giving a U value of 1725±250 W/m^{2}K.

The measured UA at the nominal heat pump operating condition was 25% lower than the design UA-value of 637 W/K. At the nominal design operating conditions the heat transfer was constrained by heat transfer surface shortage but the lower refrigerant and water flowrates than expected, gave less turbulent flow in the tubes and subsequently lower U-value. It was expected that at the design heat load of 6.4 kW the evaporator could not be operated with cold water from the mains (which could only be cooled to 0°C due to freezing) because the evaporator performance would be limited by the LMTD.

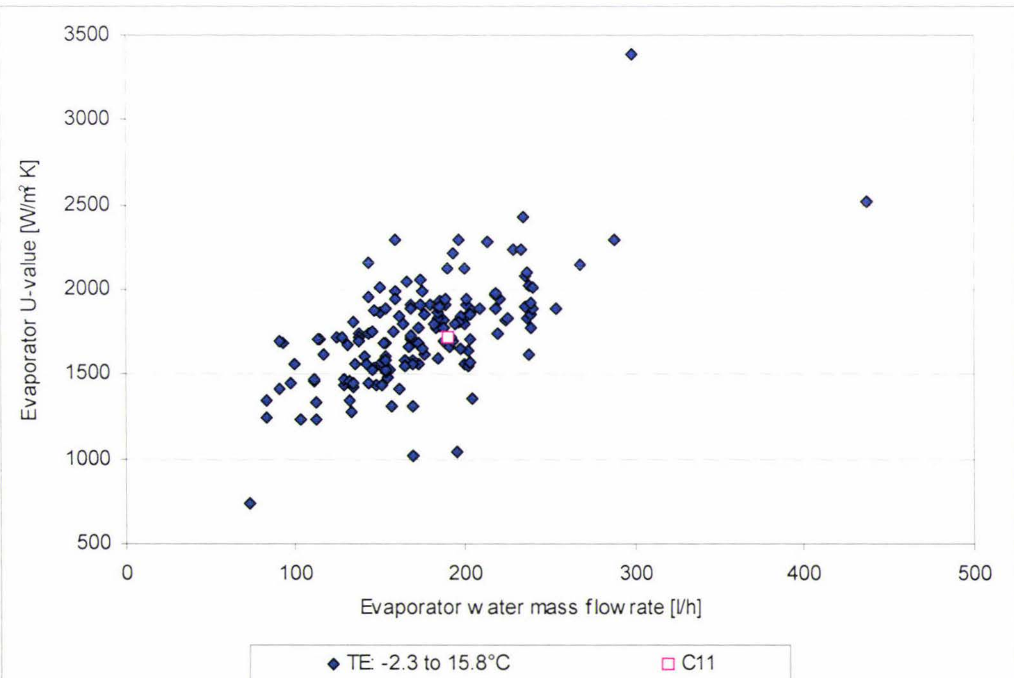

Figure 7.18: Overall U value for the evaporator as a function of the water mass flux.

Figure 7.18 shows the overall heat transfer coefficient for the flooded evaporator for all the heat pump trials as a function of the water mass flowrate and the mean heat transfer coefficient at nominal heat pump operating condition (C11).

The water side heat transfer coefficient was 1650 W/m^{2}K to 7290 W/m^{2}K at a water mass flowrate between 0.02 to 0.12 kg/s, giving a refrigerant side heat transfer coefficient of 1360 W/m^{2}K to 17680 W/m^{2}K. Figure 7.19 shows the refrigerant side heat transfer coefficient for boiling CO_2 as a function of the refrigerant mass flux.

Overall the heat transfer coefficients values were consistent to those reported in literature. Yarrall (1998) measured U-values in the range from 500-1300 W/m^2 K for a shell and tube evaporator while other literature values for boiling CO_2 inside horizontal tubes and evaporation temperatures between -28°C to 15°C ranged from 2000 to 16000 W/m^2 K (Hwang *et al* 1997a; Rieberer and Halozan, 1997; Zhao *et al*, 1997; Yun *et al* ,2001).

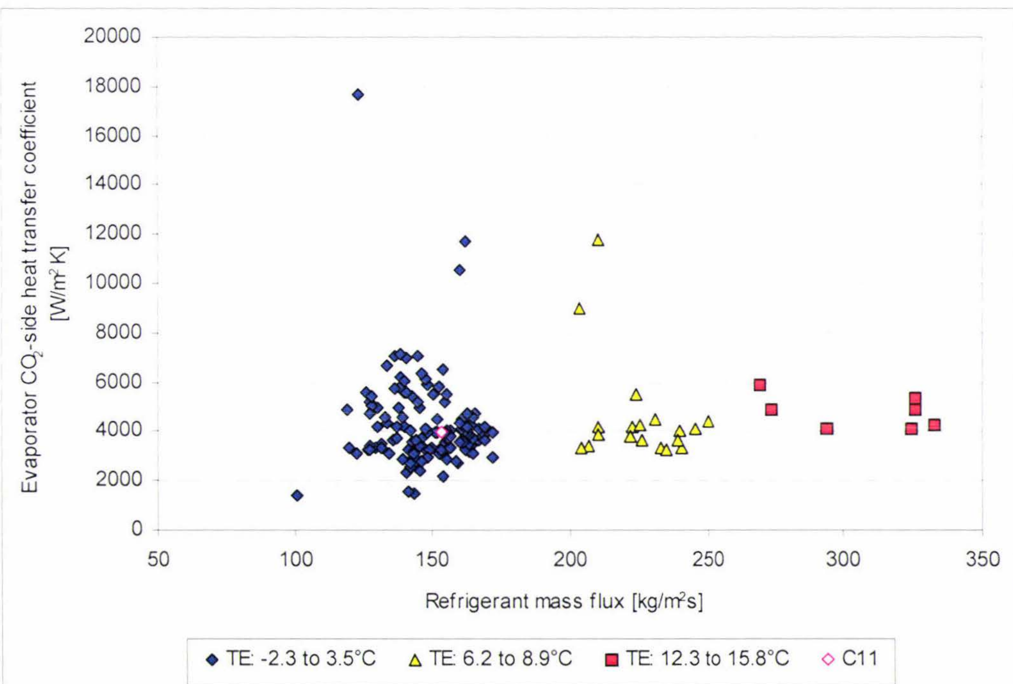

Figure 7.19: Refrigerant side heat transfer coefficient for the evaporator as a function of the refrigerant mass flux.

The pressure drop across the refrigerant side of the evaporator was less than 1.5 bar and hence within the measured uncertainty of the pressure gauges. Any effect of the pressure drop on the evaporation conditions, such as a temperature change in the saturated refrigerant between the evaporator inlet and outlet was not measured.

7.5.5 Low pressure receiver (LPR)

Separation capacity

The suction vapour quality was not directly measured but it was indicated by the suction superheat, the gas velocity in the LPR and the apparent compressor efficiency. The indicated isentropic compressor efficiency seemed related to the amount of cooling of the vapour during the compression. Hence any refrigerant droplets that were carried over into the compressor due to limited LPR separation capacity increase the indicated compressor efficiency.

The possibility of liquid carry over increases with rising gas velocity in the LPR due to the enhanced dragging force on the droplets. The liquid droplet can exist despite vapour superheat but the likelihood that such droplets exist in the CO_2 vapour phase decreases as the superheat increases. Figure 7.20 shows the vapour superheat for all heat pump trials as a function of the gas velocity in the LPR and for different evaporation conditions as well as the trend line.

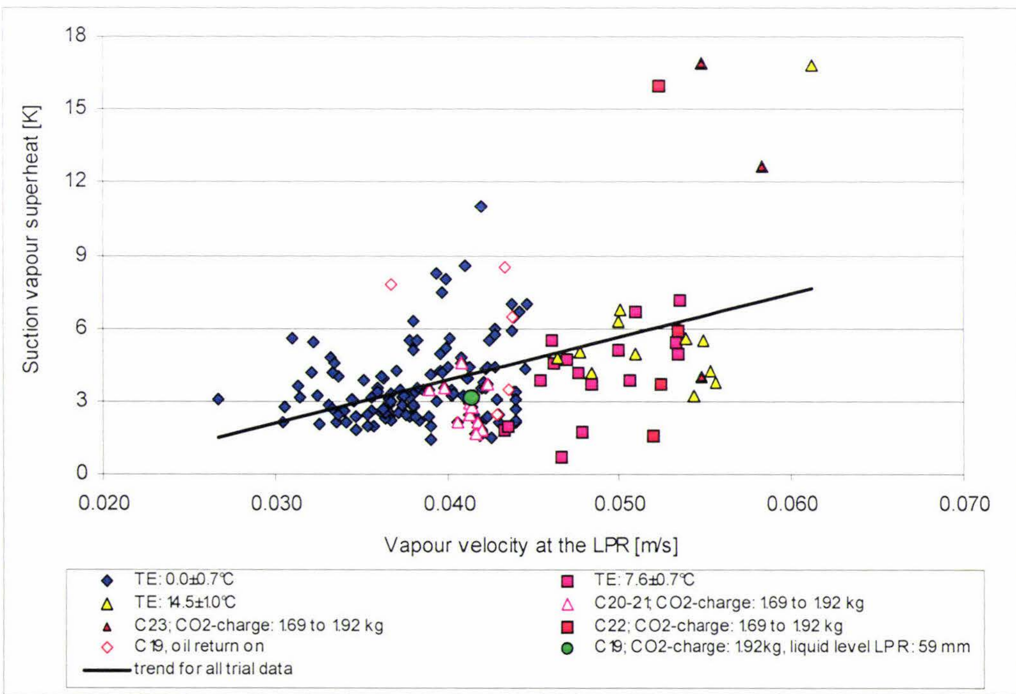

Figure 7.20: Vapour superheat as a function of the gas velocity in the LPR at different evaporation conditions.

The vapour velocity ranged from 0.027 to 0.061 m/s and the vapour superheat from 0.7 to 16.9 K. The trend line of the trial data indicates that the superheat increases with increasing vapour velocity, so while at high velocity liquid droplets were more likely to be carried over into the suction it was unlikely that the droplets could continue to exist for long because of the superheat.

Figure 7.21 shows the relationship between the amount of gas cooling during the compression (indicated isentropic efficiency) and the vapour velocity in the LPR.

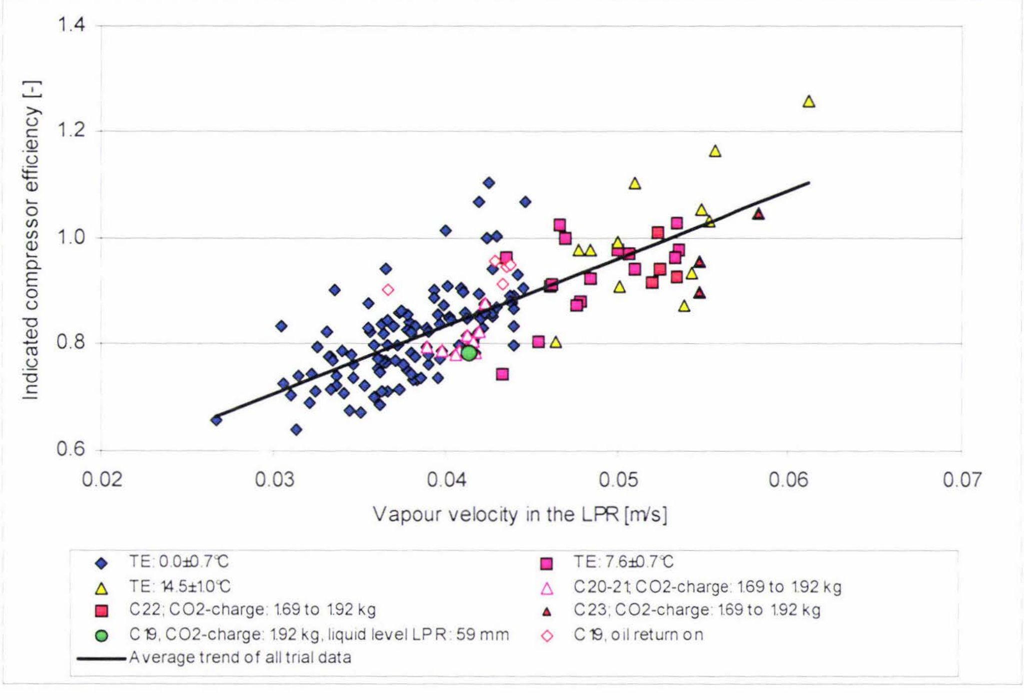

Figure 7.21: Calculated compressor efficiency as a function of the gas velocity in the LPR

The indicated isentropic compressor efficiency ranged from 0.66 to 1.26 and overall the efficiency increased with increasing gas velocity and vapour superheat (as shown in Figure 7.20). High indicated efficiency values indicate that there was significant gas cooling during the compression.

Because of the high indicated efficiency values and the overall energy- and mass flowrate-imbalance (as described in 7.4), it was postulated that some liquid droplets were carried over despite high superheat. The indicated isentropic efficiency was correlated to the pressure ratio (efficiency improves with decreasing pressure ratio) and subsequently to the mass flowrate and gas velocity in the LPR, so it was difficult to assess whether droplets were carried over at all heat pump operating conditions, the amount of liquid being carried over, and/or the critical gas velocity for liquid carry-over.

The investigated range of vapour velocity (0.03 and 0.06 m/s) was 1.7 time lower than the design velocity and about 3 times lower than the recommended terminal velocity proposed by Wiencke (2001) respectively. Problems with liquid carry over were also reported by Yarrall (1998) using a gravity liquid separator with a design separation velocity of 0.18 m/s. Possible reasons for liquid carry over despite low vapour velocity were:

- Oil foaming in the LPR.
- Lower terminal gas velocity for separation than proposed by Wiencke (2001) due to smaller droplet diameter of the CO_2 and/or CO_2/oil-mixture.
- Turbulent flow pattern in the LPR.
- Reduced separation length caused by refrigerant overcharge, oil foaming and/or oil accumulation.

Overall, there would be more droplets entering the compressor suction at high gas velocity and high superheat than at low velocity and low superheat. However, conversely the energy imbalance improved with increasing gas velocity and superheat. Possible explanations were:

- A stronger effect of the vapour superheat on the liquid carry over than the gas velocity
- Increased evaporation of the droplets in the suction line at high gas velocity
- Liquid carry over that occurred independently of the investigated gas velocity and vapour superheat (e.g. caused by oil foaming in the LPR, reduced separation length due to refrigerant overcharge, oil foaming and/or oil accumulation and/or turbulent flow pattern in the LPR).

Volumetric capacity

During the refrigerant charging trials (at conditions C19 to C21), the LPR was operated with a ballast volume between 80 and 310 g liquid CO_2 corresponding to about 14 and 59 mm liquid level at 0°C evaporation temperature and a refrigerant liquid density of 929 kg/m^3 (the system was charged with 1.69 to 1.92 kg CO_2 whereas the evaporator started to operate flooded at 1.61 kg CO_2). The vapour superheat for those trials was slightly lower than the average superheat for the rest of the trials (Figure 7.20 and Figure 7.21) but there was no other observable effect of the ballast volume and liquid level in the LPR on separation quality.

At 105 bar.g discharge pressure the refrigerant system had to be charged by an additional 75 g to keep the evaporator flooded when the evaporation conditions were changed from 0°C/33.9 bar.g to 7.5°C/41.2 bar.g and by 240 g when changing from 0°C/33.9 bar.g to 15°C/49.8 bar.g respectively. The relative increase in the ballast volume when reducing the gas cooler water inlet temperature could not be measured but the experience with the prototype suggested that more CO_2 was shifted between the high-side and the LPR when the water temperatures were changed than when changing the evaporation temperatures. Hence it was concluded that the design surge volume (200 g) for changing heat pump conditions and the design ballast volume (100 g at design conditions) were too low and the overall LPR volume was too small.

7.5.6 Heat pump process

Figure 7.22 shows the average heat pump COP for heat pump configuration 6 (hp90 to hp110 trials) as a function of the discharge pressure at different heat pump cold water inlet temperatures and varying evaporating conditions. The hot water temperature was 60±1°C and the vapour superheat varied between 0.7 K and 8.1 K. The trend of the average COP data is indicated by polynomial trend lines. The predicted performance at the nominal heat pump design condition (C11) is shown in the figures.

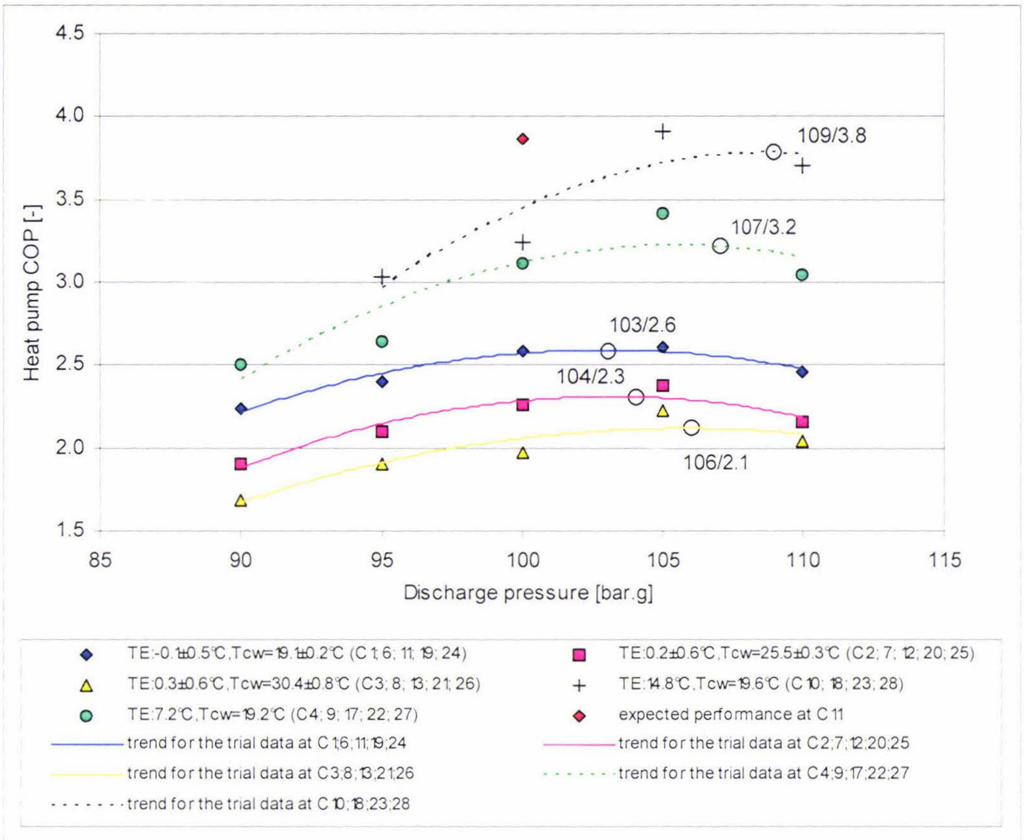

Figure 7.22: Heat pump COP as a function of the discharge pressure at 60°C hot water temperature, varying cold water temperatures and varying evaporation temperature and pressure.

At the nominal heat pump operating condition (C11) an average COP of 2.6 was measured. At -0.1°C/33.8 bar.g evaporation temperature/pressure the heat pump COP ranged from 1.7 (at 90 bar.g and 30.4°C GC water inlet temperature (C3)) to 2.6 (at 105 bar.g and 19.6°C GC water inlet temperature (C19)). Overall the efficiency of the heat pump at 0°C/33.8 bar.g evaporation temperature/pressure decreased by about 20-25% when the GC water inlet temperature was increased from 20°C to 30°C. At changing evaporation temperatures/pressures the COP was between 2.2 (at -0.1°C/33.7 bar.g evaporation temperature/pressure, 90 bar.g discharge pressure and 19.1°C GC water inlet temperature (C3)) to 3.8 (at 14.7°C/49.4 bar.g evaporation temperature/pressure, 105 bar.g discharge pressure and 19.6°C water inlet temperature (C23)).

Figure 7.23 shows the heating capacity of the heat pump as a function of the discharge temperature.

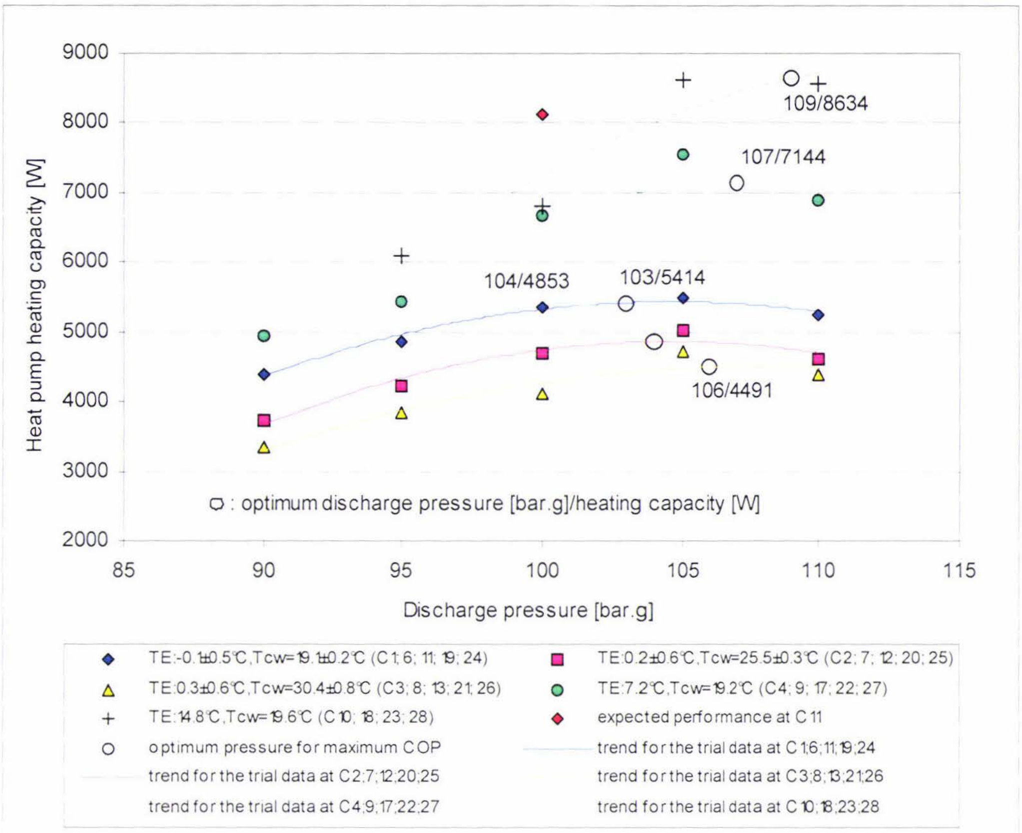

Figure 7.23: Heat pump heating capacity as a function of the discharge pressure for 60°C hot water temperature, varying cold water temperatures and evaporation temperature/pressure.

The heat pump heating capacity varied from 3.1 kW (-0.1°C/33.8 bar.g evaporation temperature/pressure, 90 bar.g and 30.4°C GC water inlet temperatures (C3)) to 8.5 kW (at 14.8°C/49.6 bar.g evaporation temperature/pressure, 105 bar.g and 19.6 GC water inlet temperature (C23)). At the nominal heat pump design condition the heat pump had a heating capacity of 5.3 kW, corresponding to 112 litres per hour of hot water at 60°C. As described by Neksa (1994), the heat pump achieved the maximum capacity at slightly higher discharge pressure than the maximum COP, however the difference was small.

The heat pump performance was not as good as predicted in design cycle calculations. At the nominal heat pump conditions (C11), the heating capacity and the COP were about 34% lower than expected. However the heat pump predictions were carried out for 15°C cold water temperature rather than the measured temperature of about 19°C so a direct comparison of the data was difficult. The main reason for the overall lower COP and heating capacity measured for the prototype was the poor compressor performance but it was expected that the design heat pump performance would not have been achieved if the design compressor performance was achieved due to the limited GC performance.

In other work, a COP 4.2 (at 0°C evaporating temperature, 10°C to 60°C water temperatures) was measured by Halozan and Rieberer (1999). Zakeri *et al* (2000) achieved a heat pump of COP 5.77 (at 15°C evaporation temperature and 6.7 to 66°C water temperatures) while field data with a seasonal COP of 3 to 4 were reported by Saikawa and Hashimoto (2000).

Figure 7.24 and Figure 7.25 show the thermal efficiency (relative to the Carnot cycle) for the heat pump based on an air source evaporator with a LMTD of 10 K, as a function of the discharge pressure for different GC water inlet temperatures and different evaporation conditions.

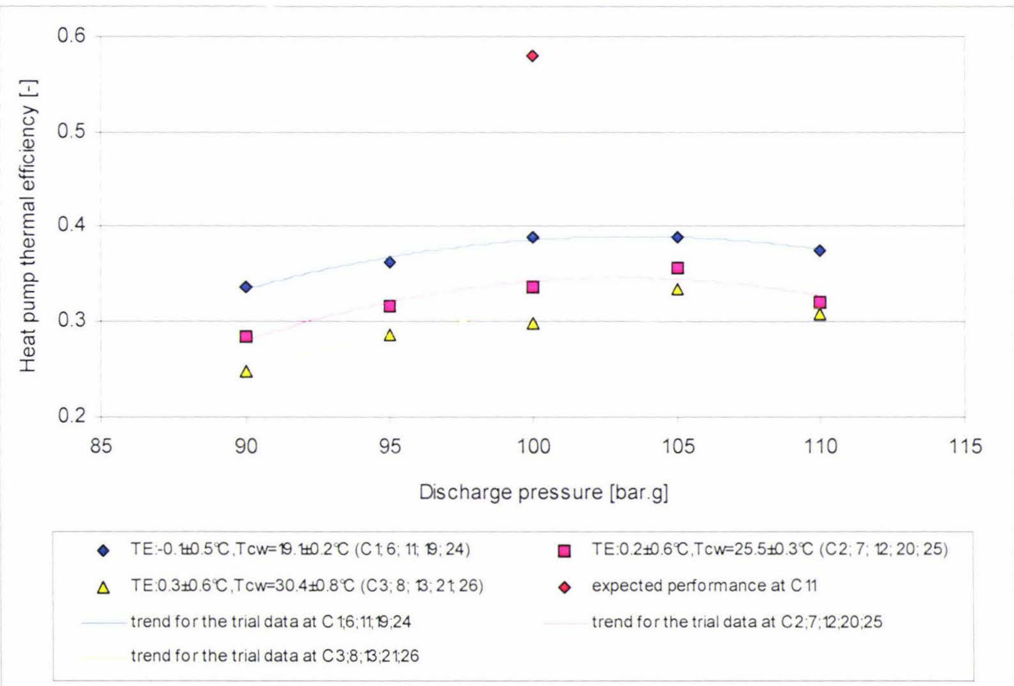

Figure 7.24: Heat pump thermal efficiency relative to the Carnot efficiency for 60°C hot water temperature and 0°C/33.8 bar.g evaporation as a function of the discharge pressure and cold water temperatures.

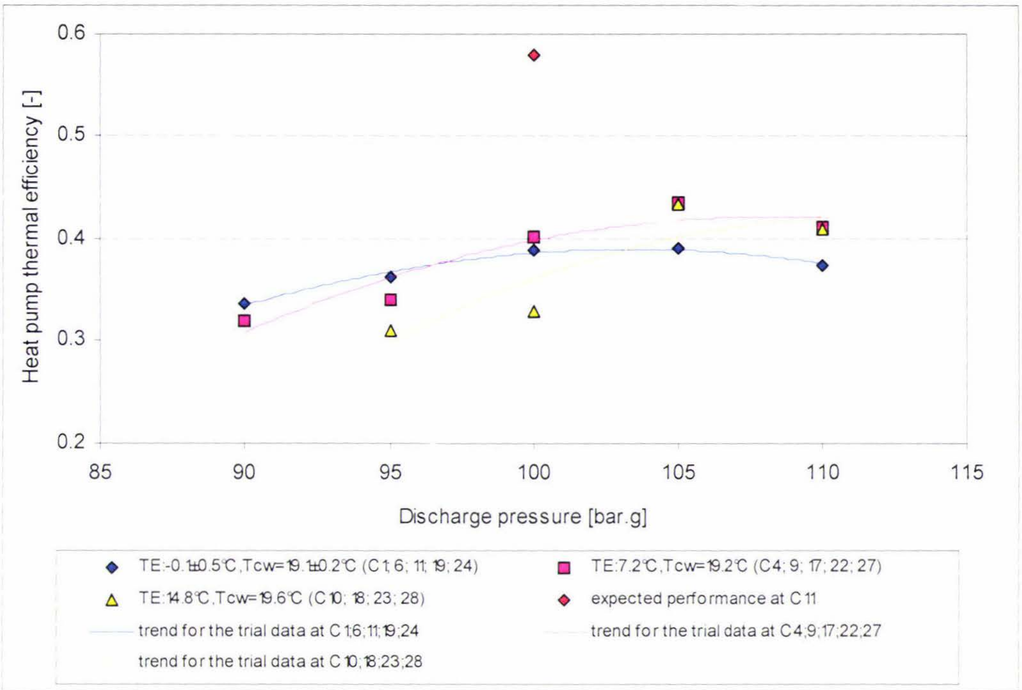

Figure 7.25: Heat pump thermal efficiency relative to the Carnot efficiency for 20 to 60°C cold to hot water temperature as a function of the discharge pressure and evaporation temperature/pressure.

The heat pump thermal efficiency ranged from 25% (at -0.1°C/33.8 bar.g evaporation temperature/pressure, 90 bar.g and 30.4°C GC water inlet temperature (C13)) to 43% (at 7.2°C/50.0 bar.g evaporation temperature/pressure, 19.2°C GC water inlet temperature and 105 bar.g (C22)). At the nominal heat pump design condition an average efficiency of 39% was measured. The heat pump thermal effectiveness at 7.5°C/41.2 bar.g evaporation temperature/pressure was higher than the efficiency at 15°C/49.8 bar.g. Reason for this was the GC performance constraints at high suction conditions. These may have been relieved by operation at higher discharge pressure.

Literature values of the thermal efficiency of CO_2 water heaters were not available but the measured values were slightly lower than the thermal efficiency of conventional heat pumps, which typically operate with maximum efficiency of about 0.5 (Egger, 1987).

Table 7.2 summarises the optimum discharge pressure and the maximal COP measured for different GC water inlet temperatures and different evaporation temperatures. These pressures were higher than the literature values for CO_2 hot water heaters, such as 90-100 bar.g optimum high pressure at 60°C hot water, 20-30°C cold water inlet temperature and 0-15°C evaporation temperature respective (Rieberer and Halozan (1998) and Neksa (1994)). Reason for the higher pressures for maximum COP was the gas cooler performance, which was sensitive to the compressor discharge temperature.

The pressure for maximum COP ranged from 103 bar.g at 0°C/33.8 bar.g evaporation temperature/pressures and 20/60°C water temperatures to 109 bar.g at 15°C/49.8 bar.g evaporation temperature/pressures respectively (Figure 7.22). Within that range, the discharge pressure had little effect on the maximum COP (Table 7.2). Deviations in the discharge pressures from the pressure for maximum COP of ±5 bar lead to COP changes of less than 3%. Even less effect of the discharge pressure on the COP of a heat pump for water heating was measured by Rieberer *et al* (2000), with ±2.5% deviation from the optimum COP at pressures of ±10 bar from the optimum. The reason for the stronger effect of the discharge pressure on the maximum COP for this prototype was the GC size which led to discharge-temperature sensitive performance. This effect was expected be greater if design compressor performance had been achieved due to the undersized GC performance.

Within the investigated range of operating conditions, control to a constant discharge of 105 bar.g would be sufficient to achieve near maximum COP's. Table 7.2 shows the maximum deviation of the COP at 105 bar.g from the optimum. Maximum COP losses of approximately 1.6% were expected at evaporation temperature of 7.5°C and 15°C respectively, while at all other conditions the losses were expected to be less than 1%.

Table 7.2: Discharge pressure for maximum COP's

Cold water temperature	Evaporation temperature	Discharge pressure for maximum COP	Maximum COP	COP at 105 bar.g discharge pressure	COP losses at constant 105 bar.g discharge pressure control
[°C]	[°C]	[bar.g]	[-]	[-]	[%]
19.2	-0.2	103	2.59	2.58	<1
25.5	0.2	104	2.31	2.30	<1
30.4	0.3	106	2.12	2.12	<1
19.4	7.5	107	3.22	3.17	1.6
19.7	14.7	109	3.78	3.72	1.6

For 15°C evaporation temperature, GC water inlet temperatures higher than 20°C were not investigated. However from the trend of the optimum pressure at 0°C/34.9 bar.g evaporation temperature/pressure it was expected that when the water temperature increases from 20°C to 25°C or 30°C, the COP would decrease to the extend that a constant pressure control may not be appropriate. However, such conditions were not likely to occur frequently if the heat pump was used with a stratified HWC.

Overall maximum heat pump performance was achieved at 105 bar.g discharge pressure, hence most subsequent heat pump trials and the HWC trials were performed at this discharge pressure. Figure 7.26 to Figure 7.29 shows the heat pump COP and the heating capacity at 105 bar.g discharge pressure as a function of the evaporation temperature (T_E) and the heat pump cold water inlet temperature (T_{cw}) respectively. The trend of the average heat pump performance at 0°C/33.9 bar.g evaporation temperature/pressure was used to develop a heat pump model for the HWSS performance prediction (as described in section 6.3.3).

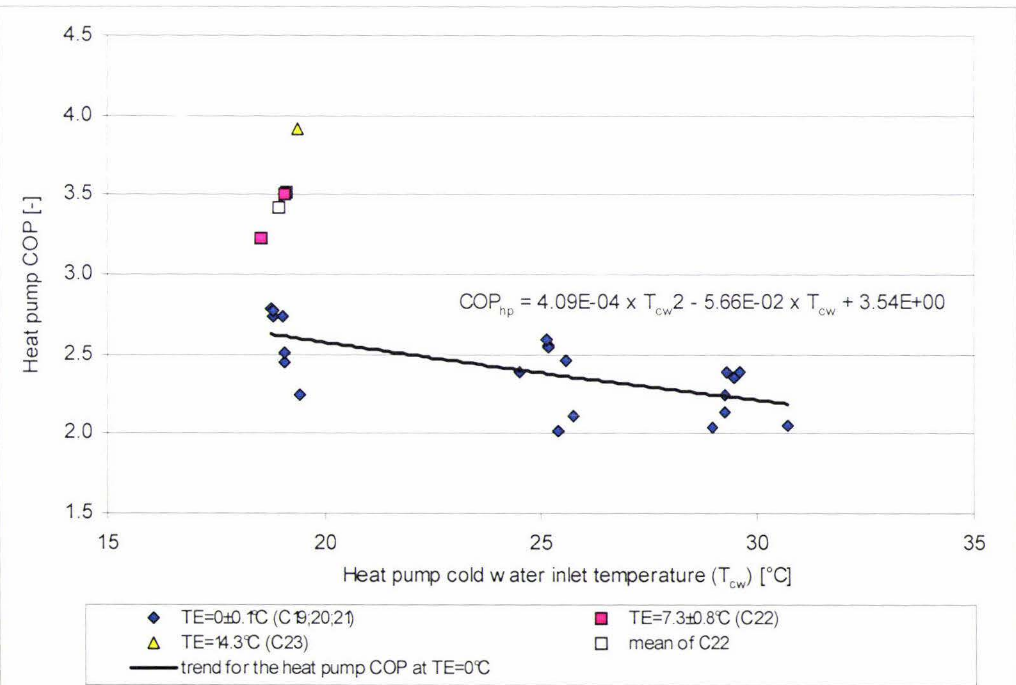

Figure 7.26: Heat pump COP at 105 bar.g discharge pressure and varying heat pump cold water (T_{cw}) inlet temperatures.

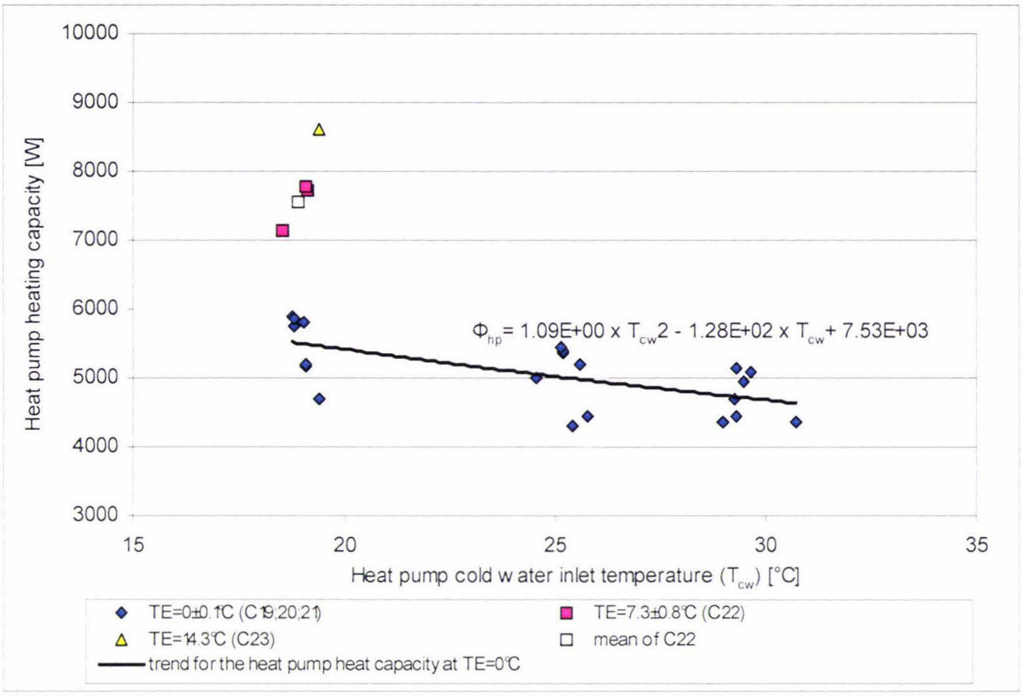

Figure 7.27: Heat pump heat capacity at 105 bar.g discharge pressure and varying heat pump cold water (T_{cw}) inlet temperatures.

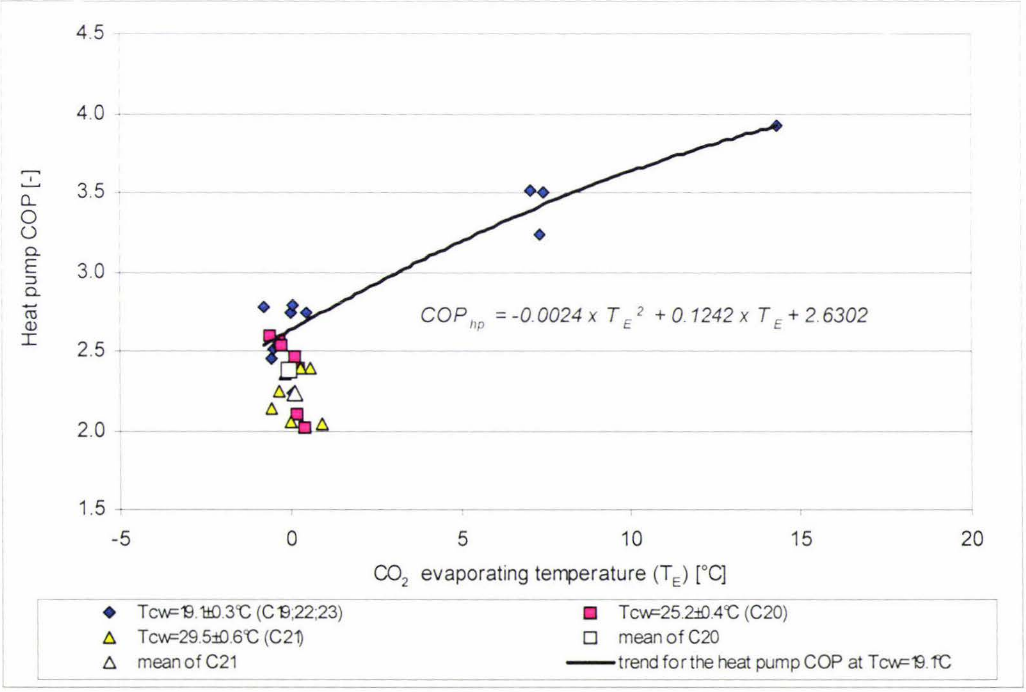

Figure 7.28: Heat pump COP at 105 bar.g discharge pressure and varying evaporating temperatures (T_E).

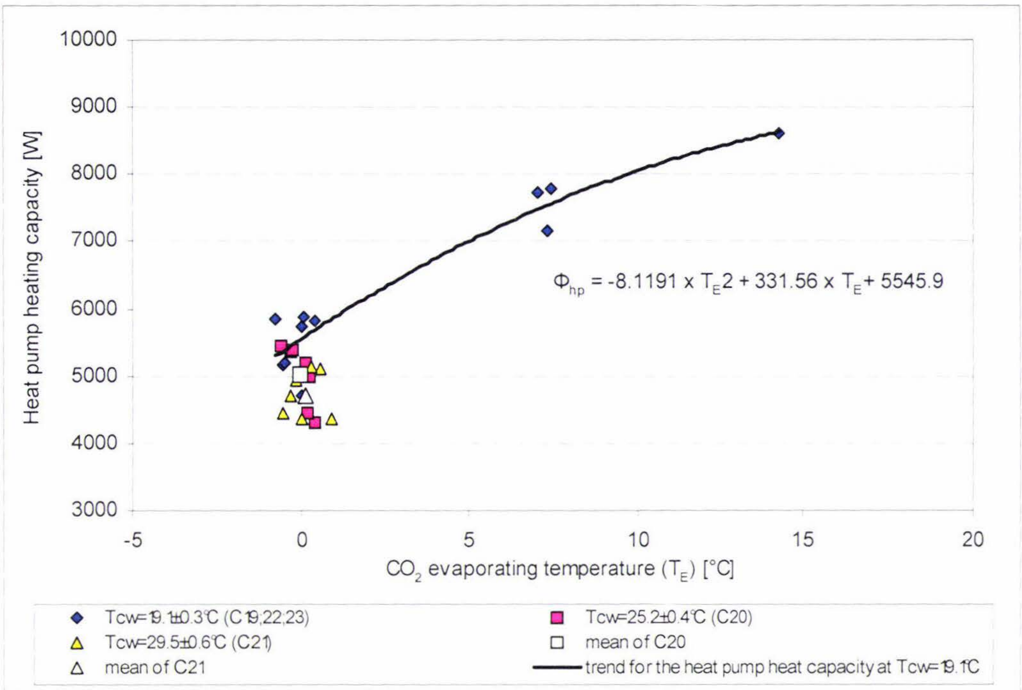

Figure 7.29: Heat pump heat capacity COP at 105 bar.g discharge pressure and varying evaporating temperatures (T_E).

7.5.7 Oil behaviour and recovery

Presence of oil films in the system (pipe and heat exchanger), oil fouling in the heat exchangers and/or evidence for excessive pressure drop caused by the oil could not be measured. Inspections of the high-side components when the configurations were changed showed no sign of oil films and/or oil accumulation in the tubes and/or the heat exchangers.

On the low-side oil accumulation was observed in the LPR. A mixture of oil and CO_2 was recovered of the bottom of the LPR at the end of the trials which where performed without recovering the oil. At atmospheric conditions, the oil and the CO_2 combined to form a mixture of low viscosity, consisting of approximately 33 % v/v CO_2, which slowly evaporated from the oil. The characteristics of the oil-CO_2 mixture at the operating pressure could not be measured; however, similar behaviour was expected when the heat pump was operated. The behaviour of the mixture would explain some of the heat pump operational problems and the refrigerant overcharge.

Oil foaming (1/3 of the height of the liquid level) was observed in the compressor oil sight glass, in particular when rapidly decreasing the suction pressures. It was expected that similar behaviour occurred in the LPR, however, this could not be measured nor observed. However oil foaming would explain the apparent liquid carry over to the compressor suction.

For the oil return trials, the oil was recovered through the needle valve (which was opened by 1-2 turns) to the compressor at a sufficient rate to achieve sustainable liquid level at the oil sight glass. However it could not be measured whether oil only or a mixture of CO_2 and oil returned to the compressor.

The effect of the returning oil or oil-CO_2 mixture on the compressor indicated isentropic efficiency is shown in Figure 7.30 as a function of the vapour superheat at the LPR outlet for 105 bar.g discharge pressure, 20°C/60°C GC water temperatures and 0°C/33.9 bar.g evaporation temperature/pressure (C19). The vapour superheat was measured at the LPR outlet, however the oil return was by-passed to the compressor suction, hence Figure 7.30 does not show the effect of the returning oil on the superheat.

Figure 7.30: Effect of the oil return on the compressor performance at 105 bar.g discharge pressure, 20°C/60°C GC water temperatures and 0°C/33.8 bar.g evaporation temperature/pressure (C19).

The indicated compressor efficiency slightly increased when the oil/CO_2-mixture was drained into the suction of the compressor. This supports the explanation that droplet liquid carry-over through the suction line outlet of the LPR contributed to the low indicated isentropic compressor performance and the energy imbalance.

7.6 Hot water cylinder (HWC) performance

Figure 7.31 shows the measured thermocline in the HWC during the heating recovery trial with the heat pump operating at 105 bar.g discharge pressure, 0°C/33.9 bar.g evaporation temperature/pressure. The heat pump control was set to 60°C water temperature resulting in hot water temperatures in the range of 59 to 62°C. The tap water temperature was 17.6°C and the ambient air temperature was 17°C. At the beginning of the trial the HWC was fully mixed at 16.5°C. The initial heat pump water flowrate was 121 l/h. The T17 and T24 positions correspond to the HWC top and bottom respectively. The HWC thermostat was located between T23 and T24.

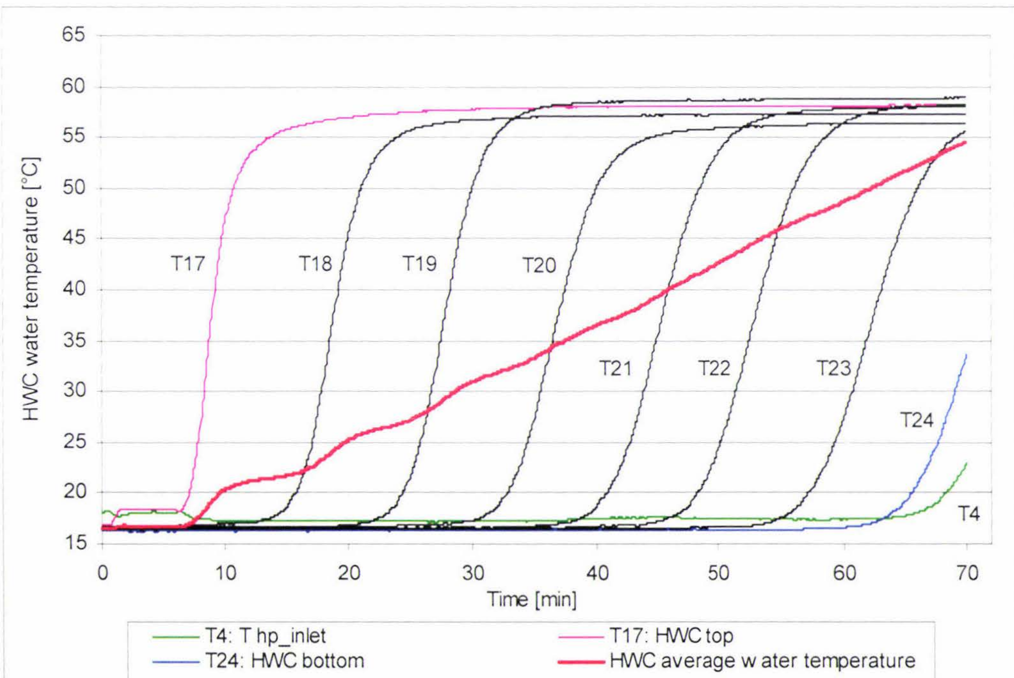

Figure 7.31: Measured water temperature in the HWC during a recovery period with the heat pump operating at 105 bar.g discharge pressure, 0°C/33.8 bar.g evaporation temperature/pressure and an initial water flowrate of 121 l/h.

The thermocouples in the HWC setup measured the temperatures within ±0.2 K, however at the end of the recovery period a difference of approximately 2 K in the measured water temperatures was observed (indicated in Figure 7.31). This was probably caused by imperfect heat conduction from the HWC shell to the thermocouples, which were mounted on the outside of the HWC shell.

There was limited mixing of the entering hot water and the cold water in the HWC and the thermocline appeared to be very sharp with a change in temperature from above 55°C at the top to less than 20°C at the bottom of the HWC. The temperature at the thermostat reached the heat pump off conditions (35°C at the HWC thermostat) after approximately 65 minutes. At this time about 75% of the HWC volume was at a useful temperature (above 55°C). The water temperature at the gas cooler water inlet temperature remained low (<25°C) during the whole heating period.

Figure 7.32 gives the average water temperature in the HWC and the heat losses to ambient air measured in the first heat loss trial as a function of time. The average air temperature was 18.2°C, the water in the HWC was initially fully mixed at 53.4°C and there was no flow through the HWC.

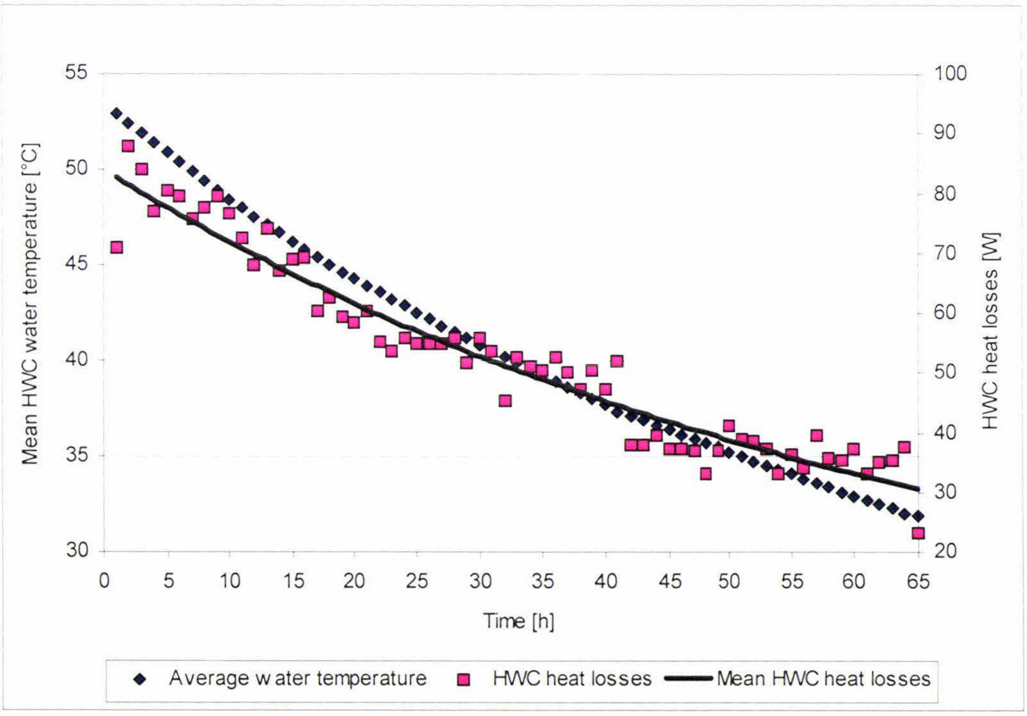

Figure 7.32: HWC mean water temperature and HWC heat losses during the first heat loss trial (heat-loss1)

The HWC heat losses ranged from approximately 84 W at an average water temperature of 50°C to about 37 W at 35°C corresponding to annual heat losses of 350 to 700 kWh/year.

The HWC UA-value, which was back-calculated using Equ. 5.47, ranged from 1.7 to 2.7 W/K with a mean of 2.3 W/K, giving an average overall heat transfer coefficient (based on the inner shell area of the HWC) of 1.3±0.1 W/m^{2}K.

Figure 7.33 shows the mean HWC water temperature and the heat losses to the ambient air measured in the second heat loss trial. This trial was started with the HWC being stratified with water temperatures between 17 and 55°C, giving a mean water temperature of 35°C. The average ambient air temperature was 17°C.

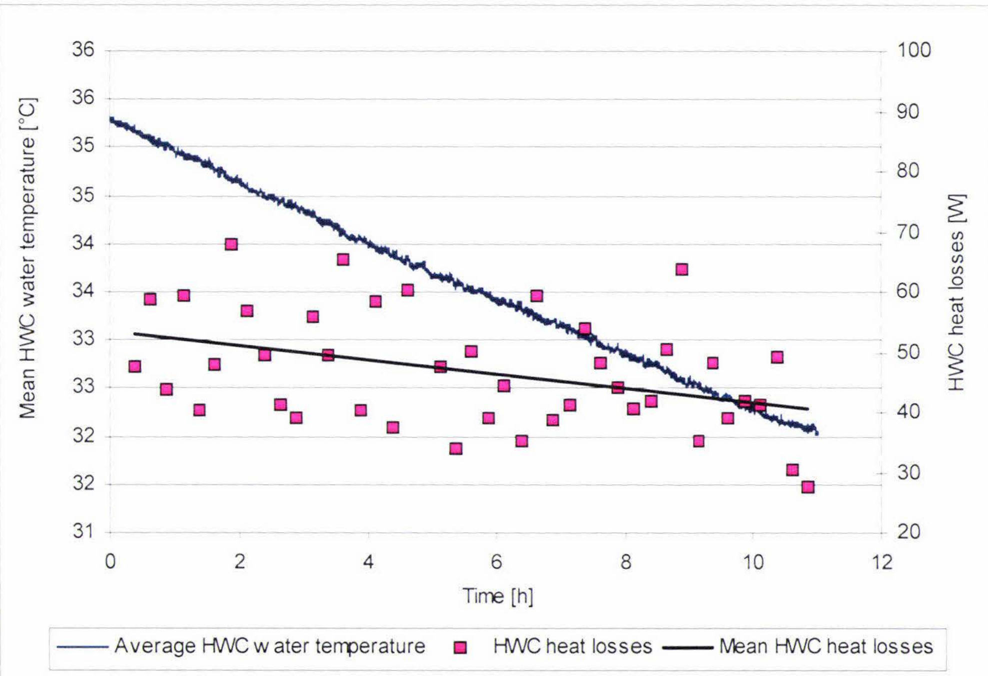

Figure 7.33: HWC mean water temperature and HWC heat losses during the second heat loss trial (heat-loss2)

The heat losses varied across a wide range from about 28 to 68 W giving a HWC UA-value of 1.4 to 4.1 W/K. On average the heat losses were 47 W and the HWC U-value 1.6±0.3 W/m^{2}K. The annual heat losses would be approximately 410 kWh/ year (at an average HWC temperature of about 33.6°C). Reason for the wide range of the back-calculated heat losses was the heat conduction of the temperature sensor and the relatively small temperature changes of less than 0.15 K over the 15 minutes between measured values.

The back-calculated average U-value for the two heat loss trials differed by about 20%. Possible reasons for the difference in the measured U-value were:

- Measurement errors due to imperfect heat conduction from the HWC shell to the thermocouples. This was supported by the relatively wide range of the heat losses measured in the second heat loss trial.
- Radial temperature gradient due to high stratification (in particular for at the heat loss1 trial) so that the measured water temperature deviated from the true average HWC temperature (e.g. Figure 7.34 which possibly indicates a radial temperature gradient).

The annual heat losses of the HWC corresponded to a modern A-grade cylinder (600-800 kWh/year, (Williamson and Clark, 2001) although based on the date of manufacture (pre 1976) the HWC was expected to be of the type D. However the basis of the heat loss data (e.g. average HWC water temperature, ambient air temperature) given by the manufacturers was unknown so a direct comparison was not possible.

Figure 7.34 shows measured the temperature profile of the HWC during the hot water withdrawal trial (first 4 hours) and the standing period after the trial (heat-loss2 trial from 4 to 12 hours). The ambient air temperature was 17°C and the tap water temperature was 18.5°C respectively.

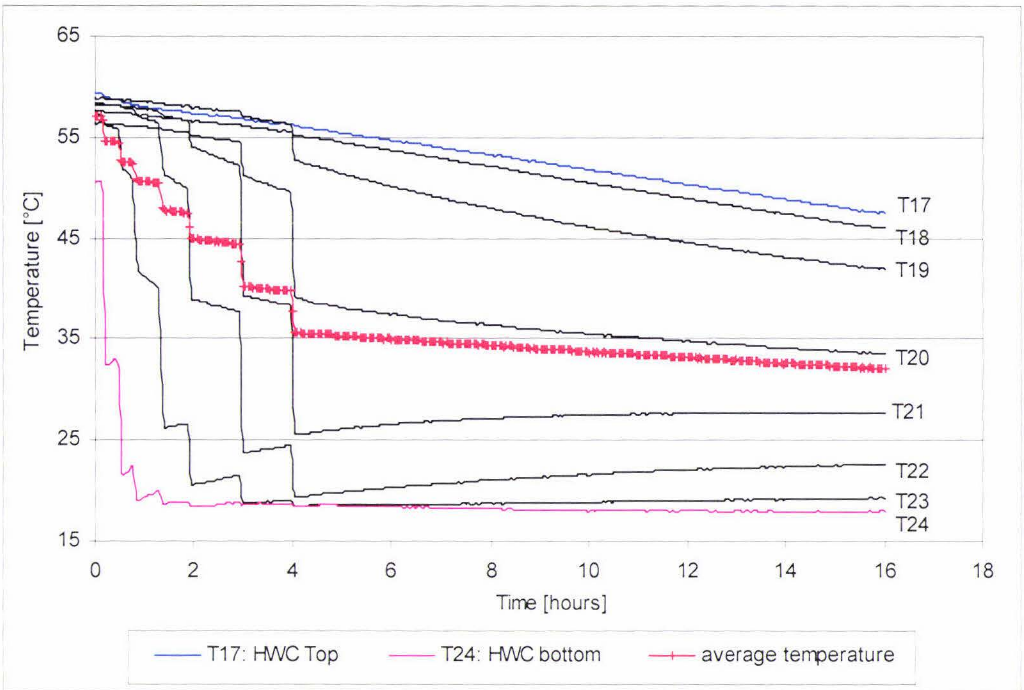

Figure 7.34: Temperature profiles in the HWC during the water withdrawal (cooling trial) and the second heat loss trial (heat-loss2).

Between the HWC withdrawal intervals, the temperature of the water at the HWC bottom slightly increased. This suggested that there was some mixing caused by the cold water which entered into the HWC through the bottom inlet. However a similar temperature increase was observed after the withdrawal when there was no flow in the HWC (between 4 to 16 hours), which indicated that there was some mixing at the bottom of the HWC due to natural convection possibly forced by the radial temperature gradient.

8 HWSS performance modelling

8.1 HWSS model validation

The measured data for the HWC trials were used to estimate the model parameters such the HWC conduction enhancement factors. The mean measured U-value for the two heat loss trials of 1.47 W/m^{2}K was applied. All modelling was performed with the HWC divided into 96 segments and a time step of 1 second.

Figure 8.1 and Figure 8.2 compares the measured and the predicted average HWC temperature and the HWC thermocline respectively for the first heat loss trial. The locations of the thermocouples are indicated by dots in Figure 8.2.

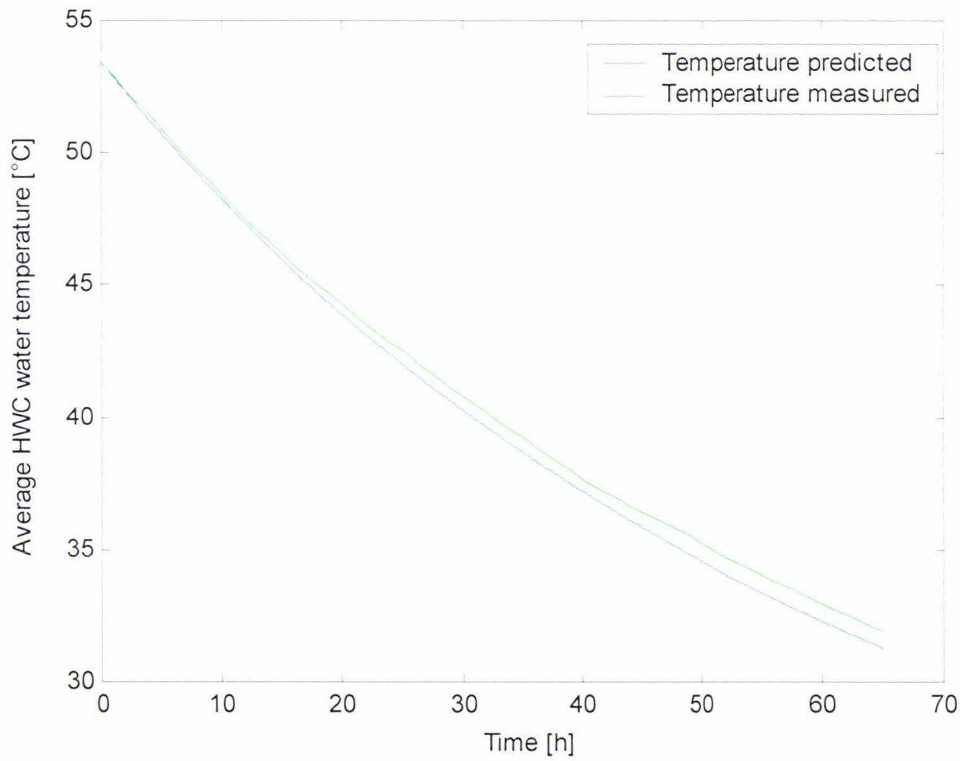

Figure 8.1: Comparison of predicted and measured HWC average temperature for the first heat loss trial (heat-loss1).

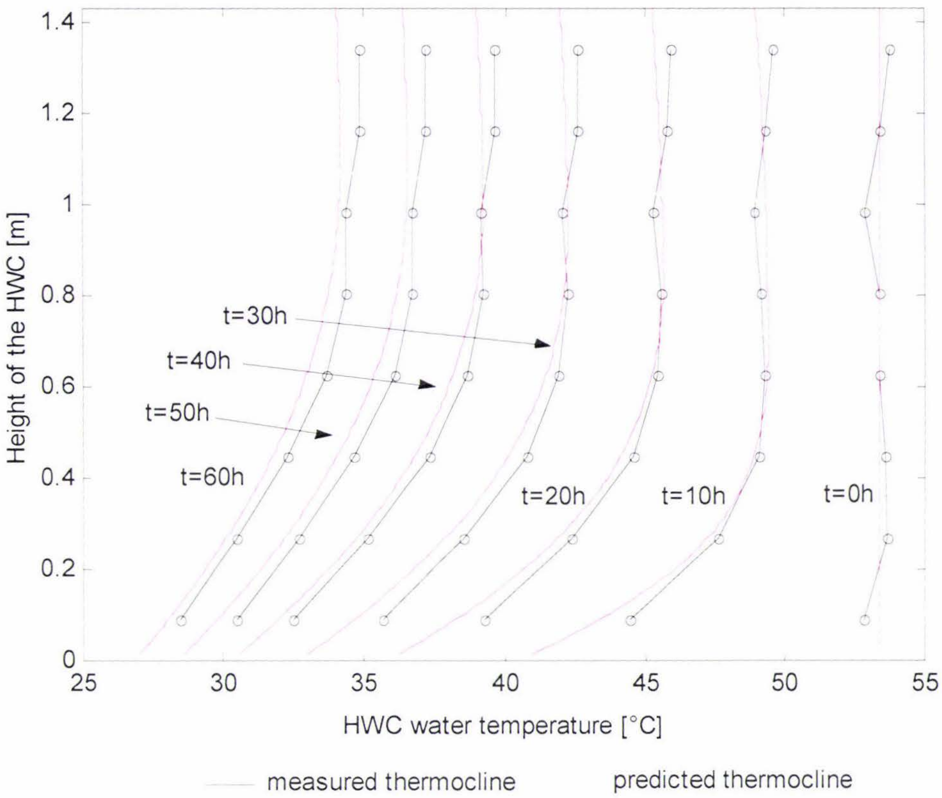

Figure 8.2: Comparison of measured and predicted thermoclines for the first heat loss trial (heat-loss1).

The predicted average water temperature after 65 hours was 1 K lower than the corresponding experimental data. The heat losses were slightly overestimated because of the average U-value was slightly higher than the effective overall heat transfer coefficient measured in the first heat loss trial.

Due to the overestimated heat losses (when using the average U-value), the average water temperature along the thermocline was slightly lower than the experimental data. However, good agreement between the shape of the predicted thermocline and the shape of the measured thermocline was achieved with a natural convection enhancement factor for a positive temperature gradient of 8 and a natural convection enhancement factor for negative temperature gradient of 40. With the average U-value the predicted temperature at the bottom of the HWC was constantly too high so the U for the bottom segment of the HWC only was arbitrarily increased by a factor of 6. To keep the overall area averaged HWC U-value at 1.47 W/m^{2}K, the U-value for the other segments was decreased (by 1.28 times) to 1.15 W/m^{2}K.

A possible explanation for the high enhancement factor for convection with a positive temperature gradient was mixing due to the radial temperature gradient in the HWC, which was not considered by the one dimensional model. Possible reasons for the higher heat losses through the bottom of the HWC were reduced insulation and the likelihood of heat conduction through the supporting construction (made of an aluminium sheet), on which the inner copper shell of the HWC was standing.

Figure 8.3 and Figure 8.4 compares the measured and the predicted average HWC temperature and the thermocline for the second heat loss trial applying the same model parameter settings as described above.

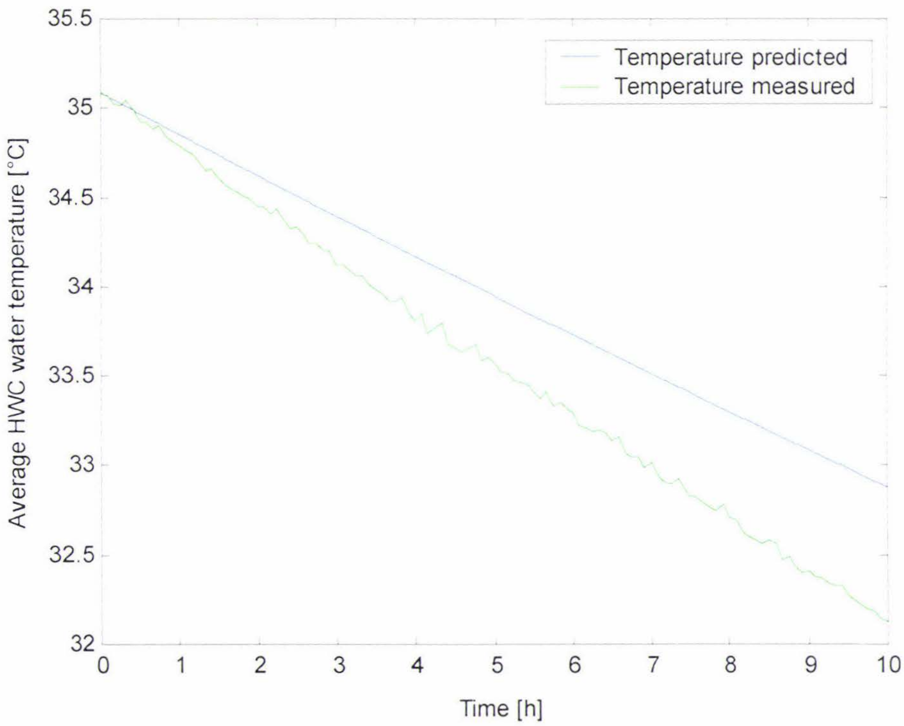

Figure 8.3: Comparison of predicted and measured HWC average temperature for the second heat loss trial (heat-loss2).

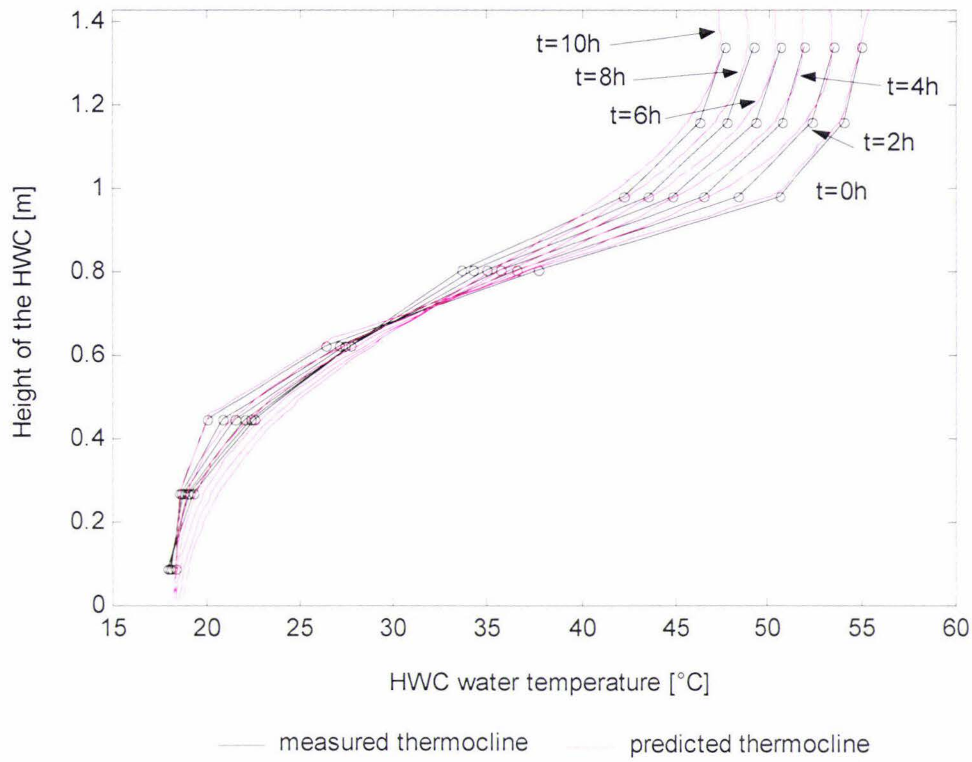

Figure 8.4: Comparison of measured and predicted thermoclines for the second heat loss trial.

The predicted overall heat losses were lower than measured, leading to slower temperature reduction of the HWC and a difference of 0.8 K after 10 hours. Overall, the disagreement between the predicted temperature and the measured data was slightly higher than for the first heat loss trial.

The predicted thermocline gave a good fit to the measured HWC temperature profile. Due to the underestimated heat losses (by using the average U-value), the average water temperature along the thermocline was slightly higher (e.g. towards the HWC bottom) than the experimental data.

Figure 8.5 and Figure 8.6 and show the predicted and measured temperatures in the HWC for the heating trial. The temperatures were predicted using the average U-value and the conduction enhancement factors as described above. A flow enhancement factor of 2.3 was used. The ambient air temperature was 17.0°C, the tap water temperature 17.6 °C, the average heat pump hot water supply temperature 59.8°C and the initial HWC temperature 16.5°C.

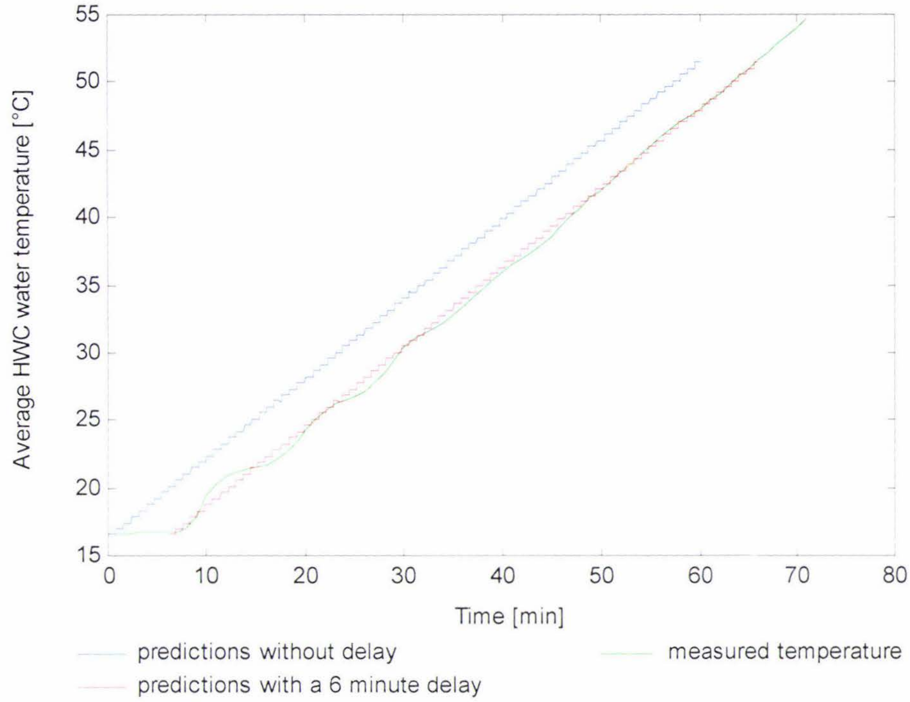

Figure 8.5: Comparison of measured and predicted average HWC temperature for the heating trial.

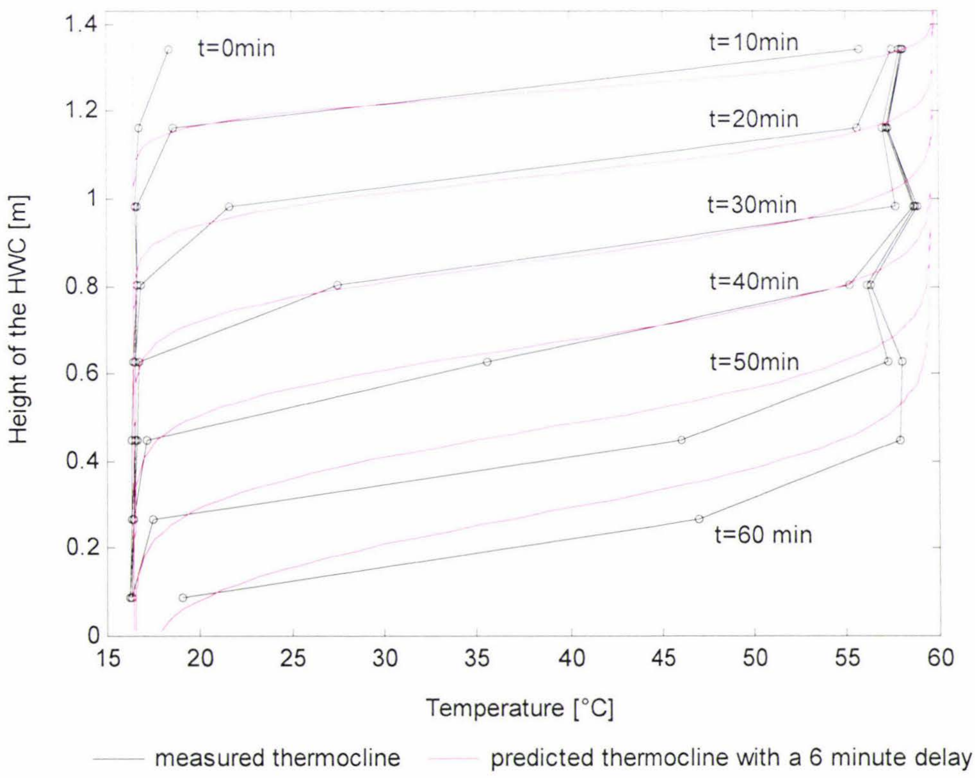

Figure 8.6: Comparison of measured and predicted temperatures in the HWC for the heating trial.

The average HWC temperature was accurately predicted if a 6 minute delay was included. This delay corresponded to the time required for the heat pump to produce hot water at 60°C from start (e.g. push water through the delivery piping) and the response of the measurement set-up to the delivered hot water.

Overall, good fit of the thermocline was achieved with a flow enhancement factor of 2.3. However it was difficult to estimate the temperature deviation in the thermocline because of the relatively large distance between the measurement points. Quality of fit was not particularly sensitive to this value.

The predicted hot water at the top of the HWC was about 2 K higher than the measured hot water temperature. Reasons for the difference were temperature measurement errors due to imperfect heat conduction to the thermocouples, heat losses between the heat pump and the HWC and/or a radial HWC temperature gradient.

Figure 8.7 shows the predicted and the measured average HWC temperature for the cooling trial, while Figure 8.8 shows the predicted and the measured thermocline during the trial. The same model parameters described above were used (Table 8.1). The tap water temperature was 18.5°C, the ambient air temperature 17.0°C and the withdrawn water flowrates were m1 to m7 as described in Table 5.10.

Overall, the HWC thermocline fitted reasonably well to the measured temperature profiles. The predicted average HWC temperature was off-set by about 2 K from the experimental data, which was good considering the small number of measurement points. The difference could be explained by uncertainty associated with thermocouple positioning alone.

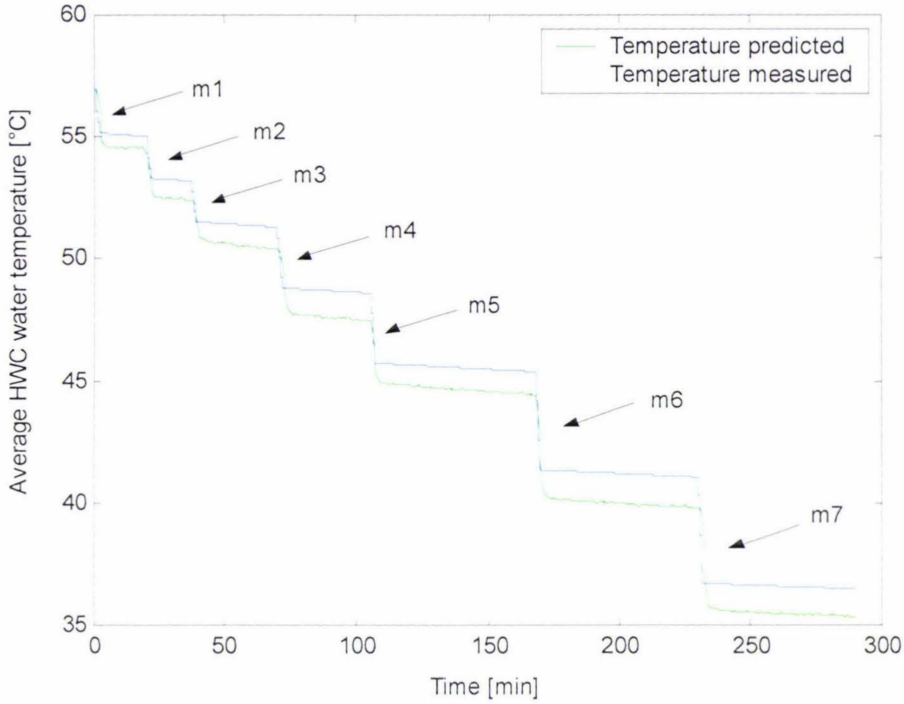

Figure 8.7: Comparison of measured and predicted average HWC temperatures for the cooling trial.

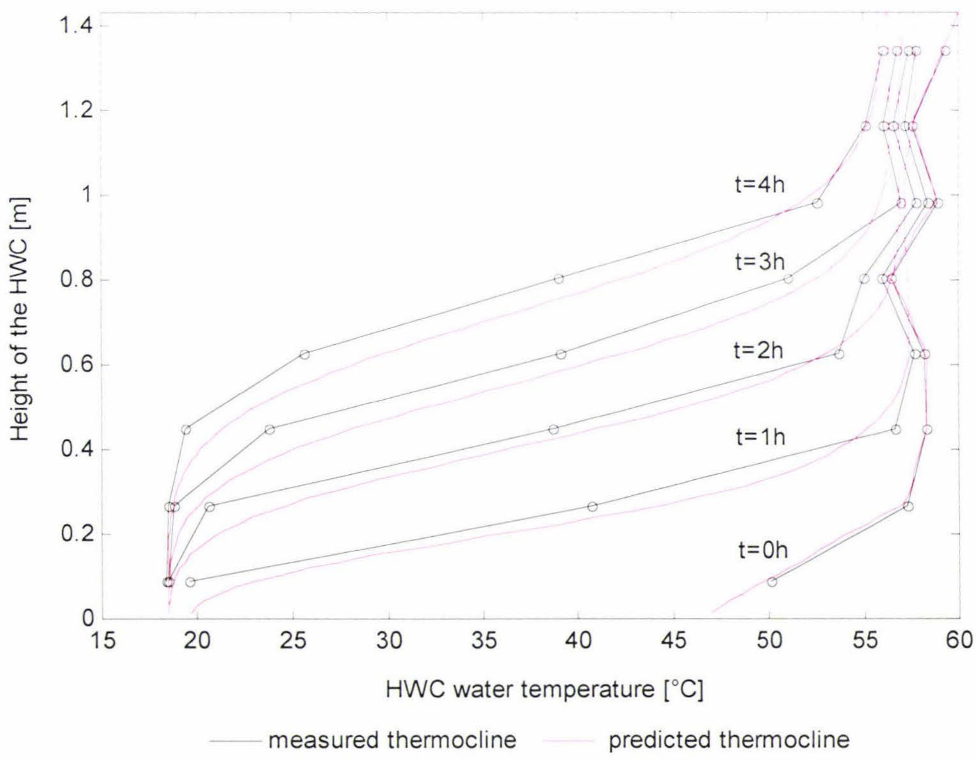

Figure 8.8: Comparison of measured and predicted thermoclines in the HWC for the cooling trial.

Overall, for the HWC parameters in Table 8.1 that were fitted based on the HWC trial data, the model gave good predictions for the other trials. Therefore these model parameters were used to predict the likely performance of the HWSS under a wider range of conditions. However, the delay of the heat pump to produce hot water at 60°C after start-up (shown in Figure 8.5) was not considered in these model predictions.

Table 8.1: Model parameter settings used for the HWSS performance modelling

Time and space	
Number of segments, J	96
Differential time (Time step), Δt	1 s
Physical properties of water	
Specific heat water, c_W	4183 J/kgK
Density of water, ρ_W	1000 kg/m3
Thermal conductivity of water, λ_W	0.621 W/mK
WSS parameters	
Cold water supply temperature, T_{tap}	15°C
HWC parameters	
Ambient air temperature, T_{air}	10°C
HWC height (inner shell), H_{HWC}	1.43 m
HWC diameter (inner shell), d_{HWC}	0.35 m
HWC volume, V_{HWC}	137 l
Overall heat transfer coefficient, U_{HWC}	1.47 W/m^{2}K
Bottom segment heat transfer coefficient enhancement factor	6
Enhancement factor for natural convection in direction of the temperature gradient, $f_{\lambda, nat\_conv\_pos}$	8
Enhancement factor for natural convection against the temperature gradient, $f_{\lambda, nat\_conv\_neg}$	40
Enhancement factor for the mixing, $f_{\lambda, mixing}$	2.3
HWSS control	
Heat pump set-point temperature, $T_{hp, on}$	25°C
Heat pump control dead-band temperature, $\Delta T_{hp, dead\text{-}band}$	10 K

8.2 Predicted HWSS performance

Figure 8.9 to Figure 8.13 show the predicted HWSS performance for the water consumption of user A, B and A&B (as described in Table 6.1). The predictions were carried out with HWSS model parameters settings summarized in Table 8.1.

Figure 8.9 shows the hot water flowrate that was withdrawn from the HWC and/or the heat pump and supplied to the users as function of the time. Figure 8.10 gives the temperature of the withdrawn water.

Figure 8.12 to Figure 8.13 shows the heat pump water inlet temperature, the heat pump COP and the heat pump heating capacity for the user A, B and A&B water consumption profiles. A heat pump water inlet temperature below 10°C indicates that the heat pump was off.

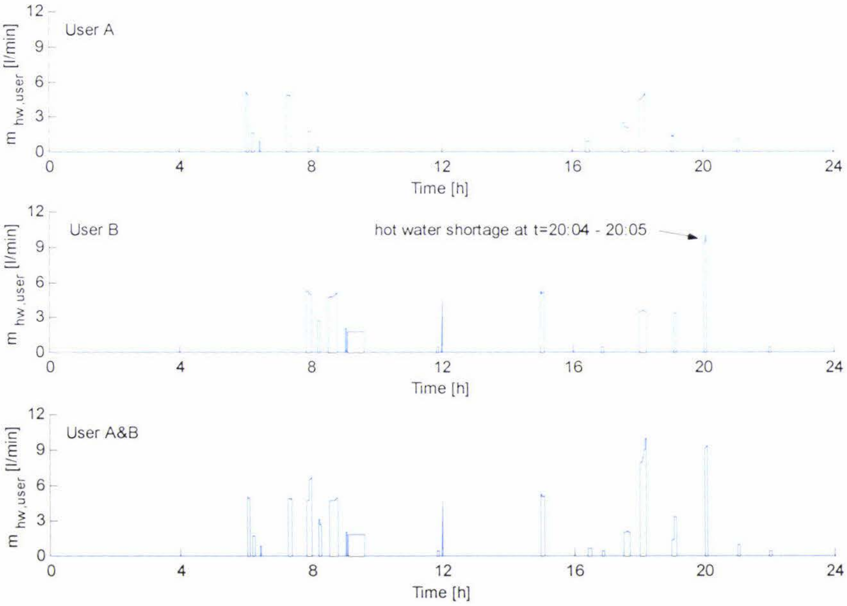

Figure 8.9: Hot water flowrate withdrawn from the HWC and/or the heat pump for user A, B and A&B water consumption.

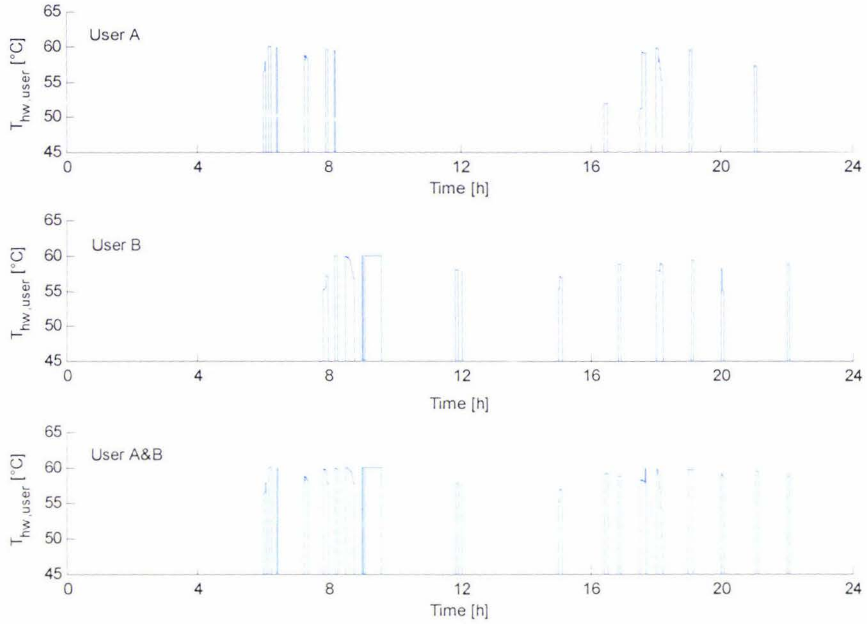

Figure 8.10: Temperature of the withdrawn hot water from the HWC and/or the heat pump for user A, B and A&B water consumption.

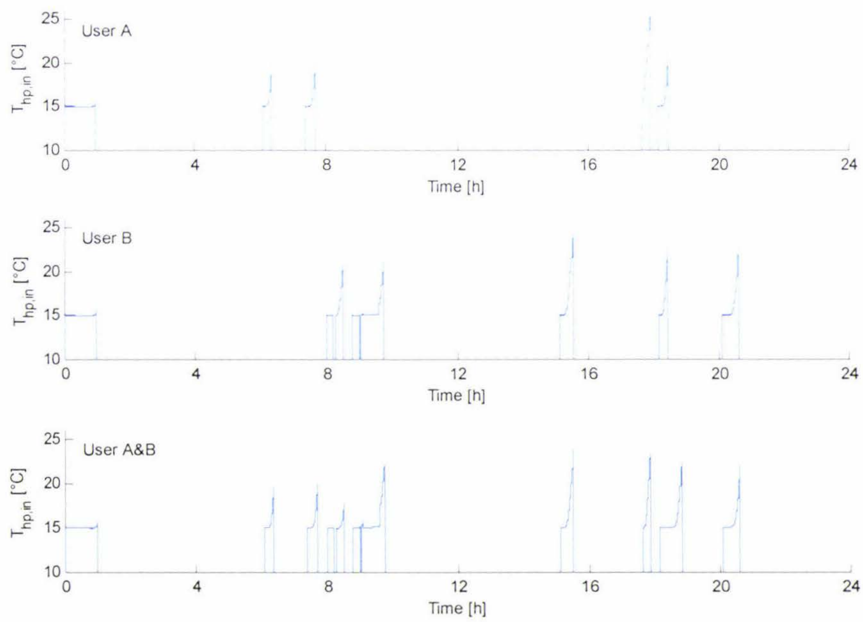

Figure 8.11: Heat pump cold water inlet temperature for user A, B and A&B water consumption.

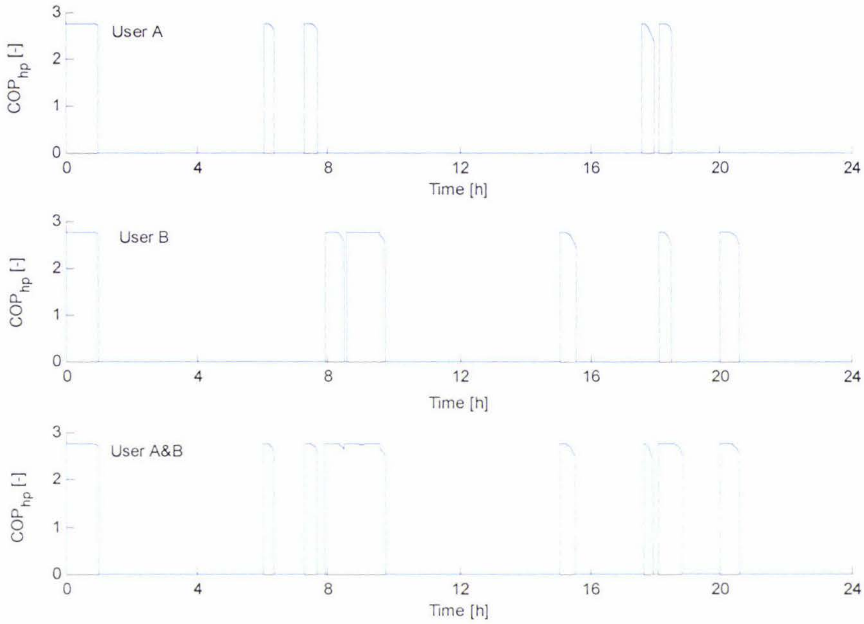

Figure 8.12: Heat pump heating COP for user A, B and A&B water consumption.

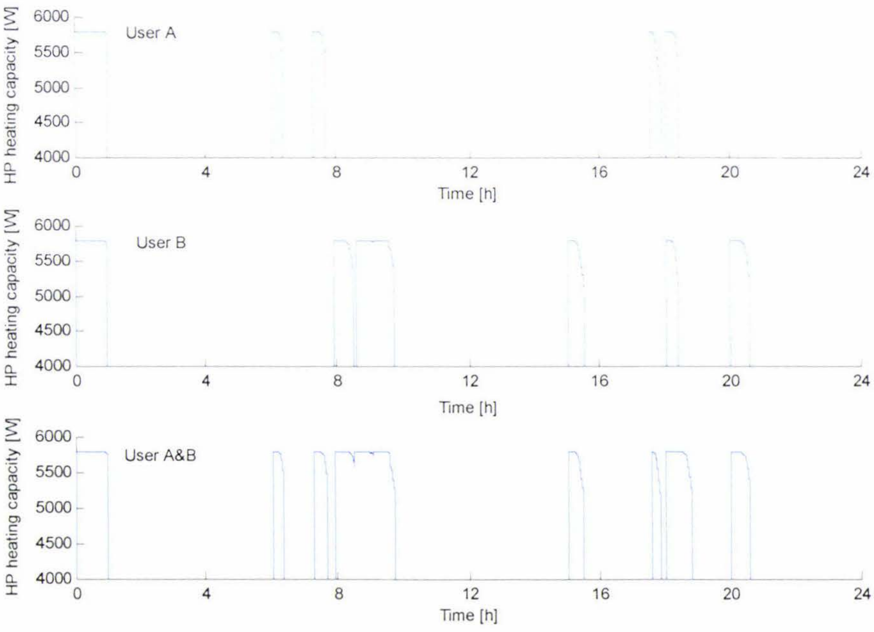

Figure 8.13: Heat pump heat capacity for user A, B and A&B water consumption.

Table 8.2 summarises the overall predicted performance of the HWSS for moderate hot water consumption (user A), excessive water consumption (user B) and when supplying both users A&B over a 24 hour period.

Table 8.2: Predicted HWSS performance for moderate hot water consumption (user A), excessive water consumption (user B) and when supplying both users A&B over a 24 hour period.

HWSS condition	**User A**	**User B**	**User A&B**
Total amount of water consumed [l]	260	468	728
Total amount of hot water withdrawn of the HWC [l]	168	346	509
Average hot water supply temperature [°C]	42.7	46.8	45.3
Energy of consumed hot water [MJ]	30.1	62.1	92.3
Heat pump electric work [MJ]	18.6	31.6	42.4
Heat losses HWC [MJ]	6.2	6.6	6.4
Average COP HWSS [-]	2.38	2.52	2.58
Periods of hot water shortage [min]	0	1	0
Operating period of the heat pump [min]	147	250	336
Number of on/off intervals [-]	5	6	8
Minimal / average operating time [min]	18 / 29	21 / 42	16 / 42
Average heat pump efficiency (COP) [-]	2.72	2.73	2.73
Average water temperature at the heat pump inlet during the heat pump operating period [°C]	15.9	15.7	15.7
Period of heat pump inlet temperature > 25°C [min / part of heat pump operating time in %]	1 / 0.5	0 / 0	0 / 0

Overall the HWSS was able to meet the user demand for all hot water consumptions and hot water shortage (temperature lower than desired) occurred for the user profile B for less than 1 minute. The reason that no shortage occurred for the user profile A&B was that the heat pump was reheating the HWC when the peak demand occurred.

The heat pump ran at near maximum COP at all HWSS conditions due to the low heat pump inlet water temperature, which was generally below 25°C. However, in actual systems the heat pump efficiency might be slightly worse because of the large number of relatively short heat pump operating periods each day. These short intervals were caused by the relatively small HWC sizing (relate to the heat pump heating capacity), the heat pump control settings and the temperature distribution in the HWC.

The heat losses of the HWC reduced the HWSS COP by 12% for the user profile A and by 6% for the user profile A&B. The HWC affects the overall system performance, particularly at moderate hot water usage. However, these losses were acceptable, considering the age of the HWC. It was expected that with an A-grade HWC the heat losses would significantly reduce.

The HWSS control temperature for the heat pump start of 25°C was a reasonable compromise between getting low heat pump water inlet temperature and long duration of heat pump operation. A lower set-point temperature would result in greater hot water shortage while a higher heat pump starting temperature gives lower overall heat pump efficiency due to higher heat pump water inlet temperatures and an increased number of the heat pump on/off intervals.

The heat pump operating duration could be optimised by increasing the control dead band. Table 8.3 shows the HWSS performance when providing user A&B and for different control dead bands, aiming to have fewer operating periods of increased durations.

Table 8.3: Predicted HWSS performance with 5 to 25 K heat pump control temperature dead band.

Control temperature dead band [K]	**5**	**10**	**15**	**20**	**25**
Heat pump stet-point temperature [°C]			25		
Periods of hot water shortage [min]	2	0	2	0	0
COP HWSS [-]	2.59	2.58	2.56	2.53	2.49
Average heat pump efficiency (COP) [-]	2.74	2.73	2.72	2.70	2.66
Operating period of the heat pump [min]	330	336	342	350	358
Number of on/off intervals [-]	9	8	7	7	7
Minimal / average operating time [min]	11 / 37	16 / 42	20 / 49	21 / 50	22 / 51
Average water temperature at the heat pump inlet during the heat pump operating period [°C]	15.4	15.7	15.9	16.5	17.4
Period of heat pump inlet temperature > 25 C [min / part of operating time in %]	0 / 0	0 / 0	3 / 1	16 / 5	36 / 10

The overall HWSS performance and the heat pump COP slightly declined as the dead band was increased from 5 to 25 K due to the increased heat pump water inlet temperature at the end of each heat pump operating period. The shortage periods remained low for all heat pump control settings. The number of the heat pump on/off intervals reduced from 9 at 5 K dead band to 7 at 15 to 25 K dead band, so 15 K dead band gave maximum system efficiency with least heat pump on/off intervals. At these settings the heat pump ran at near maximum COP and the efficiency losses due to high water inlet temperatures were less than 1% (maximum heat pump COP at 15°C cold water inlet and 10°C air temperature was 2.75). For the heat pump studied, use of a larger HWC would significantly reduce the number of on/off periods.

Figure 8.14 shows the HWC average temperature, the temperature at the HWC thermostat and the heat pump inlet temperature for the users A&B water consumption profile, and with the optimised heat pump thermostat control settings of 25°C heat pump set-point temperature and 15 K dead band. Figure 8.15 shows the thermocline in the HWC over the 24 hour period. The heat pump off intervals are indicated by the heat pump water inlet temperature below 10°C.

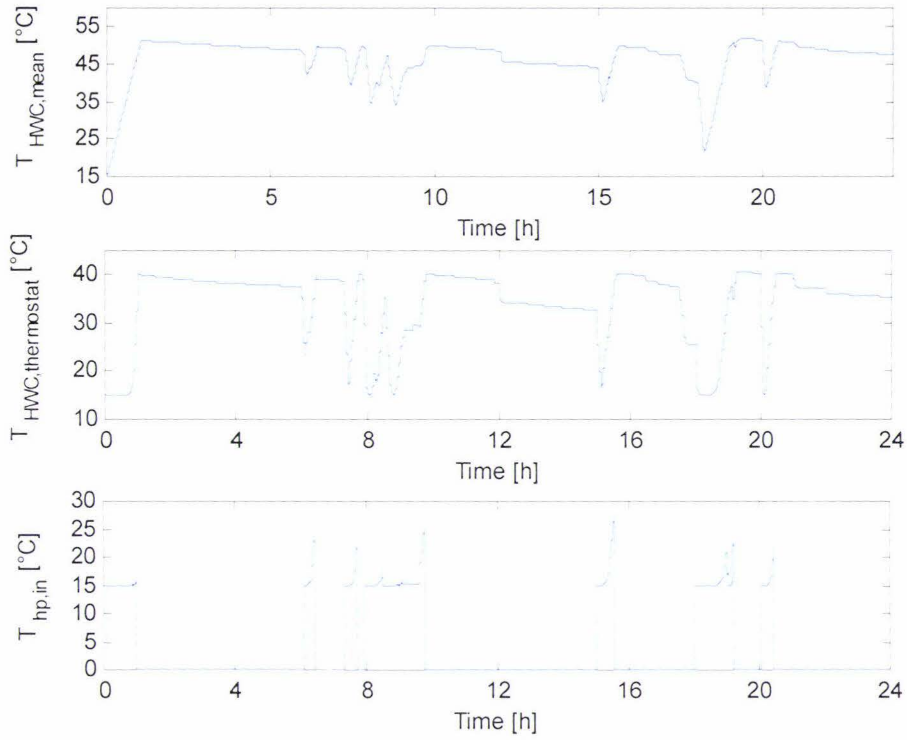

Figure 8.14: Predicted HWC temperatures when supplying the users A&B with hot water with thermostat settings of 25°C and 15 K dead band.

The HWC thermocline remained distinct with the lowest water temperature at the bottom during the periods when water was withdrawn from the HWC (e.g. after 6 to 9 hours or 9 to 21 hours) but the thermocline became less pronounced during periods with little hot water consumption and HWC recovery by the heat pump (e.g. after 9 or 15 hours).

The average HWC temperature generally remained above 45°C, however at 18 hours there was nearly no hot water left in the HWC until the heat pump started and the HWC recovered. This indicates that the HWC volume is too small for a 2 family home HWSS.

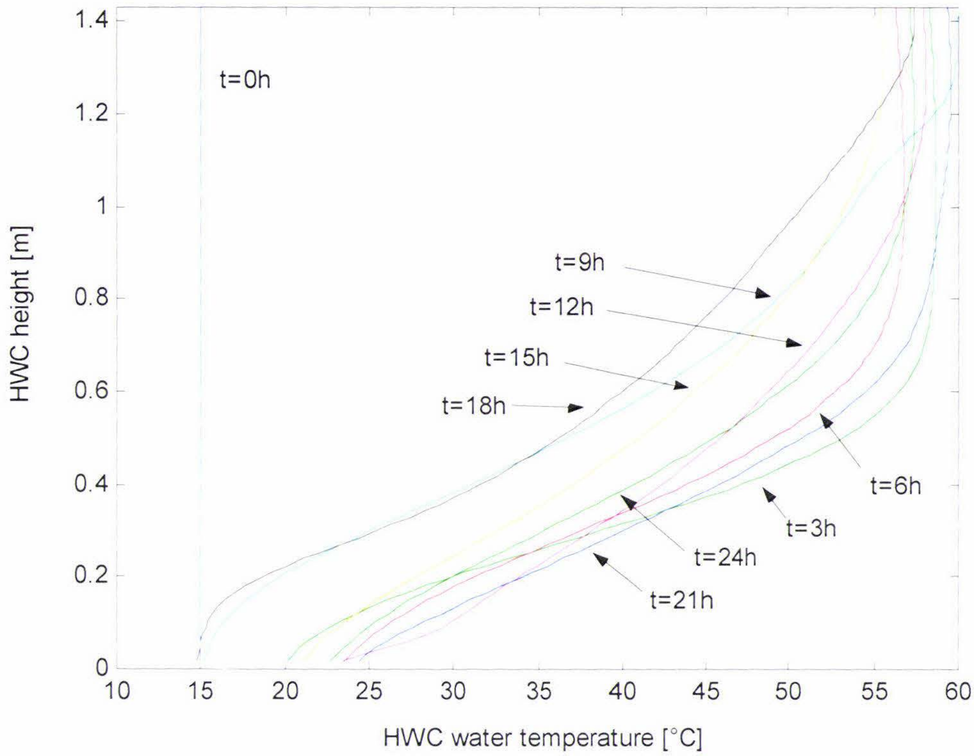

Figure 8.15: Predicted HWC thermoclines when supplying the User A&B with hot water with thermostat settings of 25°C and 15 K dead band.

The average heat pump duration of 51 minutes remained short despite the control improvements. However, this was because of the combination of the relatively small HWC (appropriate for a one family home) and the relatively large heat pump heating capacity (appropriate for a 2 to 3 family home) so the HWSS performance would significantly improve by using a bigger HWC.

Overall the HWSS performance prediction showed that the CO_2 heat pump combined with a stratified HWC achieves high efficiency. The efficiency losses due to heat pump water inlet temperatures above 25°C were moderate despite the simple heat pump thermostat control. Due to the low heat pump water inlet temperatures, constant discharge pressure control was adequate, leading to simple and cost-effective heat pump control system. Overall system efficiency improvements up to 12% could be achieved by reducing the HWC heat losses.

9 Conclusion

An 8 kW prototype water heating heat pump using a transcritical CO_2 cycle was successfully designed, constructed and operated. The design method was based on conventional prediction methods and the available correlations from the literature were of sufficient precision, except for the LPR design which needed to be oversized to ensure adequate liquid separation.

The measurement system and the heat pump control were simple and cost-effective, but they lead to significant data uncertainty and variability of the heat pump operating conditions. In particular, the evaporator temperature/pressure control and the heat pump water inlet temperature control system need to be improved to achieve appropriate control precision.

Overall the prototype was simple, easy to start and stop and generally gave stable operation. The configuration of the refrigerant cycle with the BPR for refrigerant expansion and constant discharge pressure control, and the LPR with the internal IHX located after the evaporator provided good heat pump stability at changing operating conditions.

A number of sources including the compressor, the LPR separation effectiveness and the compressor oil solubility contributed to the heat pump performance problems. It was not possible to eliminate these operational problems.

The design heat pump heating capacity and COP of 8.1 kW and 3.9 respectively were not achieved mainly due to poorer than expected compressor performance. However the measured COP of 2.6 at the 20°C to 60°C water temperatures, 0°C/33.9 bar.g evaporation temperature/pressure and 105 bar.g discharge pressure was competitive with conventional heat pump water heaters. Constant discharge pressure control to 105 bar.a was adequate and achieved near maximum COP across a wide range of operating conditions.

The piston-type compressor prototype ran quietly and was insensitive to occasional refrigerant carry over. However the apparent volumetric and isentropic efficiencies were significantly lower than claimed by the manufacturer leading to lower heating capacity and energy efficiency.

The gas cooler design using a vented, twisted double tube design was favourable due to its simplicity and cost effectiveness. The UA-values were acceptable and excessive performance losses caused by the vented design were not measured. A disadvantage was the constraints on tube diameters for the twisted-tube technology, meaning it was difficult to provide sufficient turbulence at the low refrigerant mass flowrate experienced in small scale heat pumps.

The LPR did not provide sufficient liquid / vapour separation at all operating conditions. The separation process was not measured directly but the lower than expected compressor discharge temperatures suggested that liquid droplets were carried over into the suction of the compressor at high evaporation temperature/pressure due to high gas velocity in the LPR. However, whether the LPR was undersized or other parameters, such as oil foaming and/or oil-carry over were responsible for the cooling was not clear.

The performance of the IHX was poor because of the limited heat transfer surface and the small tube diameter which were available for the project. In particular high-side pressure drop was too high and the heat transfer surface of the IHX which was used for vapour superheat needed to be larger to achieve more superheat. To achieve higher efficiency and overall more constant superheating at changing liquid level, the IHX should be designed with two coils sections, one at the LPR top that always operates in the vapour phase and one at the LPR bottom, which boils refrigerant off, unless the LPR is completely empty.

The measured oil discharge rate from the compressor was moderate and significantly less than reported in literature. The oil was carried from the compressor through the refrigerant cycle and was recovered from the LPR. No oil accumulation was apparent in the gas cooler or evaporator. The oil recovery coil at the bottom of the LPR was a simple and effective way for the oil recovery; however, the system did not return the oil continuously and requires a solenoid valve for automation. The oil phase behaviour is critical for the function of the recovery system. Manufacturers data suggested that the oil would not separate at all operating conditions, so oil return may not guaranteed at all operating conditions.

A model of the HWSS was developed and successfully used to predict the HWSS performance at conditions likely to occur in a 2 family home. The heat pump model was simplistic due to the available heat pump data and allowed performance modelling of the HWSS at the heat pump design condition of 10°C air temperature only. The thermocline in the HWC was modelled with reasonable precision when HWC model was modified to take account of enhanced heat conduction with negative temperature gradient (due to buoyancy mixing) and higher heat losses from the bottom of the HWC.

The use of a stratified HWC in combination with the CO_2 heat pump was appropriate because it allowed the water inlet temperature to the heat pump to be kept as low as possible. The HWSS performance predictions showed that the heat pump water inlet temperature seldom rose above 25°C at all operating conditions so that the heat pump efficiency losses caused by the increase in the water inlet temperature had a negligible effect on the overall HWSS efficiency. The biggest contribution to poor energy efficiency was the heat losses from the HWC, however the heat losses were expected to reduce significantly if a modern type A-grade HWC was used. Due to the low heat pump water inlet temperature, constant discharge pressure control was sufficient and lead to simple and cost-effective heat pump control.

The HWSS performance could be improved by using a bigger HWC with a volume of 200 to 300 l rather than 137 l. The higher volume would give fewer heat pump on/off intervals and longer heat pump operating duration respectively. However, the HWC heat losses would slightly increase due to the bigger size HWC.

Overall, the investigation of the HWSS has shown that the CO_2 heat pump has significant advantages compared with the conventional heat pump technology when combined with a stratified HWC, but availability and cost of components and compressor performance respectively remain critical constraints to commercial implementation.

10 Recommendations

Further work is necessary to achieve the expected heat pump performance, including:

- Improving the heat pump control and measurement system to reduce the data uncertainty so that the sources for the heat pump operational problems can be more fully identified.
- Investigate whether liquid carry-over and/or oil foaming caused the lower than expected compressor performance and if necessary replace the compressor oil, re-design the LPR and/or add an oil separator.
- Ask the manufacturer for further advice and information about the observed compressor characteristics and measured performance and eliminate the compressor operational problems.

More work needed to be done on the heat pump designs, such as:

- Re-design the IHX to achieve improved heat exchanger effectiveness, reduced pressure drop and more constant superheat at all operation conditions.
- Investigate an air-source evaporator unit.
- Investigate a strategy for sustainable oil return.

Further performance trials need to be carried out to:

- Complete the characterisation of the heat pump performance under all the likely operating conditions, such as at high water inlet temperature and high evaporation conditions.
- Improve the heat pump model (part of the HWSS model) and investigate the overall HWSS performance at varying heat pump heat source conditions (ambient air).

To measure the HWSS functionality and the overall efficiency, the heat pump control has to be fully automated. More work should be done to better characterise the HWSS, including:

- Investigate the best control strategy.
- Carry out field tests of a system operating with actual hot water demand.

11 List of References

Aarlien R., Pettersen J., Skaugen G., Neksa P. (1996). Residential Air Conditioning with CO_2 - Preliminary Results. Applications for Natural Refrigerants: Proceedings of the Conference of the International Institute of Refrigeration Commissions B1, B2, E1 and E2. Aarhus (Denmark). pp 659-666.

American Society of Heating, Refrigerating and Air-Conditioning Engineers. (1999). ASHRAE Handbook - Applications, SI Edition. American Society of Heating, Refrigerating and Air-Conditioning Engineers. Atlanta (USA).

American Society of Heating, Refrigerating and Air-Conditioning Engineers. (2001). ASHRAE Handbook - Fundamentals, SI Edition. American Society of Heating, Refrigerating and Air-Conditioning Engineers. Atlanta (USA).

Baumann, H. (2001). Oelfreier CO_2- Kleinkompressor [German]. The Swiss Federal Office of Energy SFOE.

Beaver A., Yin C., Bullard W., Hrnjak P.S. (1999). Experimental and Model Study of the Heat Pump / Air Conditioning Systems based on Transcritical Cycle with R744. Refrigeration into the Third Millennium - 20th International Congress of Refrigeration: Proceedings of the Conference of the International Institute of Refrigeration. Sydney (Australia). Paper No. 434.

Brandes H., Kruse H. (2000). High Temperature Heat Pumps for Existing Buildings using CO_2 as Working Fluids [German]. Klima Luft- und Kaeltetechnik. Vol. 7, pp 311-315.

Bredesen A.M., Hafner A., Pettersen J., Neksa P., Aflekt K. (1997). Heat Transfer and Pressure Drop for in-Tube Evaporation of CO_2. Heat Transfer Issues in Natural Refrigerants: Proceedings of the Conference of the International Institute of Refrigeration Commission B1, with E1 and E2. College Park (USA). pp 35-49.

Chen, X., Wu, M., Chen, P., Bansal, B. (1996a). Heat Transfer Performance of Several Spirally Corrugated Heat Exchanger Tubes - The effect of flow direction. IPENZ Conference. Dunedin (NZ). pp. 297-301.

Chen X., Carden P., Wu M. (1996b). Spiral Tube Heat Exchanger for Industrial Applications. IRHACE Technical Conference: Conference proceedings. Christchurch (New Zealand).

Dorin F., Neksa P. (2000). CO_2 Compressor and Equipment, Use and Availability. 9th Annual Conference of the Institute of Refrigeration. London (UK).

Egger R. (1987). New Ways to Optimization of Hot Water Heat Pump. Klima Luft- und Kaeltetechnik. Vol. 12, pp 543-548.

Fahl J. (1998). Lubricants for the Use with Carbon Dioxide as Refrigerant [German]. Klima Luft- und Kaeltetechnik. Vol. 8, pp 375-379.

Fenghour A., Wakeham W.A. (1998). The Viscosity of Carbon Dioxide. Journal of Physical and Chemical Reference Data. Vol. 27, pp 31-44.

Foersterling S., Lauterbach B., Kaiser H., Koehler J. (2000). Experimental Investigations of a Carbon Dioxide Compressor [German]. Klima Luft- und Kaeltetechnik. Vol. 6, pp 264-268.

Grohmann S., Wobst E. (1998). Control and Operation of A/C-Plants Working with CO_2 as Refrigerant [German]. Klima Luft- und Kaeltetechnik. Vol. 4, pp 185-188.

Hafner A. (2000). Experimental Study on Heat Pump Operation of Prototype CO_2 Mobile Air Conditioning System. Proceedings of the 4th IRR-Gustav Lorentzen Conference on Natural Working Fluids at Purdue: Proceedings of the Conference of the International Institute of Refrigeration Commissions B1, B2 with E1, E2. Purdue (USA).

Halozan H., Ebner T., Lawatsch H. (1994). Propane and CO_2 - Two Natural Alternatives. CFC's, The Day After: Proceedings of the Conference of the International Institute of Refrigeration Commissions B1, B2, E1 and E2. Padua (Italy). pp 329-336.

Halozan H., Rieberer R. (2000). CO_2 As Refrigerant - Possible Applications. Proceedings of the 4th IRR-Gustav Lorentzen Conference on Natural Working Fluids at Purdue: Proceedings of the Conference of the International Institute of Refrigeration Commissions B1, B2 with E1, E2. Purdue (USA). pp 89-96.

Halozan H., Rieberer R. (1999). CO_2 - an Interesting Alternative [German]. Klima Luft und Kaeltetechnik. Vol. 1, pp 20-23.

Hasegawa H., Ikoma M., Nishiwaki F., Shintaku H., Yakumaru Y. (2000). Experimental and Theoretical Study of Hermetic CO_2 Scroll Compressor. Proceedings of the 4th IRR-Gustav Lorentzen Conference on Natural Working Fluids at Purdue: Proceedings of the Conference of the International Institute of Refrigeration Commissions B1, B2 with E1, E2. Purdue (USA). pp 358-364.

Hashimoto K., Saikawa M. (1997). Preliminary Experimental Results of CO_2 Gas-Cooling Over-All Heat Transfer Coefficient Under Super Critical Condition. Heat Transfer Issues in Natural Refrigerants: Proceedings of the Conference of the International Institute of Refrigeration Commission B1, with E1 and E2. College Park (USA). pp 50-58.

Hauk A., Fahl J., Weidner E. (2001). Thermo- and Fluiddynamics of Lubricants with CO_2 at Transcritical Conditions [German]. Klima Luft- und Kaeltetechnik. Vol. 1, pp 13-19.

Heide R., Fahl J. (2001). Miscibility of Lubricating Oils with Carbon Dioxide [German]. Klima Luft- und Kaeltetechnik. Vol. 10, pp 466-470.

Hesse U. (1997). Lubricants for Carbon Dioxide [German]. Klima Luft- und Kaeltetechnik. Vol. 5, pp 206-208.

Hesse U., Spauschus H.O. (1996). Lubricants for Carbon Dioxide. Applications for Natural Refrigerants: Proceedings of the Conference of the International Institute of Refrigeration Commissions B1, B2, E1 and E2. Aarhus (Denmark). pp 605-608.

Heyl P., Kraus W.E., Quack H. (1998). Expander-Compressor for a More Efficient Use of CO_2 as Refrigerant. Natural Working Fluids '98 - IIR Gustav Lorentzen Conference: Proceedings of the Conference of the International Institute of Refrigeration Section B and E. Oslo (Norway). pp 195-203.

Heyl P., Quack H. (1999). Free Piston Expander-Compressor for CO_2 - Design, Applications and Results. Refrigeration into the Third Millennium - 20th International

Congress of Refrigeration: Proceedings of the Conference of the International Institute of Refrigeration. Sydney (Australia). Paper No. 516.

Heyl P., Mauer T. (2001). Practical Experiences With Transcritical CO_2-Refrigeration Systems Utilizing Expanders [German]. Klima Luft- und Kaeltetechnik. Vol. 12, pp 572-578.

Heyl P., Maurer T. (2002). Test Results Transcritical CO_2-Refrigeration Systems Utilizing Expanders. Klima Luft- Und Kaeltetechnik. Vol. 1, pp 19-22.

Hihara E., Tanaka S. (2000). Boiling Heat Transfer of Carbon Dioxide in Horizontal Tube. Proceedings of the 4th IRR-Gustav Lorentzen Conference on Natural Working Fluids at Purdue: Proceedings of the Conference of the International Institute of Refrigeration Commissions B1, B2 with E1, E2. Purdue (USA). pp 290-296.

Hiller C. (2002). Heat Pump Water Heater Operating: Experience in a Residence. ASHRAE Transactions. pp 108.

Hubacher B., Groll E. A. (2003). Performance Measurements of a Hermetic, Two-Stage Carbon Dioxide Compressor. 21st International Congress of Refrigeration. Washington DC, (USA), Paper No. 029.

Hwang Y., Kim B.H., Radermacher R. (1997a). Boiling Heat Transfer Correlation for Carbon Dioxide. Heat Transfer Issues in Natural Refrigerants: Proceedings of the Conference of the International Institute of Refrigeration Commission B1, with E1 and E2. College Park (USA). pp 81-95.

Hwang Y., Radermacher R. (1997b). Evaluation of Carbon Dioxide Heat Exchanger. Heat Transfer Issues in Natural Refrigerants: Proceedings of the Conference of the International Institute of Refrigeration Commission B1, with E1 and E2. College Park (USA). pp 105-115.

Kasper G., Halozan H. (1997). CO_2 - an Old New Refrigerant. Heat Pump Systems, Energy Efficiency, and Global Warming: Proceedings of the Conference of the International Institute of Refrigeration Commission E2, with E1 and B2. Linz (Austria). pp 121-127.

Kim J.H., Yoon H.S., Kim M.S. (2001). An Experimental Investigation of Heat Transfer Characteristics During in-Tube Gas Cooling Process of Carbon Dioxide. Proceedings of the Conference of the International Institute of Refrigeration Commission B2. Paderborn (Germany). pp 526-533.

Klein S.A., Reindl. T. D., Brownell K.A. (1999). Refrigeration System Performance Using Liquid-Suction Heat Exchanger. Refrigeration into the Third Millennium - 20th International Congress of Refrigeration: Proceedings of the Conference of the International Institute of Refrigeration. Sydney (Australia). Paper No. 71.

Knudsen H. J., Jensen P. H. (1997). Heat Transfer Coefficient for Boiling Carbon Dioxide. Proceeding Meeting of International Institute of Refrigeration on CO_2 Technologies in Heat Pumps and Air Conditioning. Trondheim (Norway).

Koyama S., Kuwahara K., Shinmura E., Shinichiro I. (2001). Experimental Study on Flow Boiling of Carbon Dioxide in a Horizontal Small Diameter Tube. Proceedings of the Conference of the International Institute of Refrigeration Commission B2. Paderborn (Germany). pp 526-533.

Leisenheimer B., Fritz T. (2000). Interaction Between CO_2 and Elastomers With Respect to Permeation and Explosive Decompression. Proceedings of the 4th IRR-Gustav Lorentzen Conference on Natural Working Fluids at Purdue: Proceedings of the Conference of the International Institute of Refrigeration Commissions B1, B2 with E1, E2. Purdue (USA). pp 207-215.

Lemke N., Tegethoff W., Schuetz S., Koehler J. (1999). Stratified Tap-Water-Storage System for Carbon Dioxide Heat Pumps. Refrigeration into the Third Millennium - 20th International Congress of Refrigeration: Proceedings of the Conference of the International Institute of Refrigeration. Sydney (Australia). Paper No. 49

Liao S., Jakobsen A. (1998). Optimal Heat Rejection Pressure in Transcritical Carbon Dioxide Air Conditioning and Heat Pump Systems. Natural Working Fluids '98 - IIR Gustav Lorentzen Conference: Proceedings of the Conference of the International Institute of Refrigeration Section B and E. Oslo (Norway). pp 301-310.

Lorentzen G. (1993). Method and Device for High Side Pressure Regulation in Transcritical Vapor Compression Cycle. United State Patent No. 5.245.836.

Lorentzen G. (1994a). Revival of Carbon Dioxide as Refrigerant. International Journal of Refrigeration. Vol. 17, pp 292-301.

Lorentzen G. (1994b). Natural Refrigerants, a Complete Solution. CFC's, The Day After: Proceedings of the Conference of the International Institute of Refrigeration Commissions B1, B2, E1 and E2. Padua (Italy). pp 317-328.

Lorentzen G., Pettersen J. (1993). A New, Efficient and Environmentally Benign System for Car Air-Conditioning. International Journal of Refrigeration. Vol. 16, pp 4-12.

Man-Hoe K., Clark W.B. (2001). Development of a Microchannel Evaporator Model for a CO_2 Air-Conditioning System. Energy, Elsevier Science Ltd. Vol. 26, pp 931-948.

Ministry of Economic Development (2000), Annual Report of the Ministry of Economic Development. Wellington (NZ).

Neksa P. (1994). Trans-Critical Vapour Compression Heat Pumps. New Applications of Natural Working Fluids in Refrigeration and Air Conditioning: Proceedings of the Conference of the International Institute of Refrigeration Commission B2. Hannover (Germany). pp 395-404.

Neksa P., Dorin F., Rekstad H., Bredesen A., Serbisse A. (1999). Development of Semi-Hermetic CO_2-Compressor. Refrigeration into the Third Millennium - 20th International Congress of Refrigeration: Proceedings of the Conference of the International Institute of Refrigeration. Sydney (Australia). Paper No. 424.

Neksa P., Girotto S., Schiefloe P.A. (1998). Commercial Refrigeration Using CO_2 As Refrigerant - System Design and Experimental Results. Natural Working Fluids '98 - IIR Gustav Lorentzen Conference: Proceedings of the Conference of the International Institute of Refrigeration Section B and E. Oslo (Norway). pp 227-236.

Neksa P., Rekstad H., Zakeri G. (1997). CO_2 Prototype Hot Water Heat Pump - Characteristics, System Design and Experimental Results. Heat Pump Systems, Energy Efficiency, and Global Warming: Proceedings of the Conference of the International Institute of Refrigeration Commission E2, with E1 and B2. Linz (Austria).

Nelson J., Balakrihnan A., Murthy S. (1998). Experiments on Stratified Chilled Water Tanks. International Journal of Refrigeration. Vol. 22, pp 216-234.

Novelli I. (1994). CFC's Substitutes: New Threats for the Ozone Layer and Global Warming - the Greenpeace Campaign. CFC's, The Day After: Proceedings of the Conference of the International Institute of Refrigeration Commissions B1, B2, E1 and E2. Padua (Italy). pp 71-78.

Olson D. (1999). Heat Transfer in Supercritical Carbon Dioxide With Convective Boundary Conditions. Refrigeration into the Third Millennium - 20th International Congress of Refrigeration: Proceedings of the Conference of the International Institute of Refrigeration. Sydney (Australia). Paper No. 641.

Oppel F.J., Ghajar A.J., Moretti P. (1986). a Numerical and Experimental Study of Stratified Thermal Storage. International Journal of Refrigeration. Vol. 92, pp 293-309.

Ortiz T., Groll E. (2000). Steady-State Thermal Finite Element Analysis of a Microchannel CO_2 Evaporator. Proceedings of the 4th IRR-Gustav Lorentzen Conference on Natural Working Fluids at Purdue: Proceedings of the Conference of the International Institute of Refrigeration Commissions B1, B2 with E1, E2. Purdue (USA). pp 297-305.

Pettersen J. (1995). Refrigerating, Air Conditioning and Heat Pump Systems Based on CO_2. Workshop Proceedings: Compression Systems with Natural Working Fluid - Applications, Experience and Developments. IEA Heat Pump Center. Trondheim (Norway). pp 163-179.

Pettersen J. (1999a). CO_2 as Working Fluid - Components, Part B. Refrigeration into the Third Millennium - 20th International Congress of Refrigeration: Proceedings of the Conference of the International Institute of Refrigeration. Sydney (Australia). Short course No. 3 (SC3).

Pettersen J. (1999b). Comparison of Explosion Energy in Residential Air-Conditioning Systems Based on HCFC-22 and CO_2. Refrigeration into the Third Millennium - 20th International Congress of Refrigeration: Proceedings of the Conference of the International Institute of Refrigeration. Sydney (Australia). Paper No. 240.

Pettersen J., Rieberer R., Leister A. (2000a). Heat Transfer and Pressure Drop Characteristics of Super-Critical Carbon Dioxide in Microchannel Heat Exchanger. Proceedings of the 4th IRR-Gustav Lorentzen Conference on Natural Working Fluids at Purdue: Proceedings of the Conference of the International Institute of Refrigeration Commissions B1, B2 with E1, E2. Purdue (USA). pp 315-323.

Pettersen J., Rieberer R., Munkejord S. (2000b). Heat Transfer and Pressure Drop Characteristics of Evaporating Carbon Dioxide in Microchannel Tube. Proceedings of the 4th IRR-Gustav Lorentzen Conference on Natural Working Fluids at Purdue: Proceedings of the Conference of the International Institute of Refrigeration Commissions B1, B2 with E1, E2. Purdue (USA). pp 324-331.

Pettersen J., Skaugen G. (1994). Operating of Transcritical CO_2 Vapour Compression Circuits in Vehicles Air Conditioning. New Applications of Natural Working Fluids in Refrigeration and Air Conditioning: Proceedings of the Conference of the International Institute of Refrigeration Commission B2. Hannover (Germany). pp 495-405.

Preissner M., Cutler B., Singanamalla S., Hwang Y., Radermacher R. (2000). Comparison of Automotive Air-Conditioning Systems Operating with CO_2 and R134a. Proceedings of the 4th IRR-Gustav Lorentzen Conference on Natural Working Fluids at Purdue: Proceedings of the Conference of the International Institute of Refrigeration Commissions B1, B2 with E1, E2. pp 191-198.

Richter M., Song S., Yin J., Kim M., Bullard C., Hrnjak P. (2000). Transcritical CO_2 Heat Pump for Residential Application. Proceedings of the 4th IRR-Gustav Lorentzen Conference on Natural Working Fluids at Purdue: Proceedings of the Conference of the International Institute of Refrigeration Commissions B1, B2 with E1, E2. Purdue (USA). pp 59-66.

Rieberer R., Gasser M., Halozan H. (2000). Control of CO_2 Heat Pumps. Proceedings of the 4th IRR-Gustav Lorentzen Conference on Natural Working Fluids at Purdue: Proceedings of the Conference of the International Institute of Refrigeration Commissions B1, B2 with E1, E2. Purdue (USA). pp 109-116.

Rieberer R., Halozan H. (1997). Design of Heat Exchanger for CO_2-Heat Pump Water Heaters. Heat Transfer Issues in Natural Refrigerants: Proceedings of the Conference of the International Institute of Refrigeration Commission B1, with E1 and E2. College Park (USA). pp 96-104.

Rieberer R., Halozan H. (1998). CO_2 Heat Pumps in Controlled Ventilation Systems. Natural Working Fluids '98 - IIR Gustav Lorentzen Conference: Proceedings of the Conference of the International Institute of Refrigeration Section B and E. Oslo (Norway). pp 167-176.

Robinson D., Groll E. (2000). Introducing ACCO2 - a Public Domain Air-to-Air Simulation Model of the Transcritical Carbon Dioxide Cycle. Proceedings of the 4th IRR-Gustav Lorentzen Conference on Natural Working Fluids at Purdue: Proceedings of the Conference of the International Institute of Refrigeration Commissions B1, B2 with E1, E2. Purdue (USA). pp 77-85.

Rossouw, P. (2000). Energy Efficiency Recourse Assessment, Energy Efficiency and Conservation Authority, Wellington (New Zealand).

Runacres K. (2002). World Water Heater Market. IRHACE Journal. Vol. 14, pp 31-34.

Saikawa M., Hashimoto K. (1998). An Experimental Study on the Behaviour of CO_2 Heat Pump Cycle. Natural Working Fluids '98 - IIR Gustav Lorentzen Conference: Proceedings of the Conference of the International Institute of Refrigeration Section B and E. Oslo (Norway). pp 177-182.

Saikawa M., Hashimoto K. (2000). Development of Prototype of CO_2 Heat Pump Water Heater for Residential Use. Proceedings of the 4th IRR-Gustav Lorentzen Conference on Natural Working Fluids at Purdue: Proceedings of the Conference of the International Institute of Refrigeration Commissions B1, B2 with E1, E2. Purdue (USA). pp 97-102.

Schmidt E.L., Kloecker K., Flacke N., Steimle F. (1998). Applying the Transcritical CO_2 Process to a Drying Heat Pump. International Journal of Refrigeration. Vol. 21, pp 202-211.

Schmidt F., Fredsted J. (1999). Optimal Control of Electronic Expansion Valve in Modern Low Charge Evaporator Systems Requires Fast Reacting Expansion Valves and New Controller Design. Refrigeration into the Third Millennium - 20th International

Congress of Refrigeration: Proceedings of the Conference of the International Institute of Refrigeration. Sydney (Australia). Paper No. 394

Schoenfeld H., Krauss W.E. (1997). Calculation and Simulation of a Heat Exchanger: Supercritical Carbon Dioxide - Water. Heat Transfer Issues in Natural Refrigerants: Proceedings of the Conference of the International Institute of Refrigeration Commission B1, with E1 and E2. College Park (USA). pp 72-80.

Silvares M.O., Huerta A.S. (1999). Influence of the Thermophysical Properties of Refrigerant-Oil Mixture on Refrigeration Components Performance. Refrigeration into the Third Millennium - 20th International Congress of Refrigeration: Proceedings of the Conference of the International Institute of Refrigeration. Sydney (Australia). Paper No. 266.

Sinnott, R. (1999). Chemical Engineering (3th ed.). Pergamon Press, Oxford New York.

Skaugen G., Svensson M. (1998). Dynamic Modelling and Simulation of a Trans-Critical CO_2 Heat Pump Unit. Natural Working Fluids '98 - IIR Gustav Lorentzen Conference: Proceedings of the Conference of the International Institute of Refrigeration Section B and E. Oslo (Norway). pp 183-190.

Suess J. (1998). Indicated Process of CO_2-Compressor [German]. Klima Luft- und Kaeltetechnik. Vol. 10, pp 463-470.

Suess J. (2001). Expansion of the Transcritical CO_2-Process [German]. Klima Luft- und Kaeltetechnik. Vol. 1, pp 33-36.

Suess J., Kruse H. (1997a). Design Criteria of CO_2-Compressor for Vapour Compression Cycles. Heat Pump Systems, Energy Efficiency, and Global Warming: Proceedings of the Conference of the International Institute of Refrigeration Commission E2, with E1 and B2. Linz (Austria). pp 139-146.

Suess J., Kruse H. (1997b). Influence of Leakage on Efficiency of Compressor for Carbon Dioxide [German]. Klima Luft- und Kaeltetechnik. Vol. 4, pp 173-470.

Suzai T., Sato A., Tadano M., Komatsubara T., Ebara T., Oda A. (1999). Development of a Carbon Dioxide Compressor for Refrigerators and Air Conditioners. Conference of the Japan Society of Refrigerating and Air Conditioning Engineers. Tokyo (Japan).

Toshio H., Kenichi F. (1998). Improvements of Mobile Air Conditioning Systems From Point of Global Warming Problems. Natural Working Fluids '98 - IIR Gustav Lorentzen Conference: Proceedings of the Conference of the International Institute of Refrigeration Section B and E. Oslo (Norway). pp 269-278.

Vaisman I. (2000). Thermodynamic analysis of carbon dioxide cycles. Proceedings of the 4th IRR-Gustav Lorentzen Conference on Natural Working Fluids at Purdue: Proceedings of the Conference of the International Institute of Refrigeration Commissions B1, B2 with E1, E2. Purdue (USA). pp 69-75.

Vaisman I. (2002). COP Analysis of Carbon Dioxide Cycles. ASHRAE Transactions. Vol. 108.

Vesovic V., Wakeham W.A., Olchowy G.A., Sengers J.V., Watson J.T.R., Millat J. (1990). the Transport Properties of Carbon Dioxide. Journal of Physical and Chemical Reference Data. Vol. 19, pp 763-808.

White S., Yarrall M., Cleland D. (1999). Modelling the Performance of a Transcritical CO_2 Heat Pump for High Temperature Heating. Refrigeration into the Third Millennium - 20th International Congress of Refrigeration: Proceedings of the Conference of the International Institute of Refrigeration. Sydney (Australia). Paper No. 641

Williamson, A. and Clark, S. (2000), Domestic Hot Water: Options and Solutions Centre for Advanced Engineering CAE, Christchurch (New Zealand).

Wiencke B. (2001). Gravity Liquid Separators for Industrial Refrigeration. ASHRAE Annual Meeting Cincinnati (USA). Seminar No. 32.

Yanagisawa T., Fukata M., Saika T., Kato H. (2000). Basis Operating Characteristics of Reciprocating Compressor for CO_2 Cycle. Proceedings of the 4th IRR-Gustav Lorentzen Conference on Natural Working Fluids at Purdue: Proceedings of the Conference of the International Institute of Refrigeration Commissions B1, B2 with E1, E2. Purdue (USA). pp 343-349.

Yanagisawa T., Fukuta M., Ogi Y., Ishii D. (1999). Performance Characteristics of Compressors Working With Carbon Dioxide. Refrigeration into the Third Millennium - 20th International Congress of Refrigeration: Proceedings of the Conference of the International Institute of Refrigeration. Sydney (Australia). Paper No. 328.

Yarrall, M.G (1998). Performance of a Transcritical Carbon Dioxide Heat Pump for Simultaneous Refrigeration and Water Heating. Thesis for a Masters of Technology at Massey University (NZ). New Zealand.

Yarrall M.G., White S.D., Cleland D.J. (1998). Performance of Transcritical CO_2 Heat Pump for the Food Processing Industries. Natural Working Fluids '98 - IIR Gustav Lorentzen Conference: Proceedings of the Conference of the International Institute of Refrigeration Section B and E. Oslo (Norway). pp 159-166.

Yin J., Park C., Boewe D., McEnaney R., Beaver A., Bullard C.W., Hrnjak P.S. (1998). Experimental and Model Comparison of Transcritical CO_2 Versus R134a and R410 System Performance. Natural Working Fluids '98 - IIR Gustav Lorentzen Conference: Proceedings of the Conference of the International Institute of Refrigeration Section B and E. Oslo (Norway). pp 331-340.

Yun R., Hwang J.H., Kim Y.C. (2001). Evaporation Heat Transfer Characteristics of Carbon Dioxide in a Horizontal Smooth Tube. Proceedings of the Conference of the International Institute of Refrigeration Commission B2. Paderborn (Germany).

Zakeri G., Neska P., Havard R., Land-Ree K., Olsen T. (2000). Results and Experiences with the First Commercial Pilot Plant CO_2 Heat Pump Water Heater. Proceedings of the 4th IRR-Gustav Lorentzen Conference on Natural Working Fluids at Purdue: Proceedings of the Conference of the International Institute of Refrigeration Commissions B1, B2 with E1, E2. Purdue (USA). pp 103-107.

Zhao Y., Ohadi M.M., Dessiatoun S.V., Schuster A., McNiar A., Radermacher R., Darabi J. (1997). Evaporation Heat Transfer Coefficients of Ammonia and CO_2 Inside a Smooth Tube. Heat Transfer Issues in Natural Refrigerants: Proceedings of the Conference of the International Institute of Refrigeration Commission B1, with E1 and E2. College Park (USA). pp 116-130.

Zingerli A.P., Groll E.A. (2000). Influence of Refrigeration Oil on the Heat Transfer and Pressure Drop of Supercritical CO_2 during in-Tube Cooling. Proceedings of the 4th IRR-Gustav Lorentzen Conference on Natural Working Fluids at Purdue: Proceedings of the Conference of the International Institute of Refrigeration Commissions B1, B2 with E1, E2. Purdue (USA). pp 279-289.

12 Nomenclature

12.1 List of abbreviations

ASHRAE	American Society of Heating, Refrigerating and Air-conditioning Engineers
CFC	Chloro-fluorocarbon based refrigerants
COP	Coefficient of performance
CO_2	Carbon dioxide
EERA	Energy End-Use Database NZ
E-P	Evan-Perkins refrigerant cycle
GC	Gas cooler
GWP	Global warming potential
HCFC	Hydro-chloro-fluorocarbon based refrigerants
HWC	Hot water (storage) cylinder
HWSS	Hot water supply system
IHX	Internal heat exchanger
IPR	Intermediate pressure receiver
LMTD	Log mean temperature difference
LPR	Low pressure receiver
NZ	New Zealand
ODP	Ozone depletion potential
POE	Polyolester-oil (synthetic oil)
R	Refrigerant
SFOE	Swiss Federal Office of Energy (SFOE)
UA-Value	Overall heat transfer coefficient times the heat transfer surface area
WPRV	main water-supply pressure reducing valve
WSS	Water supply system

12.2 Symbols

Symbols used for the experimental data analysis

$A_{CS,LPR}$	Cross sectional area of the LPR [m^2]
$A_{CO2,GC}$	Heat transfer surface area of the refrigerant-side [m^2]
$A_{i,HWC}$	Surface of the inner HWC shell [m^2]
$A_{mean,E}$	Mean heat transfer surface of the evaporator [m^2]
$A_{mean,GC}$	Mean heat transfer surface of the gas cooler [m^2]
$A_{mean,GC,n}$	Mean heat transfer surface of the n^{th} segment of the gas cooler [m^2]
$A_{O,comp}$	Surface area of the compressor [m^2]
$A_{O,IHX}$	Outer heat transfer surface of the IHX [m^2]

$A_{W,GC}$	GC heat transfer surface at the water-side [m^2]
COP_{hp}	Heat pump heating coefficient of performance [-]
COP_{Carnot}	Carnot coefficient of performance of the heat pump [-]
$H_{CO2\text{-}level,\ LPR}$	Height of liquid CO_2 level in the LPR [m]
H_{HWC}	Height of the inner HWC shell [m]
$LMTD_E$	Log mean temperature difference in the evaporator [K]
$LMTD_{GC,n}$	Log mean temperature difference of the n^{th} gas cooler segment [K]
$LMTD_{IHX}$	Log mean temperature difference of the IHX [K]
M_{CO2}	Refrigerant charge [kg]
$M_{CO2,\ E\text{-}flooded}$	Refrigerant charge when the evaporator starts to be flooded[kg]
$M_{HWC,\ j}$	Mass of the HWC j^{th} segment [kg]
M_{HWC}	Total mass of the HWC [kg]
P_{el}	Power consumption of the electric compressor motor [W]
PR	Compressor pressure ratio [-]
$T_{W,\ GC\_in}$	Water temperature at the gas cooler inlet [°C]
$T_{W,\ GC\_out}$	Water temperature at the gas cooler outlet [°C]
$T_{W,\ GC\_centre}$	Water temperature between the first and the second gas cooler unit [°C]
T_{CO2,GC_in}	Refrigerant temperature at the gas cooler inlet [°C]
T_{CO2,GC_out}	Refrigerant temperature at the gas cooler outlet [°C]
$T_{CO2,\ IHX\_in}$	High-side refrigerant temperature at the IHX inlet [°C]
$T_{CO2,\ IHX\_out}$	High-side refrigerant temperature at the IHX outlet [°C]
$T_{CO2,\ LPR\_in}$	Refrigerant temperature at the LPR inlet [°C]
$T_{CO2,\ LPR\_out}$	Refrigerant temperature at the LPR outlet [°C]
$T_{CO2,E}$	Refrigerant evaporation temperature [°C]
$T_{W,\ E\_in}$	Water temperature at the evaporator inlet [°C]
T_{W,E_out}	Water temperature at the evaporator outlet [°C]
$T_{O,\ comp}$	Average compressor body surface temperature [°C]
T_{air}	Ambient air temperature near the compressor surface [°C]
$T_{w\text{-}mean}$	Mean temperature of the water in the HWC at the time t [°C]
T_j	Water temperature measured for the j^{th} segment [°C]
U_E	Overall heat transfer coefficient of the evaporator [W/m^2K]
U_{GC}	Overall U value of the gas cooler, based on the mean heat transfer surface area [W/m^2K]
U_{IHX}	Overall IHX heat transfer coefficient [W/m^2K]
U_{HWC}	Overall heat transfer coefficient based in the inner HWC shell [W/m^2K]
V_{theo}	Nominal swept volume of the compressor [m^3/s]
c_W	Specific heat capacity of water [J/kgK]
d_{HWC}	Diameter of the inner HWC shell [m]
f_{vent}	Overall heat transfer reduction factor due to the vented GC design [-]
h_{air}	Overall heat transfer coefficient at the compressor body surface [W/m^2K]

$h_{CO2,comp\_out\text{-}is}$	Enthalpy of the refrigerant at the compressor outlet if the compression was isentropic [J/kg]
$h_{CO2,comp\_in}$	Enthalpy of the refrigerant at the compressor inlet [J/kg]
$h_{CO2,comp\_out}$	Enthalpy of the refrigerant at the compressor outlet if the compression was isentropic [J/kg]
$h_{CO2,E}$	Refrigerant side heat transfer coefficient [W/m^{2}K]
h_{CO2,E_in}	Enthalpy of the refrigerant at evaporator inlet [J/kg]
$h_{CO2,GC}$	Refrigerant-side heat transfer coefficient [W/mK]
$h_{CO2,\ GC\_centre}$	Enthalpy of the refrigerant between the first and the second gas cooler unit [J/kg]
$h_{CO2,\ GC\_in}$	Enthalpy of the refrigerant at the gas cooler inlet [J/kg]
$h_{CO2,\ GC\_out}$	Enthalpy of the refrigerant at the gas cooler outlet [J/kg]
h_{CO2,IHX_in}	Enthalpy of carbon dioxide at the IHX inlet [J/kg]
h_{CO2,IHX_out}	Enthalpy of carbon dioxide at the IHX outlet [J/kg]
$h_{CO2,\ LPR\_out}$	Enthalpy of the refrigerant at LPR outlet [J/kg]
$h_{W,E}$	Evaporator water side heat transfer coefficient [W/m^{2}K]
$h_{W,GC}$	GC water-side heat transfer coefficient [W/mK]
m_{CO2}	Mean CO_2 mass flowrate [kg/s]
$m_{CO2,\ E}$	Evaporator refrigerant mass flowrate back-calculated of the low-side heat balance [kg/s]
$m_{CO2,\ GC}$	GC refrigerant mass flowrate in the gas cooler [kg/s]
$m_{CO2,\ GC\text{-}1st}$	Refrigerant mass flowrate back-calculated from the heat balance of the first GC [kg/s]
$m_{CO2,\ GC\text{-}2nd}$	Refrigerant mass flowrate back-calculated from the heat balance of the second GC [kg/s]
$m_{W,\ E}$	Water mass flow rate in the evaporator [kg/s]
$m_{W,\ GC}$	Water mass flowrate in the gas cooler [kg/s]
$p_{discharge}$	Compressor discharge pressure [bar_g]
$p_{suction}$	Compressor suction pressure [bar_g]
$r_{i,\ GC}$	Radius of the inner GC tube [m]
$r_{o,\ GC}$	Radius of the inner tube of the GC annulus [m]
t_{tube}	Wall thickness of the tube [m]
v_{CO2}	Vertical velocity of the refrigerant vapour in the LPR [m/s]
$\Delta m_{CO2,imbalance}$	Refrigerant mass flowrate imbalance [%]
Δt	Time interval in-between the temperature measurements [s]
ϕ_{GC}	Heat transfer rate for the gas cooler [W]
$\phi_{W,GC}$	Rate of heat gain by the water mass in the gas cooler [W]
$\phi_{CO2,\ GC}$	Rate of heat rejection by the CO_2 in the gas cooler [W]
$\phi_{GC\text{-}1st}$	Heat transfer rate for the first gas cooler unit [W]
$\phi_{GC\text{-}2nd}$	Heat transfer rate for the second gas cooler unit [W]
$\phi_{GC,\ n}$	Heat transfer rate of the nth gas cooler segment [W]

ϕ_{IHX}	Heat transfer rate of the IHX [W]
ϕ_{E}	Heat transfer rate in the evaporator [W]
$\phi_{W.E}$	Heat transfer rate rejected by the evaporator water [W]
$\phi_{CO2,\ lps}$	Heat rate required for the evaporation and superheating of the refrigerant flow at the low-pressure side [W]
$\phi_{losses,\ comp}$	Heat losses of the compressor calculated by the compressor energy balance [W]
$\phi_{losses\text{-}conv,\ comp}$	Heat losses of the compressor calculated by the heat convection to the ambient air [W]
$\phi_{unspecified}$	Unspecified energy imbalance [W]
$\phi_{losses,\ HWC}$	Heat losses of the HWC to the ambient air [W]
η_{vol}	Overall compressor volumetric efficiency [-]
$\eta_{is,\ eff}$	Effective isentropic compressor efficiency [-]
$\eta_{is,\ ind}$	Indicated isentropic compressor efficiency [-]
η_{hp}	Thermal efficiency of the heat pump [-]
ε_{IHX}:	IHX effectiveness [-]
ε_{GC}	Gas cooler effectiveness [-]
λ_{tube}	Thermal conductivity of the tube [W/mK]
$\rho_{CO2\text{-}l,\ LPR}$	Density of the liquid refrigerant in the LPR [m^3/kg]
$\rho_{CO2\text{-}g,\ LPR\_outlet}$	Density of the refrigerant vapour at the LPR outlet [kg/m^3]
$\rho_{CO2,\ comp\_in}$	Refrigerant (vapour) density at the compressor inlet [kg/m^3]

Symbols used in the HWSS Model

COP_{hp}	Heat pump heating COP [-]
COP_{HWSS}	HWSS coefficient of performance [-]
E_{hw}	Total energy in the supplied hot water [J]
J	Number of segments [-]
M_{buffer}	Mass accumulated in the buffer segment [kg]
M_{HWC}	Mass of the water in the HWC [kg]
M_{seg}	Mass of the water in the segment [kg]
$P_{el,\ hp}$:	Power consumption of the heat pump compressor [W]
T_{air}	Ambient air temperature [°C]
T_{h}	Water temperature at the height h of the HWC [°C]
$T_{hp,\ in}$	Temperature of the water at the heat pump inlet [°C]
$T_{hp,\ on}$	Heat pump temperature set-point [°C]
$T_{hp,\ out}$	Temperature of the water at the heat pump outlet [°C]
$T_{HWC,\ bot}$	Temperature of the water at the HWC bottom outlet [°C]
$T_{HWC,\ top}$	Temperature of the water at the HWC top outlet [°C]
$T_{HWC,\ t=0}$	Initial water temperature in the HWC [°C]

$T_{hw,\ user}$	Temperature of the hot water supplied to the user [°C]
T_j	Water temperature of the j[th] segment in the HWC [°C]
T_{tap}	Cold water supply temperature [°C]
$T_{thermostat}$	Temperature at the HWC thermostat [°C]
T_{user}	Temperature of the water demanded by the user [°C]
$T_{user,\ supplied}$	Temperature of the water supplied to the user [°C]
U_{HWC}	Overall heat transfer coefficient of the HWC based on the inner surface [W/m²K]
$W_{el,\ hp}$	Electric work of the heat pump compressor [J]
c_W	Specific heat capacity of water [J/kgK]
d_{HWC}	Inner diameter of the HWC [m]
$f_{\lambda,\ flow}$	Conductivity enhancement factor for mixing due to the flow [-]
$f_{\lambda,\ flow}$	Conductivity enhancement factor for mixing effects [-]
$f_{\lambda,\ nat\_conv\_pos}$	Conductivity enhancement factor for the natural convection with a positive temperature gradient between the segments [-]
$f_{\lambda,\ nat\_conv\_neg}$	Conductivity enhancement factor for natural convection with a negative temperature gradient between the segments [-]
h	Distance from bottom at the HWC [m]
$h_{thermostat}$	Position of the thermostat [m]
m_{user}	Mass flowrate of water supplied to the user [l/s]
$m_{cw,\ user}$	Mass flowrate of cold water supplied to the user [l/s]
$m_{hw,\ user}$	Mass flowrate of hot water supplied to the user [l/s]
m_{hp}	Mass flowrate of hot water produced by the heat pump [l/s]
m_{HWC}	Mass flowrate of water down though the HWC [l/s]
$m_{HWC,\ tap}$	Mass flowrate of cold water at the HWC tap [l/s]
m_{HWC}	Water mass flowrate through the HWC [l/s]
$switch$	Heat pump switch indicating whether the heat pump is on (1) or off (0)
t	Time [s]
$t_{reliable\_supply}$	Total time at which the HWSS was able to meet the users demand [s]
t_{supply}	Total time hot water is required [s]
Δh	Thickness of the segment [m]
ΔT_{DB}	Temperature dead band for thermostat [K]
Δt	Time step [s]
$\Delta t_{cond+heal\_losses}$	Maximal time step for numerically stable conduction and heat loss term [s]
$\Delta t_{m\_user>0}$	Periods for which the user was supplied with the hot water [s]
$\Delta t_{plug\text{-}flow}$	Differential time for numerical stable plug-flow-term [s]
$\Delta t_{T\_user,\ supply \geq T\_hw,\ user}$	Period for which the user was supplied with the demanded hot water temperature [s]
ΔT_{HWC}	Change of the mean HWC temperature [K]
ϕ_A	Heat losses to the ambient air [W]

ϕ_{hp}	Predicted heat pump heat capacity [W]
$\phi_{seg,h}$	Heat accumulated in the segment at the height h of the HWC [W]
ϕ_{m}	Heat transferred by the water mass flowrate [W]
$\phi_{m,\ h\pm\Delta h/2}$	Heat-rate transferred through the surface h+Δh/2 and h-Δh/2 of the segment at the height h in the HWC [W]
ϕ_{λ}	Heat transferred by the heat conduction [W]
$\phi_{\lambda,h\pm\Delta h/2}$	Heat rate transferred through the surface h+Δh/2 or h-Δh/2 of the segment at the height h in the HWC [W]
$\lambda_{eff,h\pm\Delta h/2}$	Pseudo conduction thermal conductivity at the surface h+Δh/2 or h-Δh/2, which considered heat conduction, natural convection and/or mixing of the water between the segments [W/mK]
λ_{W}	Conductivity of water [W/mK]
ρ_{W}	Density of water [kg/m^3]

13 Appendix

A.1 Refrigerant property data

CO_2 property data proposed by Vesovic *et al* (1990) and Fenghour and Wakeham (1998) were used to develop equations that give the viscosity and thermal conductivity at 100 bar.g pressure as a function of the temperature.

Equation for viscosity:

$$\eta_{CO2} = -7.55E-18 \times T_{CO2}^{\,6} + 6.22E-15 \times T_{CO2}^{\,5} - 1.50E-12 \times T_{CO2}^{\,4} + 1.86E-10 \times T_{CO2}^{\,3} + 5.48E-09 \times T_{CO2}^{\,2} - 2.11E-06 \times T_{CO2} + 1.15E-04$$

Equ. 13.1

Equation for thermal conductivity:

$$\lambda_{CO2} = -4.42E-15 \times T_{CO2}^{\,6} + 4.34E-12 \times T_{CO2}^{\,5} - 1.56E-9 \times T_{CO2}^{\,4} + 2.32E-07 \times T_{CO2}^{\,3} - 6.82E-06 \times T_{CO2}^{\,2} - 1.40E-03 \times T_{CO2} + 1.22E-01$$

Equ. 13.2

Where:

η_{CO2}	Viscosity of CO_2 [kg/ms]
λ_{CO2}	Thermal conductivity of CO_2 [W/mK]
T_{CO2}	CO_2 temperature [°C]

These equations give the viscosity and the conductivity of CO_2 at 100 bar.g in the range -33°C to 276°C within 10% except near the critical temperature where the deviation was about 30% for viscosity and 20% for conductivity.

A.2 Heat pump design

A.2.1 Heat pump process design model

A model of the heat pump process was developed to design the heat pump process and to predict the performance at varying operating conditions. The heat pump model included:

- Compressor calculations based on the manufacturers data
- GC heat transfer calculations based on gliding refrigerant and water temperatures
- IHX heat transfer calculations
- Evaporator heat transfer calculations
- Heat pump efficiency calculations

The heat pump process input parameters were:

- Ambient air temperature
- Compressor discharge pressure
- Suction vapour superheat
- Temperature approach in the heat exchangers (for the nominal heat pump design condition) or heat exchangers UA-values (for heat pump process performance predictions at conditions other than the nominal heat pump design)

The following temperature approaches in the heat exchangers were used for the nominal heat pump design condition:

GC:	5 K temperature difference between the inlet water and the outlet refrigerant.
IHX:	5K temperature difference between the high-side refrigerant outlet and the refrigerant evaporating temperature.
Evaporator:	10 K temperature difference between the ambient air and the refrigerant evaporating temperature.

Figure 13.1 shows the heat pump process in the p-h diagram at the nominal design condition and the nomenclature used:

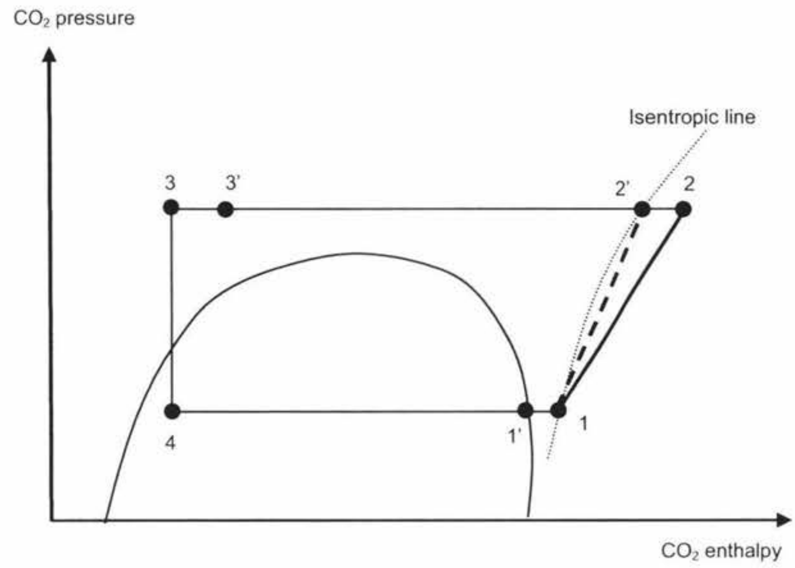

Figure 13.1: Schematic of the transcritical CO_2 refrigerant cycle

1'	State of the refrigerant at the evaporator outlet [-]
1	State of the refrigerant at the compressor suction (superheated vapour) [-]
2'	State of the refrigerant at the compressor discharge if the compression was isentropic [-]
2	State of the refrigerant at the compressor discharge [-]
3'	State of the refrigerant at the GC outlet [-]
3	State of the refrigerant at the IHX outlet [-]
4	State of the refrigerant at the evaporator inlet [-]

A.2.1.1 Compressor calculations

The compressor efficiencies were defined by Neksa *et al* (1999) as followed:

- Volumetric efficiency

$$\eta_{vol} = \frac{m_{CO2}}{V_{theo}\ \rho_{CO2,1}} \qquad \text{Equ. 13.3}$$

- Isentropic efficiency

$$\eta_{is,eff} = \frac{m_{CO2}\left(h_{CO2,2'} - h_{CO2,1}\right)}{P_{el}} \qquad \text{Equ. 13.4}$$

and:

$$\eta_{is,eff} = \eta_{is,ind} \ \eta_{motor} \ \eta_{mech+valves} \qquad \text{Equ. 13.5}$$

- Indicated isentropic efficiency

$$\eta_{is,ind} = \frac{h_{CO2,2'} - h_{CO2,1}}{h_{CO2,2} - h_{CO2,1}} \qquad \text{Equ. 13.6}$$

Where:

η_{vol}	Volumetric compressor efficiency [-]
$\eta_{is,\,eff}$	Effective isentropic efficiency [-]
$\eta_{is,\,ind}$	Indicated isentropic efficiency [-]
η_{motor}	Compressor motor efficiency [-]
$\eta_{motor,\,mech+valve}$	Compressor motor, mechanical and valve effectiveness [-]
m_{CO2}	Refrigerant mass flow rate [kg/s]
V_{theo}	Nominal swept volume of the compressor [m^3/s]
$\rho_{CO2,\,1}$	Refrigerant (vapour) density at the compressor suction [kg/m^3]
$h_{CO2,\,2'}$	Refrigerant enthalpy at the compressor outlet if the compression was isentropic [J/kg]
$h_{CO2,\,2}$	Refrigerant enthalpy at the compressor outlet [J/kg]
$h_{CO2,\,1}$	Refrigerant enthalpy at the compressor suction [J/kg]
P_{el}	Compressor motor power consumption [W]

Literature data of a compressor model similar to the compressor used were given by Neksa *et al* (1999). These data was used to fit equations which describes the compressor performance as a function of the pressure ratio.

$$\eta_{vol} = 6.905 \times 10^{-3} \ \pi^2 - 1.565 \ \pi + 1.142 \qquad \text{Equ. 13.7}$$

$$\eta_{is,eff} = 4.761 \times 10^{-3} \ \pi^2 - 9.619 \times 10^{-2} \ \pi + 0.940 \qquad \text{Equ. 13.8}$$

$$\eta_{is,ind} = -1.607 \times 10^{-3} \ \pi^2 - 2.925 \times 10^{-2} \ \pi + 0.986 \qquad \text{Equ. 13.9}$$

with:

$$\pi = \frac{p_{CO2,2}}{p_{CO2,1}} \qquad \text{Equ. 13.10}$$

Where:

π	Pressure ratio [-]
$p_{CO2,2}$	Compressor discharge pressure [bar.a]
$p_{CO2,1}$	Compressor suction pressure [bar.a]

The refrigerant mass flowrate was given by:

$$m_{CO2} = V_{theo}\ \rho_{CO2,1}\ \eta_{vol} \qquad \text{Equ. 13.11}$$

The compressor discharge temperature was evaluated from refrigerant enthalpy and pressure at the compressor discharge and refrigerant property data.

$$T_{CO2,2} = f(h_{CO2,2}, p_{CO2,2}) \qquad \text{Equ. 13.12}$$

with:

$$h_{CO2,2} = h_{CO2,1} + \frac{h_{CO2,2'} - h_{CO2,1}}{\eta_{is,ind}} \qquad \text{Equ. 13.13}$$

Where:

$T_{CO2,2}$	Refrigerant temperature at the compressor discharge [°C]

The refrigerant enthalpy at the compressor discharge for isentropic compression ($h_{CO2,2'}$) was evaluated from the compressor discharge pressure and the entropy at the compressor suction.

$$h_{CO2,2'} = f(s_{CO2,2'}, p_{CO2,2}) \qquad \text{Equ. 13.14}$$

with:

$$s_{CO2,2'} = s_{CO2,1} \qquad \text{Equ. 13.15}$$

Where:

$s_{CO2,2'}$	Refrigerant entropy at the compressor discharge [J/kgK]
$s_{CO2,1}$	Refrigerant entropy at the compressor suction [J/kgK]

The compressor power requirement was calculated from the effective isentropic efficiency:

$$P_{el} = \frac{m_{CO2}\left(h_{CO2,2'} - h_{CO2,1}\right)}{\eta_{is,eff}}$$ Equ. 13.16

At constant discharge pressure and varying suction, the compressor power has a maximum because the enthalpy change in the CO_2 for isentropic compression ($h_{CO2,2'}$ - $h_{CO2,1}$) declines as the suction pressure increases while the refrigerant mass flowrate (m_{CO2}) increases due to increasing suction CO_2 density and increasing volumetric compressor efficiency.

The compressor heat losses were calculated by:

$$\phi_{comp,losses} = P_{el} - m_{CO2}\left(h_{CO2,2} - h_{CO2,1}\right)$$ Equ. 13.17

Where:

$\phi_{comp,\ losses}$ Compressor heat losses to ambient temperature [W]

A.2.1.2 GC heat transfer calculations

The gas cooler heat transfer capacity was calculated by:

$$\phi_{CO2,GC} = m_{CO2}\left(h_{CO2,2} - h_{CO2,3'}\right)$$ Equ. 13.18

The water mass flowrate was calculated from the overall GC heat balance:

$$m_{W,GC} = \frac{\phi_{CO2,GC}}{c_w\left(T_{W,GC\_out} - T_{W,GC\_in}\right)}$$ Equ. 13.19

Where:

$\phi_{CO2,GC}$	Heat transfer rate of the GC [W]
$h_{CO2,\ 3'}$	Refrigerant enthalpy at the gas cooler outlet [J/kg]
$m_{W,\ GC}$	GC water mass flowrate [l/s]
$T_{W,\ GC\_out}$	GC water outlet temperature [°C]
$T_{W,\ GC\_in}$	GC water inlet temperature [°C]
c_W	Specific heat capacity of water [J/kgK]

The heat transfer performance predictions of the GC requires a steady-state model of the GC, which predicts the heat transfer process at gliding refrigerant and water temperatures and supercritical CO_2 conditions. The method used for the calculation of the GC UA-value is described in sections A.2.2, Equ. 13.44.

The overall GC LMTD value was given by:

$$LMTD_{GC} = \frac{\phi_{GC}}{UA_{GC}} \qquad \text{Equ. 13.20}$$

Where:

$LMTD_{GC}$ Log mean temperature of the GC [K]

UA_{GC} GC UA-value [W/K]

The gas cooler effectiveness was calculated by:

$$\varepsilon_{GC} = \frac{T_{CO2,2} - T_{CO2,3'}}{T_{CO2,2} - T_{GC,W\_in}} \qquad \text{Equ. 13.21}$$

Where:

ε_{GC} GC effectiveness [-]

A.2.1.3 IHX heat transfer calculations

The IHX heat transfer capacity was given by:

$$\phi_{IHX} = m_{CO2}\left(h_{CO2,3'} - h_{CO2,3}\right) \qquad \text{Equ. 13.22}$$

Where:

ϕ_{IHX} Heat transfer rate of the IHX [W]

$h_{CO2,3}$ Refrigerant enthalpy at the IHX high-pressure side outlet [J/kg]

The IHX UA-value was calculated by:

$$UA_{IHX} = \frac{\phi_{IHX}}{LMTD_{IHX}} \qquad \text{Equ. 13.23}$$

with:

$$LMTD_{IHX} = \frac{(T_{CO2,3'} - T_{CO2,1}) - (T_{CO2,3} - T_{CO2,1'})}{\ln\left(\frac{T_{CO2,3'} - T_{CO2,1}}{T_{CO2,3} - T_{CO2,1'}}\right)} \qquad \text{Equ. 13.24}$$

Where:

UA_{IHX}	IHX UA-Value [W/K]
$LMTD_{IHX}$	Log mean temperature difference of the IHX [K]
$T_{CO2,1}$	Refrigerant temperature at the IHX suction side outlet [°C]

The refrigerant temperature at the IHX outlet $T_{CO2,3}$ and subsequently the refrigerant enthalpy was given by the IHX effectiveness:

$$\varepsilon_{IHX} = \frac{T_{CO2,3'} - T_{CO2,3}}{T_{CO2,3'} - T_{CO2,1'}} \qquad \text{Equ. 13.25}$$

Where:

ε_{IHX}	IHX effectiveness [-]
$T_{CO2,1'}$	Evaporation temperature [°C]

A.2.1.4 Evaporator heat transfer calculations

The evaporator was designed to be flooded. Because of the unknown amount of liquid carry over from the evaporator to the LPR, the evaporator heat transfer had to be calculated from the overall low-side heat balance:

$$\phi_{lp-side} = \phi_E + \phi_{IHX} \qquad \text{Equ. 13.26}$$

with:

$$\phi_{lp-side} = m_{CO2}\,(h_{CO2,1} - h_{CO2,4}) \qquad \text{Equ. 13.27}$$

$$\phi_E = UA_E\ TD_E \qquad \text{Equ. 13.28}$$

and:

$$TD_E = T_{air} - T_{CO2,1'}$$ Equ. 13.29

Solving for the evaporation temperature:

$$T_{CO2,1'} = T_{air} - \frac{m_{CO2}\left(h_{CO2,1} - h_{CO2,4}\right) - \phi_{IHX}}{UA_E}$$ Equ. 13.30

Where:

$\phi_{lp\text{-}side}$	Heat flow required for the refrigerant evaporation and vapour superheating [W]
ϕ_E	Heat transfer rate for the evaporator [W]
$h_{CO2,4}$	Refrigerant enthalpy at the evaporator inlet [J/kg]
TD_E	Temperature difference for the evaporator [K]
UA_E	Evaporator UA-value [W/K]
T_{air}	Ambient air temperature [°C]

Equ. 13.30, Equ. 13.22 and Equ. 13.25 were solved iteratively for the evaporation temperature $T_{CO2,1}$ noting that:

$$h_{CO2,4} = h_{CO2,3}$$ Equ. 13.31

A.2.1.5 Heat pump efficiency calculations

The overall heat pump coefficient of performance (COP) was calculated by:

$$COP_{hp} = \frac{\phi_{GC}}{P_{el}}$$ Equ. 13.32

Where:

COP_{hp} Coefficient of performance of the heat pump [-]

The maximal possible efficiency of the heat pump process is given by the Carnot efficiency, which is a function of the heat sink and the heat source temperatures.

$$COP_{Carnot} = \frac{T_{W,GC\_out} + 273}{T_{W,GC\_out} - T_{air}}$$ Equ. 13.33

Where:

COP_{Carnot} Carnet coefficient of performance of the heat pump [-]

The overall thermal heat pump thermal efficiency was defined as the ratio between the achieved efficiency and the Carnot efficiency:

$$\eta_{hp} = \frac{COP_{hp}}{COP_{Carnot}} \quad \text{Equ. 13.34}$$

Where:

η_{hp} Thermal efficiency of the heat pump [-]

A.2.2 Gas cooler performance predictions

The performance predictions of the GC requires a steady-state model of the GC, which predicts the heat transfer process at gliding refrigerant and water temperatures and supercritical CO_2 conditions. The modelling process involved:

1. Division of the GC in segments of equal refrigerant temperature change and prediction of the GC temperature profile and the GC-UA-value for each segment
2. Calculation of the GC tube dimensions
3. Calculation of the heat transfer coefficient for the water and refrigerant sides for each segment based on the average properties over the gliding temperatures.
4. Calculating the overall heat transfer coefficient for each segment.
5. Prediction of the GC length required to transfer the heat flow for each segment.
6. Prediction of the refrigerant mass flow and the pressure drop in the GC.

Gas cooler temperature profile

The heat transfer in the GC takes place at gliding refrigerant and water temperatures. To predict the heat transfer, the GC was divided into J segments. The segments had the mid points at the centre and equal CO_2 temperature difference between the upstream (j+1/2) and downstream (j-1/2) face of the segment (Figure 13.2). This method was applied because the refrigerant properties, such as the enthalpy at supercritical conditions and at given pressure were available as a function of the temperature.

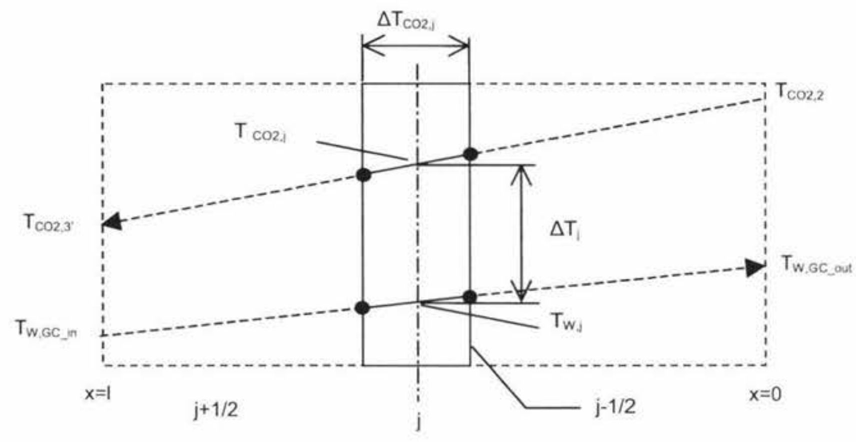

Figure 13.2: General segment j, somewhere in the gas cooler

The heat balance for the general segment is given by:

$$\phi_{CO2,j} = \phi_{W,j} \qquad \text{Equ. 13.35}$$

with:

$$\phi_{CO2,j} = m_{CO2}\left(h_{CO2,j+1/2} - h_{CO2,j-1/2}\right) \qquad \text{Equ. 13.36}$$

and:

$$\phi_{W,j} = m_W \; c_W \; \left(T_{W,j-1/2} - T_{W,j+1/2}\right) \qquad \text{Equ. 13.37}$$

The enthalpies of CO_2 at the segment faces were evaluated from the refrigerant pressure and temperatures:

$$h_{CO2,j\pm1/2} = f(T_{CO2,j\pm1/2}, p_{CO2.2}) \qquad \text{Equ. 13.38}$$

with:

$$T_{CO2,j+1/2} = T_{CO2,2} - j \; \Delta T_{CO2,j} \qquad \text{Equ. 13.39}$$

$$T_{CO2,j-1/2} = T_{CO2,2} - (j-1) \; \Delta T_{CO2,j} \qquad \text{Equ. 13.40}$$

and:

$$\Delta T_{CO2,j} = \frac{T_{CO2,2} - T_{CO2,3'}}{J}$$ Equ. 13.41

Where:

$\phi_{CO2,j}$	Heat transfer rate in the j[th] segment rejected by the refrigerant [W]
$\phi_{W,j}$	Heat transfer rate j[th] segment absorbed by the water [W]
$h_{CO2,j\pm1/2}$	Refrigerant enthalpy at the faces of the j[th] segment [J/kgK]
$\Delta T_{CO2,j}$	Temperature difference across the refrigerant side of the segment [K]
$\Delta T_{CO2,j\pm1/2}$	Refrigerant temperatures at the faces of the j[th] segment [°C]
$T_{W,j\pm1/2}$	Water temperatures at the faces of the j[th] segment [°C]
J	Number of segments [-]
j	Index of segment starting with 1 at the GC refrigerant side inlet [-]

The water temperature at the faces of the segments was given by:

$$T_{W,j-1/2} = T_{W,GC\_out} - \frac{m_{CO2}}{m_W\ c_W}\left(h_{CO2,2} - h_{CO2,j-1/2}\right)$$ Equ. 13.42

$$T_{W,j+1/2} = T_{W,GC\_out} - \frac{m_{CO2}}{m_W\ c_W}\left(h_{CO2,2} - h_{CO2,j+1/2}\right)$$ Equ. 13.43

The overall GC UA-value was the sum of the UA-values in the segments. It was calculated by the heat transfer rate and the logarithmic temperature difference for each segment.

$$UA_{GC} = \sum_{1}^{J} UA_{GC,j} = \sum_{1}^{J} \frac{\phi_{GC,j}}{LMTD_{GC,j}}$$ Equ. 13.44

and:

$$LMTD_{GC,j} = \frac{\left(T_{CO2,j+1/2} - T_{W,j+1/2}\right) - \left(T_{CO2,j-1/2} - T_{W,j-1/2}\right)}{ln\left(\dfrac{T_{CO2,j+1/2} - T_{W,j+1/2}}{T_{CO2,j-1/2} - T_{W,j-1/2}}\right)}$$ Equ. 13.45

Where:

UA_{GC}	GC UA-value [W/K]
$UA_{GC,j}$	GC UA-value of the j[th] segment [W/K]

$LMTD_{GC,j}$ Log mean temperature difference of the j[th] segment [K]

The overall GC LMTD value was given by:

$$LMTD_{GC} = \frac{\phi_{GC}}{UA_{GC}}$$ Equ. 13.46

Where:

$LMTD_{GC}$ Log mean temperature of the GC [K]

The gas cooler effectiveness was calculated by:

$$\varepsilon_{GC} = \frac{T_{CO2,2} - T_{CO2,3'}}{T_{CO2,2} - T_{GC,W\_in}}$$ Equ. 13.47

Where:

ε_{GC} GC effectiveness [-]

Gas cooler tube dimensions

The annulus of the double pipe GC's were made of twisted tubes. The following twisted tube parameters were required for the heat transfer predictions:

- Heat transfer surface
- Cross sectional area for flow
- Hydraulic diameter

The outside diameter of the twisted tube was equal to the outside diameter of the straight tube before the twisting process. Assuming that the wall thickness of the tubes did not change through the twisting process, the outside surface area of the twisted tube was equal to the outside surface area of the straight tube.

$$A_{outside,twisted\_tube} = d_{outside,straight,tube}\ \pi\ L_{straight\_tube}$$ Equ. 13.48

$$A_{inside,twisted\_tube} = d_{inside,straight,tube}\ \pi\ L_{straight\_tube}$$ Equ. 13.49

Noting that:

$$d_{outside,straight,tube} = d_{outside,twisted,tube}$$ Equ. 13.50

Where:

$A_{outside,\ twisted\_tube}$	Outside heat transfer surface of the twisted tube [m^2]
$A_{inside,\ twisted\_tube}$	Inside heat transfer surface of the twisted tube [m^2]
$d_{outside,straight\_tube}$	Outside diameter of the straight tube [m]
$d_{outside,twisted\_tube}$	Outside diameter of the straight tube [m]
$d_{inside,\ straight\_tube}$	Inside diameter of the straight tube [m]
$L_{straight\_tube}$	Tube length before the twisting process [m]

The equivalent hydraulic diameter of any shaped tube is defined by:

$$d_h = 4\frac{A_{cs}}{C_{cs}}$$ Equ. 13.51

Where:

d_h	Hydraulic diameter [m]
A_{cs}	Cross sectional area of the tube available for flow [m^2]
C_{cs}	Wetted circumference of the cross sectional area [m]

The wetted circumference of the twisted tube was calculated by:

$$C_{outside,twisted\_tube} = d_{outside,straight\_tube}\,\pi\,\frac{L_{straight\_tube}}{L_{twisted\_tube}}$$ Equ. 13.52

$$C_{inside,twisted\_tube} = d_{inside,straight\_tube}\,\pi\,\frac{L_{straight\_tube}}{L_{twisted\_tube}}$$ Equ. 13.53

The wetted cross section of the annulus was hence given by:

$$C_{CS,annulus} = d_{outside,annulus}\,\pi + C_{outside,twisted\_tube}$$ Equ. 13.54

Where:

$C_{outside,\ twisted\_tube}$	Outside circumference of the twisted tube [m]
$C_{outside,\ twisted\_tube}$	Inside circumference of the twisted tube [m]
$L_{twisted\_tube}$	Length of the twisted tube [m]

The cross sectional area of the twisted tube was not known precisely due to the shape of the twisted tube so the cross sectional area was approximated as follows by the mean diameters of the twisted tube.

$$d_{mean-outside,twisted,tube} = \frac{d_{outside,twisted\_tube} + \left(d_{inside,twisted\_tube} + 2\, s_{twisted\_tube}\right)}{2} \qquad \text{Equ. 13.55}$$

$$d_{mean-inside,twisted,tube} = \frac{d_{inside,twisted\_tube} + \left(d_{outside,twisted\_tube} - 2\, s_{twisted\_tube}\right)}{2} \qquad \text{Equ. 13.56}$$

The cross sectional area was hence given by:

$$A_{cs,annulus} = \frac{\left(d_{outside,annulus}{}^{2} - d_{mean-outside,twisted\_tube}{}^{2}\right)\pi}{4} \qquad \text{Equ. 13.57}$$

$$A_{cs,twisted\_tube} = \frac{d_{mean-inside,twisted\_tube}{}^{2}\,\pi}{4} \qquad \text{Equ. 13.58}$$

Where:

$A_{cs,\ annulus}$	Cross sectional area of the annulus available for flow [m^2]
$A_{cs,\ twisted\_tube}$	Cross sectional area of the twisted available for (in-tube) flow [m^2]
$d_{mean\text{-}outside,\ twisted\_tube}$	Mean outside diameter of the twisted tube [m]
$d_{mean\text{-}inside,\ twisted\_tube}$	Mean inside diameter of the twisted tube [m]
$d_{inside,\ twisted\_tube}$	Inner diameter of the twisted tube. (Smallest inner diameter, no relationship to the tube length was found.) [m]
$d_{outside,\ annulus}$	Outside diameter of the annulus [m]
$s_{twisted\_tube}$	Tube wall thickness of the twisted tube [m]

Heat transfer coefficient calculations

The heat transfer coefficient was estimated for each of the GC segments (Figure 13.2) using the refrigerant temperatures at the mid point of each segment. For the twisted tubes a heat transfer coefficient enhancement factor of 1.4 was applied (Chen *et al*, 1996a, 1996b).

- Supercritical refrigerant heat transfer coefficient was calculated using the correlation given by Kim *et al* (2001):

$$h_{CO2} = \frac{Nu_b \ \lambda_{CO2}}{d_h} f_{tube} \qquad \text{Equ. 13.59}$$

with:

$$f_{tube} = \begin{cases} 1 & \text{for straight tubes} \\ 1.4 & \text{for twisted tubes} \end{cases} \qquad \text{Equ. 13.60}$$

$$Nu_b = 0.03246 \ Re_b^{\ 0.8062} \ Pr_b^{\ 0.7960} \left(\frac{\rho_{CO2,b}}{\rho_{CO2,w}}\right)^{1.209} \left(\frac{c_{p,CO2\_h}}{c_{p,CO2\_b}}\right)^{0.7181} \qquad \text{Equ. 13.61}$$

The CO_2 property changes near the critical point were considered by using the mean integrated specific heat (Kim, *et al*, 2001), which was defined by:

$$c_{p,CO2\_h} = \frac{h_{CO2,w} - h_{CO2,b}}{T_{CO2,w} - T_{CO2,b}} \qquad \text{Equ. 13.62}$$

Where:

h_{CO2}	Heat transfer coefficient for CO_2 [W/m^2K]
Nu_b	Nussel number at the bulk temperature [-]
λ_{CO2}	Thermal conductivity of CO_2 [W/mK]
d_h	Tube diameter or hydraulic diameter of annulus [m]
$T_{CO2,w}$	Refrigerant side wall temperature [K]
$T_{CO2,b}$	Refrigerant side bulk temperature [K]
Re_b	Renolds number at the bulk temperature [-]
Pr_b	Prandtl number at the bulk temperature [-]
$\rho_{CO2,b}$	Refrigerant density at bulk temperature [kg/m^3]
$\rho_{CO2,w}$	Refrigerant density at wall temperature [kg/m^3]
$c_{p,CO2\_b}$	Specific heat capacity of the refrigerant at the bulk temperature [J/kgK]
$c_{p,CO2\_h}$	Integrated mean specific heat capacity of the refrigerant [J/kgK]
$h_{CO2,w}$	Refrigerant enthalpy at the wall temperature [J/kg]
$h_{CO2,b}$	Refrigerant enthalpy at the bulk temperature [J/kg]
f_{tube}	Heat transfer enhancement factor for twisted tubes [-]

- Water side heat transfer coefficient for turbulent water flow inside the tube / annulus were estimated using the McAdams correlation (ASHRAE, 2001):

$$h_W = \frac{0.023\, c_{W,b}\, G}{Pr_b^{\,2/3}\, Re_b^{\,0.2}} \left(\frac{\mu_{W,b}}{\mu_{W,w}} \right)^{0.14} f_{tube} \qquad \text{Equ. 13.63}$$

Where:

h_W	Water side heat transfer coefficient [W/m^{2}K]
G	Mass velocity [kg/m^{2}s]
$c_{W,b}$	Specific heat capacity of water at bulk temperature [J/kgK]
$\mu_{W,b}$	Water viscosity at bulk temperature [kg/ms]
$\mu_{W,w}$	Water viscosity at the wall temperature [kg/ms]

The overall heat transfer coefficient is a function of the individual heat transfer coefficients weighted by their surface area and the overall tube-wall resistance. Since the overall surface areas of the GC were unknown, the surface areas per 1 meter GC length were applied. The resistance of the vented tube was taken into account by a correction factor of 0.7 which was consistent with the experience of the heat exchanger manufacturer.

$$U_j = \frac{f_{vent}}{\left(\frac{1}{h_{CO2,j}\, A_{CO2,1m}} + \frac{r_{i,GC}\, \ln\left(r_{o,GC} / r_{i,GC}\right)}{\lambda_{tube}\, A_{mean,1m}} + \frac{1}{h_{W,j}\, A_{W,1m}} \right) A_{mean,1m}} \qquad \text{Equ. 13.64}$$

with:

$$A_{mean,1m} = \frac{A_{CO2,1m} + A_{W,1m}}{2} \qquad \text{Equ. 13.65}$$

Where:

U_j	Overall heat transfer coefficient of the jth GC segment based on the mean heat transfer surface area [W/m^{2}K]
$h_{CO2,j}$	Refrigerant-side heat transfer coefficient in the jth GC segment [W/mK]
$h_{W,j}$	Water-side heat transfer coefficient in the jth GC segment [W/mK]
$A_{mean,1m}$	Mean heat transfer surface of the gas cooler per one meter GC length [m^2]
$A_{CO2,1m}$	Heat transfer surface area on the refrigerant-side per one meter GC length [m^2]
$A_{W,1m}$	Heat transfer surface area on the water-side per one meter GC length [m^2]
$r_{i,GC}$	Radius of the inner tube for straight tube or ½ of the mean inner diameter of the

	twisted tube [m]
$r_{o,\,GC}$	Radius of the inner tube of the annulus for straight tubes or ½ of the mean outside diameter of the twisted tube [m]
λ_{tube}	Thermal conductivity of the tube [W/mK]
f_{vent}	Overall heat transfer reduction factor due to the vented GC design [-]

Gas cooler length calculation

The overall gas cooler length was calculated as followed:

$$L_{GC} = \sum_{1}^{J} L_{GC,j} = \sum_{1}^{J} \frac{A_{mean,j}}{A_{mean,1m}} \quad \text{Equ. 13.66}$$

with:

$$A_{mean,j} = \sum_{1}^{J} \frac{UA_j}{U_j} \quad \text{Equ. 13.67}$$

Where:

L_{GC}	Overall length of the gas cooler [m]
$L_{GC,\,j}$	Length of the j[th] GC segment [m]
$A_{mean,\,j}$	Mean heat transfer surface of the j[th] GC segment [m^2]

Mass and pressure drop calculations

The overall refrigerant side volume and CO_2 mass was calculated by summing the volume and mass respectively for the individual segments.

$$V_{CO2,GC} = L_{GC}\ A_{CS,CO2-side} \quad \text{Equ. 13.68}$$

$$M_{CO2,GC} = \sum_{1}^{J} L_{GC,j}\ A_{CS,CO2-side}\ \rho_{CO2,j} \quad \text{Equ. 13.69}$$

with:

$$\rho_{CO2,j} = f\left(T_{CO2,j}, p_{CO2,2}\right) \quad \text{Equ. 13.70}$$

The overall pressure drop was given by the sum of the pressure drops of the segments.

$$\Delta p_{GC} = \sum_{1}^{J} \Delta p_j = \sum_{1}^{J} \xi \frac{L_{GC,j}\ \rho_{CO2,j}\ v_{CO2,j}^{2}}{2\ d_{h,CO2-side}} \qquad \text{Equ. 13.71}$$

with:

$$v_{CO2,j} = \frac{m_{CO2}}{\rho_{CO2,j}\ A_{CS,CO2-side}} \qquad \text{Equ. 13.72}$$

Where:

$V_{CO2,\ GC}$	Refrigerant side volume of the GC [m^3]
$A_{CS,\ CO2\text{-}side}$	Cross sectional area of the refrigerant side of the GC [m^2]
$M_{CO2,GC}$	Refrigerant mass in the GC [kg]
Δp_{GC}	Overall GC pressure drop [Pa]
Δp_j	Pressure drop of the j^{th} GC segment [Pa]
$\rho_{CO2,j}$	Density of the refrigerant in the j^{th} GC segment [kg/m^3]
$v_{CO2,j}$	Velocity of the refrigerant-flow in the j^{th} segment [m/s]
$d_{h,\ CO2\text{-}side}$	Hydraulic diameter of the refrigerant side [m]
ξ	Pressure drop coefficient [-]

The pressure drop coefficient (ASHRAE, 2001) was calculated for a smooth tube (Equ. 13.73). The increased pressure drop caused by the turbulent flow in the twisted tubes of the GC was not considered.

$$\xi = 0.0054 + \frac{0.3964}{Re^{0.3}} \qquad \text{Equ. 13.73}$$

with:

$$Re = \frac{d_{h,CO2-side}\ \rho_{CO2}\ v_{CO2}}{\mu_{CO2}} = \frac{4\ m_{CO2}}{d_{h,CO2-side}\ \pi\ \mu_{CO2}} \qquad \text{Equ. 13.74}$$

Where:

Re	Reynolds coefficient [-]
$d_{h,\ CO2\text{-}side}$	Refrigerant side hydraulic diameter [m]

μ_{CO2} Refrigerant viscosity [kg/ms]

Gas cooler modelling procedure

The overall gas cooler length of 5 meters for GC 1, GC 2.1 and GC 2.2 was given by the maximum length of the available tubes for the twisting process so the performance predictions were carried out to predict the GC heat transfer rate and the temperature approach at the refrigerant side outlet of the GC. The refrigerant mass flowrate, the GC refrigerant inlet temperature and the GC water in- and outlet temperatures were known from the cycle calculations.

The necessary GC length was calculated iteratively by changing the refrigerant temperature at the outlet of the GC until the calculated GC length matched the effective length of the GC units.

A.2.3 Evaporator

A water source evaporator unit was used to mimic an air source evaporator unit. The heating requirements were given by the overall process calculations.

At the nominal design condition, cold water from the mains supply at approximately 20°C was used. The water outlet temperature was designed to be 5°C or greater which is well above the freezing point of water. The required water mass flowrate was back-calculated from the evaporator heat balance such as:

$$m_{W,E} = \frac{\phi_E}{c_W \left(T_{W,E\_out} - T_{W,E\_in}\right)} \qquad \text{Equ. 13.75}$$

Where:

ϕ_E Heat transfer rate in the evaporator [W]

$m_{W,E}$ Water mass flow rate in the evaporator [kg/s]

T_{W,E_in} Water temperature at the evaporator inlet [°C]

T_{W,E_out} Water temperature at the evaporator outlet [°C]

The nominal UA-Value of the evaporator for the heat exchanger specifications was calculated by:

$$UA_E = \frac{\phi_E}{LMTD_E}$$ Equ. 13.76

with:

$$LMTD_E = \frac{\left(T_{W,E\_in} - T_{W,E\_out}\right)}{ln\left(\frac{T_{W,E\_in} - T_{CO2,1'}}{T_{W,E\_out} - T_{CO2,1'}}\right)}$$ Equ. 13.77

Where:

UA_E UA-Value of the evaporator [W/K]

$LMTD_E$ Log mean temperature difference in the evaporator [K]

The evaporator unit was designed and built by Vaportec Ltd. (NZ) based on the specifications as described in Table 4.10.

A.2.4 Internal heat exchanger

The IHX was made of a 3.5 meter long copper coil. However, the high-side refrigerant pressure drop was predicted for a straight and smooth tube, using ASHRAE (2001) correlations.

$$\Delta p_{IHX} = -\xi \frac{L_{tube}\ \rho_{CO2,3'}\ v_{CO2}^{\ 2}}{2\ d_{tube}}$$ Equ. 13.78

with:

$$v_{CO2} = \frac{m_{CO2}\left(d_{tube}^{\ 2}\ \pi\right)}{4\ \rho_{CO2,3'}}$$ Equ. 13.79

and ξ *as* described in Equ. 13.74

Where:

Δp_{IHX} IHX pressure drop [Pa]

m_{CO2} Refrigerant mass flowrate [kg/s]

d_{tube} IHX tube (inside) diameter [m]

L_{tube} Length of the IHX copper coil [m]

The size of the IHX was constrained by the available space in the LPR and the available tube diameter. Therefore heat transfer predictions were not performed.

A.2.5 Low pressure receiver

The LPR was designed based on saturated vapour and liquid conditions (state 1', Figure 13.1). The design criteria for the LPR cross sectional area was the maximal allowed gas velocity for good vapour/liquid separation, which had to be lower than the terminal velocity (Wiencke, 2001). The terminal velocity describes the gas velocity at which the droplet stay in suspension:

$$v_t = \sqrt{\frac{4\ g\ d_D\left(\rho_{CO2-l,1'} - \rho_{CO2-v,1'}\right)}{3\ \rho_{CO2-v,1'}\ C_D}} \qquad \text{Equ. 13.80}$$

with:

$$C_D = 0.445 \quad at \quad 1000 \le \mathrm{Re} \le 350000 \qquad \text{Equ. 13.81}$$

and:

$$Re = \frac{4\ m_{CO2}}{d_{LPR}\ \pi\ \mu_{CO2}} \qquad \text{Equ. 13.82}$$

Where:

v_t Terminal velocity for gas of the vertical gaseous refrigerant-flow in the LPR [m/s]

g Acceleration due to gravity force [m/s^2]

$\rho_{CO2\text{-}l,1'}$ Density of the liquid refrigerant at the LPR inlet [kg/m^3]

$\rho_{CO2\text{-}v,1'}$ Density of the refrigerant vapour at the LPR outlet [kg/m^3]

d_D Diameter of the droplet [m]

d_{LPR} LPR diameter for flow [m^2]

C_D Drag coefficient [-]

For pure CO_2 droplets a diameter of 0.1 mm was recommended by Wiencke (2001).

Hence for the gas velocity in the LPR it followed that:

$$v_{CO2,LPR} = \frac{m_{CO2}}{A_{CS,LPR}\ \rho_{CO2-v,1'}} \leq v_t \qquad \text{Equ. 13.83}$$

Solving for the LPR cross sectional area:

$$A_{CS,LPR} \geq \frac{m_{CO2}}{\sqrt{\frac{4\ g\ d_D\ (\rho_{CO2-l,1'} - \rho_{CO2-v,1'})}{3\ \rho_{CO2-v,1'}\ C_D}}\ \rho_{CO2-v,1'}} \qquad \text{Equ. 13.84}$$

The LPR was made of a hydraulic tube, hence the inner diameter of the tube was given by:

$$d_{i,LPR} = \sqrt{\frac{4\ A_{CS,LPR}}{\pi}} \qquad \text{Equ. 13.85}$$

Where:

$v_{CO2,\ v\_LPR}$	Velocity of the vertical gaseous refrigerant-flow in the LPR [m/s]
$A_{CS,\ LPR}$	Cross sectional area of the LPR [m^2]
$\rho_{CO2\text{-}v,\ 1}$	Density of the gaseous refrigerant at the LPR outlet [kg /m^3]
m_{CO2}	Refrigerant mass flowrate [kg/s]
$d_{i,\ LPR}$	Inner diameter of the LPR [m]

The LPR volume was given by the volumetric requirements as described in section 4.5.5.

A.2.6 Pipe work

The refrigerant system charge at the nominal design condition was assessed for the different heat pump configurations by calculating the charge of the individual components, which was given by the volume and the refrigerant density (given by the refrigerant pressure and temperature). The charge of the GC units was calculated by the GC model and the evaporator was assumed to contain 1/3 liquid and 2/3 refrigerant vapour.

The gas velocity in the pipe system was calculated from the refrigerant mass flowrate and the refrigerant density (given by the temperature and pressure). The pressure drop was calculated by:

$$\Delta p_{pipe} = -\xi \frac{L_{pipe}\, \rho_{CO2}\, v_{CO2}^{\;2}}{2\, d_{pipe}}$$ Equ. 13.86

with:

$$v_{CO2} = \frac{m_{CO2} \left(d_{pipe}^{\;2}\, \pi\right)}{4\, \rho_{CO2}}$$ Equ. 13.87

and ξ *as* described in Equ. 13.74

Where:

Δp_{pipe}	Pressure drop in the pipe [Pa]
ρ_{CO2}	Density of the refrigerant given by the pressure and temperature [kg /m^3]
v_{CO2}	Velocity of the refrigerant-flow [m/s]
d_{pipe}	Inner diameter of the pipe [m]
L_{pipe}	Pipe length [m]

A.3 Experimental data

Table 13.1 summarises the experimental heat pump and HWC trials.

Table 13.1: List of the heat pump and HWC trials

Date	Trial name	Objectives of the investigations	Heat pump conditions	Heat pump measurement set-up	Comment(s)
3.7.2002	Ref-process	Produce a guideline for the compressor efficiency to control whether the compressor performance reduced during the experimental work	ref1, ref2, ref3	S1	Hot water temperature: 45°C
5.7.2002	gc1_v1.1	Heat transfer of GC1 at varying discharge pressure	C01; C11; C24; C29	S1	Problems with hp control
5.7.2002	gc1_v1.2	Heat transfer of GC1 at varying cold water inlet temperature	C12; C13	S1	Problems with hp control
5.7.2002	gc1_v1.3	Heat transfer of GC1 at varying hot water outlet temperature	C11; C16	S1	Problems with hp control
9.7.2002	gc1_v2.1	Heat transfer of GC1 at varying discharge pressure	C01;C11; C24;C29	S1	Repeat g1_v1.1
9.7.2002	gc1_v2.2	Heat transfer of GC1 at varying cold water inlet temperature	C11, C12, C13	S1	Repeat g1_v1.2
9.7.2002	gc1_v2.3	Heat transfer of GC1 at varying evaporation temperature	C11, C17; C18	S1	-
12.7.2002	gc2.1_v1.1	Heat transfer of GC2.1 at varying hot water outlet temperature	C11; C15; C16	S2	Repeat g1_v1.3
12.7.2002	gc2.1_v1.2	Heat transfer of GC2.1 at varying cold water inlet temperature	C11; C12; C13; C14	S2	-
12.7.2002	gc2.1_v1.3	Heat transfer of GC2.1 at varying discharge pressure	C01; C11; C24; C29	S2	-
12.7.2002	gc2.1_v1.4	Heat transfer of GC2.1 at varying evaporation temperature	C11;C17; C18	S2	-

21.7.2002	gc2.2_v1.1	Heat transfer of GC2.2 at varying hot water outlet temperature	C11; C15; C16	S3	-
21.7.2002	gc2.2_v1.2	Heat transfer of GC2.2 at varying cold water inlet temperature	C12, C13, C14	S4	-
21.7.2002	gc2.2_v1.3	Heat transfer of GC2.2 at varying discharge pressure	C01; C11; C24; C29	S4	-
21.7.2002	gc2.2_v1.4	Heat transfer of GC2.2 at varying evaporation temperature	C11; C17; C18	S4	-
30.7.2002	gc3.1_v1.1	Heat transfer of GC3.1 at varying cold water inlet temperature	C11; C12; C13; C15	S4	Variation in mains warm water
3.8.2002	gc3.1_v2.1	Heat transfer of GC3.1 at varying cold water inlet temperature Heat transfer of GC3.1 at varying discharge pressure Heat transfer of GC3.1 at varying evaporation temperature and pressure	C01; C06; C11; C12; C13; C17; C18; C19; C24;	S4	Repeat gc3.1_v1.1
15.8.2002	gc3.2_v1.1	Heat transfer of GC3.2 at varying cold water inlet temperature Heat transfer of GC3.2 at varying discharge pressure Heat transfer of GC3.2 at varying evaporation temperature and pressure	C01; C06; C11; C12; C13; C17; C18; C19; C24;	S5	-
20.8.2002	comp1	Reproducibility of the compressor performance Clarify whether there was a compressor mechanical problem Effect of compressor body temperature, oil temperature and crankcase oil level on the compressor performance	C11	S6	-
22.8.2002	comp4	Compressor performance at body cooling	C11	S6	Additional compressor body cooling
25.8.2002	comp2	Reproducibility of the compressor performance Clarify whether there was a compressor mechanical problem Effect of compressor body temperature, oil temperature and crankcase oil level on the compressor performance	C11	S6	-
24.8.2002	comp3	Reproducibility of the compressor performance Clarify whether there was a compressor mechanical problem	C11	S6	-

		Effect of compressor body temperature, oil temperature and crankcase oil level on the compressor performance			
23.9.2002	hp90_v1	Heat pump performance at varying GC water inlet temperature, varying evaporation conditions and 90 bar.g discharge pressure	C01; C02; C03, C04	S6	-
23.9.2002	hp95_v1	Heat pump performance at varying GC water inlet temperature, varying evaporation conditions and 95 bar.g discharge pressure	C06; C07; C08, C09, C10	S7	-
23.9.2002	hp100_v1	Heat pump performance at varying GC water inlet temperature, varying evaporation conditions and 100 bar.g discharge pressure	C11; C12; C13, C17, C18	S7	-
24.9.2002	hp105_v1	Heat pump performance at varying GC water inlet temperature, varying evaporation conditions and 105 bar.g discharge pressure	C19; C20; C21, C22, C23	S7	-
24.9.2002	hp110_v1	Heat pump performance at varying GC water inlet temperature, varying evaporation conditions and 110 bar.g discharge pressure	C24; C25; C26, C27, C28	S7	-
26.9.2002	hp95_v2	Heat pump performance at varying GC water inlet temperature, varying evaporation conditions and 95 bar.g discharge pressure	C06; C09	S7	Repeat hp95_v1
26.9.2002	hp105_v2	Heat pump performance at varying GC water inlet temperature, varying evaporation conditions and 95 bar.g discharge pressure	C19; C20; C21, C22, C23	S7	Repeat hp105_v1
26.9.2002	hp110_v2	Heat pump performance at varying GC water inlet temperature, varying evaporation conditions and 110 bar.g discharge pressure	C24; C25; C26, C27	S7	Repeat hp110_v1
2.10.2002	hp90_v3	Heat pump performance at varying GC water inlet temperature, varying evaporation conditions and 90 bar.g discharge pressure	C01; C02; C03	S7	Repeat hp90_v2
2.10.2002	hp95_v3	Heat pump performance at varying GC water inlet temperature, varying evaporation conditions and 95 bar.g discharge pressure	C06; C07; C08, C09; C10	S7	Repeat hp95_v2
2.10.2002	hp100_v3	Heat pump performance at varying GC water inlet temperature, varying evaporation conditions and 100 bar.g discharge pressure	C11; C12; C13, C17; C18	S7	Repeat hp100_v1
2.10.2002	hp105_v3	Heat pump performance at varying GC water inlet temperature, varying evaporation conditions and 105 bar.g discharge pressure	C19; C20; C21; C22; C23	S7	Repeat hp105_v1 and v2
2.10.2002	hp110_v3	Heat pump performance at varying GC water inlet temperature, varying evaporation conditions and 110 bar.g discharge pressure	C24; C25; C26, C27; C28	S7	Repeat hp105_v1 and v2
5.10.2002	CO2_charge1	Heat pump performance at 105 bar.g discharge pressure, a refrigerant charge of 1.685 kg varying GC cold water inlet temperatures and	C19; C20; C21;	S7	No measurements at C23 because of

		varying evaporation temperatures / pressures	C22		low CO_2 charge
5.10.2002	CO2_charge2	Heat pump performance at 105 bar.g discharge pressure, a refrigerant charge of 1.760 kg varying GC cold water inlet temperatures and varying evaporation temperatures / pressures	C19; C20; C21; C22; C23	S7	-
5.10.2002	CO2_charge3	Heat pump performance at 105 bar.g discharge pressure, a refrigerant charge of 1.815 kg varying GC cold water inlet temperatures and varying evaporation temperatures / pressures	C19; C20; C21; C22; C23	S7	-
5.10.2002	CO2_charge4	Heat pump performance at 105 bar.g discharge pressure, a refrigerant charge of 1.915 kg varying GC cold water inlet temperatures and varying evaporation temperatures / pressures	C19; C20; C21; C22; C23	S7	-
6.10.2002	heat_loss1	Measure thermocline over a period of HWC standing looses	-	S8	Initial ambient air temperature:18.2°C
10.10.2002	reheat	Measure thermocline in the HWC during reheating period, test functionality of the oil return	C19 (initial condition)	S8	Initial ambient air temperature:17.0°C
15.10.2002	cooling	Measure thermocline during a period of water withdrawal and HWC standing losses	-	S8	Initial ambient air temperature:17.2°C
15.10.2002	heat_loss2	Measure thermocline over a period of HWC standing looses	-	S8	Initial ambient air temperature:17.0°C

Table 13.2 gives the heat pump raw data in chronological order, while Table 13.3 gives the HWC raw data.

Table 13.2: Heat pump raw data

Trial name		ref_process	ref_process	ref_process	gc1_v1.1	gc1_v1.1	gc1_v1.1	gc1_v1.1	gc1_v1.2	gc1_v1.2	gc1_v1.2	gc1_v1.3	gc1_v1.3	gc1_v1.3	gc1_v1.3	gc1_v2.1	gc1_v2.1	gc1_v2.1	gc1_v2.1	gc1_v2.2	gc1_v2.2	gc1_v2.2	gc1_v2.3
Data point number		1	2	3	4	5	6	7	8	9	10	11	12	13	14	15	16	17	18	19	20	21	22
Heat pump setup no.(S-)		1	1	1	1	1	1	1	1	1	1	1	1	1	1	1	1	1	1	1	1	1	1
Heat pump condition no. (C-)		ref1	ref2	ref3	01	11	24	29	13	-	12	11	-	16	-	29	24	11	01	12	13	-	18
Configuration / measurement setup																							
1st gas cooler		GC1	GC1	GC1	GC1	GC1	GC1	GC1	GC1	GC1	GC1	GC1	GC1	GC1	GC1	GC1	GC1	GC1	GC1	GC1	GC1	GC1	GC1
2nd gas cooler		-	-	-	-	-	-	-	-	-	-	-	-	-	-	-	-	-	-	-	-	-	-
Gas cooler overall		GC1	GC1	GC1	GC1	GC1	GC1	GC1	GC1	GC1	GC1	GC1	GC1	GC1	GC1	GC1	GC1	GC1	GC1	GC1	GC1	GC1	GC1
IHX (on/off):		on	on	on	on	on	on	on	on	on	on	on	on	on	on	on	on	on	on	on	on	on	on
HWC (on/off):		off	off	off	off	off	off	off	off	off	off	off	off	off	off	off	off	off	off	off	off	off	off
Oil return (on/off):		off	off	off	off	off	off	off	off	off	off	off	off	off	off	off	off	off	off	off	off	off	off
CO2 charge:		-	-	-	-	-	-	-	-	-	-	-	-	-	-	-	-	-	-	-	-	-	-
Raw data																							
data	d/m/y	3/7/02	3/7/02	3/7/02	5/7/02	5/7/02	5/7/02	5/7/02	5/7/02	5/7/02	5/7/02	5/7/02	5/7/02	5/7/02	5/7/02	9/7/02	9/7/02	9/7/02	9/7/02	9/7/02	9/7/02	9/7/02	9/7/02
Time		800.0	1400.0	2200.0	350.0	900.0	1350.0	1700.0	1000.0	1700.0	2900.0	1300.0	1800.0	2400.0	2900.0	400.0	701.0	1100.0	1500.0	600.0	1400.0	1800.0	550.0
T1 (CO2 gc in)	°C	82.1	92.8	101.3	77.5	91.4	100.9	107.0	94.4	91.1	98.7	90.3	92.9	91.5	94.4	108.5	104.0	94.8	86.2	95.5	96.3	96.3	76.1
T2 (CO2 gc inner)	°C	-	-	-	-	-	-	-	-	-	-	-	-	-	-	-	-	-	-	-	-	-	-
T3 (CO2 gc out)	°C	27.8	21.6	20.4	42.1	40.3	33.4	29.0	42.1	44.3	39.9	39.8	32.2	26.6	21.8	27.2	31.4	39.1	39.9	40.8	42.1	43.7	43.7
T4 (water gc in)	°C	18.3	16.9	16.9	18.1	18.2	18.0	17.9	30.7	35.0	24.4	17.6	17.6	17.4	17.1	16.7	16.8	16.9	16.9	25.3	30.0	34.6	17.1
T5 (water gc inner)	°C	-	-	-	-	-	-	-	-	-	-	-	-	-	-	-	-	-	-	-	-	-	-
T6 (water gc out)	°C	44.3	44.5	44.6	60.2	61.1	61.2	61.1	60.9	60.6	60.1	60.4	55.4	50.1	45.1	59.9	60.0	59.7	59.5	59.9	60.2	60.2	59.9
T7 (CO2 evaporator in)	°C	-0.5	-0.5	-0.1	3.5	0.7	0.3	0.7	3.8	-0.1	-1.7	-0.1	-0.4	-0.9	-0.9	0.8	0.8	0.6	0.7	0.5	0.3	-0.2	14.7
T8 (CO2 evaporator out)	°C	-0.8	-0.5	-0.1	3.1	0.5	-0.1	0.4	3.6	-0.6	-2.1	-0.5	-0.6	-1.2	-1.0	0.6	0.6	0.3	0.3	0.0	-0.2	-0.7	14.5
T9 (water evaporator in)	°C	18.1	16.8	16.8	17.1	17.8	17.8	17.7	17.4	16.6	17.6	17.3	17.5	17.3	17.0	16.5	16.5	16.5	16.3	16.5	16.6	16.4	26.2
T10 (water evaporator out)	°C	0.5	0.8	1.2	3.7	1.4	1.0	1.6	4.5	0.0	-1.1	0.8	0.8	0.4	0.7	1.8	1.6	1.2	1.0	0.9	0.6	0.1	15.7
T11 (CO2 IHX in)	°C	27.4	21.4	20.2	41.3	39.8	32.9	28.4	42.2	43.7	39.1	39.3	31.6	26.4	21.5	26.8	31.3	38.6	39.3	40.0	41.5	42.8	42.8
T12 (CO2 IHX out)	°C	2.1	4.2	7.7	29.5	16.1	9.1	9.7	29.9	30.3	19.5	11.7	13.6	11.3	10.8	18.3	18.3	24.2	33.8	15.7	23.3	27.2	36.3
T13 (CO2 LPR out)	°C	2.8	2.7	2.5	5.0	2.7	2.3	2.8	5.5	1.6	0.7	2.0	2.0	1.9	2.3	3.6	3.3	2.9	2.9	2.4	2.4	2.0	18.9
T14 (oil compressor out)	°C	50.3	55.3	61.5	54.8	56.6	59.7	62.8	66.2	64.5	68.3	44.6	50.2	54.7	58.6	72.0	72.5	71.8	70.2	67.6	68.9	69.3	63.7
T15 (oil comp. in)	°C	48.2	52.8	58.7	52.7	54.3	57.1	59.9	63.2	61.6	64.9	42.6	47.9	52.3	55.9	68.5	69.1	68.4	67.0	64.3	65.5	65.9	60.8
T16 (comp. body)	°C	51.4	58.9	65.1	47.1	56.4	63.3	68.7	60.9	57.3	64.1	55.4	57.4	58.2	61.8	70.3	67.5	61.3	55.3	60.6	61.3	61.4	51.0
we [kW]	kW	2.0	2.1	2.2	2.0	2.1	2.2	2.3	2.1	2.1	2.0	2.1	2.2	2.1	2.1	2.3	2.2	2.1	2.0	2.1	2.1	2.1	2.2
p1 [bar]	bar	33.0	33.0	34.0	34.0	34.0	34.0	34.0	34.0	32.0	32.0	33.0	34.0	32.0	32.0	34.0	34.0	34.0	34.0	34.0	34.0	33.0	48.0
p2 [bar]	bar	90.0	100.0	110.0	90.0	100.0	110.0	120.0	100.0	100.0	100.0	100.0	100.0	100.0	100.0	120.0	110.0	100.0	90.0	100.0	100.0	100.0	100.0
p3' [bar]	bar	90.0	100.0	110.0	89.0	100.0	110.0	120.0	100.0	100.0	100.0	100.0	100.0	100.0	100.0	120.0	110.0	100.0	89.0	100.0	100.0	100.0	96.0
p3 [bar]	bar	-	-	-	-	-	-	-	-	-	-	-	-	-	-	-	-	-	-	-	-	-	-
p4 [bar]	bar	34.0	34.0	35.0	34.0	34.0	34.0	34.0	-	-	-	34.0	34.0	34.0	34.0	-	-	-	-	-	-	-	-
p_oil [bar']	bar	36.0	36.0	36.0	38.0	36.0	36.0	36.0	36.0	35.0	34.0	35.0	36.0	35.0	35.0	36.0	36.0	36.0	36.0	36.0	35.0	35.0	50.0
m_gc [l/min]	l/min	2.7	2.6	2.5	0.9	1.2	1.3	1.3	1.3	1.6	1.4	1.1	1.6	1.9	2.4	1.5	1.5	1.4	1.0	1.5	1.6	1.7	1.6
m_eva [l/min]	l/min	2.7	3.1	3.1	1.6	1.9	2.2	2.4	1.5	0.9	1.4	1.7	2.4	2.5	2.8	2.9	2.9	2.2	1.4	1.9	1.7	1.3	3.9
oil level [mm]	mm	-	-	-	-	-	-	-	-	-	-	-	-	-	-	-	-	-	-	-	-	-	-
Refrigerant properties																							
Enthalpy h1 [kJ/kg]	kJ/kg	437.7	437.4	435.0	439.1	435.1	434.6	435.5	439.7	438.0	436.5	436.5	434.0	438.4	439.0	436.8	436.1	435.6	435.5	434.8	434.6	436.3	432.2
Enthalpy h2' [kJ/kg]	kJ/kg	479.0	483.6	483.5	479.3	479.3	483.1	488.1	485.1	485.8	483.8	482.2	477.7	486.3	487.2	489.8	485.0	479.8	474.8	478.7	478.6	482.1	460.3
Enthalpy h2 [kJ/kg]	kJ/kg	483.2	491.1	496.5	475.5	488.8	495.7	498.6	493.7	488.3	500.6	487.2	491.3	489.2	493.9	501.1	500.9	494.4	489.8	495.5	496.8	496.8	461.0
Enthalpy h3" [kJ/kg]	kJ/kg	-	-	-	-	-	-	-	-	-	-	-	-	-	-	-	-	-	-	-	-	-	-
Enthalpy h3' [kJ/kg]	kJ/kg	267.7	246.4	241.7	365.4	313.9	278.0	262.4	324.2	339.0	311.1	311.1	278.0	260.1	246.7	257.3	271.7	306.9	342.5	316.2	324.8	334.8	347.0
Enthalpy h3 [kJ/kg]	kJ/kg	200.7	204.6	211.9	273.9	232.4	215.0	215.6	270.3	271.6	240.7	221.8	226.3	220.6	219.7	235.2	236.5	253.2	292.6	231.1	251.0	261.9	298.0
Enthalpy h4 [kJ/kg]	kJ/kg	200.7	204.6	211.9	273.9	232.4	215.0	215.6	270.3	271.6	240.7	221.8	226.3	220.6	219.7	235.2	236.5	253.2	292.6	231.1	251.0	261.9	298.0
Density CO2 suction [kg/m3]	kg/m3	90.6	90.8	95.2	92.6	95.1	95.4	94.9	92.2	87.7	88.6	91.4	95.9	87.5	87.1	94.0	94.4	94.8	94.9	95.3	95.4	91.5	137.5
p1' based on T7 [bar]	bar	33.4	33.4	33.8	37.2	34.5	34.1	34.5	37.5	33.8	32.3	33.8	33.5	33.0	33.0	34.6	34.6	34.4	34.5	34.3	34.1	33.7	49.5

gc1_v2.3	gc1_v2.3	gc2.1_v1.1	gc2.1_v1.1	gc2.1_v1.1	gc2.1_v1.1	gc2.1_v1.2	gc2.1_v1.2	gc2.1_v1.2	gc2.1_v1.2	gc2.1_v1.3	gc2.1_v1.3	gc2.1_v1.3	gc2.1_v1.3	gc2.1_v1.4	gc2.1_v1.4	gc2.1_v1.4	gc2.2_v1.1	gc2.2_v1.1	gc2.2_v1.1	gc2.2_v1.1	gc2.2_v1.2	gc2.2_v1.2
23	24	25	26	27	28	29	30	31	32	33	34	35	36	37	38	39	40	41	42	43	44	45
1	1	2	2	2	2	2	2	2	2	2	2	2	2	2	2	2	3	3	3	3	3	3
17	11	11	-	16	15	14	13	12	11	01	11	24	29	11	17	18	15	16	-	11	14	14
GC1	GC1	GC2.1	GC2.1	GC2.1	GC2.1	GC2.1	GC2.1	GC2.1	GC2.1	GC2.1	GC2.1	GC2.1	GC2.1	GC2.1	GC2.1	GC2.1	GC2.2	GC2.2	GC2.2	GC2.2	GC2.2	GC2.2
-	-	-	-	-	-	-	-	-	-	-	-	-	-	-	-	-	-	-	-	-	-	-
GC1	GC1	GC2.1	GC2.1	GC2.1	GC2.1	GC2.1	GC2.1	GC2.1	GC2.1	GC2.1	GC2.1	GC2.1	GC2.1	GC2.1	GC2.1	GC2.1	GC2.2	GC2.2	GC2.2	GC2.2	GC2.2	GC2.2
on	on	on	on	on	on	on	on	on	on	on	on	on	on	on	on	on	on	on	on	on	on	on
off	off	off	off	off	off	off	off	off	off	off	off	off	off	off	off	off	off	off	off	off	off	off
off	off	off	off	off	off	off	off	off	off	off	off	off	off	off	off	off	off	off	off	off	off	off
-	-	-	-	-	-	-	-	-	-	-	-	-	-	-	-	-	-	-	-	-	-	-
9/7/02	9/7/02	12/7/02	12/7/02	12/7/02	12/7/02	12/7/02	12/7/02	12/7/02	12/7/02	12/7/02	12/7/02	12/7/02	12/7/02	12/7/02	12/7/02	12/7/02	21/7/02	21/7/02	21/7/02	21/7/02	21/7/02	21/7/02
1300.0	1750.0	500.0	1100.0	1400.0	1750.0	1200.0	1700.0	2200.0	2800.0	1950.0	2100.0	2500.0	3100.0	400.0	900.0	1600.0	200.0	800.0	1400.0	1700.0	1300.0	1600.0
79.8	94.2	92.8	95.5	95.4	95.1	95.5	95.1	96.0	97.0	91.4	93.1	102.2	112.3	95.9	84.7	80.5	92.7	93.8	94.5	95.5	95.1	97.6
-	-	-	-	-	-	-	-	-	-	-	-	-	-	-	-	-	-	-	-	-	-	-
42.8	39.3	38.2	31.9	28.6	23.7	45.7	42.8	40.4	37.0	37.8	37.6	32.5	26.6	37.5	41.7	43.6	20.1	23.2	27.0	31.0	41.9	42.3
16.9	16.9	19.0	17.9	17.8	17.7	36.2	30.5	24.9	18.6	18.4	18.3	18.1	17.7	17.7	17.8	18.1	17.5	17.2	17.4	17.5	36.6	34.8
-	-	-	-	-	-	-	-	-	-	-	-	-	-	-	-	-	-	-	-	-	-	-
59.8	59.9	60.3	54.8	50.1	40.0	59.7	59.2	59.1	59.7	60.2	60.3	60.4	60.3	60.1	60.1	60.2	39.7	49.6	54.5	59.6	57.0	61.3
7.6	0.4	-0.7	-0.6	-0.3	0.3	1.2	-0.1	-0.2	0.2	-1.4	-0.4	0.0	-0.2	0.7	8.0	14.8	1.1	0.3	0.7	0.0	-0.4	0.2
7.2	0.0	-0.6	-0.6	-0.2	0.3	1.0	-0.3	-0.4	0.1	-1.3	-0.2	0.2	0.0	0.7	7.7	14.9	1.0	0.0	0.5	-0.2	-0.8	0.0
16.7	16.4	18.2	17.5	17.6	17.4	18.0	18.0	18.2	18.1	17.9	17.8	17.7	17.4	17.2	17.3	37.5	17.1	16.9	17.0	17.0	16.8	17.4
8.0	0.9	0.1	0.3	0.8	1.5	1.5	0.4	0.4	1.0	0.0	1.2	1.5	1.2	1.4	8.5	15.6	2.2	1.2	1.7	0.8	-0.2	0.6
42.1	38.8	37.4	31.2	27.9	23.2	43.7	41.2	38.9	35.7	28.1	24.7	20.8	17.8	36.4	40.4	42.6	20.0	23.3	27.2	31.5	42.7	43.2
28.8	6.1	7.2	7.0	8.4	10.6	34.7	31.3	26.9	23.5	26.9	24.2	18.6	15.2	20.2	33.9	38.1	10.6	8.0	13.6	14.7	30.5	29.3
10.8	3.9	1.9	1.7	1.9	2.5	3.4	2.6	2.3	3.0	1.6	2.5	2.9	2.6	3.1	9.7	19.7	4.5	2.8	3.2	2.4	2.8	3.4
62.0	64.0	52.4	57.2	59.3	60.9	63.0	63.7	64.5	65.3	55.8	57.1	60.5	66.0	64.4	64.5	62.6	54.0	56.7	58.7	59.9	62.7	63.7
59.2	61.0	50.1	54.4	56.3	58.0	59.6	60.3	60.9	61.7	53.2	54.5	57.5	62.6	61.1	61.3	59.5	51.1	53.6	55.5	56.4	59.1	60.0
50.0	60.0	54.3	56.2	56.3	56.5	57.0	56.9	57.5	58.1	51.3	53.9	59.9	67.5	57.3	51.4	51.3	52.6	54.2	55.4	54.0	54.2	56.7
2.2	2.1	2.1	2.1	2.1	2.1	2.1	2.1	2.1	2.1	1.2	2.1	2.2	2.3	2.2	2.2	2.1	2.1	2.1	2.1	2.1	2.1	2.1
40.0	34.0	33.0	33.0	34.0	34.0	34.0	34.0	34.0	34.0	33.0	33.0	34.0	34.0	34.0	41.0	49.0	34.0	34.0	34.0	34.0	34.0	34.0
100.0	100.0	100.0	100.0	100.0	100.0	101.0	99.0	100.0	100.0	90.0	100.0	110.0	120.0	100.0	100.0	103.0	100.0	100.0	100.0	100.0	100.0	100.0
98.0	100.0	100.0	100.0	100.0	100.0	100.0	99.0	100.0	100.0	90.0	100.0	110.0	120.0	100.0	100.0	103.0	100.0	99.0	99.0	100.0	99.0	99.0
-	-	-	-	-	-	-	-	-	-	-	-	-	-	-	-	-	-	-	-	-	-	-
-	-	-	-	-	-	-	-	-	-	-	-	-	-	-	-	-	-	-	-	-	-	-
43.0	36.0	35.0	35.0	35.0	36.0	34.0	35.0	35.0	36.0	35.0	35.0	36.0	35.0	36.0	43.0	51.0	36.0	35.0	36.0	36.0	35.0	36.0
1.4	1.2	1.3	1.7	2.1	3.3	1.8	1.6	1.5	1.4	0.9	1.3	1.4	1.4	1.4	1.6	1.8	3.5	2.2	1.8	1.5	2.1	1.7
3.9	2.1	1.8	2.4	2.8	3.3	1.4	1.4	1.9	2.3	1.2	2.2	2.6	2.6	2.5	5.0	2.4	3.9	3.3	3.2	2.7	1.5	1.5
-	-	-	-	-	-	-	-	-	-	-	-	-	-	-	-	-	-	-	-	-	-	-
435.3	437.3	436.3	436.0	434.0	435.0	436.5	435.0	434.6	435.8	435.8	437.1	435.6	435.0	435.8	431.0	431.2	438.3	435.5	436.0	434.8	435.3	436.5
472.0	482.1	482.1	481.7	477.7	478.9	481.4	478.5	478.6	480.1	476.5	483.1	484.3	487.4	480.1	465.5	459.5	483.3	479.6	480.3	478.7	479.4	480.8
468.4	493.4	491.3	495.5	495.5	494.9	494.8	495.9	496.3	497.9	497.9	491.8	498.0	507.1	496.3	477.5	466.4	491.0	492.9	494.1	495.7	495.0	498.8
-	-	-	-	-	-	-	-	-	-	-	-	-	-	-	-	-	-	-	-	-	-	-
333.7	307.9	302.9	277.0	266.2	252.1	348.9	331.1	313.9	296.9	316.7	300.1	275.1	256.0	299.6	322.3	328.1	242.2	250.7	261.6	274.2	325.0	328.3
267.5	208.8	211.2	211.0	214.2	219.2	287.3	275.4	261.3	251.6	264.7	253.5	237.0	228.0	242.7	284.6	299.5	219.2	213.3	226.2	228.7	273.0	269.1
267.5	208.8	211.2	211.0	214.2	219.2	287.3	275.4	261.3	251.6	264.7	253.5	237.0	228.0	242.7	284.6	299.5	219.2	213.3	226.2	228.7	273.0	269.1
111.9	93.7	91.5	91.7	95.9	95.2	94.2	95.2	95.4	94.7	91.8	91.0	94.8	95.2	94.7	118.3	141.4	93.1	94.9	94.5	95.3	95.0	94.2
41.3	34.2	33.3	33.3	33.6	34.1	35.0	33.8	33.6	34.0	32.5	33.5	33.8	33.7	34.5	41.8	49.6	34.9	34.1	34.5	33.9	33.5	34.0

gc2.2_v1.2	gc2.2_v1.2	gc2.2_v1.2	gc2.2_v1.3	gc2.2_v1.3	gc2.2_v1.3	gc2.2_v1.3	gc2.2_v1.3	gc2.2_v1.4	gc2.2_v1.4	gc2.2_v1.4
46	47	48	49	50	51	52	53	54	55	56
3	3	3	3	3	3	3	3	3	3	3
13	12	11	01	11	24	29	06	18	17	11
GC2.2	GC2.2	GC2.2	GC2.2	GC2.2	GC2.2	GC2.2	GC2.2	GC2.2	GC2.2	GC2.2
-	-	-	-	-	-	-	-	-	-	-
GC2.2	GC2.2	GC2.2	GC2.2	GC2.2	GC2.2	GC2.2	GC2.2	GC2.2	GC2.2	GC2.2
on	on	on	on	on	on	on	on	on	on	on
off	off	off	off	off	off	off	off	off	off	off
off	off	off	off	off	off	off	off	off	off	off
-	-	-	-	-	-	-	-	-	-	-
21/7/02	21/7/02	21/7/02	21/7/02	21/7/02	21/7/02	21/7/02	21/7/02	21/7/02	21/7/02	21/7/02
2000.0	2400.0	2900.0	2200.0	2750.0	3200.0	3600.0	3950.0	200.0	700.0	1400.0
98.1	99.5	99.4	85.0	94.9	104.9	112.4	87.6	78.2	81.0	95.9
-	-	-	-	-	-	-	-	-	-	-
39.8	37.1	32.5	36.7	31.9	24.6	22.4	36.9	41.1	38.8	31.6
30.4	26.7	18.3	17.5	17.6	17.6	17.6	17.5	18.1	18.1	18.1
-	-	-	-	-	-	-	-	-	-	-
59.7	59.7	61.1	59.5	60.1	60.3	60.1	59.9	60.7	60.2	59.9
-0.6	-0.7	-0.2	-0.4	0.0	-0.7	0.4	1.6	15.2	7.7	-0.3
-0.8	-1.0	-0.5	-0.7	-0.2	-0.8	0.7	1.2	17.4	7.4	-0.5
17.6	17.8	17.7	16.7	17.0	17.1	17.0	16.9	33.5	28.4	17.2
-0.1	0.0	0.6	0.1	0.8	0.4	1.6	2.1	16.4	8.2	0.4
40.7	38.0	33.2	36.8	32.1	24.6	22.4	37.3	41.5	39.4	31.8
25.8	23.1	20.8	23.6	17.3	14.8	15.9	27.0	37.0	31.2	14.8
3.1	3.1	3.7	2.7	3.4	3.5	6.0	5.1	20.2	9.7	3.0
64.5	65.3	66.2	55.0	57.8	61.0	64.4	63.7	59.3	58.6	60.7
60.8	61.6	62.3	52.0	54.7	57.5	60.6	60.1	56.1	55.5	57.4
57.2	58.5	58.6	47.6	53.8	59.9	65.3	51.9	49.4	48.2	55.4
2.1	2.1	2.1	2.0	2.1	2.2	2.3	2.0	2.2	2.2	2.1
35.0	34.0	34.0	35.0	35.0	35.0	36.0	36.0	49.0	40.0	33.0
100.0	100.0	100.0	90.0	100.0	110.0	120.0	95.0	103.0	100.0	100.0
98.0	99.0	98.0	88.0	99.0	110.0	120.0	93.0	100.0	98.0	99.0
-	-	-	-	-	-	-	-	-		-
-	-	-	-	-	-	-	-	-	-	-
35.0	35.0	35.0	35.0	35.0	35.0	36.0	36.0	51.0	43.0	35.0
1.7	1.6	1.5	1.2	1.5	1.5	1.6	1.4	1.9	1.6	1.5
1.6	2.1	2.5	1.9	2.8	2.8	3.1	2.7	3.5	2.4	2.5
-	-	-	-	-	-	-	-	-	-	-
433.5	436.0	437.0	432.8	434.0	434.3	436.3	434.6	432.5	433.3	438.1
475.7	480.3	481.5	470.0	476.4	481.3	486.3	473.5	461.0	469.4	484.5
499.6	501.9	501.8	487.9	494.5	502.3	507.4	487.3	461.6	470.7	496.3
-	-	-	-	-	-	-	-	-	-	-
314.2	298.3	280.5	313.1	277.8	252.2	245.3	304.4	318.6	308.5	276.8
258.6	250.4	244.7	254.6	235.2	228.1	229.8	263.6	297.3	275.5	229.3
258.6	250.4	244.7	254.6	235.2	228.1	229.8	263.6	297.3	275.5	229.3
99.1	94.5	93.9	99.6	98.7	98.5	100.0	101.2	140.1	113.6	90.4
33.3	33.2	33.7	33.5	33.9	33.2	34.2	35.3	50.0	41.5	33.6

gc3.1_v1.1	gc3.1_v1.1	gc3.1_v1.1	gc3.1_v1.1	gc3.1_v2.1	gc3.1_v2.1	gc3.1_v2.1	gc3.1_v2.1	gc3.1_v2.1	gc3.1_v2.1	gc3.1_v2.1	gc3.1_v2.1
57	58	59	60	61	62	63	64	65	66	67	68
4	4	4	4	4	4	4	4	4	4	4	4
11	12	13	15	11	12	13	01	26	11	17	18
GC1	GC1	GC1	GC1	GC1	GC1	GC1	GC1	GC1	GC1	GC1	GC1
GC2.2	GC2.2	GC2.2	GC2.2	GC2.2	GC2.2	GC2.2	GC2.2	GC2.2	GC2.2	GC2.2	GC2.2
GC3.1	GC3.1	GC3.1	GC3.1	GC3.1	GC3.1	GC3.1	GC3.1	GC3.1	GC3.1	GC3.1	GC3.1
on	on	on	on	on	on	on	on	on	on	on	on
off	off	off	off	off	off	off	off	off	off	off	off
off	off	off	off	off	off	off	off	off	off	off	off
-	-	-	-	-	-	-	-	-	-	-	-
30/7/02	30/7/02	30/7/02	30/7/02	3/8/02	3/8/02	3/8/02	3/8/02	3/8/02	3/8/02	3/8/02	3/8/02
100.0	1100.0	2000.0	2400.0	4300.0	3700.0	2000.0	4700.0	5400.0	4300.0	7100.0	6200.0
93.9	92.5	92.0	90.6	92.0	90.9	89.3	82.9	106.0	92.0	87.1	87.5
44.6	46.9	48.0	49.0	46.2	47.5	48.3	48.0	37.6	46.2	47.8	48.2
20.5	28.1	36.3	40.2	23.8	29.8	34.8	35.1	20.2	23.8	28.4	31.1
17.6	24.3	31.0	35.1	20.2	25.2	29.9	20.1	19.8	20.2	20.2	20.4
35.8	40.0	42.8	44.1	39.1	41.5	43.1	42.9	27.5	39.1	41.6	42.1
59.4	60.0	59.9	60.2	60.2	60.7	60.5	60.6	59.8	60.2	60.4	60.7
-0.2	0.7	0.5	2.1	0.2	0.4	-0.8	0.6	-0.7	0.2	7.7	14.0
-0.4	0.5	0.2	1.9	0.3	0.4	-0.8	0.6	8.4	0.3	8.8	33.3
17.0	17.1	17.4	17.5	19.6	20.0	19.7	19.4	19.8	19.6	37.2	44.2
1.8	2.7	2.2	3.8	2.4	2.3	0.7	2.2	2.9	2.4	10.3	18.9
20.4	28.1	36.4	40.1	23.9	29.9	34.9	35.2	20.3	23.9	28.6	31.0
10.8	14.8	18.5	25.1	16.5	19.0	19.8	20.9	18.8	16.5	26.6	29.8
2.8	3.5	3.1	4.6	2.9	2.7	1.6	2.7	10.3	2.9	14.8	30.8
62.8	62.2	62.0	62.1	56.8	55.7	50.4	56.5	59.2	56.8	58.4	58.5
65.6	64.9	64.6	64.6	59.3	58.2	52.5	58.8	62.0	59.3	60.9	60.9
49.7	48.0	47.6	47.1	40.7	39.8	37.9	36.1	52.6	40.7	42.0	48.4
2.1	2.1	2.1	2.1	2.1	2.1	2.1	2.0	2.1	2.1	2.1	2.1
34.0	34.0	34.0	35.0	33.0	34.0	32.0	34.0	32.0	33.0	40.0	47.0
100.0	100.0	100.0	100.0	100.0	100.0	100.0	90.0	110.0	100.0	100.0	100.0
100.0	100.0	100.0	100.0	100.0	100.0	100.0	89.0	110.0	100.0	98.0	96.0
-	-	-	-	-	-	-	-	-	xx	xx	xx
-	-	-	-	-	-	-	-	-	xx	xx	xx
35.0	36.0	35.0	37.0	35.0	36.0	35.0	36.0	35.0	35.0	43.0	50.0
1.6	1.8	1.9	2.0	2.0	2.1	2.1	1.6	1.9	2.0	2.6	3.0
3.7	3.7	2.7	2.6	3.3	2.9	2.2	2.5	3.3	3.3	2.9	4.0
0.0	0.0	0.0	0.0	-	-	-	-	-	-	-	-
435.5	436.5	435.8	436.2	437.9	435.1	437.9	435.3	450.8	437.9	442.4	455.5
479.6	480.8	480.1	479.3	484.1	479.3	485.7	474.6	507.7	484.1	480.8	489.2
493.1	490.7	489.8	487.7	489.8	488.2	485.5	484.6	504.1	489.8	481.7	482.2
341.8	357.4	365.5	371.3	353.2	362.2	366.8	399.7	292.0	353.2	364.2	366.8
243.2	264.9	294.2	313.4	252.1	270.0	288.0	299.8	240.9	252.1	266.5	276.5
219.7	228.9	238.1	256.1	233.3	239.4	241.4	246.8	237.5	233.3	260.7	271.9
219.7	228.9	238.1	256.1	233.3	239.4	241.4	246.8	237.5	233.3	260.7	271.9
94.9	94.2	94.7	97.2	90.5	95.1	87.8	95.0	80.7	90.5	106.7	115.5
33.7	34.5	34.3	35.8	34.1	34.2	33.1	34.4	33.2	34.1	41.4	48.6

gc3.2_v1.1	gc3.2_v1.1	gc3.2_v1.1	gc3.2_v1.1	gc3.2_v1.1	gc3.2_v1.1	gc3.2_v1.1	gc3.2_v1.1	gc3.2_v1.1	gc3.2_v1.1	gc3.2_v1.1
69	70	71	72	73	74	75	76	77	78	79
5	5	5	5	5	5	5	5	5	5	5
12	13	01	06	11	19	24	11	06	17	18
GC2.2	GC2.2	GC2.2	GC2.2	GC2.2	GC2.2	GC2.2	GC2.2	GC2.2	GC2.2	GC2.2
GC1	GC1	GC1	GC1	GC1	GC1	GC1	GC1	GC1	GC1	GC1
GC3.2	GC3.2	GC3.2	GC3.2	GC3.2	GC3.2	GC3.2	GC3.2	GC3.2	GC3.2	GC3.2
on	on	on	on	on	on	on	on	on	on	on
off	off	off	off	off	off	off	off	off	off	off
off	off	off	off	off	off	off	off	off	off	off
-	-	-	-	-	-	-	-	-	-	-
15/8/02	15/8/02	15/8/02	15/8/02	15/8/02	15/8/02	15/8/02	15/8/02	15/8/02	15/8/02	15/8/02
3850.0	4950.0	5700.0	1400.0	2100.0	9500.0	9900.0	9100.0	2900.0	8600.0	8000.0
95.9	97.5	86.6	86.7	94.2	99.4	106.9	92.3	103.1	83.5	78.3
46.0	46.8	45.2	45.7	44.5	41.3	35.4	45.1	40.3	47.8	50.2
32.3	35.1	35.8	34.4	27.1	23.0	21.3	26.9	22.7	32.6	37.6
25.3	29.6	20.5	20.5	20.0	19.7	19.8	19.5	19.8	19.6	20.5
40.9	42.2	40.3	40.9	38.2	32.1	26.7	38.1	31.0	41.7	43.9
60.2	60.0	59.5	59.3	59.8	59.9	60.0	59.7	60.1	59.0	59.5
0.3	0.2	0.2	-0.4	-0.1	-0.6	-0.1	-0.2	-0.2	7.2	14.6
0.2	0.2	0.1	-0.5	-0.1	-0.5	0.3	-0.1	1.9	7.1	17.9
19.1	19.6	19.5	18.9	19.0	18.8	18.8	18.7	18.9	18.8	44.6
1.5	1.6	1.4	0.5	1.5	1.2	2.2	1.3	2.3	9.4	16.6
32.5	35.3	36.2	34.6	27.1	23.0	21.3	27.2	22.8	32.9	38.1
23.1	28.6	30.6	20.5	20.4	17.0	17.9	17.2	20.0	27.8	34.2
4.4	5.8	4.3	1.6	3.8	4.4	8.2	3.3	8.4	10.9	21.3
60.6	60.8	60.3	51.2	54.3	57.3	59.3	55.7	58.6	54.2	54.7
63.5	63.8	63.3	53.6	57.1	60.6	62.7	58.7	61.7	57.0	57.4
82.8	84.1	75.1	74.0	80.9	85.0	91.0	78.7	88.4	73.0	70.0
2.1	2.1	2.2	2.0	2.1	2.1	2.1	2.1	2.1	2.2	2.1
34.0	34.0	34.0	34.0	33.0	33.0	33.0	33.0	33.0	40.0	49.0
100.0	100.0	90.0	95.0	100.0	105.0	110.0	100.0	105.0	100.0	100.0
100.0	100.0	90.0	94.0	100.0	105.0	110.0	100.0	105.0	100.0	98.0
-	-	-	-	-	-	-	-	-	-	-
-	-	-	-	-	-	-	-	-	-	-
36.0	35.0	35.0	35.0	36.0	35.0	36.0	36.0	35.0	42.0	50.0
1.9	1.9	1.5	1.6	1.7	1.8	1.8	1.8	1.8	2.2	2.3
2.7	2.5	2.2	2.3	3.1	3.1	3.4	3.1	3.5	7.3	2.7
-	-	-	-	-	-	-	-	-	-	-
438.1	440.2	437.9	433.3	439.3	440.1	445.8	438.5	446.1	435.5	434.8
483.1	485.7	477.9	474.4	486.0	489.4	499.5	485.0	497.5	472.2	462.6
496.3	498.7	490.5	486.0	493.6	497.6	505.3	490.3	503.3	475.2	465.3
351.8	357.4	384.7	366.7	341.1	311.9	284.3	344.7	307.1	363.5	379.1
278.7	289.3	302.5	290.5	261.9	248.9	243.7	261.3	248.4	279.4	302.2
250.5	266.5	277.5	244.3	243.0	233.7	235.5	234.8	241.1	263.7	287.0
250.5	266.5	277.5	244.3	243.0	233.7	235.5	234.8	241.1	263.7	287.0
93.2	91.9	93.3	96.3	89.7	89.2	85.9	90.1	85.7	111.8	137.9
34.1	34.1	34.0	33.5	33.8	33.3	33.8	33.6	33.7	40.9	49.3

comp1	comp1	comp1	comp1	comp4	comp4	comp4	comp2	comp2	comp2	comp2	comp2
80	81	82	83	85	86	87	88	89	90	91	92
6	6	6	6	6	6	6	6	6	6	6	6
11	11	11	11	11	11	11	11	11	11	11	11
GC1	GC1	GC1	GC1	GC1	GC1	GC1	GC1	GC1	GC1	GC1	GC1
GC2.2	GC2.2	GC2.2	GC2.2	GC2.2	GC2.2	GC2.2	GC2.2	GC2.2	GC2.2	GC2.2	GC2.2
GC3.1	GC3.1	GC3.1	GC3.1	GC3.1	GC3.1	GC3.1	GC3.1	GC3.1	GC3.1	GC3.1	GC3.1
on	on	on	on	on	on	on	on	on	on	on	on
off	off	off	off	off	off	off	off	off	off	off	off
off	off	off	off	off	off	off	off	off	off	off	off
-	-	-	-	-	-	-	-	-	-	-	-
20/8/02	20/8/02	20/8/02	20/8/02	22/8/02	22/8/02	22/8/02	25/8/02	25/8/02	25/8/02	25/8/02	25/8/02
800.0	1200.0	3300.0	4600.0	1800.0	3000.0	5400.0	1400.0	2000.0	2600.0	3200.0	3800.0
95.3	92.3	93.5	96.1	92.0	91.1	91.6	90.8	92.4	91.4	92.5	94.3
45.6	45.8	45.2	45.0	45.1	45.8	45.5	46.2	45.8	45.9	46.0	45.5
25.0	24.9	23.6	22.9	22.6	23.4	23.4	25.3	23.8	24.9	24.4	23.6
20.6	20.0	19.5	19.6	18.2	18.6	18.7	19.4	19.0	19.1	19.1	18.9
41.7	41.6	40.8	39.5	40.6	41.5	41.2	42.4	41.5	42.1	41.8	41.1
60.4	59.9	60.1	59.8	59.4	59.9	59.1	60.2	60.4	60.3	60.5	60.4
-1.7	-0.3	0.2	-0.8	0.4	0.7	0.0	-0.2	-0.4	-0.2	-0.3	-0.7
-1.9	-0.6	-0.1	-1.1	0.3	0.5	0.0	-0.5	-0.7	-0.5	-0.5	-0.8
19.7	19.1	18.9	19.0	17.3	17.8	18.3	18.3	18.1	18.4	18.2	18.4
2.1	2.1	1.9	2.3	2.5	2.7	2.7	1.4	1.3	1.4	1.4	1.4
24.5	24.4	23.4	22.5	22.3	23.2	23.1	25.0	23.5	24.6	24.2	23.4
11.6	15.2	19.3	20.6	18.6	20.8	21.5	19.4	20.0	20.5	20.9	21.0
3.9	4.1	3.4	3.4	6.4	3.7	6.9	3.4	3.0	2.2	2.7	4.1
48.2	50.2	55.8	59.0	46.7	52.6	45.5	50.5	53.1	55.1	56.5	57.8
46.4	48.3	54.4	57.5	45.4	51.0	43.8	49.4	51.9	53.6	55.2	56.1
87.1	84.0	85.9	88.1	83.9	83.2	82.6	82.2	83.8	83.2	84.0	86.1
2.1	2.1	2.1	2.1	2.1	2.1	2.1	2.1	2.1	2.1	2.1	2.1
32.0	34.0	34.0	34.0	34.0	34.0	33.0	34.0	33.0	34.0	34.0	34.0
100.0	100.0	100.0	100.0	100.0	100.0	100.0	100.0	100.0	100.0	100.0	100.0
-	-	-	-	x	x	x	xx	xx	xx	xx	xx
97.0	97.0	97.0	97.0	96.0	97.0	97.0	97.0	97.0	97.0	97.0	97.0
xx	xx	xx	xx	xx	xx	xx	xx	xx	xx	xx	xx
35.0	35.0	36.0	35.0	36.0	36.0	36.0	36.0	35.0	35.0	35.0	35.0
1.7	1.9	1.9	1.9	1.9	1.9	1.8	1.9	2.0	1.9	1.9	1.8
2.8	3.3	3.4	3.4	4.0	4.0	4.0	3.4	3.4	3.4	3.4	3.4
18.0	17.0	8.0	2.0	18.0	6.0	3.0	10.0	7.0	4.0	2.0	2.0
441.4	437.6	436.5	436.5	441.1	437.0	444.0	436.3	437.9	434.3	435.1	437.6
490.3	482.4	480.8	480.8	487.0	481.5	492.3	480.7	484.1	478.2	479.3	482.4
495.2	490.3	492.4	496.6	489.8	488.5	489.2	488.0	490.5	488.8	490.8	493.7
348.9	350.4	345.4	344.0	344.7	350.4	347.5	352.5	349.6	350.4	351.8	348.2
255.5	255.5	251.8	249.6	248.8	251.3	251.3	256.3	252.4	255.2	254.1	251.8
221.6	230.3	240.9	244.3	239.0	244.6	246.5	240.9	242.7	244.0	244.8	245.4
221.6	230.3	240.9	244.3	239.0	244.6	246.5	240.9	242.7	244.0	244.8	245.4
85.7	93.5	94.2	94.2	91.3	93.9	86.9	94.3	90.5	95.6	95.1	93.5
32.3	33.6	34.0	33.1	34.2	34.5	33.8	33.7	33.4	33.6	33.5	33.2

comp2	comp2	comp3	comp3	comp3	comp3	comp3	comp3	hp90bar_v1	hp90bar_v1	hp90bar_v1	hp90bar_v1	hp95bar_v1	hp95bar_v1	hp95bar_v1	hp95bar_v1	hp95bar_v1	hp100bar_v1	hp100bar_v1	hp100bar_v1	hp100bar_v1
93	94	95	96	97	98	99	100	101	102	103	104	105	106	107	108	109	110	111	112	113
6	6	6	6	6	6	6	6	6	6	6	6	6	6	6	6	6	6	6	6	6
11	11	11	11	11	11	11	11	01	02	03	04	06	07	08	09	10	11	12	13	17

GC1	GC1	GC1	GC1	GC1	GC1	GC1	GC1	GC1	GC1	GC1	GC1	GC1	GC1	GC1	GC1	GC1	GC1	GC1	GC1	GC1
GC2.2	GC2.2	GC2.2	GC2.2	GC2.2	GC2.2	GC2.2	GC2.2	GC2.2	GC2.2	GC2.2	GC2.2	GC2.2	GC2.2	GC2.2	GC2.2	GC2.2	GC2.2	GC2.2	GC2.2	GC2.2
GC3.1	GC3.1	GC3.1	GC3.1	GC3.1	GC3.1	GC3.1	GC3.1	GC3.1	GC3.1	GC3.1	GC3.1	GC3.1	GC3.1	GC3.1	GC3.1	GC3.1	GC3.1	GC3.1	GC3.1	GC3.1
on	on	on	on	on	on	on	on	on	on	on	on	on	on	on	on	on	on	on	on	on
off	off	off	off	off	off	off	off	off	off	off	off	off	off	off	off	off	off	off	off	off
off	off	off	off	off	off	off	off	off	off	off	off	off	off	off	off	off	off	off	off	off
-	-	-	-	-	-	-	-	-	-	-	-	-	-	-	-	-	-	-	-	-

25/8/02	25/8/02	4/9/02	4/9/02	4/9/02	4/9/02	4/9/02	4/9/02	23/9/02	23/9/02	23/9/02	23/9/02	23/9/02	23/9/02	23/9/02	23/9/02	23/9/02	11/9/02	11/9/02	11/9/02	11/9/02
4400.0	5000.0	1200.0	1800.0	2400.0	3000.0	3600.0	4200.0	400.0	1000.0	2100.0	3300.0	1200.0	2200.0	3600.0	4600.0	6000.0	200.0	800.0	1600.0	2300.0
96.1	96.9	94.2	91.5	91.5	93.6	94.9	95.4	81.9	82.9	84.0	77.1	85.3	85.2	88.5	79.2	72.3	92.3	92.4	92.3	82.2
45.2	45.1	45.8	46.6	46.2	45.7	45.6	45.4	46.3	46.4	46.7	47.6	46.7	46.9	46.9	48.3	48.5	45.7	46.7	47.3	48.5
23.4	23.2	23.2	24.8	24.4	23.9	23.8	23.7	34.9	36.7	38.3	36.2	30.7	35.9	37.6	36.3	36.9	23.0	30.3	35.8	31.6
19.1	18.9	18.7	18.6	18.9	19.0	19.1	18.9	19.2	25.9	31.5	19.3	19.0	25.2	29.6	19.4	19.3	18.6	25.9	31.7	19.6
40.6	40.5	41.6	42.8	41.8	41.5	41.3	41.2	43.9	44.1	44.7	44.8	44.1	44.8	45.0	45.9	45.3	41.0	43.4	44.9	45.4
60.3	60.3	60.8	61.1	60.5	60.5	60.6	60.5	59.4	59.3	59.8	59.6	60.1	60.0	60.2	60.8	58.6	60.3	59.9	60.4	60.5
-0.7	-1.0	-2.3	0.8	0.5	0.5	0.5	0.5	0.7	0.1	1.1	7.3	-0.1	-0.6	-0.9	7.8	14.6	0.2	-0.5	-0.2	7.3
-0.9	-1.1	-2.5	0.5	0.6	0.3	0.4	0.4	0.3	-0.3	0.6	6.9	-0.3	-0.9	-1.3	7.4	17.6	-0.1	-0.8	-0.5	7.0
18.3	18.2	17.8	18.0	18.3	18.3	18.2	18.1	18.2	18.3	18.4	25.1	17.9	18.3	18.7	22.0	32.5	18.1	18.3	18.5	39.5
1.4	1.2	1.9	2.6	2.6	2.7	2.7	2.8	2.0	1.3	2.2	9.0	1.2	0.5	0.1	9.5	16.8	2.2	1.2	1.5	9.1
23.2	23.1	23.0	24.6	24.2	23.7	23.6	23.6	34.2	36.0	37.7	35.5	29.9	35.3	36.9	35.5	36.0	22.7	29.9	35.3	31.1
21.1	20.8	13.7	19.8	21.4	22.0	22.0	21.9	29.9	32.2	34.3	32.2	7.3	22.8	25.3	32.0	30.3	16.4	16.7	22.2	27.7
5.0	5.7	3.2	5.1	3.9	6.4	7.0	7.5	3.8	3.4	5.1	12.8	1.5	1.7	1.8	11.7	20.9	4.5	2.4	1.2	8.9
59.5	60.5	47.3	50.4	52.6	54.4	56.3	57.8	53.1	54.0	55.8	55.8	48.8	51.4	55.3	54.9	52.3	50.1	52.3	54.7	54.1
58.1	59.3	45.6	48.5	51.0	52.4	54.5	56.3	51.6	52.5	54.2	53.8	47.5	49.7	53.4	52.8	50.2	48.0	50.0	52.3	51.9
88.0	88.8	85.0	82.8	82.4	85.2	86.6	87.3	74.4	75.4	76.5	71.3	77.6	77.3	80.9	73.7	69.0	84.0	84.2	84.2	75.9
2.1	2.0	2.0	2.1	2.1	2.1	2.1	2.0	2.0	1.9	2.0	2.0	2.0	2.0	2.0	2.1	2.0	2.1	2.1	2.1	2.1
33.0	32.0	31.0	34.0	34.0	34.0	34.0	34.0	34.0	35.0	35.0	40.0	34.0	34.0	34.0	40.0	49.0	34.0	34.0	33.0	40.0
100.0	100.0	100.0	100.0	100.0	100.0	100.0	100.0	90.0	90.0	90.0	90.0	95.0	95.0	95.0	95.0	95.0	100.0	100.0	100.0	100.0
xx	xx	xx	xx	xx	xx	xx	xx	-	-	-	-	-	-	-	-	-	-	-	-	-
97.0	97.0	97.0	97.0	97.0	97.0	97.0	97.0	90.0	90.0	90.0	89.0	95.0	94.0	95.0	92.0	90.0	100.0	100.0	100.0	98.0
xx	xx	xx	xx	xx	xx	xx	xx	-	-	-	-	-	-	-	-	-	-	-	-	-
35.0	35.0	34.0	36.0	36.0	36.0	36.0	36.0	36.0	36.0	37.0	43.0	36.0	36.0	35.0	43.0	50.0	36.0	36.0	35.0	42.0
1.9	1.8	1.7	1.9	1.9	1.9	1.9	1.9	1.6	1.6	1.8	1.8	1.7	1.7	1.8	1.9	2.2	1.9	1.9	2.0	2.1
3.4	3.4	3.3	4.0	3.9	3.9	4.0	4.0	2.8	2.2	1.9	3.2	3.0	2.2	1.9	4.8	4.3	3.8	2.8	2.5	2.3
2.0	2.0	15.0	13.0	2.0	4.0	2.0	2.0	-	-	-	-	-	-	-	-	-	-	-	-	-

441.2	444.2	442.6	439.2	437.3	441.1	442.2	442.8	437.0	434.2	436.8	438.9	433.3	433.6	433.6	436.9	433.9	438.3	434.6	435.2	432.0
488.5	494.1	493.4	484.5	482.1	487.0	488.3	489.2	476.7	471.8	475.1	471.6	474.4	474.9	474.9	471.7	459.3	483.3	478.6	480.7	467.9
496.6	497.7	493.4	489.2	489.0	492.6	494.5	495.5	482.8	484.6	486.4	474.8	483.6	483.5	488.9	472.8	459.5	490.3	490.7	490.3	472.8
346.1	345.4	350.4	356.0	352.5	349.6	348.2	347.5	390.7	391.3	393.5	398.2	374.5	375.9	375.2	384.6	385.8	348.9	356.7	360.8	368.7
251.3	250.7	250.5	255.2	253.8	252.4	252.4	252.1	297.8	308.4	321.9	307.6	275.5	298.2	305.5	302.4	309.8	249.9	271.9	291.7	276.9
245.4	244.6	226.6	241.9	246.5	247.8	247.8	247.5	275.2	284.6	294.6	285.4	212.0	251.0	257.7	281.8	276.8	232.8	233.8	248.0	264.4
245.4	244.6	226.6	241.9	246.5	247.8	247.8	247.5	275.2	284.6	294.6	285.4	212.0	251.0	257.7	281.8	276.8	232.8	233.8	248.0	264.4
88.6	84.1	82.4	92.5	93.7	91.3	90.7	90.3	93.9	98.6	96.8	109.2	96.3	96.1	96.1	110.7	138.7	93.1	95.4	92.3	114.6
33.2	32.9	31.8	34.6	34.3	34.3	34.3	34.3	34.5	33.9	34.9	41.0	33.8	33.3	33.1	41.6	49.4	34.0	33.4	33.7	41.0

hp100bar_v1	hp105bar_v1	hp105bar_v1	hp105bar_v1	hp105bar_v1	hp105bar_v1	hp110bar_v1	hp110bar_v1	hp110bar_v1	hp110bar_v1	hp110bar_v1	hp95bar_v2	hp95bar_v2	hp105bar_v2	hp105bar_v2	hp105bar_v2	hp105bar_v2	hp105bar_v2	hp110bar_v2
114	115	116	117	118	119	120	121	122	123	124	125	126	127	128	129	130	131	132
6	6	6	6	6	6	6	6	6	6	6	6	6	6	6	6	6	6	6
18	19	20	21	22	23	24	25	26	27	28	06	09	19	20	21	22	23	24
GC1	GC1	GC1	GC1	GC1	GC1	GC1	GC1	GC1	GC1	GC1	GC1	GC1	GC1	GC1	GC1	GC1	GC1	GC1
GC2.2	GC2.2	GC2.2	GC2.2	GC2.2	GC2.2	GC2.2	GC2.2	GC2.2	GC2.2	GC2.2	GC2.2	GC2.2	GC2.2	GC2.2	GC2.2	GC2.2	GC2.2	GC2.2
GC3.1	GC3.1	GC3.1	GC3.1	GC3.1	GC3.1	GC3.1	GC3.1	GC3.1	GC3.1	GC3.1	GC3.1	GC3.1	GC3.1	GC3.1	GC3.1	GC3.1	GC3.1	GC3.1
on	on	on	on	on	on	on	on	on	on	on	on	on	on	on	on	on	on	on
off	off	off	off	off	off	off	off	off	off	off	off	off	off	off	off	off	off	off
off	off	off	off	off	off	off	off	off	off	off	off	off	off	off	off	off	off	off
-	-	-	-	-	-	-	-	-	-	-	-	-	-	-	-	-	-	-
11/9/02	24/9/02	24/9/02	24/9/02	24/9/02	24/9/02	25/9/02	25/9/02	25/9/02	25/9/02	25/9/02	26/9/02	26/9/02	26/9/02	26/9/02	26/9/02	26/9/02	26/9/02	26/9/02
3700.0	600.0	1100.0	1600.0	2000.0	3300.0	5100.0	6000.0	6700.0	3100.0	4000.0	1000.0	1700.0	1800.0	2600.0	3000.0	3700.0	4000.0	500.0
72.8	99.2	98.0	93.7	88.8	81.4	101.3	102.5	103.6	94.3	81.0	83.5	73.4	101.6	100.4	99.6	89.6	84.3	104.6
49.5	42.9	45.1	47.5	47.5	50.1	41.0	43.2	44.3	40.7	50.4	47.4	49.5	41.5	44.1	45.2	47.2	47.4	35.5
37.3	20.6	27.4	34.8	26.4	31.8	20.2	26.4	29.9	21.3	29.5	31.8	37.4	20.4	26.8	30.4	25.5	30.4	20.1
19.7	19.1	25.4	30.7	19.1	19.8	19.0	25.4	29.6	19.9	19.7	19.5	19.7	19.4	25.8	29.0	20.1	19.9	19.7
46.4	34.2	39.7	44.1	42.9	46.0	31.4	36.1	38.2	31.0	45.2	45.1	47.3	32.5	38.0	40.7	41.6	43.4	27.0
59.0	59.9	60.2	60.3	60.5	61.4	60.6	60.3	61.0	57.7	61.4	60.3	59.8	59.5	59.9	60.2	60.6	59.7	57.9
15.8	-0.6	0.4	0.0	7.1	14.4	-0.5	-0.1	0.2	6.2	14.5	-0.4	7.1	0.0	0.2	0.9	8.9	9.2	0.1
15.8	-0.7	0.1	-0.3	6.9	17.2	-0.8	-0.3	0.2	6.1	14.6	-0.8	6.5	-0.2	0.0	0.6	8.9	9.3	0.1
38.4	18.6	18.9	18.8	28.9	40.0	18.4	18.6	18.6	39.0	46.0	18.5	24.0	18.4	19.2	19.0	38.4	38.2	19.1
18.0	1.9	2.3	1.5	10.0	17.4	1.4	1.8	1.7	8.6	16.6	1.1	8.1	1.7	1.6	2.2	11.0	11.2	1.7
36.6	20.4	27.1	34.5	26.2	31.4	20.2	26.2	29.6	21.4	29.2	31.0	36.4	20.1	26.5	29.9	25.2	29.8	19.9
32.5	16.1	20.3	20.9	23.4	29.1	13.2	20.8	22.9	19.4	26.8	5.9	29.5	16.5	18.5	21.1	23.6	24.1	16.1
19.6	4.7	4.7	3.0	12.5	20.0	2.9	5.4	5.3	10.7	17.7	1.3	7.7	4.0	2.6	2.7	13.0	11.6	4.2
52.8	57.0	58.8	59.1	58.3	53.9	60.5	61.6	62.7	58.1	55.5	45.7	47.2	58.9	60.8	61.6	60.9	60.0	60.9
50.5	54.6	56.3	56.5	55.7	51.4	58.5	59.7	60.4	56.1	53.2	44.3	45.4	57.0	58.7	59.4	58.7	58.0	58.9
68.2	91.2	90.4	85.5	82.4	75.2	92.8	94.0	95.2	86.6	75.2	75.1	67.0	94.4	93.0	92.6	83.2	79.4	96.9
2.1	2.1	2.1	2.1	2.2	2.2	2.1	2.2	2.2	2.3	2.3	2.0	2.1	2.1	2.1	2.1	2.2	2.2	2.2
49.0	33.0	34.0	34.0	40.0	49.0	34.0	34.0	34.0	39.0	49.0	34.0	40.0	34.0	34.0	34.0	41.0	47.0	34.0
100.0	105.0	105.0	105.0	105.0	105.0	110.0	110.0	110.0	110.0	110.0	95.0	95.0	105.0	105.0	105.0	105.0	105.0	110.0
-	-	-	-	-	-	-	-	-	-	-	-	-	-	-	-	-	-	-
96.0	105.0	105.0	105.0	103.0	101.0	110.0	110.0	110.0	110.0	108.0	94.0	93.0	105.0	105.0	105.0	104.0	101.0	110.0
-	-	-	-	-	-	-	-	-	-	-	-	-	-	-	-	-	-	-
52.0	35.0	37.0	36.0	42.0	50.0	35.0	35.0	36.0	42.0	51.0	36.0	42.0	35.0	36.0	36.0	45.0	49.0	36.0
2.5	1.8	1.8	2.1	2.7	2.8	1.8	2.0	2.1	2.6	3.0	1.7	1.8	1.7	1.9	2.0	2.5	2.7	1.8
3.9	3.4	3.2	2.6	4.2	4.3	3.2	3.1	2.9	2.6	3.6	2.8	3.2	3.0	2.6	2.6	2.9	3.7	2.8
-	-	-	-	-	-	-	-	-	-	-	-	-	-	-	-	-	-	-
431.0	440.6	438.4	435.6	438.5	432.0	435.6	439.7	439.4	437.6	426.9	432.8	429.6	437.4	435.0	435.1	437.2	417.3	437.8
458.1	490.1	485.9	482.2	478.3	461.4	484.3	489.9	489.4	480.4	457.1	473.7	462.8	484.5	481.3	481.5	475.4	445.3	487.3
454.2	497.3	495.4	488.1	479.7	465.7	496.5	498.3	500.3	484.5	459.3	480.6	462.0	501.0	499.2	497.9	481.0	471.5	501.7
374.4	320.7	333.2	348.0	347.3	363.8	305.4	315.1	320.9	304.5	353.0	379.1	390.8	312.8	326.8	333.8	346.1	347.3	284.9
303.1	242.7	261.1	285.0	259.0	276.5	240.9	257.1	267.2	243.7	266.7	279.8	307.5	242.4	259.6	270.4	256.2	271.5	240.9
281.3	231.7	242.2	243.4	250.7	267.4	224.4	242.4	248.0	239.2	258.9	208.7	271.9	232.7	237.6	244.0	250.7	253.0	231.2
281.3	231.7	242.2	243.4	250.7	267.4	224.4	242.4	248.0	239.2	258.9	208.7	271.9	232.7	237.6	244.0	250.7	253.0	231.2
141.6	88.9	93.0	94.8	109.5	140.5	94.8	92.2	92.4	107.4	145.9	96.7	116.6	93.6	95.2	95.1	113.3	150.6	93.4
50.8	33.3	34.2	33.9	40.8	49.1	33.4	33.8	34.1	39.9	49.2	33.5	40.8	33.9	34.0	34.7	42.7	43.1	33.9

hp110bar_v2	hp110bar_v2	hp110bar_v2	hp110bar_v2	hp90bar_v3	hp90bar_v3	hp90bar_v3	hp95bar_v3	hp95bar_v3	hp95bar_v3	hp95bar_v3	hp95bar_v3	hp100bar_v3	hp100bar_v3	hp100bar_v3	hp100bar_v3	hp100bar_v3	hp105bar_v3	hp105bar_v3
133	134	135	136	137	138	139	140	141	142	143	144	145	146	147	148	149	150	151
6	6	6	6	6	6	6	6	6	6	6	6	6	6	6	6	6	6	6
25	26	24	27	01	02	03	06	07	08	09	10	11	12	13	17	18	19	20
GC1	GC1	GC1	GC1	GC1	GC1	GC1	GC1	GC1	GC1	GC1	GC1	GC1	GC1	GC1	GC1	GC1	GC1	GC1
GC2.2	GC2.2	GC2.2	GC2.2	GC2.2	GC2.2	GC2.2	GC2.2	GC2.2	GC2.2	GC2.2	GC2.2	GC2.2	GC2.2	GC2.2	GC2.2	GC2.2	GC2.2	GC2.2
GC3.1	GC3.1	GC3.1	GC3.1	GC3.1	GC3.1	GC3.1	GC3.1	GC3.1	GC3.1	GC3.1	GC3.1	GC3.1	GC3.1	GC3.1	GC3.1	GC3.1	GC3.1	GC3.1
on	on	on	on	on	on	on	on	on	on	on	on	on	on	on	on	on	86.0	on
off	off	off	off	off	off	off	off	off	off	off	off	off	off	off	off	off	off	off
off	off	off	off	off	off	off	off	off	off	off	off	off	off	off	off	off	off	off
-	-	-	-	-	-	-	-	-	-	-	-	-	-	-	-	-	-	-
26/9/02	26/9/02	26/9/02	26/9/02	2/10/02	2/10/02	2/10/02	2/10/02	2/10/02	2/10/02	2/10/02	2/10/02	2/10/02	2/10/02	2/10/02	2/10/02	2/10/02	2/10/02	2/10/02
1000.0	1600.0	2000.0	2900.0	1600.0	3000.0	3400.0	600.0	1500.0	2200.0	2700.0	3200.0	1300.0	1800.0	2300.0	700.0	2700.0	2000.0	1500.0
105.7	105.7	107.6	92.4	83.9	82.9	82.8	86.0	85.5	86.5	81.2	72.3	92.4	92.5	92.2	83.8	73.0	103.0	101.9
38.9	43.1	40.4	46.4	47.0	47.6	47.6	47.1	47.3	47.8	48.2	50.5	45.3	46.4	47.2	48.4	50.5	41.5	44.4
26.2	30.1	25.7	22.8	35.2	37.6	38.8	31.5	36.5	38.7	36.4	38.9	24.3	32.0	36.8	32.5	38.6	20.2	26.5
26.0	29.7	25.4	19.3	18.7	26.3	31.3	19.3	25.7	30.6	19.6	20.3	19.0	26.2	31.3	19.3	20.1	19.1	24.5
32.4	37.2	33.1	38.3	44.9	45.7	46.0	44.4	45.3	45.9	45.6	48.2	41.2	43.7	45.1	45.0	48.0	32.9	38.4
58.1	59.8	59.5	60.7	60.8	60.7	60.9	60.2	60.2	60.5	60.5	60.1	59.6	59.6	60.0	60.9	60.1	59.7	59.9
0.3	0.4	-0.3	8.1	-1.0	0.9	1.1	0.3	0.9	1.2	8.0	15.0	0.2	0.6	0.6	8.0	15.8	-0.5	0.3
0.1	0.3	-0.4	8.7	-1.4	0.5	0.6	0.0	0.4	0.8	7.9	15.8	0.0	0.2	0.5	8.1	17.0	-0.6	0.6
19.0	19.2	19.3	30.0	17.4	18.3	18.6	18.7	18.7	20.1	34.6	44.8	18.4	18.2	18.2	32.9	44.8	18.2	18.1
1.8	1.8	1.2	10.5	0.1	1.9	2.0	1.8	2.0	2.4	9.9	16.4	2.0	1.9	1.5	10.2	17.7	1.2	1.9
25.8	29.5	25.3	22.6	34.2	36.7	37.9	30.9	35.9	38.0	35.7	38.0	24.1	31.5	36.2	32.1	37.8	20.2	26.3
19.4	20.3	18.5	20.4	21.2	33.9	34.6	23.3	28.4	31.5	33.2	31.8	21.0	26.2	29.2	29.8	33.2	17.2	23.2
5.1	5.0	5.1	12.9	3.4	4.1	4.4	2.5	3.0	3.5	14.6	20.0	4.5	4.3	3.9	12.9	20.0	7.6	7.7
62.9	64.2	64.9	63.4	50.7	53.3	54.0	54.8	56.8	57.5	56.9	51.6	57.3	58.5	58.3	56.3	51.9	62.2	61.3
60.7	61.8	62.4	61.0	51.0	53.1	54.1	54.6	56.7	57.3	56.9	51.3	57.1	58.5	57.9	56.3	51.5	62.1	61.1
98.7	98.4	100.3	85.7	75.8	75.2	75.3	78.0	78.1	78.9	75.2	67.9	84.8	84.9	84.4	77.2	68.4	95.5	93.6
2.2	2.2	2.1	2.3	1.9	2.0	2.0	2.0	2.0	2.0	2.0	2.0	2.1	2.1	2.1	2.1	2.1	2.1	2.1
34.0	34.0	34.0	40.0	33.0	34.0	34.0	34.0	34.0	34.0	41.0	49.0	34.0	34.0	34.0	40.0	50.0	33.0	34.0
110.0	110.0	110.0	110.0	90.0	90.0	90.0	95.0	95.0	95.0	95.0	98.0	100.0	100.0	100.0	100.0	100.0	105.0	105.0
-	-	-	-	-	-	-	-	-	-	-	-	-	-	-	-	-	-	-
110.0	110.0	110.0	109.0	89.0	89.0	89.0	95.0	94.0	95.0	93.0	94.0	100.0	100.0	100.0	98.0	97.0	105.0	105.0
-	-	-	-	xx	xx	xx	xx	xx	xx	xx	xx	xx	xx	xx	xx	xx	xx	xx
36.0	36.0	35.0	42.0	35.0	36.0	36.0	36.0	36.0	37.0	43.0	51.0	36.0	36.0	36.0	43.0	52.0	35.0	36.0
2.0	2.0	1.8	2.4	1.4	1.5	1.6	1.7	1.8	1.9	2.0	2.1	1.9	2.0	2.1	2.3	2.4	1.8	2.0
2.6	2.4	2.4	4.0	2.4	2.2	1.7	3.1	2.6	2.2	2.5	2.3	3.6	3.1	2.6	3.2	2.9	3.3	3.3
-	-	-	-	12.0	2.0	2.0	6.0	2.0	2.0	2.0	2.0	4.0	2.0	2.0	2.0	2.0	2.0	2.0
439.1	438.9	439.2	439.0	438.7	437.6	437.9	434.8	435.8	436.6	440.0	432.0	438.3	437.9	437.3	439.2	429.5	444.9	443.2
489.0	488.7	489.2	481.2	480.1	477.4	477.9	476.4	477.6	478.7	474.4	458.3	483.3	482.8	482.1	476.8	455.5	495.9	492.1
503.4	503.6	506.4	481.2	486.1	484.5	484.3	484.6	483.8	485.5	476.5	455.8	490.7	490.8	490.3	475.7	454.7	503.3	501.6
297.3	314.7	303.3	331.1	394.6	398.2	397.7	376.5	377.8	381.6	384.1	387.1	346.8	354.6	359.4	368.1	380.8	312.8	328.5
256.5	267.5	255.2	247.9	301.0	317.9	330.6	278.4	301.3	312.7	301.6	316.1	253.5	277.7	296.4	280.5	308.8	241.9	258.5
238.9	241.4	237.0	241.8	247.3	293.6	297.5	251.9	268.1	278.1	286.1	280.2	244.6	258.9	268.4	270.7	283.3	234.2	249.5
238.9	241.4	237.0	241.8	247.3	293.6	297.5	251.9	268.1	278.1	286.1	280.2	244.6	258.9	268.4	270.7	283.3	234.2	249.5
92.6	92.7	92.5	109.1	90.0	93.5	93.3	95.3	94.7	94.1	111.1	140.5	93.1	93.3	93.7	109.0	146.0	86.4	90.0
34.1	34.3	33.6	41.9	33.0	34.7	34.9	34.1	34.7	34.9	41.8	49.8	34.0	34.4	34.4	41.8	50.8	33.4	34.1

hp105bar_v3	hp105bar_v3	hp105bar_v3	hp110bar_v3	hp110bar_v3	hp110bar_v3	hp110bar_v3	hp110bar_v3	CO2_tr1	CO2_tr1	CO2_tr1	CO2_tr1	co2_tr2	co2_tr2	co2_tr2	co2_tr2	co2_tr2	co2_tr3	co2_tr3	co2_tr3
152	153	154	155	156	157	158	159	160	161	162	163	164	165	166	167	168	169	170	171
6	6	6	6	6	6	6	6	6	6	6	6	6	6	6	6	6	6	6	6
21	22	23	24	25	26	27	28	19	20	21	22	19	20	21	22	23	19	20	21
GC1	GC1	GC1	GC1	GC1	GC1	GC1	GC1	GC1	GC1	GC1	GC1	GC1	GC1	GC1	GC1	GC1	GC1	GC1	GC1
GC2.2	GC2.2	GC2.2	GC2.2	GC2.2	GC2.2	GC2.2	GC2.2	GC2.2	GC2.2	GC2.2	GC2.2	GC2.2	GC2.2	GC2.2	GC2.2	GC2.2	GC2.2	GC2.2	GC2.2
GC3.1	GC3.1	GC3.1	GC3.1	GC3.1	GC3.1	GC3.1	GC3.1	GC3.1	GC3.1	GC3.1	GC3.1	GC3.1	GC3.1	GC3.1	GC3.1	GC3.1	GC3.1	GC3.1	GC3.1
on	on	on	86.0	on	on	on	on	on	on	on	on	on	on	on	on	on	on	on	on
off	off	off	off	off	off	off	off	off	off	off	off	off	off	off	off	off	off	off	off
off	off	off	off	off	off	off	off	off	off	off	off	off	off	off	off	off	off	off	off
-	-	-	-	-	-	-	-	1.7	1.7	1.7	1.7	1.8	1.8	1.8	1.8	1.8	1.8	1.8	1.8
2/10/02	2/10/02	2/10/02	2/10/02	2/10/02	2/10/02	2/10/02	2/10/02	5/10/02	5/10/02	5/10/02	5/10/02	5/10/02	5/10/02	5/10/02	5/10/02	5/10/02	5/10/02	5/10/02	5/10/02
800.0	3900.0	1600.0	1900.0	2600.0	3300.0	4200.0	1100.0	2850.0	5300.0	5750.0	3850.0	3850.0	850.0	250.0	2800.0	3300.0	300.0	2300.0	2700.0
100.0	88.5	79.1	100.4	100.4	101.8	94.3	82.9	96.3	98.1	98.5	99.0	98.2	99.3	97.6	85.1	93.0	96.7	96.4	95.9
45.2	45.7	49.8	41.6	43.5	44.5	46.2	50.5	41.9	43.3	44.8	45.3	40.2	43.2	44.7	47.8	46.4	41.6	42.7	44.1
30.8	23.7	33.6	20.2	26.6	31.1	22.8	30.7	20.5	26.7	31.0	23.5	20.3	26.4	30.9	26.5	25.5	20.3	26.3	30.9
29.3	18.6	19.5	18.8	25.4	30.4	19.0	19.4	18.8	25.6	29.5	19.5	19.0	25.2	29.2	19.3	19.6	18.8	25.2	29.6
41.2	40.1	46.1	32.5	37.0	39.4	38.7	45.9	33.2	36.9	40.4	38.6	30.8	36.5	40.1	42.6	40.5	32.6	36.1	39.5
59.8	59.5	60.6	60.3	60.3	60.1	61.1	62.0	60.2	60.5	61.1	62.8	59.0	60.2	60.2	62.6	62.4	59.7	59.4	60.0
-0.6	7.3	15.6	-0.2	-0.1	-0.6	6.2	15.0	0.0	0.1	-0.2	7.9	0.4	-0.3	-0.3	8.9	12.3	0.1	-0.3	0.6
-0.9	7.2	17.5	-0.3	-0.3	-0.8	6.1	17.4	-0.1	0.0	-0.4	23.7	0.3	-0.5	-0.5	8.6	32.0	-0.1	-0.5	0.3
18.3	30.7	45.6	18.1	18.3	18.4	25.8	45.7	18.0	18.1	18.4	42.2	18.5	18.3	18.4	41.9	42.9	18.3	18.5	18.2
1.2	9.6	18.0	1.6	1.3	0.6	8.5	17.5	1.7	1.9	1.2	10.8	2.2	1.3	1.1	10.8	17.2	1.8	1.1	1.8
30.6	23.8	33.1	19.9	26.3	30.6	22.8	30.3	20.3	26.6	30.8	23.3	20.1	26.2	30.7	26.3	25.3	20.2	26.2	30.8
26.9	21.3	30.3	18.0	21.8	23.8	19.6	28.2	16.3	22.5	24.4	23.2	17.1	20.9	21.3	23.3	25.2	14.8	16.8	19.6
5.8	12.5	21.0	3.4	3.0	2.4	10.0	20.5	2.9	3.8	3.4	23.8	3.2	4.2	3.2	10.4	29.2	2.2	1.9	2.3
60.5	58.2	55.6	56.0	58.5	60.0	60.2	56.1	58.2	62.3	62.8	60.8	60.3	63.3	62.9	58.5	58.9	60.6	59.5	60.3
61.0	58.4	55.6	55.9	58.6	60.0	60.3	55.8	60.6	64.8	65.3	63.1	62.7	65.9	65.5	60.7	61.1	63.1	61.8	62.6
92.1	82.1	74.1	91.9	91.7	92.9	86.3	77.2	85.7	87.1	87.7	89.3	87.4	88.0	86.8	76.0	84.1	85.9	85.6	85.1
2.1	2.2	2.2	2.1	2.2	2.1	2.3	2.3	2.1	2.1	2.1	2.2	2.1	2.1	2.1	2.2	2.2	2.1	2.1	2.1
34.0	40.0	49.0	34.0	34.0	33.0	40.0	49.0	34.0	33.0	34.0	41.0	34.0	34.0	34.0	41.0	48.0	34.0	34.0	34.0
105.0	105.0	105.0	110.0	110.0	110.0	110.0	110.0	105.0	105.0	105.0	105.0	105.0	105.0	105.0	105.0	105.0	105.0	105.0	105.0
-	-	-	-	-	-	-	-	-	-	-	-	-	-	-	-	-	-	-	-
105.0	104.0	102.0	110.0	110.0	110.0	110.0	107.0	102.0	103.0	103.0	99.0	102.0	103.0	101.0	98.0	95.0	102.0	102.0	100.0
xx	xx	xx	xx	xx	xx	xx	xx	-	-	-	-	-	-	-	-	-	xx	xx	xx
36.0	43.0	42.0	36.0	36.0	35.0	41.0	51.0	36.0	35.0	35.0	43.0	35.0	35.0	35.0	44.0	48.0	36.0	35.0	36.0
2.1	2.5	2.8	1.8	2.0	2.1	2.3	2.8	2.0	2.1	2.2	2.5	2.1	2.2	2.2	2.5	2.9	2.1	2.3	2.4
2.8	3.9	3.0	3.4	3.0	2.6	4.5	3.6	3.6	3.3	2.8	2.7	3.7	3.1	2.8	2.7	4.1	3.6	3.1	3.1
2.0	2.0	2.0	6.0	2.0	2.0	2.0	2.0	8.0	4.0	4.0	6.0	-	-	-	-	-	-	-	-
440.2	438.3	433.9	436.3	435.8	437.1	434.0	433.1	435.6	439.3	436.5	454.6	436.0	437.6	436.0	432.3	451.2	434.3	433.8	434.5
488.1	478.1	463.7	485.2	484.7	487.8	474.7	464.6	482.2	488.4	483.3	497.3	482.6	484.8	482.6	469.4	485.4	480.5	479.7	480.6
498.4	479.0	461.0	494.9	494.9	497.2	484.5	463.0	492.6	495.4	496.0	496.8	495.5	497.5	494.6	472.8	486.9	493.2	492.8	491.8
333.2	336.2	362.1	308.4	317.0	321.9	330.5	354.1	314.9	322.3	331.5	334.4	307.1	322.3	330.9	349.2	341.1	313.3	319.6	327.4
271.6	251.3	282.0	241.2	257.9	270.5	247.8	270.6	242.7	259.4	271.9	250.3	241.9	258.5	271.9	258.5	255.7	242.2	257.9	271.9
259.6	244.6	270.8	235.5	244.9	250.1	239.4	263.1	232.3	248.0	253.4	251.0	234.6	244.0	245.4	251.5	257.4	229.0	233.8	241.2
259.6	244.6	270.8	235.5	244.9	250.1	239.4	263.1	232.3	248.0	253.4	251.0	234.6	244.0	245.4	251.5	257.4	229.0	233.8	241.2
91.9	109.6	138.7	94.3	94.7	91.0	113.0	139.5	94.8	89.7	94.2	101.2	94.5	93.5	94.5	117.2	121.1	95.6	96.0	95.5
33.3	41.1	50.5	33.7	33.7	33.3	39.9	49.8	33.9	34.0	33.7	41.7	34.3	33.5	33.6	42.7	46.6	33.9	33.6	34.4

co2_tr3	co2_tr3	co2_tr4	co2_tr4	co2_tr4	co2_tr4	co2_tr4	reheat1	reheat1	reheat1	reheat1
172	173	174	175	176	177	178	181	182	183	184
6	6	6	6	6	6	6	7	7	7	7
22	23	19	20	21	22	23	19.0	19.0	19.0	19.0
GC1	GC1	GC1	GC1	GC1	GC1	GC1	GC1	GC2	GC3	GC4
GC2.2	GC2.2	GC2.2	GC2.2	GC2.2	GC2.2	GC2.2	GC2.2	GC2.3	GC2.4	GC2.5
GC3.1	GC3.1	GC3.1	GC3.1	GC3.1	GC3.1	GC3.1	GC3.1	GC3.2	GC3.3	GC3.4
on	on	on	on	on	on	on	on	on	on	on
off	off	off	off	off	off	off	on	on	on	on
off	off	off	off	off	off	off	on-2 turns	on-2 turns	on-2 turns	on-2 turns
1.8	1.8	1.9	1.9	1.9	1.9	1.9	-	-	-	-
5/10/02	5/10/02	5/10/02	5/10/02	5/10/02	5/10/02	5/10/02	6/10/02	6/10/02	6/10/02	6/10/02
1300.0	1800.0	1450.0	1100.0	600.0	1900.0	2800.0	2000.0	3000.0	5000.0	6000.0
87.6	90.3	97.0	95.8	95.1	89.6	78.5	98.1	96.3	99.7	100.2
44.2	47.2	40.8	43.3	44.6	44.9	48.6	0.0	0.0	0.0	0.0
22.7	26.1	20.3	26.6	30.8	23.7	31.0	19.5	19.2	18.7	22.9
19.1	19.0	18.8	25.1	29.3	19.6	19.4	18.0	17.3	17.4	23.0
36.6	41.5	31.6	37.2	39.9	38.2	44.3	0.0	0.0	0.0	0.0
59.1	62.8	59.0	59.5	59.9	60.3	61.3	59.6	59.6	59.3	60.2
7.4	12.6	-0.8	-0.6	0.3	8.4	14.3	-1.0	0.2	-0.3	0.5
7.4	26.3	-1.0	-0.8	0.0	8.9	14.5	9.9	0.3	1.4	0.5
42.5	43.1	18.0	18.2	18.2	41.1	42.5	17.2	16.9	16.6	16.7
9.6	16.2	1.0	0.9	1.6	10.7	16.6	2.7	2.1	1.9	2.4
22.6	26.1	20.1	26.4	30.6	23.6	30.9	0.0	0.0	0.0	0.0
21.0	25.4	13.1	14.6	15.9	21.8	28.2	15.6	15.7	15.8	18.8
11.1	25.3	2.4	1.8	2.1	14.3	18.3	6.5	6.6	8.2	8.3
58.8	58.8	60.7	60.9	60.1	60.6	56.7	0.0	0.0	0.0	0.0
61.1	61.0	63.2	63.4	62.5	62.9	58.7	0.0	0.0	0.0	0.0
78.4	81.7	86.0	85.1	84.1	80.6	71.0	0.0	0.0	0.0	0.0
2.2	2.2	2.1	2.1	2.2	2.2	2.2	2.1	2.1	2.1	2.1
40.0	46.0	34.0	34.0	34.0	41.0	49.0	34.0	34.0	34.0	34.0
105.0	105.0	105.0	105.0	105.0	105.0	105.0	105.0	105.0	105.0	105.0
-	-	-	-	-	-	-	-	-	-	-
98.0	95.0	102.0	102.0	100.0	97.0	90.0	103.0	103.0	103.0	103.0
xx	xx	xx	xx	xx	xx	xx	xx	xx	xx	xx
53.0	48.0	35.0	36.0	36.0	44.0	50.0	35.0	36.0	35.0	36.0
2.8	2.9	2.1	2.3	2.4	2.8	3.0	2.0	2.0	2.0	2.1
2.6	3.9	3.5	3.1	3.1	2.9	3.8	4.3	4.3	4.3	3.1
-	-	-	-	-	-	-	15.0	18.0	20.0	20.0
436.0	448.2	434.6	433.8	434.3	439.3	428.3	441.4	441.6	444.0	444.2
475.2	483.8	480.8	479.7	480.5	478.1	456.8	489.8	489.9	493.2	493.4
477.6	482.2	493.6	491.8	490.4	481.2	460.0	495.5	492.6	497.9	498.7
327.9	345.5	309.4	322.3	329.7	331.5	354.8	195.5	195.5	195.5	195.5
248.4	257.7	242.2	259.1	271.6	250.8	271.9	240.1	239.4	237.9	248.7
244.9	258.3	224.7	228.5	231.9	247.5	269.1	230.8	231.0	231.3	238.7
244.9	258.3	224.7	228.5	231.9	247.5	269.1	230.8	231.0	231.3	238.7
111.4	118.3	95.4	96.0	95.6	111.7	144.4	91.1	91.0	89.6	89.5
41.2	46.9	33.2	33.3	34.1	42.2	49.0	32.9	34.0	33.6	34.3

Table 13.3: HWC raw data

Heat standing loss trial: heat_loss1
Date: 6.10.2002
Measurement set-up: S8
System configuration: heat pump off, no water flowing in the HWC

Time [min]	T17 (HWC top) [°C]	T18 [°C]	T19 [°C]	T20 [°C]	T21 [°C]	T22 [°C]	T23 [°C]	T24 (HWC bottom) [°C]
0	53.8	53.4	52.9	53.4	53.4	53.6	53.7	52.8
60	53.2	52.8	52.1	52.9	53.2	53.5	53.5	52.3
120	52.7	52.4	51.8	52.5	52.8	53.0	52.8	51.1
180	52.4	52.0	51.5	52.1	52.3	52.5	52.1	50.1
240	52.0	51.6	51.2	51.7	51.9	52.0	51.5	49.1
300	51.6	51.2	50.9	51.3	51.5	51.6	50.8	48.2
360	51.2	50.8	50.5	50.8	51.0	51.1	50.2	47.4
420	50.8	50.5	50.1	50.4	50.6	50.6	49.5	46.7
480	50.4	50.1	49.7	50.0	50.2	50.1	48.9	45.9
540	50.0	49.7	49.3	49.6	49.7	49.6	48.2	45.2
600	49.6	49.3	48.9	49.2	49.3	49.1	47.6	44.5
660	49.2	48.9	48.5	48.8	48.9	48.6	47.0	43.8
720	48.9	48.6	48.1	48.5	48.5	48.2	46.4	43.2
780	48.4	48.2	47.7	48.0	48.1	47.7	45.9	42.7
840	48.1	47.9	47.3	47.7	47.7	47.2	45.3	42.1
900	47.7	47.5	47.0	47.3	47.3	46.8	44.8	41.6
960	47.3	47.1	46.6	46.9	46.9	46.3	44.3	41.0
1020	47.0	46.8	46.3	46.6	46.5	45.9	43.8	40.6
1080	46.6	46.4	45.9	46.2	46.1	45.4	43.3	40.1
1140	46.3	46.1	45.6	45.9	45.8	45.0	42.8	39.7
1200	45.9	45.8	45.3	45.6	45.4	44.6	42.4	39.3
1260	45.5	45.4	44.9	45.2	45.0	44.2	42.0	38.9
1320	45.2	45.1	44.6	44.9	44.7	43.8	41.6	38.5
1380	44.9	44.8	44.3	44.6	44.4	43.4	41.2	38.2
1440	44.6	44.5	44.0	44.2	44.0	43.1	40.8	37.8
1500	44.2	44.2	43.6	43.9	43.7	42.7	40.4	37.5
1560	43.9	43.9	43.3	43.6	43.3	42.3	40.1	37.1
1620	43.6	43.5	43.0	43.3	43.0	41.9	39.7	36.7
1680	43.2	43.2	42.7	42.9	42.6	41.6	39.3	36.4
1740	42.9	42.9	42.4	42.6	42.3	41.2	38.9	36.0
1800	42.6	42.6	42.1	42.3	41.9	40.8	38.5	35.7
1860	42.3	42.3	41.8	42.0	41.6	40.5	38.1	35.3
1920	42.0	42.0	41.5	41.7	41.3	40.1	37.8	35.1
1980	41.7	41.7	41.2	41.4	40.9	39.7	37.5	34.7
2040	41.4	41.4	40.9	41.1	40.6	39.4	37.1	34.4
2100	41.1	41.1	40.6	40.8	40.3	39.0	36.8	34.1
2160	40.8	40.8	40.3	40.4	40.0	38.7	36.4	33.7
2220	40.5	40.5	40.0	40.1	39.6	38.3	36.1	33.4
2280	40.2	40.2	39.7	39.8	39.3	38.0	35.8	33.1
2340	39.9	39.9	39.4	39.5	39.0	37.7	35.4	32.8
2400	39.7	39.7	39.1	39.2	38.7	37.3	35.1	32.5
2460	39.4	39.4	38.8	38.9	38.3	37.0	34.8	32.2
2520	39.1	39.1	38.6	38.7	38.1	36.7	34.5	31.9
2580	38.9	38.9	38.4	38.5	37.8	36.4	34.2	31.7
2640	38.7	38.6	38.2	38.2	37.6	36.2	34.0	31.5
2700	38.4	38.4	37.9	38.0	37.3	35.9	33.7	31.3
2760	38.2	38.2	37.7	37.7	37.1	35.6	33.5	31.1
2820	38.0	37.9	37.5	37.5	36.8	35.4	33.3	31.0
2880	37.7	37.7	37.2	37.3	36.6	35.2	33.1	30.8
2940	37.5	37.4	37.0	37.0	36.3	34.9	32.9	30.7
3000	37.2	37.2	36.7	36.7	36.1	34.6	32.7	30.5
3060	36.9	36.9	36.5	36.5	35.8	34.4	32.4	30.3
3120	36.7	36.7	36.2	36.2	35.6	34.1	32.2	30.1
3180	36.5	36.4	36.0	36.0	35.3	33.9	32.0	29.9
3240	36.2	36.2	35.8	35.8	35.1	33.7	31.8	29.7
3300	36.0	36.0	35.5	35.5	34.8	33.4	31.6	29.5
3360	35.8	35.8	35.3	35.3	34.6	33.2	31.4	29.4
3420	35.5	35.5	35.1	35.0	34.4	33.0	31.2	29.1
3480	35.3	35.3	34.8	34.8	34.1	32.7	31.0	28.9
3540	35.1	35.0	34.6	34.6	33.9	32.5	30.7	28.7
3600	34.8	34.8	34.4	34.3	33.6	32.3	30.5	28.5
3660	34.6	34.6	34.2	34.1	33.4	32.1	30.3	28.3
3720	34.4	34.4	33.9	33.9	33.2	31.8	30.1	28.1
3780	34.2	34.2	33.7	33.7	33.0	31.6	29.9	27.9
3840	33.9	33.9	33.5	33.4	32.7	31.4	29.6	27.7
3900	33.8	33.8	33.4	33.3	32.6	31.2	29.5	27.5

HWC reheating trial: reheat1
Date: 10.10.2002
Measurement set-up: S8
System configuration: S8, heat pump on (C11)

time [sec.]	T17 (HWC top) [°C]	T18 [°C]	T19 [°C]	T20 [°C]	T21 [°C]	T22 [°C]	T23 [°C]	T24 (HWC bottom) [°C]
1800.0	16.9	16.8	16.5	16.6	16.4	16.3	16.3	16.2
1860.0	17.4	16.7	16.5	16.6	16.4	16.3	16.4	16.3
1920.0	18.4	16.8	16.5	16.6	16.4	16.4	16.4	16.3
1980.0	18.3	16.7	16.5	16.6	16.4	16.4	16.4	16.2
2040.0	18.4	16.8	16.5	16.6	16.5	16.4	16.4	16.2
2100.0	18.4	16.8	16.6	16.6	16.5	16.4	16.4	16.3
2160.0	18.2	16.8	16.5	16.6	16.5	16.4	16.4	16.3
2220.0	20.1	16.9	16.6	16.7	16.5	16.5	16.4	16.3
2280.0	27.6	16.9	16.6	16.7	16.5	16.4	16.4	16.3
2340.0	39.1	16.9	16.7	16.7	16.5	16.5	16.4	16.3
2400.0	46.9	17.0	16.7	16.7	16.5	16.6	16.4	16.3
2460.0	51.0	17.0	16.6	16.7	16.5	16.4	16.4	16.2
2520.0	53.2	17.1	16.6	16.7	16.5	16.4	16.4	16.3
2580.0	54.4	17.3	16.6	16.7	16.5	16.6	16.4	16.3
2640.0	55.2	17.8	16.7	16.7	16.5	16.6	16.4	16.3
2700.0	55.7	18.7	16.7	16.7	16.5	16.6	16.4	16.3
2760.0	56.1	20.7	16.8	16.7	16.5	16.6	16.4	16.3
2820.0	56.4	24.6	16.7	16.7	16.5	16.5	16.4	16.3
2880.0	56.6	31.0	16.7	16.7	16.5	16.5	16.4	16.3
2940.0	56.8	38.5	16.8	16.7	16.5	16.5	16.4	16.3
3000.0	57.0	44.9	16.9	16.7	16.5	16.6	16.5	16.3
3060.0	57.1	49.5	17.0	16.7	16.5	16.5	16.4	16.3
3120.0	57.2	52.3	17.3	16.7	16.6	16.6	16.4	16.3
3180.0	57.4	54.0	17.9	16.8	16.6	16.5	16.5	16.3
3240.0	57.4	55.0	19.3	16.8	16.5	16.5	16.4	16.3
3300.0	57.5	55.6	21.7	16.8	16.6	16.5	16.4	16.3
3360.0	57.5	56.0	25.9	16.9	16.6	16.6	16.4	16.3
3420.0	57.6	56.3	31.9	16.9	16.6	16.6	16.4	16.3
3480.0	57.7	56.5	38.8	17.0	16.6	16.6	16.5	16.3
3540.0	57.7	56.6	45.2	17.2	16.7	16.5	16.5	16.4
3600.0	57.8	56.7	50.0	17.3	16.6	16.5	16.5	16.4
3660.0	57.8	56.8	53.3	17.8	16.6	16.5	16.5	16.4
3720.0	57.9	56.9	55.3	18.7	16.6	16.5	16.4	16.3
3780.0	57.9	56.9	56.5	20.6	16.7	16.7	16.5	16.3
3840.0	57.9	57.0	57.3	23.3	16.7	16.6	16.5	16.3
3900.0	57.9	57.0	57.8	27.5	16.8	16.7	16.5	16.4
3960.0	58.0	57.0	58.0	32.6	16.8	16.7	16.5	16.3
4020.0	58.0	57.1	58.3	38.1	17.0	16.6	16.5	16.4
4080.0	58.0	57.1	58.3	42.9	17.2	16.7	16.5	16.3
4140.0	58.0	57.1	58.4	46.9	17.7	16.7	16.5	16.4
4200.0	58.0	57.1	58.5	49.9	18.6	16.7	16.5	16.4
4260.0	58.0	57.1	58.5	51.9	20.3	16.8	16.5	16.4
4320.0	58.0	57.2	58.5	53.3	22.7	16.8	16.5	16.3
4380.0	58.0	57.2	58.6	54.2	26.1	16.8	16.5	16.3
4440.0	58.0	57.2	58.6	54.8	30.7	16.9	16.5	16.4
4500.0	58.0	57.2	58.6	55.2	35.6	17.2	16.5	16.4
4560.0	58.1	57.2	58.7	55.5	40.6	17.6	16.5	16.4
4620.0	58.1	57.2	58.7	55.7	45.0	18.2	16.5	16.3
4680.0	58.1	57.3	58.7	55.8	48.7	19.7	16.7	16.4
4740.0	58.0	57.2	58.6	55.8	51.4	21.5	16.6	16.3
4800.0	58.0	57.2	58.7	55.9	53.6	24.4	16.6	16.3
4860.0	58.0	57.2	58.7	56.0	55.0	28.0	16.7	16.3
4920.0	58.0	57.2	58.7	56.1	55.9	32.4	16.8	16.3
4980.0	58.0	57.2	58.7	56.1	56.5	37.2	16.9	16.3
5040.0	58.0	57.2	58.7	56.1	57.0	41.9	17.1	16.3
5100.0	58.1	57.3	58.8	56.2	57.3	46.1	17.5	16.3
5160.0	58.1	57.3	58.8	56.2	57.5	49.6	18.2	16.3
5220.0	58.1	57.3	58.8	56.2	57.6	52.1	19.6	16.5
5280.0	58.1	57.3	58.8	56.3	57.7	54.0	21.3	16.5
5340.0	58.1	57.3	58.8	56.3	57.8	55.4	23.9	16.5
5400.0	58.1	57.3	58.8	56.3	57.8	56.3	27.2	16.6
5460.0	58.1	57.3	58.8	56.3	57.9	56.9	31.1	16.7
5520.0	58.1	57.3	58.8	56.3	57.9	57.4	35.4	16.9
5580.0	58.1	57.3	58.9	56.3	57.9	57.6	39.7	17.3
5640.0	58.1	57.3	58.8	56.4	58.0	57.8	43.7	18.0
5700.0	58.1	57.3	58.9	56.4	58.0	58.0	47.0	19.1
5760.0	58.1	57.3	58.8	56.3	57.9	58.0	49.8	20.9
5820.0	58.1	57.4	58.9	56.4	58.0	58.1	52.1	23.2
5880.0	58.1	57.3	58.8	56.4	58.0	58.1	53.6	26.1
5940.0	58.2	57.4	58.9	56.4	58.1	58.2	54.8	29.7
6000.0	58.2	57.4	58.9	56.4	58.1	58.3	55.7	33.7

HWC water withdrawal: cooling								
Date: 10.10.2002								
Measurement set-up: S8								
System configuration: heat pump off								
withdrawal period:		1	2	3	4	5	6	7
Time [min]:		0:00 – 0:02	0:20 – 0:22	0:37 – 0:39	1: 10 – 1:12	1:45 – 1:47	2:48 – 2:52	3:50 - 3:54
water mass flowrate [l/min]:$		2.91	2.9	3	4.6	4.6	7.54	7.45
min [sec.]	T17: HWC Top [°C]	T10 (T2 cyl) [°C]	T11 (T3 cyl) [°C]	T12 (T4 cyl) [°C]	T13 (T5 cyl) [°C]	T14 (T6 cyl) [°C]	T15 (T7 cyl) [°C]	T24: HWC bottom [°C]
0	59.38	57.55	58.86	56.40	58.12	58.35	57.22	50.46
180	59.33	57.53	58.83	56.38	58.12	58.31	57.20	50.54
360	59.28	57.56	58.85	56.42	58.17	58.32	57.20	50.62
540	59.22	57.58	58.86	56.34	58.22	58.32	57.03	47.16
720	58.96	57.50	58.80	56.29	58.15	58.21	56.25	32.53
900	58.92	57.50	58.81	56.31	58.16	58.22	56.19	32.50
1080	58.84	57.48	58.80	56.27	58.13	58.20	56.09	32.61
1260	58.83	57.47	58.77	56.26	58.12	58.17	55.97	32.76
1440	58.77	57.45	58.76	56.27	58.12	58.18	55.90	32.95
1620	58.74	57.49	58.81	56.28	58.13	58.17	55.72	32.12
1800	58.50	57.40	58.72	56.22	58.03	57.98	52.85	21.88
1980	58.40	57.36	58.69	56.21	58.05	57.92	52.02	21.44
2160	58.34	57.34	58.63	56.16	57.97	57.86	51.66	21.65
2340	58.32	57.33	58.67	56.15	57.98	57.86	51.40	21.89
2520	58.27	57.33	58.64	56.12	57.96	57.81	51.09	22.13
2700	58.22	57.28	58.62	56.11	57.93	57.75	50.76	22.33
2880	58.13	57.30	58.58	56.08	57.87	57.15	42.76	18.97
3060	58.03	57.21	58.54	56.03	57.79	57.01	41.88	18.97
3240	57.93	57.14	58.50	56.01	57.77	56.96	41.60	19.05
3420	57.97	57.20	58.51	56.04	57.78	56.93	41.38	19.23
3600	57.96	57.18	58.52	56.03	57.79	56.87	41.20	19.34
3780	57.86	57.10	58.45	55.94	57.69	56.74	40.95	19.40
3960	57.86	57.10	58.48	55.96	57.71	56.69	40.79	19.56
4140	57.79	57.04	58.44	55.91	57.67	56.58	40.58	19.63
4320	57.75	57.03	58.41	55.88	57.64	56.51	40.41	19.76
4500	57.73	56.98	58.37	55.82	57.61	56.43	40.24	19.89
4680	57.72	56.96	58.34	55.84	57.50	56.32	40.08	19.99
4860	57.67	56.92	58.28	55.73	57.22	52.01	27.73	18.53
5040	57.63	56.88	58.27	55.69	57.06	51.40	26.21	18.64
5220	57.61	56.82	58.18	55.64	56.97	51.21	26.20	18.64
5400	57.66	56.89	58.22	55.67	56.98	51.07	26.28	18.73
5580	57.63	56.87	58.22	55.64	56.91	50.89	26.30	18.75
5760	57.59	56.83	58.17	55.60	56.88	50.71	26.34	18.74
5940	57.56	56.78	58.13	55.52	56.78	50.51	26.35	18.72
6120	57.57	56.81	58.16	55.58	56.81	50.41	26.47	18.83
6300	57.50	56.75	58.09	55.50	56.70	50.22	26.47	18.80
6480	57.45	56.66	58.07	55.46	56.64	50.05	26.54	18.79
6660	57.45	56.70	58.09	55.48	56.62	49.93	26.61	18.87
6840	57.41	56.65	58.03	55.37	55.74	43.96	23.16	18.39
7020	57.32	56.58	57.90	55.15	54.10	39.09	20.52	18.41
7200	57.30	56.57	57.89	55.12	53.96	38.93	20.51	18.43
7380	57.29	56.61	57.91	55.10	53.89	38.84	20.59	18.49
7560	57.28	56.53	57.87	55.06	53.76	38.75	20.61	18.46
7740	57.24	56.49	57.82	55.01	53.64	38.64	20.62	18.44
7920	57.24	56.51	57.84	55.03	53.55	38.59	20.71	18.48
8100	57.21	56.49	57.83	54.95	53.46	38.51	20.79	18.50
8280	57.13	56.46	57.77	54.92	53.34	38.42	20.81	18.47
8460	57.12	56.43	57.74	54.88	53.24	38.38	20.89	18.46
8640	57.10	56.39	57.69	54.85	53.12	38.30	20.92	18.47
8820	57.15	56.42	57.75	54.86	53.07	38.28	21.04	18.57
9000	57.10	56.34	57.68	54.78	52.94	38.22	21.09	18.56
9180	57.05	56.34	57.66	54.75	52.84	38.12	21.11	18.51
9360	57.02	56.31	57.64	54.71	52.72	38.06	21.17	18.64
9540	57.04	56.32	57.64	54.72	52.66	38.06	21.28	18.66
9720	57.02	56.28	57.63	54.69	52.57	38.00	21.32	18.76
9900	56.91	56.20	57.56	54.60	52.42	37.88	21.29	18.69
10080	56.92	56.21	57.55	54.57	52.35	37.84	21.40	18.73
10260	56.94	56.22	57.55	54.58	52.27	37.82	21.46	18.72
10440	56.91	56.21	57.52	54.54	52.16	37.75	21.51	18.75
10620	56.87	56.14	57.44	53.83	47.92	30.19	19.86	18.42
10800	56.79	56.09	57.06	51.31	39.47	23.80	18.87	18.57
10980	56.74	56.06	57.02	51.15	39.28	23.75	18.86	18.54
11160	56.69	56.04	56.96	51.02	39.18	23.76	18.82	18.58
11340	56.68	55.99	56.93	50.95	39.13	23.81	18.82	18.63
11520	56.62	55.93	56.87	50.78	39.03	23.82	18.83	18.60
11700	56.53	55.86	56.82	50.69	38.98	23.85	18.80	18.52
11880	56.58	55.90	56.85	50.67	38.97	23.92	18.86	18.67
12060	56.55	55.87	56.76	50.53	38.91	23.99	18.88	18.70
12240	56.50	55.85	56.71	50.44	38.83	24.00	18.87	18.67
12420	56.49	55.82	56.70	50.35	38.81	24.03	18.88	18.65

12600	56.47	55.79	56.68	50.31	38.77	24.10	18.90	18.67
12780	56.38	55.71	56.59	50.18	38.68	24.10	18.87	18.62
12960	56.37	55.68	56.57	50.12	38.66	24.17	18.91	18.61
13140	56.36	55.67	56.53	50.03	38.61	24.22	18.92	18.65
13320	56.38	55.66	56.50	49.94	38.57	24.26	18.91	18.63
13500	56.33	55.62	56.45	49.85	38.52	24.28	18.91	18.62
13680	56.41	55.69	56.49	49.83	38.55	24.36	19.00	18.67
13860	56.38	55.66	56.45	49.76	38.46	24.36	18.98	18.65
14040	56.33	55.62	56.37	49.64	38.41	24.39	18.97	18.62
14220	56.26	55.54	56.33	49.52	38.37	24.43	18.97	18.59
14400	56.23	55.52	54.98	45.34	31.95	21.21	18.58	18.41
14580	56.07	55.21	52.70	39.43	25.68	19.35	18.48	18.39
14760	56.02	55.15	52.62	39.14	25.59	19.36	18.50	18.40
14940	56.00	55.12	52.55	38.99	25.60	19.38	18.49	18.40
15120	55.94	55.08	52.46	38.89	25.61	19.39	18.50	18.42
15300	55.86	55.02	52.35	38.80	25.63	19.41	18.50	18.41
15480	55.86	54.98	52.30	38.73	25.64	19.42	18.48	18.43
15660	55.84	54.96	52.22	38.69	25.67	19.46	18.52	18.48
15840	55.82	54.93	52.16	38.65	25.74	19.53	18.55	18.50
16020	55.76	54.89	52.09	38.57	25.75	19.54	18.55	18.47
16200	55.77	54.89	52.05	38.56	25.80	19.58	18.55	18.50
16380	55.69	54.83	51.95	38.50	25.83	19.58	18.55	18.49
16560	55.69	54.80	51.90	38.45	25.85	19.59	18.57	18.51
16740	55.67	54.74	51.84	38.43	25.94	19.67	18.59	18.51
16920	55.63	54.73	51.77	38.40	25.93	19.65	18.56	18.52
17100	55.61	54.71	51.70	38.33	25.97	19.70	18.59	18.52
17280	55.58	54.68	51.67	38.32	26.03	19.78	18.64	18.55
17460	55.50	54.60	51.56	38.24	26.03	19.77	18.60	18.51

Heat standing loss trial: heat_loss2

Date: 10.10.2002

Measurement set-up: S8

System configuration: heat pump off, no water flowing in the HWC

Time	T17: HWC Top	T10 (T2 cyl)	T11 (T3 cyl)	T12 (T4 cyl)	T13 (T5 cyl)	T14 (T6 cyl)	T15 (T7 cyl)	T24: HWC bottom
[sec.]	[°C]	[°C]	[°C]	[°C]	[°C]	[°C]	[°C]	[°C]
20000	55.0	54.0	50.6	37.7	26.4	20.0	18.6	18.4
21800	54.6	53.6	50.0	37.4	26.6	20.3	18.6	18.3
23600	54.3	53.3	49.5	37.1	26.8	20.5	18.6	18.3
25400	53.9	52.9	48.9	36.8	26.9	20.7	18.6	18.2
27200	53.5	52.4	48.4	36.6	27.0	20.8	18.7	18.2
29000	53.2	52.1	47.9	36.4	27.2	21.1	18.7	18.1
30800	52.8	51.6	47.3	36.1	27.2	21.2	18.7	18.1
32600	52.4	51.2	46.9	35.9	27.3	21.3	18.7	18.0
34400	52.0	50.8	46.4	35.6	27.4	21.5	18.8	18.0
36200	51.6	50.4	46.0	35.4	27.4	21.6	18.8	18.0
38000	51.3	50.1	45.7	35.3	27.6	21.8	18.9	18.0
39800	51.0	49.7	45.2	35.1	27.6	21.8	18.9	18.0
41600	50.6	49.3	44.9	35.0	27.6	22.0	19.0	18.0
43400	50.3	48.9	44.5	34.8	27.7	22.1	19.0	18.0
45200	49.9	48.5	44.2	34.6	27.7	22.2	19.1	18.0
47000	49.5	48.1	43.8	34.4	27.7	22.2	19.0	17.9
48800	49.2	47.7	43.5	34.3	27.7	22.3	19.1	17.9
50600	48.8	47.4	43.1	34.1	27.7	22.4	19.1	17.9
52400	48.4	47.0	42.8	33.9	27.7	22.4	19.2	17.9
54200	48.1	46.6	42.5	33.8	27.7	22.5	19.2	17.9
56000	47.7	46.2	42.2	33.7	27.7	22.5	19.2	17.9